SORPTION AND REACTION OF OXIDES OF NITROGEN AND CARBON ON HETEROPOLY OXOMETALATES

by

Raymond Bélanger

A thesis
presented to the University of Waterloo
in fulfilment of the
thesis requirement for the degree of
Doctor of Philosophy
in
Chemistry

Waterloo, Ontario, Canada, 1996

BORROWER'S PAGE

The University of Waterloo requires the signatures of all persons using or photocopying this thesis. Please sign below, and give address and date.

ABSTRACT

Nitric oxide and nitrogen dioxide can be removed from a gas stream by heteropoly oxometalates having the Keggin structure (KU). NO_2 can be sorbed (physisorbed and/or chemisorbed) into the bulk structure of 12-tungstophosphoric acid (HPW), 12-tungstosilicic acid (HSiW), and 12-molybdophosphoric acid (HPMo), however with the latter, small quantities were sorbed. A portion of the gas phase NO_2 reacts with the water on and in the solid acids to produce nitric acid which desorbs into the gas phase. Infrared, Raman, and NMR spectroscopies indicate that the remainder of the NO_2 remains bound in the solid acids through association with the protons contained within to form a nitronium salt. NO cannot be directly sorbed by the acids, but can be sorbed if the catalysts were first exposed to NO_2. No reduction of NO nor NO_2 to N_2 is observed with the heteropoly acids.

With ammonium 12-tungstophosphate and ammonium 12-molybdophosphate, N_2 (and small quantities of NO) are found to be the principal products in the effluent of the reactor held at temperatures below 200°C, from the surface (and bulk) reaction of nitrogen dioxide contained in the gas stream and ammonia from the catalyst. At temperatures higher than 200°C, nitrous oxide is produced, as well as N_2. Nitric oxide can be reduced, to a certain extent, to N_2. However, the NO conversion is significantly increased when NO_2 or HNO_3 are injected first on the ammonium catalysts. The spent ammonium 12-tungstophosphate sorbs quantities of NO_2, while ammonium 12-molybdophosphate does not. Both catalysts are regenerated through injection of gaseous ammonia.

With silica supported 12-tungstophosphoric acid, as with the bulk acid, quantities of NO_2 are sorbed. Although the surface area is increased, the number of NO_2 per anion decreases from the bulk stoichiometry of 3 NO_2/KU to smaller values for lower loadings. As with its bulk acid, silica supported 12-molybdophosphoric acid sorbs vanishingly small quantities of NO_2. Little or no NO is sorbed or reduced by the supported acids .

As with the bulk ammonium salts, the injection of nitrogen dioxide on silica supported heteropoly acids, pre-exposed to gaseous ammonia, produces mainly nitrogen. The conversion of NO_2 to nitrogen reaches a maximum with approximately 20% loading. Results on the conversion of N_2O to N_2 by silica supported 12-molybdophosphoric acid, pre-exposed to gaseous ammonia, are also reported.

Since little or no NO or NO_2 are sorbed or reduced by the Li, Na, K, Rb, and Cs salts of HPW, protons evidently participate, directly or indirectly in the sorption and reaction of NO and NO_2 by the heteropoly oxometalates.

Heteropoly acids, both pure and SiO_2-supported, reduce quantities of CO_2 to carbon deposits at temperatures as low as room temperature. As with NOx, the protons contained within the catalysts are necessary for the reduction of CO_2. The carbon containing deposits are reoxidized and released to the gas stream when the catalysts are heated to temperatures higher than 550°C. Also, the unsupported and supported heteropoly acids oxidize CO to CO_2, without added O_2. The addition of traces of oxygen enhances the reaction and regenerates the surface of the catalysts.

In view of the present results and the more stringent regulations for the control of emissions, the heteropoly oxometalates offer an interesting alternative for removal of oxides of nitrogen and carbon from a gas stream.

ACKNOWLEDGEMENTS

This thesis would have not been possible without the continuous support and encouragement of my supervisor, John B. Moffat. I want to thank him greatly.

I also want to thank Alexandre G. Brolo for his help with the Raman data, and Sandra Mooibroek for her help with the NMR data. Their respective contribution is greatly appreciated.

My thanks to Michelle A. Parent and Senquan Gao for helping in the preparation of some of the catalysts used.

A ma mère...

TABLE OF CONTENTS

LIST OF TABLES

LIST OF FIGURES

LIST OF SYMBOLS AND ABBREVIATIONS

%	percent
μ	micro or reduced mass
α	Alpha
ν	nu
λ	wavelength
π	pi
ω	omega
θ	theta
□	atom vacancy
μL	microlitre
μmol	micromole
* or i	isotope (or stated otherwise)
ads	adsorbed
A/F	Air/Fuel ratio
amu	Atomic Mass Unit
B.E.T. or BET	Brunauer, Emmett, and Teller isotherm
cm	centimeter
CsPW	Cesium 12-tungstophosphate
dec.	decreasing
e	electron
g	gram
h	Planck's constant
HPMo	12-molybdophosphoric acid
HPW	12-tungstophosphoric acid
HSiW	12-tungstosilicic acid
hr	hour
i.d.	internal diameter
ICR	Isothermal Continuous Reaction
inc.	increasing
K	degree Kelvin
kHz	kilohertz
KU	Keggin Unit
kV	kilovolt
LEV	Low Emission Vehicles

LiPW	Lithium 12-tungstophosphate
m	meter or mass
mA	milliampere
MF	molecular fragment
Mhz	megahertz
min	minute
mL	millilitre
MOCC	Metal-Oxygen Cluster Compounds
mol	mole
MS	Molecular Sieve
NaPW	Sodium 12-tungstophosphate
NH_4PMo	Ammonium 12-molybdophosphate
NH_4PW	Ammonium 12-tungstophosphate
N.M. or N/M	Not Measured
nm	nanometer
NOx	Nitrogen Oxides
NSCR	Non-selective catalytic reduction
o.d.	outside diameter
°C	degree Celcius
KPW	Potassium 12-tungstophosphate
ppm	parts per million
RbPW	Rubidium 12-tungstophosphate
SCR	Selective Catalytic Reduction
sec	second
SNCR	Selective Non-Catalytic Reduction
SPE-VT	Single-Pulse Experiments at a Variety of Temperatures
T	Temperature or tesla
t	time
TCD	Thermal conductivity detector
TGA	Thermogravimetric analysis
TLEV	Transitional Low Emission Vehicles
TPD	Temperature-Programmed Desorption
TPR	Temperature-Programmed Reaction
TWC	Three-Way-Catalyst
VOC	Volatile Organic Compounds
w	weight

CHAPTER I

INTRODUCTION

A. Air pollution and nitrogen oxides

Although air pollution is mainly associated with human activities, the atmosphere always contained noxious substances, from lightning, burning forests, volcano eruptions, decomposition processes, or bacteria. Only the concentration of these substances varied in history.

As a result of the introduction of toxic chemicals by natural and human-made causes, it is virtually impossible to determine what the composition of "pure" air could be. Pure air is in fact diluted polluted air. The Engineers Joint Council developed the following definition of air pollution (Ref.1.1): "*Air pollution means the presence in the outdoor atmosphere of one or more contaminants, such as dust, fumes, gas, mist, odor, smoke, or vapor, in quantities, of characteristics, and of duration such as to be injurious to human, plant or animal life or to property, or which unreasonably interfere with the comfortable enjoyment of life and property.*". Table 1.1 gives the gaseous composition of "unpolluted" air (Ref.1.2). Any change of concentration or the introduction of other components cited in Table 1.1 should be considered as "pollution".

Forest dieback, damage to buildings and structures caused by acid precipitation, photochemical smog in cities from combustion processes, and health deterioration for people are just a few problems caused by atmospheric pollution. The socio-economic costs of pollutants are high. The shift towards a more environmentally friendly society by the introduction of different legislations from our governments, and with the pressure of the scientific community, has improved the quality of the air we breathe.

The sources are well known, both natural and human-made. Smoke and ashes are now more than just a dark emanation from a combustion process. Their chemical compositions are known. The components of air pollution are identified. Table 1.2 presents a summary and estimated concentration of the most important pollutants, both naturally and human-made, produced globally in 1978 (Ref.1.2).

TABLE 1.1

COMPOSITION OF "UNPOLLUTED AIR"

Chemicals	Concentration (ppm-vol)
Nitrogen	756 500
Oxygen	202 900
Water	31 200
Argon	9 000
Carbon dioxide	305
Neon	17.4
Helium	5
Methane	0.97-1.16
Krypton	0.97
Nitrous oxide	0.49
Hydrogen	0.49
Xenon	0.08
Organic vapours	0.02

TABLE 1.2

ESTIMATED ANNUAL GLOBAL EMISSION OF POLLUTANTS

Pollutant	Natural[a]	Human-made[a]	Total[a]
CO_2	1 000 000	22 000	1 022 000
CO	2 100	700	2 800
SO_2	20	212	232
CH_4	1 050	160	1 210
NO, NO_2	180	75	255
Total non-CH_4 hydrocarbons	20 000	40	20 040
NH_3	260	6	266
HCl, Cl_2	150	4	154
N_2O	340	3	343
H_2S	84	3	87
CH_3Cl	5	2	7
Isoprene and terpenes	830	0	830
TOTAL:	1 025 019	23 205	1 048 224

[a] 10^6 metric tons per year.

The quantity of human-made pollutants corresponds approximately to 2.2% of the total quantity emitted on earth. However, the pollutants emitted tend to be more concentrated around and downwind from the sources and thus their concentration will be higher in cities than in the countryside. Diffusion processes are slower in cities. Since the majority of the population lives in or near major cities, the air quality can deteriorate rapidly when the meteorological conditions prevail. The real problem is not the quantity of pollutants emitted but their diffusion and further dilution. We cannot change the atmospheric conditions to promote dilution. So the only solution remains the reduction or elimination of emissions at the source.

In order to reduce the quantity of contaminants emitted by human-made sources, it is important to know their nature and the action on our environment once released. For example, nitric oxide, NO, is released from combustion. Nitric oxide is a primary pollutant, as well as all the molecules presented in Table 1.2, but reacts readily with atmospheric O_2 to generate nitrogen dioxide, NO_2. Nitrogen dioxide is the secondary pollutant and is extremely toxic. Nitrogen dioxide is known to cause photochemical smog in cities, and nitric acid (HNO_3) when reacting with water vapor. Nitric acid is also a secondary pollutant.

Today's economy is based on consumption of goods. The more products we consume, the better the economy is. However, it takes energy to manufacture and most sources of energy used produce pollution.

The two general sources of atmospheric pollution are combustion, and handling and processing of chemicals. Many polluting chemicals are released into the atmosphere. However, two classes, sulfur oxides and nitrogen oxides, are well known for the damages which they cause to the environment and to our health.

Thirty years ago, the regulations were set mainly to reduce the emissions of sulfur oxides from all sources. Nitrogen oxides were also known to be a major pollutant, but, the efforts in the reduction were centred on sulfur emissions because it was related to numerous deaths in pollution episodes. However, legislation came rapidly around for the immediate reduction of nitrogen oxides from all sources. Since the present work deals mainly with the nitrogen oxides, the discussion will be limited to this class of pollutants.

The two categories of sources are: 1) stationary, and 2) mobile.

As said earlier, nitrogen oxides are substantially destructive air pollutants (after sulfur oxides) and various forms of these can theoretically exist in the environment. The reaction of N_2

and O_2 in combustion processes causes the formation of; N_2O, NO, NO_2, NO_3, N_2O_3, N_2O_4, and N_2O_5. Two hydrates are also known to exist in the atmosphere; HNO_2 and HNO_3.

Reference 1.3b presents the emissions of NOx, VOC, CO_2, and N_2O across Canada. Since 1992 a reduction of 16% of air pollutants has been recorded. The global contribution of greenhouse gases (i.e N_2O and CO_2) from Canada was evaluated to be less than 2% in 1992.

Nitrous oxide (N_2O) is a normal constituent of the atmosphere and is found at concentrations of about 5 ppm. Most N_2O comes from biochemical reactions in the soil. Nitrous oxide was not considered as a potential pollutant because of its high stability at normal conditions. Its atmospheric residence time is estimated from 20 to 100 years. Possible accumulation could cause problems, but little is known of the effect of nitrous oxide on the ecosystem. However, its role into the reduction of the ozone layer and the global warming is now known.

Nitric oxide (NO) represents 90 to 95% of the total nitrogen oxides formation. Nitric oxide is primordial to life, because it is an important neurotransmitter (Ref.1.4). However, once nitric oxide is released in the atmosphere, it reacts readily with many other molecules and thus is considered as an atmospheric pollutant. Nitric oxide is partly responsible for the production of NO_2 when oxidised.

Nitrogen dioxide (NO_2) can also be further oxidised in the atmosphere to N_2O_5 which reacts with water to produce nitric acid (HNO_3) and thus, acidic precipitations. High concentrations (0.1 ppm or more) of NO and NO_2, from motorised vehicles in cities, along with low altitude ozone, are responsible for the formation of photochemical smog (Ref.1.5).

Los Angeles is well known for its photochemical smog. In 1542, Juan Rodriguez Cabrillo observed the behavior of the smoke from Indians burning fires and called the San Pedro Bay the "Bay of Smokes".

The formation of photochemical smog is the result of the reaction of NO_2 with solar radiation and subsequent cascade of reactions with NO, O_3 and hydrocarbons, and special atmospheric conditions limiting dilution and transportation away from the sources. On an average day, the unreacted pollutants usually reach a maximum in concentration at around 6:00 to 8:00 a.m. because at this time in the morning, motor vehicle emission is at its peak, meteorological conditions restrict dilution, and the sun is rising. As time passes, the intensity of sunlight increases and the photoreactions start. When NO_2 absorbs light ($\lambda < 400$ nm), it decomposes to NO and oxygen atoms. The oxygen atoms will react with molecular oxygen to

produce ozone (O_3). NO is consumed and reaches a minimum as the concentration in NO_2 increases. Nitrogen dioxide concentration increases, goes through a maximum, and then decreases with the increase in ozone concentration. Nitric oxide and ozone react together to form nitrogen dioxide and molecular oxygen. NO_2 colors the atmosphere red-brown and reduces the visibility. During the passage of day-time, the quantity of hydrocarbons slowly drops to a minimum because of side reactions with NO, NO_2, O, and O_3. Figure 1.1 represents the complex sequence of events in terms of concentration of NO, NO_2, O_3 and hydrocarbons during a typical photochemical smog episode (Los Angeles, September 3, 1964) (Ref.1.6). The basic cycle of nitric oxide, nitrogen dioxide and ozone photochemical smog reactions can be seen in the following diagram (Fig.1.2).

Because of the direct impact of NO and NO_2 in our urban lives, their reduction and elimination has become a major concern.

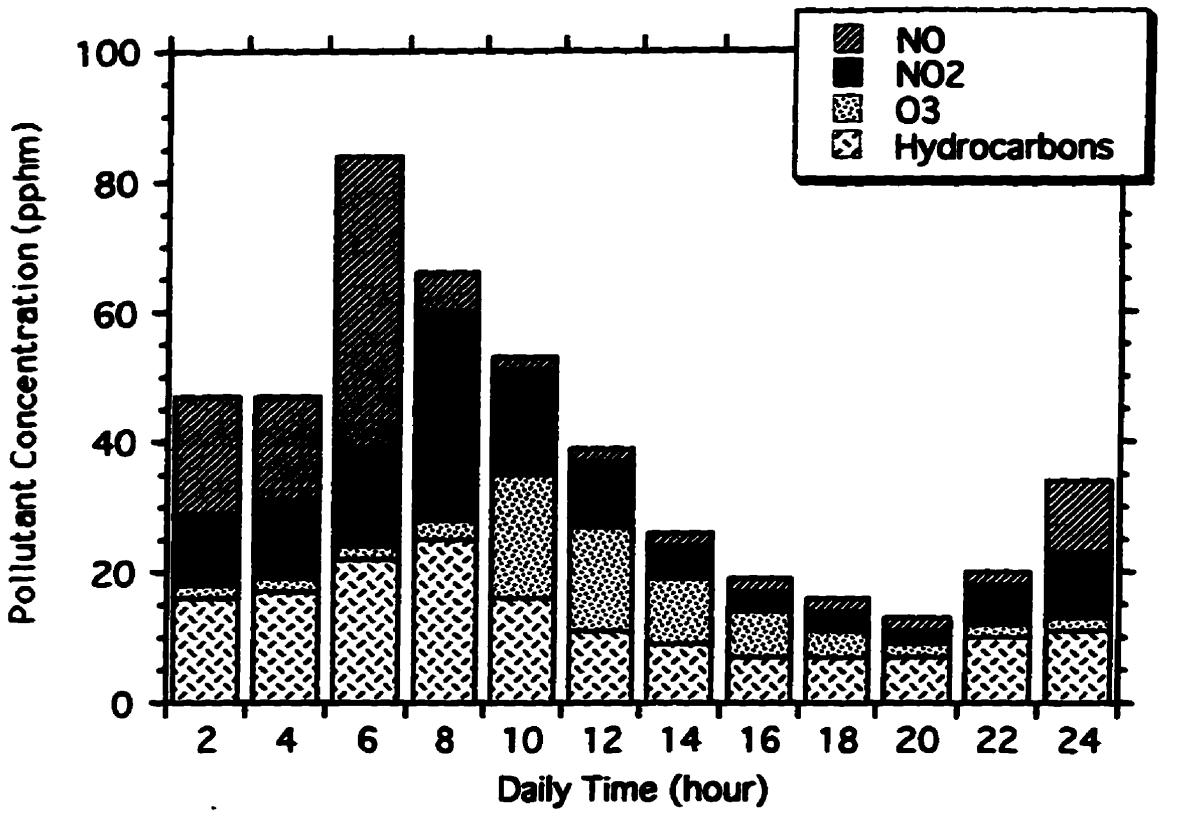

Fig.1.1 Concentration of NO, NO_2, O_3 and hydrocarbons in the atmosphere of Los Angeles on September 3, 1964.

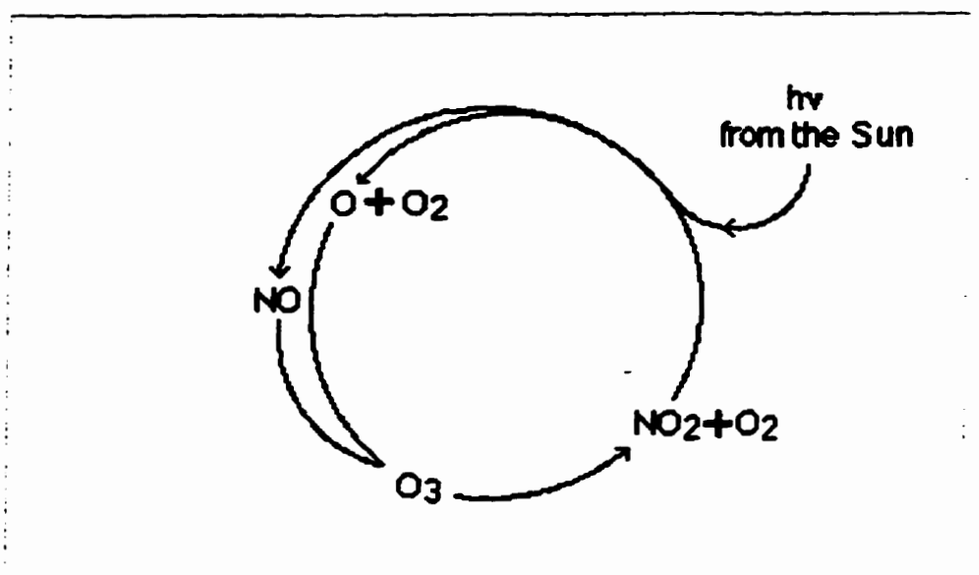

Fig.1.2 **Photochemical smog cycle.**

B. History of Catalysts used for the Removal of Nitrogen Oxides; Stationary and mobile sources

The U.S. Federal Clean Air Act of 1967 set the standards for automobile exhaust emission (Refs.1.7 and 1.8). Engine modifications were sufficient to meet the regulation. After its first amendment in 1970, catalytic technology had to be used. The law required a 90% reduction of NO_2 of all cars for the first 50 000 miles, by 1976. This triggered an intense activity in catalytic research (Ref.1.8). Between 1970 and 1975, more than 470 papers and patents were published for automobile exhaust catalysts.

By 1994 the new standards featured an additional 30% reduction in hydrocarbons as well as an additional 60% reduction of nitrogen oxides. The state of California requirements used new categories for the different class of vehicles. Standards were set to 0.125, 3.4, and 0.4 g/mi in hydrocarbons, carbon monoxide, and nitrogen oxides, respectively, for transitional low emission vehicles (TLEV), 0.075, 3.4, and 0.2 g/mi in hydrocarbons, carbon monoxide, and nitrogen oxides, respectively, for low emission vehicles (LEV), and 0.04, 1.7, and 0.2 g/mi in hydrocarbons, carbon monoxide, and nitrogen oxides, respectively, for ultra-low emission vehicules (Ref.1.7B). In 1992, in Europe, combined emissions in hydrocarbons and nitrogen oxides were limited to 1.55 g/mi, and 4.35 g/mi for carbon monoxide. In 1996, tighter emission standards were expected to be introduced. In other parts of the world, new standards, similar to the ones in the United States were also introduced (Ref.1.9).

Larger stationary sources were also subjected to legislations, but not the smaller ones (<100 tons/year). Taken collectively, the smaller stationary souces emit unacceptable quantities of pollutants. Since 1990, all stationary sources are subject to the new legislation. During the 1990's, the SO_2 and NOx emissions are to be reduced by approximately 10 and 2 million tons/year, respectively, and be capped to 8.9 million tons/year (for SO_2) (Ref.1.10).

Although better catalytic technologies are used, the problem is, however, increasing because of the increase in the number of sources emitting the noxious pollutants. For example, during the last forty years the number of vehicles increased by ten-fold to over 500 million, and for the next forty years, it is expected to rise to one billion (Ref.1.11).

The technology adopted for the mobile sources was and is still different from the technology utilised for the stationary sources.

The type of catalytic converter chosen for mobile sources of NOx is based on supported precious metals (Pt/Pd , Rh, Pt/Rh, Pd/Rh, and Ce/Pd/Rh, on alumina) and is now applied on most vehicles. (Refs.1.8, 1.10, 1.12a, 1.12b, 1.12c, and 1.12d). This type of nitrogen oxide control is referred to as non-selective catalytic reduction (NSCR).

Rhodium-containing catalysts are known as Three-Way-Catalysts (TWC) because of their ability to oxidize hydrocarbons and carbon monoxide to carbon dioxide (and water), and to reduce nitric oxide to molecular nitrogen (and water). In a typical flow-through catalytic converter, the catalyst is deposited on a corderite monolith ($2MgO \cdot 2Al_2O_3 \cdot 5SiO_2$). The monolith has a honeycomb structure. Before receiving the rhodium (1-2%), the corderite is covered with a thin layer of alumina (called the washcoat). Lanthanum is added to the washcoat for thermal stabilization. Cerium can also be added (0-10%) to enhance the reduction of NO by extending the time before the rhodium is deactivated by the accumulation of surface oxygen from the nitric oxide decomposition. The cerium is believed to act as an oxygen storage device. Sometimes, nickel oxide is added to suppress the formation of hydrogen sulfide. The TWC is normally heated to temperatures between 350 and 650°C. Below 350°C the conversion is low and at temperatures higher than 650°C thermal deterioration of the catalytic converter becomes significant.

The Rh-based catalysts are efficient only in a very narrow window of operation. They are known to be adequate for a stoichiometric air/fuel (A/F = 14.7) mixture. In fuel-rich operation (A/F < 14.7), or net reducing atmosphere, the TWC cannot oxidize efficiently carbon monoxide to carbon dioxide. In fuel-lean operation (A/F>14.7), or net oxidizing, the TWC is unable to reduce efficiently nitric oxide to molecular nitrogen. The TWC system requires a tight control of the air/fuel ratio ($A/F = 14.7 \pm 0.3$). The optimum air-to-fuel ratio is controlled by an electronic control module and an exhaust oxygen sensor.

The TWC catalyst is excellent to control the emissions from mobile sources. However, during the next decade, the law will require a higher reduction in the emissions from all sources (4-stroke, 2-stroke, and diesel engines), as well as better fuel economy. In order to achieve this,

all motors will have to run under fuel-lean conditions (net excess of air). Under lean conditions the TWC is unable to reduce NO to N_2. New catalytic formulations will be needed to comply with the law.

More recently, catalytic research has been centered on copper-exchanged zeolites as an alternative to noble metal based catalysts for the reduction of NO (Refs.1.13 to 1.16) for operation under fuel-lean conditions. However, the Cu-ZSM-5 catalyst activity is not high enough for commercial use (Ref.1.17).

As mentioned earlier, the technology for the catalytic reduction of stationary emissions is based on a different type of catalytic science (Ref.1.18a). In the 1970s, Exxon developed a selective non-catalytic reduction (SNCR) process (Ref.1.18b). In the process NOx reacts with ammonia (NH_3), homogeneously in the gas phase, to produce molecular nitrogen and water vapour. Nitrogen oxides are reduced selectively by NH_3. Typically, a temperature of 850-1050°C is needed to maximize the reduction process. Although the process is inexpensive, only 50% reduction levels can be achieved. Furthermore, the process is only effective in the temperature range mentioned above. The high quantity of ammonia injected also increases the ammonia slip problem (20 ppm). This solution for the NOx elimination is also not attractive because of the adsorption of ammonia on the fly ash and also because of corrosion of the elements downstream from the boiler.

The technology used for the stationary sources is mainly based on supported metal-oxides in a process called selective catalytic reduction (SCR) where oxygen and ammonia are added to the gas stream prior to the catalyst. The catalyst is held at 150-450°C. Although patented in the U.S. in 1959, SCR was first applied in Japan and later in Germany (Ref.1.19). The predominant metal oxide, which was adopted by most industries, is vanadia oxide (V_2O_5) supported on titania (TiO_2) (Refs.1.19 to 1.30). This catalyst is a very good catalyst because of its high resistance to SO_2 poisoning. The reactions between NOx and ammonia on this catalyst produce mainly N_2 and H_2O in the gas phase (Ref.1.22). Although most of the results reported were for the reaction between NO and NH_3, the catalytic reduction of NO_2 on metal oxides was reported only in a limited number of studies (Ref.1.31). It was found that the conversion of NO_2 on V_2O_5 catalysts was very low. Other reducing agents (such as CO, H_2, CH_4, and

hydrocarbons) were tested but only NH_3 is very selective to the reduction of NOx. The SCR process removes 60-85% of NOx by using 0.6-0.9 mole NH_3 per mole NO_2. Increasing the amount of NH_3 improves the reduction process but increases the ammonia slip (>5 ppm).

Although this latter technology is quite effective for the reduction of NO, the process could be improved and extended to NO_2 by the use of new catalysts where the need to inject ammonia could be reduced and even eliminated. Further, for mobile sources, new and cheaper catalysts, which could also reduce NOx under fuel-lean conditions, would be welcome by all car builders since the cost of precious metals is increasing and the availability is decreasing.

C. Metal-Oxygen Cluster Compounds

Metal-oxygen cluster compounds, also known as heteropoly oxometalates, exist with a variety of structures and stoichiometries (Refs.1.32 and 1.33). Of particular interest for their catalytic properties are those with anions of Keggin structure.

Heteropoly oxometalates are ionic solids with discrete and large, approximately spherical anions with atoms such as phosphorus or silicon at their centers (Fig.1.3). This central atom is bonded to four oxygen atoms arranged tetrahedrally. Surrounding this central tetrahedron and sharing oxygen atoms with it and each other are 12 octahedra with a peripheral metal atom such as tungsten or molybdenum at their approximate centers and oxygen atoms at their vertices. Three types of oxygen atoms exist in the structure of the anion; those which interconnect the peripheral metal atoms with each other, those which interconnect the central atom to the peripheral metal atoms, and those which protrude from the twelve octahedra. The anion is also known as the Keggin Unit (KU).

X-ray and neutron diffraction experiments show that 6-hydrated 12-tungstophosphoric acid ($H_3PW_{12}O_{40} \cdot 6H_2O$, abbreviated as HPW) has a cubic Pn3m structure with the proton surrounded by two, approximately co-planar, water molecules hydrogen-bonded to the terminal oxygen atoms of the anions (Fig.1.4) (Ref.1.34). As shown from the stoichiometry above, three protons are associated with each Keggin Unit (e.g. $3H^+$/KU).

Semiempirical quantum mechanical (EXH) calculations have predicted that solid heteropoly acids containing tungsten as their peripheral metal atoms should have a higher acidity

than those with molybdenum as their peripheral metal atoms (Ref.1.35). These calculations also show that 12-molybdophosphoric acid is expected to have more labile oxygen atoms than 12-tungstophosphoric acid. The lability of the oxygen was observed from experiments on the partial oxidation of methane to methanol (Ref.1.36). The strength of the acids was later confirmed by microcalorimetric measurements of the differential heat of adsorption of ammonia (Ref.1.37). These experiments have shown that the acidity of heteropoly acids is in the range expected for superacids. Further, the following sequence of acidic strengths was derived: HPW>HSiW>>HPMo·HSiMo.

Although the surface areas of these solid acids are small (approximately 10 m^2/g), photoacoustic-FTIR studies have shown that polar molecules such as ammonia, pyridine, and methanol are capable of penetrating from the vapour phase into the bulk structure, that is between the cations and the anions, where interaction with the protons may occur (Refs.1.38 to 1.40).

Derivatives of the heteropoly acids can also be prepared by aqueous precipitation with other cations (Na^+, K^+, Rb^+, and Cs^+ are some examples) (Refs.1.32, 1.41 to 1.43, and 1.44). These salts will possess different surface and catalytic properties (Refs.1.38, and 1.45 to 1.48). Ammonium salts can be produced by either injection of gaseous ammonia or by aqueous precipitation using a heteropoly acid and adding any ammonium salt (Refs.1.38, 1.42, and 1.46). Only the latter method will produce a salt with a high surface area (approximately 150 m^2/g). PAS-FTIR has shown that residual protons (approximately 0.40 H^+/KU) were present in the structure of ammonium 12-tungstophosphate (NH_4PW), giving residual Brønsted acid sites within the structure (Ref.1.38).

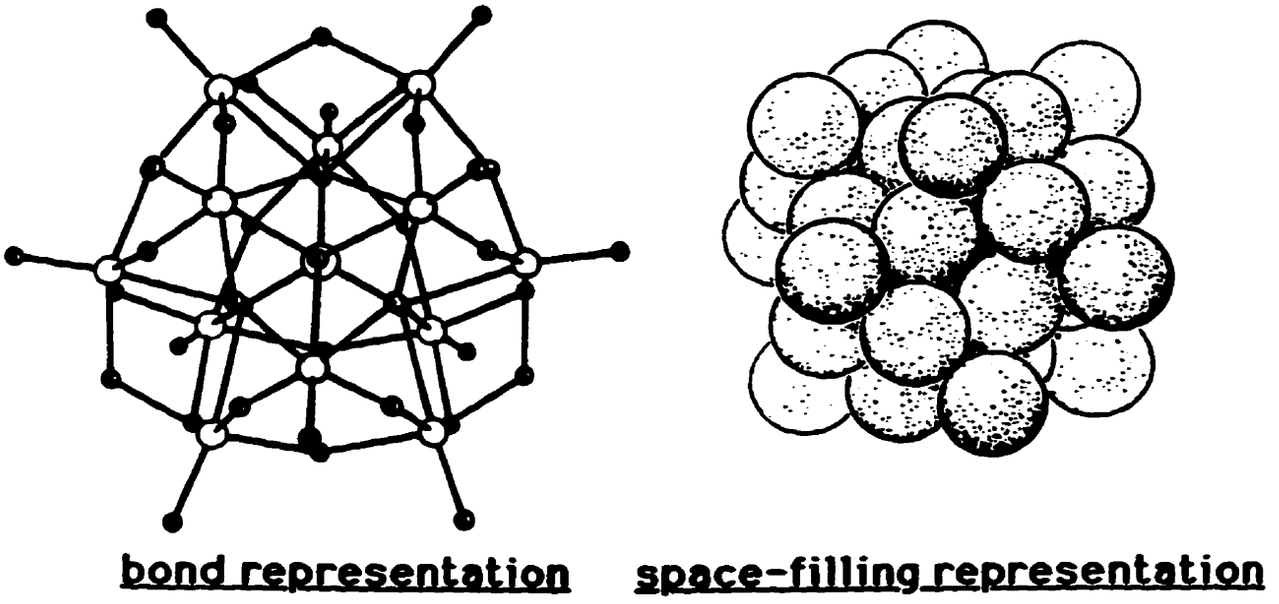

Fig.1.3 Structural representation of the anion (Keggin Structure).

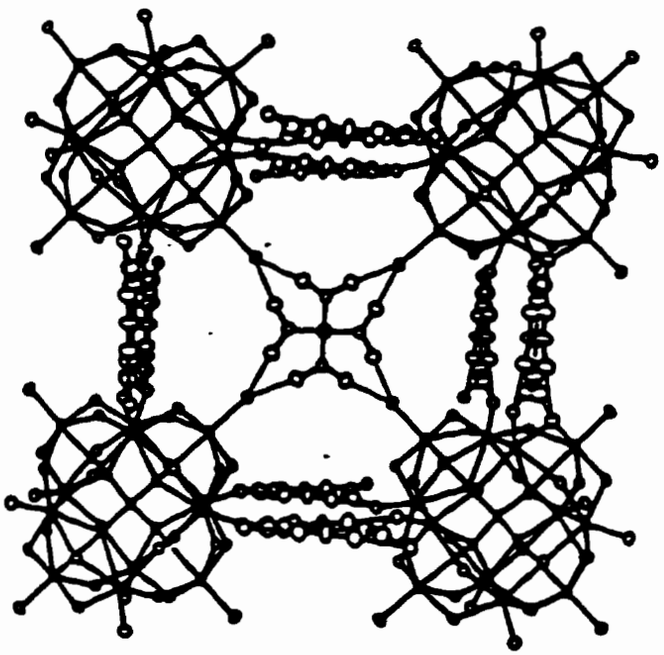

Fig.1.4 Structure of 12-tungstophosphoric acid (Ref.1.34).

As mentioned earlier, the heteropoly acids have small surface areas and thermally decompose at temperatures above 500°C (Refs.1.49 and 1.50). High surface area and stability of the catalyst are important from a catalytic point-of-view, and these two characteristics, for the present acid catalysts, can be improved by sorbing the acids on a high surface area solid support such as silica. Temperature-programmed desorption, infrared spectroscopy, Raman spectroscopy, X-ray photoelectron spectroscopy (XPS), ion scattering spectroscopy (ISS), and ^{31}P NMR spectroscopy studies have shown that silica supported 12-molybdophosphoric acid is thermally stable to temperatures up to 650°C, compared with approximately 450°C for the bulk material (Refs.1.51 to 1.53). The increase in thermal stability has been proposed to be due to interaction between the Keggin unit of the heteropoly acid and adsorption sites on the silica.

D. Objectives of Research

In view of the current interest in nitrogen oxides (NO and NO_2) and catalytic technology, it appeared both interesting and worthwhile to study the sorption and interaction of these gases on metal-oxygen cluster compounds having the Keggin structure.

The first part of this thesis focuses on the sorption and interaction of NOx with heteropoly oxometalates having protons as the cations, and provides information on the effect of the elemental composition of the anions. The effect of changes in the central atom of the anion is examined by comparing the results obtained with 12-tungstophosphoric acid and 12-tungstosilicic acid. The effect of changes in the peripheral metal atom of the anion is examined by comparing the results obtained with 12-tungstophosphoric acid and 12-molybdophosphoric acid.

The effect of changes in the cations is also examined in subsequent sections. In particular, the ammonium salts of HPW and HPMo have been examined. Further, the stoichiometry of the ammonium 12-tungstophosphate was varied to examine the influence of the quantity of residual protons contained in the structure on the catalytic process. The effect of the source of the ammonium cation was studied using different preparations for ammonium 12-molybdophosphate.

To study the role of the protons in the sorption of NOx, derivatives of the IA series of the periodic table of elements and a thallium salt were prepared in order to obtain salts containing little or no protons.

HPW and HPMo supported on silica were also examined for the sorption and conversion of NOx, together with the aforementioned solids exposed to gaseous ammonia.

Unsupported and supported heteropoly acids were also found to sorb substantial quantities of CO_2, and oxidize CO to CO_2. The parameters affecting the sorption and the oxidation mechanism were examined on HPMo, HPMo/SiO_2, HPW, and HPW/SiO_2.

REFERENCES

1.1 Bishop, C.A., *Chem. Eng. Progr.*, **53**, 146 (1957).

1.2 Stern, A.C., Boubel, R.W, Turner, D.B., Fox, D.L. Fundamentals of Air Pollution. Second edition, Academic Press Inc., Orlando, Florida, 1984.

1.3a Koziol, M.J., Whatley, F.R. Gaseous air pollutants and plant metabolism. Butterworths, Toronto, 1984.

1.3b West, B., Paton, R., and Sugalski, T., Reducing Emissions 4, 1995 Emissions Inventory and Five-Year Projections, Canadian Chemical Producers'Association.

1.4 Burnett, A.L., Lowenstein, C.J., Bredt, D.S., Chang, T.S.K., Snyder, S.H. *Science*, **257**, July, 401 (1992).

1.5 Faith, W.L., Atkisson, A.A.J. Air Pollution. Second Edition. Wiley-Interscience, New York, 1972.

1.6 Bagg, J. *The formation and Control of Oxides of Nitrogen in Air Pollution*, in Air Pollution Control, Wiley-Interscience, New York, 1971.

1.7 Hightower, J.W. Preparation of Catalysts. Elsevier, Amsterdam, 1976.

1.8 Hegedus, L.L., and Gumbleton, J.J. *Chemtech*, **Oct.**, 630 (1980).

1.9 Summers, J.C., and Silver, R.G., *Catalyst Technologies To Meet Future Emission Requirements for Light-Duty Vehicles*, in Catalytic Control of Air Pollution, Mobile and Stationary Sources, 202nd National Meeting of the American Chemical Society, American Chemical Society, Washington, DC, 1992.

1.10 Summers, J.C., Sawyer, J.E., and Frost, A.C., *The 1990 Clean Air Act and Catalytic Emission Control Technology for Stationary Sources*, in Catalytic Control of Air Pollution, Mobile and Stationary Sources, 202nd National Meeting of the American Chemical Society, American Chemical Society, Washington, DC, 1992.

1.11 Williamson, W.B, Summers, J.C., and Scaparo, J.A., *Automotive Catalyst Strategies for Future Emission Systems*, in Catalytic Control of Air Pollution, Mobile and Stationary Sources, 202nd National Meeting of the American Chemical Society, American Chemical Society, Washington, DC, 1992.

1.12a Taylor, K.C. *Chemtech*, **Sept.**, 551 (1990).

1.12b Taylor, K.C. *Catal.Rev.-Sci.Eng.*, **35**, 457 (1993).

1.12c Shelef, M., and Graham, G.W. *Catal.Rev.-Sci.-Eng.*, **36**, 433 (1994).

1.12d Cooper, B.J. *Platinum Metals Rev.*, **38**, 2 (1994).

1.13 Sato, S., Yu-u, Y., Yahiro, H., Mizuno, N., and Iwamoto, M. *Appl.Catal.*, **70**, L1 (1991).

1.14 Bennett, C.J., Bennett, P.S., Golunski, S.E., Hayes, J.W., and Walker, A.P. *Appl.Catal. A:General*, **86**, L1 (1992).

1.15 Hall, W.K., and Valyon, J. *Catal.Let.*, **15**, 311 (1992).

1.16 Witzel, F., Sill, G.A., and Hall, W.K. *J.Catal.*, **149**, 229 (1994).

1.17 Kung, M.C. *Catal.Let.*, **18**, 111 (1993).

1.18a Bosch, H., and Janssen, F. *Catalysis Today*, **2**, 369 (1987).

1.18b Lyon, R.K, *Int.J.Chem.Kinet.*, **3**, 440, 1976.

1.19 Boer, F.P., Hegedus, L.L., Gouker, T.R., and Zak, K.P. *Chemtech*, **May**, 312 (1990).

1.20 Cai, Y., and Ozkan, U.S. *Appl.Catal.*, **78**, 241 (1991).

1.21 Bjorklund, R.B., Jīrâs, S., Ackelid, U., Odenbrand, C.U.I., Anderson, L.A.H., and Brandin, J.G.M. *J.Catal.*, **128**, 574 (1991).

1.22 Dines, T.J., Rochester, C.H., and Ward, A.M. *J.Chem.Soc.Faraday Trans.*, **87**, 1473 (1991).

1.23 Dines, T.J., Rochester, C.H., and Ward, A.M. *J.Chem.Soc.Faraday Trans.*, **87**, 1617 (1991).

1.24 Ramis, G., Busca, G., and Bregani, F. *Gaz.Chimi.Italiana*, **122**, 79 (1992).

1.25 Chen, J.P., and Yang, R.T. *Appl.Catal A:General*, **80**, 135 (1992).

1.26 Lintz, H.G., and Turek, T. *Appl.Catal. A:General*, **85**, 13 (1992).

1.27 Baiker, A., Handy, B., Nickl, J., Schraml-Marth, M., and Wokaun, A. *Catal.Let.*, **14**, 89 (1992).

1.28 Schneider, M., Maciejewski, M., Tschudin, S., Wokaun, A., and Baiker, A. *J.Catal.*, **149**, 326 (1994).

1.29 Scharf, U., Schneider, M., Baiker, A., and Wokaun, A. *J.Catal.*, **149**, 344 (1994).

1.30 Matsuda, S., and Kato, A. *Appl.Catal.*, **8**, 149 (1983).

1.31 Shomokawabe, M., Ohi, A., and Takezawa, N. *Appl.Catal. A:General*, **85**, 129 (1992).

1.32 Pope, M.T., Heteropoly and Isopoly Oxometalates, Springer-Verlag, Berlin, 1983.

1.33 Bonardet, J., Carr, K., Fraissard, J., McGarvey, G.B., McMonagle, J.B., Seay, M., and Moffat, J.B., Invited paper in Advanced Techniques in Catalysis Synthesis, 1996, under press.

1.34 Brown, G.M., Noe-Spirlet, M.R., Busing, W.R., and Levy, H.A., *Acta Crystallogr Sect.*, **B33**, 1038 (1977).

1.35 Moffat, J.B., *J.Mol.Catal.*, **26**, 385 (1984).

1.36 Kasztelan, S., and Moffat, J.B., *J.Catal.*, **106**, 512 (1987).

1.37 Jozefowicz, L.C., Karge, H.G., Vasilyeva, E., and Moffat, J.B., *Microporous Materials*, **1**, 313 (1993).

1.38 Highfield, J.G., and Moffat, J.B., *J.Catal.*, **88**, 177 (1984).

1.39 Highfield, J.G., and Moffat, J.B., *J.Catal.*, **89**, 185 (1984).

1.40 Highfield, J.G., and Moffat, J.B., *J.Catal.*, **95**, 108 (1985).

1.41 Tsigdinos, G.A., *Ind. Eng. Chem., Prod. Res. Develop.*, **13**, 267 (1974).

1.42 Lapham, D., and Moffat, J.B., *Langmuir*, **7**, 2273 (1991).

1.43 Soled, S., Miseo, S., McVicker, G.B., Baumgartner, J.E., and Gates, W.E., Symposium on Advanced Techniques in Catalysis Preparation, 209th National Meeting, American Chem. Soc., Anaheim Meeting, April 2-7, 1995, pp.122-127.

1.44 Hayashi, H., and Moffat, J.B., *J.Catal.*, **87**, 67 (1982).

1.45 Ghosh, A.K., and Moffat, J.B., *J.Catal.*, **101**, 238 (1986).

1.46 Moffat, J.B., *J.Molec.Catal.*, **52**, 169 (1989).

1.47 McGarvey, G.B., and Moffat, J.B., *J.Catal.*, **128**, 69 (1991).

1.48 McGarvey, G.B., and Moffat, J.B., *J.Catal.*, **130**, 483 (1991).

1.49 Hodnett., B.K., and Moffat, J.B., *J.Catal.*, **88**, 253 (1984).

1.50 Southward, B.W., Vaughan, J.S., and O'Connor, C.T., *J.Catal.*, **153**, 293 (1995).

1.51 Kasztelan, S., and Moffat, J.B., *J.Catal.*, **109**, 206 (1988).

1.52 Kasztelan, S., Payen, E., and Moffat, J.B., *J.Catal.*, **125**, 45 (1990).

1.53 Kasztelan, S., Payen, E., and Moffat, J.B., *J.Catal.*, **128**, 479 (1991).

CHAPTER II

MATERIALS AND METHODS

A. Chemicals

The chemicals, gases, and column packing materials employed in the present work, together with their sources and purity are listed in Tables 2.1, 2.2, and 2.3, respectively. Except where otherwise stated, these were used as received.

B. Preparation and Pretreatment of Catalysts

The salts of the heteropoly acids were prepared by precipitation from aqueous solutions of the acid and of an appropriate source of the cation (Table 2.1) and, with the ammonium salts, by direct reaction of the acid with ammonia. By variation of the relative amounts of the preparative reagents in the former method both stoichiometric and non-stoichiometric ammonium salts were prepared. $^{15}NH_4PW$ and ND_4PW were prepared from $^{15}NH_4NO_3$ and ND_4Cl, respectively. The former was first dried on a hot water bath. All salts formed were further dried under vacuum at room temperature for more than 24 hours.

The heteropoly acids supported on silica were prepared by adding SiO_2 to the acid dissolved in a minimum of water (20-30 mL), stirred for 24 hours at room temperature, heated on a hot water bath and evacuated at room temperature. Particle sizes smaller than 80 mesh were used.

For HPW/SiO_2, loadings of 9.1, 16.7, 23.1, 35.0, 50.0, and 75.0 %w(HPW)/w(total) were prepared.

For $HPMo/SiO_2$ loadings of 1.0, 5.0, 9.0, 20.0, and 50.0 %w(HPMo)/w(total) were prepared.

NH_4PW/SiO_2 and NH_4PMo/SiO_2 were prepared from HPW/SiO_2 and $HPMo/SiO_2$, respectively, which have been heated to the desired temperature, exposed to ammonia and purged with helium (>20 mL/min) for 30 min until the effluent tested neutral.

All the supported samples were pretreated in helium flow (from 15 to 40 mL/min) in situ at the desired temperature prior to the experiments.

Additional information about the catalytic samples is found in Tables 2.4 and 2.5.

TABLE 2.1

CHEMICALS USED

Name	Chemical Formula	Supplier
12-Tungstophosphoric acid	$H_3PW_{12}O_{40}\cdot xH_2O$[a]	BDH
12-Molybdophosphoric acid	$H_3PMo_{12}O_{40}\cdot 24H_2O$[a]	BDH
12-Tungstosilicic acid	$H_4SiW_{12}O_{40}\cdot 26H_2O$[a]	BDH
Ammonium Chloride	NH_4Cl	J.T. Baker
d_4-Ammonium Chloride	ND_4Cl (98 atom% D)	CDN Isotopes
Ammonium Carbonate	$NH_4HCO_3\cdot NH_2COONH_4$	BDH
Ammonium Nitrate	NH_4NO_3	Mallinckrodt
^{15}N-Ammonium Nitrate	$^{15}NH_4NO_3$(98 atom% ^{15}N)	CDN Isotopes
Cesium Carbonate	Cs_2CO_3	Sigma
Lithium Carbonate	Li_2CO_3	J.T. Baker
Potassium Carbonate	K_2CO_3	J.T. Baker
Rubidium Carbonate	Rb_2CO_3	Aldrich
Sodium Carbonate	$Na_2CO_3.H_2O$	BDH
Thallium Nitrate	$TlNO_3$	BDH
Carbon Tetrachloride	CCl_4	
Copper	Cu	Fisher
CAB-O-SIL Fumed Silica (grade M-5)	SiO_2	Davison Chemical
Nitric Acid	HNO_3	BDH
Potassium Bromide	KBr	Aldrich

[a] abbreviated as HPW, HPMo, and HSiW, respectively.

TABLE 2.2

GASES USED

Name	Chemical Formula	Supplier
Ammonia	NH_3	Linde
d_3-Ammonia	ND_3 (99.1 atom% D)	ICON
Carbon Dioxide	CO_2	Praxair
Carbon Monoxide	CO	Matheson
^{18}O-Carbon Monoxide	$C^{18}O$ (97.8 atom% ^{18}O)	Isotec Inc.
Helium	He	Praxair
Hydrogen	H_2	Praxair
Nitric Oxide	NO (98.9% NO)	Linde
Nitric Oxide/He	NO in He (4950 ppm)	Praxair
Nitrogen Dioxide	NO_2 (99% N_2O_4)	Matheson
Nitrogen Dioxide/He	NO_2 in He (4960 ppm)	Praxair
^{15}N-Nitrogen Dioxide	$^{15}NO_2$ (99 atom% ^{15}N)	ICON
Nitrous Oxide	N_2O	Matheson
Oxygen	O_2	Linde

TABLE 2.3

PACKING MATERIALS FOR GC-COLUMNS

Name	Supplier
Chromosorb 103	Manville
Molecular Sieve 5A	Chromatographic Specialties Inc.
Porapak Q	Waters Associates Inc.

TABLE 2.4

ADDITIONNAL INFORMATIONS ON CATALYSTS USED

Chemical Formula	Molecular weight [a]	Surface area [b]	Pore volume [c]	Density [d]
$H_3PW_{12}O_{40}$	2880.77 g/mol	5-10 m^2/g	-	4-6 g/mL
$H_3PMo_{12}O_{40}$	1825.25 g/mol	5-10 m^2/g	-	4-6 g/mL
$H_4SiW_{12}O_{40}$	2878.89 g/mol	5-10 m^2/g	-	4-6 g/mL
$(NH_4)_3PW_{12}O_{40}$ [e]	1934.80 g/mol	100-150 m^2/g	2.7-2.9	2-4 g/mL
$(NH_4)_3PMo_{12}O_{40}$ [e]	1876.28 g/mol	75-150 m^2/g	2.7-2.9	2-4 g/mL
$(^{15}NH_4)_3PW_{12}O_{40}$ [e]	1937.80 g/mol	100-150 m^2/g	2.7-2.9	2-4 g/mL
$(^{15}NH_4)_3PMo_{12}O_{40}$ [e]	1879.28 g/mol	75-150 m^2/g	2.7-2.9	2-4 g/mL
$Li_3PW_{12}O_{40}$ [e]	2898.59 g/mol	3-10 m^2/g	-	4-7 g/mL
$Na_3PW_{12}O_{40}$ [e]	2946.74 g/mol	3-10 m^2/g	-	4-7 g/mL
$K_3PW_{12}O_{40}$ [e]	2995.08 g/mol	80-120 m^2/g	2.6-2.8	2-6 g/mL
$Rb_3PW_{12}O_{40}$ [e]	3134.18 g/mol	80-120 m^2/g	-	2-6 g/mL
$Cs_3PW_{12}O_{40}$ [e]	3276.49 g/mol	120-180 m^2/g	0.9-1.5	2-6 g/mL
$Tl_3PW_{12}O_{40}$ [e]	3490.88 g/mol	100-150 m^2/g	4.2-4.7	2-6 g/mL

a Calculated on a dry basis.

b Pretreated in He at 300°C and measured by N_2-BET at 77K.

c $cm^3/g \times 10^2$.

d Evaluated from helium volume displacement at room temperature.

e Prepared from aqueous precipitation method.

TABLE 2.5

ADDITIONNAL INFORMATIONS ON SUPPORTED CATALYSTS USED

Chemical Formula	Surface area[a]	Density[b]
SiO_2	190-200 m^2/g	1-10 mg/mL
9.1%HPW/SiO_2	150-160 m^2/g	0.5-2 g/mL
23.1%HPW/SiO_2	120-125 m^2/g	1-3 g/mL
50.0%HPW/SiO_2	90-95 m^2/g	2-4 g/mL
75.0%HPW/SiO_2	50-55 m^2/g	3-5 g/mL

a Pretreated in He at 200°C and measured by N_2-BET at 77K.

b Evaluated from helium volume displacement at room temperature.

C. Pulse Experiments and Gas Analysis

1. Analysis of O_2, N_2 and NO:

For the pulse reactions, a 4 mm i.d. X 25 cm quartz reactor was employed with the catalyst held in place by quartz wool. The flow of helium in the reactor was fixed at 15 mL/min. The selected reaction temperature was held for 10 minutes prior to the injection of nitrogen oxides. The NO was passed through a 1 m tubing cooled to dry ice-acetone temperature prior to use. Each pulse of NO_2 (17 μmoles, 24°C and 1 atm) or NO (10 μmoles, 24°C and 1 atm) was injected into the reactor with a standard gas sampling valve equipped with a Teflon rotor. All gas lines were made of stainless steel 1/8" o.d. with those after the reactor heated to 130°C. The reactants were heated to 150°C immediately prior to the entry of the reactor. A schematic diagram of the setup is presented on Figure 2.1.

The outlet of the reactor was directed to a gas chromatograph (Shimadzu GC-9A) equipped with a 4 mm o.d. by 30 cm MS-5A (60-80 mesh particle size) column. For analysis of O_2, N_2 and NO the chromatographic column was preconditioned at 300°C for 3 hours and then saturated with NO and held at 30°C (Ref.2.1). Under these conditions the retention times of O_2, N_2, and NO were at 1.1, 2.0, and 2.9 min, respectively. All calibration parameters were verified periodically.

2. Analysis of NO_2:

A cold trap (dry ice-acetone) placed between the outlet of the reactor and line leading to the gas chromatograph was employed to trap NO_2 which was subsequently measured volumetrically. After each pulse, the trap was transferred to a standard volumetric system equipped with teflon valves and a chemically inert pressure transducer. Once the system was evacuated, with the trap attached, the trap was rapidly heated to 25°C with water and the pressure due to NO_2 was immediately measured. The calibration was verified periodically.

3. Analysis of N_2O:

For analysis of N_2O, the MS-5A column was replaced by a 4 mm o.d. by 2.5 m Porapak Q column (Ref.2.2). This column was preconditioned at 200°C for 3 hours and then held at 40°C for analysis. The determination of N_2O was done with a fresh sample. The calibration was verified periodically.

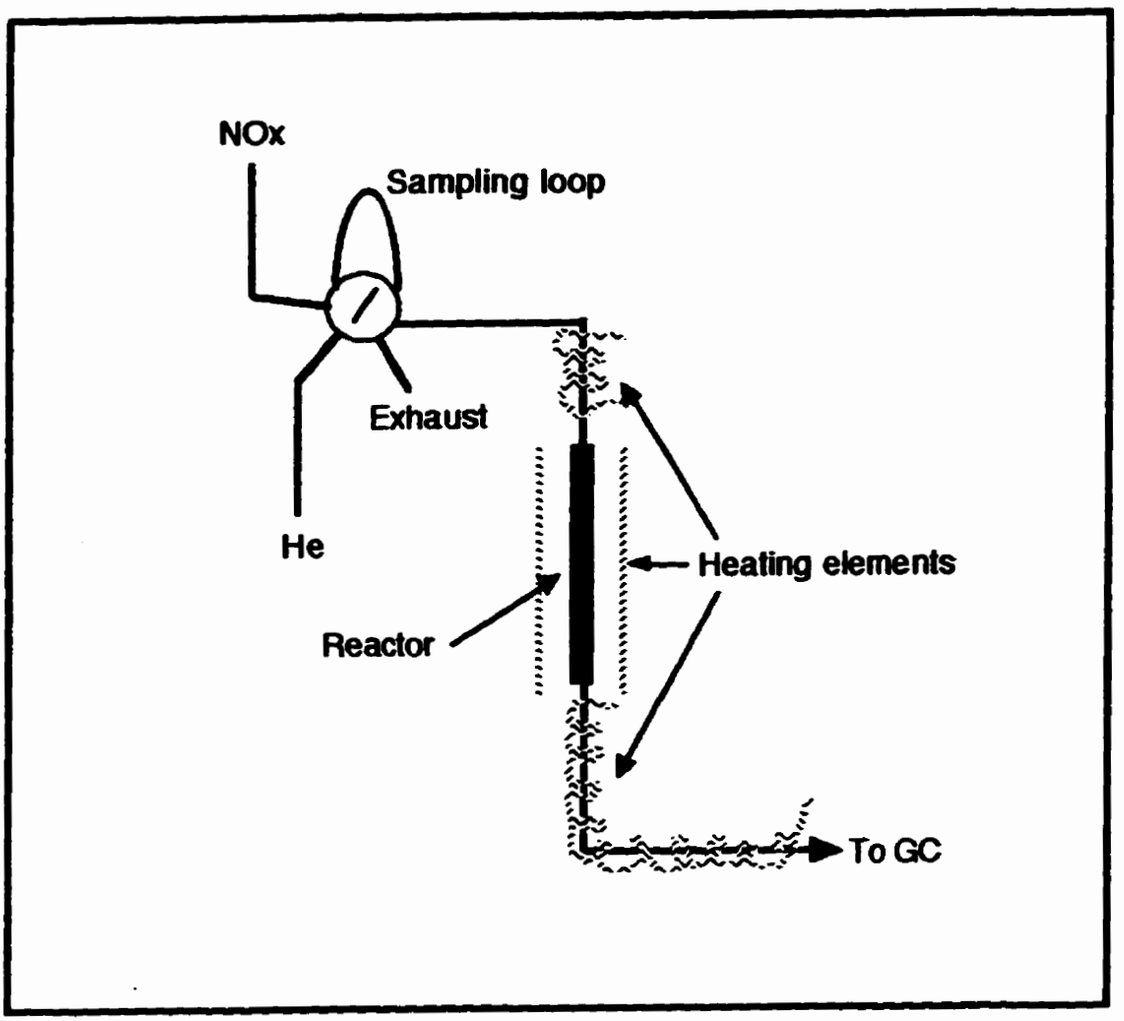

Fig.2.1 Schematic diagram for pulse experiments.

4. Analysis for total nitrogen:

For the analysis of the total nitrogen, separate reaction experiments were carried out with a modified reactor system. The effluent from the reactor was passed through a 1 meter coil kept at 700°C, subsequently through copper wool at 550°C and finally introduced to the GC. All connecting lines were maintained at 130°C. Under these conditions NO_2 and HNO_3 will be decomposed completely into NO and N_2. The method was tested by injecting a known quantity of HNO_3 through the system.

The quantities of nitrogen containing compounds exiting the reactor after each pulse were determined chromatographically and, after the desired number of pulses, the catalyst was flash heated in order to desorb any nitrogen containing material. From these values and those found from the measurement of N_2, NO, NO_2, and the total nitrogen on the catalyst after reaction, the amount of HNO_3 found in the effluent could be determined with acceptable accuracy (error < 5%) with a good nitrogen mass balance (85-100%).

5. Analysis of NH_3:

For the analysis of the quantity of nitrogen (as NH_3) on the ammonium salts the chromatographic column (MS-5A) was replaced by a Chromosorb 103 column held at 150°C (Ref.2.3). Exactly 0.033 g of ammonium salt was packed into the reactor and heated to the desired pretreatment temperature for 10 min under a flow of helium (15 mL/min). A cold trap was located downstream cooled to liquid nitrogen temperature to condense the NH_3 desorbing as the pretreatment temperature was increased. The trap was heated rapidly to about 200°C and its contents admitted to the GC for analysis. The catalytic reactor was then flash heated to decompose the ammonium salt contained in it. By using a standard ammonium salt which was known to contained 3 N/KU, the total integrated area of all peaks found on the chromatogram of this sample was compared to the total integrated area found for the pretreated sample. This method provided repetitive results within an acceptable accuracy (error < 5%).

6. GC-MS setup:

Aliquots (0.025 to 0.200 g) of catalyst were loaded into a 4mm i.d. quartz reactor connected to a gas chromatograph (HP5890) equipped with a 20 m long empty capillary deactivated fused silica column (J&W Scientific) held at 150°C. The outlet of the capillary column is directed to a mass selective detector (HP-MS5970). The range of masses monitored was set between 10 and 150 amu at a rate of 5.5 scans/sec. All data recorded were stored in the computer (IBM750P90) for analysis.

This micro-reactor system was used for pre- and post-reactor pulse analysis as well as injection of pulses of gas mixtures for single pulse reaction (SPR) experiments, isothermal continuous reaction (ICR) with gas mixtures, temperature-programmed desorption analysis (TPD), and temperature-programmed reaction (TPR).

D. Temperature-Programmed Desorption (TPD)

1. With TCD as detector:

For temperature-programmed desorption the chromatographic column in the gas chromatograph used for the pulse experiments (section C.1) was replaced by an empty column and the effluent from the reactor was passed directly over the thermal conductivity detector (TCD).

The reactor was loaded with the same amount of catalyst as with the pulse experiments and the samples were pretreated under the same conditions. The NO_x was then introduced by use of a gas sampling valve. Thereafter the sample was flushed with helium (15 mL/min) and cooled to room temperature.

The temperature of the reactor was ramped linearly (60°C/min) with a temperature programmer (Tempstar II, Thermo Electric Instruments, NJ) and the trace of the TPD recorded via the electronic integrator.

2. With MS as detector:

A series of temperature-programmed desorption experiments were recorded using the GC-MS system.

For these TPD experiments, the valves were set so that the effluent of the reactor passed directly into the GC-MS detection system (see section C.6). The samples were pretreated in helium and exposed to the selected gas mixture at the desired temperature(s) directly in the reactor. After the reactor was cooled to room temperature, the micro-reactor was flushed with helium at 15 mL/min for 15 to 30 min. The temperature of the reactor was then increased linearly from 30 to 650°C at 10°C/min with a temperature controller/programmer (Tempstar II, Thermo Electric Instruments, NJ).

All data recorded were stored in the computer for analysis. Atomic mass units corresponding to the selected molecules (Table 2.4) were extracted from the total-ion TPD or presented as the latter. Appropriate corrections for fragmentation were made, where necessary.

TABLE 2.6

ATOMIC MASS UNITS CORRESPONDING TO THE SELECTED MOLECULES

Mass (amu)	Chemical Formula
16.0	NH_2
18.0	H_2O, $^{15}NH_3$
20.0	ND_3
28.0	N_2, CO
29.0	^{15}NN, ^{13}CO
30.0	NO, $^{15}N^{15}N$, $C^{18}O$
32.0	O_2
44.0	N_2O, CO_2
45.0	^{15}NNO
46.0	NO_2, $^{15}N^{15}NO$, ^{18}OCO
47.0	$^{15}NO_2$
48.0	$^{18}OC^{18}O$

3. Thermogravimetry:

Aliquots of heteropoly oxometalates, some of which were previously exposed to NOx, were loaded into a Cahn microbalance and the weight recorded with increase in temperature.

E. Temperature-Programmed Reaction (TPR)

1. Standard TPR:

For TPR experiments, the samples were pretreated *in situ* with helium followed by exposure to a continuous flow of gas mixture (15-20 mL/min) at 30°C, while the effluent was passed to the GC-MS. After steady state had been achieved, as evidenced from the MS signals, the temperature of the reactor was increased from 30 to 650°C at 10°C/min.

The signal was recorded and the data analysed for each ion.

2. Single-pulse experiments at a variety of temperatures (SPE-VT):

For SPE-VT experiments, the samples were pretreated *in situ* under a continuous flow of helium (20 mL/min) at the desired temperature. A single pulse of reactant gas was introduced with a sampling loop directly into the helium flow. The effluent of the reactor was directed to the GC and the products analysed using the procedure described above. The temperature of the reactor was then increased (or decreased) and the procedure repeated with the same aliquot.

F. Isothermal Continuous Reaction (ICR)

For ICR experiments, the samples were pretreated *in situ* in a continuous flow of helium at the desired temperature for 2 minutes at which time the gas mixture was introduced into the reactor and the effluent was passed to the GC-MS. The reactions were continued for one to two hours.

The data were recorded using the computer and, where appropriate, the area under the curve was integrated for each related ion. The values were corrected as discussed previously.

G. Infrared Spectroscopy

The catalyst to be analysed using infrared spectroscopy was pretreated according to the above procedures. Two different mulling methods were used in this study.

In the absence of sorbed NOx, KBr was used. About 1 mg of catalyst was mixed and ground with 50 to 100 mg of spectroscopic FTIR-grade potassium bromide. No evidence was found for the reaction of HPW with the KBr under the present conditions.

When NOx was present, the catalyst was mixed with NUJOL and placed between two silver bromide (AgBr) windows (Bicron). No evidence was found for the reaction of NO_2 and HPW with the mulling agent, nor the windows.

Infrared spectra were obtained with a BOMEM MB-100 Michelson infrared spectrophotometer, from 500 to 4000 cm^{-1} and a spectral resolution of 4 cm^{-1}. For semi-quantitative analysis, each spectrum was normalized with the band for P-O stretching at 1063.3 cm^{-1}.

H. Powder X-Ray Diffraction

Powder X-ray diffraction patterns were measured on a D500-Siemens diffractometer at 40kV and 30 mA with the CuKα radiation line. The samples were incorporated in silicon grease after pretreatment and saturation with NOx in the reactor.

I. B.E.T. Surface Area

Surface areas were calculated, using the BET equation (Ref.2.4), from nitrogen adsorption isotherms obtained at 77 K. The catalysts were evacuated for 15 hours at the desired temperature prior to the adsorption measurements.

J. Pulsed MAS-NMR

Single pulse magic angle spinning nuclear magnetic resonance spectra were obtained on a Bruker AMX 500 spectrometer with a 11.7 T magnet.

Each sample was pretreated and treated as for the pulse experiments above (Section C). For determination of ^{15}N spectra, the samples were treated with enriched isotopic gas. The samples were then packed in a zirconia rotor and measured at 298 K.

The rotor frequency varied between 5.0 and 10.0 kHz. The magic angle was set at 54.7°. The resonance frequencies were 500.18 and 50.67 MHz for ^{1}H and ^{15}N, respectively. ^{1}H decoupling was used occasionally for ^{15}N. The pulse (P1) was 1 μsec. The acquisition time (AQ) was taken at 0.03 and 0.13 sec and the delay time was 4 and 5 sec for decoupled and coupled experiments, respectively. 8k or 16k data points were recorded for each spectrum. All ^{1}H spectra recorded were referenced to TMS (tetramethylsilane), using an external sample of benzene (δ = 7.24 ppm). Labelled ammonium nitrate ($^{15}NH_4NO_3$) (δ = -360 ppm) was used as external reference for ^{15}N (Ref.2.5).

K. Raman Spectroscopy

Raman spectral measurements were obtained on a Dilor OMARS-89 Raman spectrometer equipped with a microscope attachment (Olympus Model BHT). The spectrometer is interfaced to an IBM-AT computer. The detector is a 512-channel diode array. The 514.5 nm line of the Coherent Innova 70 argon ion laser was used for excitation. The spectral region was from 50 to 3000 cm^{-1}. Each sample was packed in a sealed capillary tube. Only the regions with observable peak intensities were recorded.

Other samples were analysed on a Renishaw Ramascope using the 632.8 nm line of a He/Ne laser for excitation. The spectrometer was equipped with a microscope attachment.

REFERENCES

2.1 Dietz, R.N., *Anal. Chem.*, **40**, 1576 (1968).

2.2. Whilhite, W.F., and Hollis, O.L., *J. Chromatog. Sci.*, **6**, 84 (1968).

2.3 Mindrup, R., *J. Chromatog. Sci.*, **16**, 380 (1978).

2.4 Adamson, A.W., Physical Chemistry of Surfaces, Fifth Edition, John Wiley & Sons, Inc., New York, 1990.

2.5 Mason, J., *Multinuclear NMR*, Pleneum Press, New York, 1987.

CHAPTER III

SORPTION AND REACTION OF NO AND NO_2 ON HPW, HPMo, AND HSiW

A. Results

On contact of any one of the three heteropoly acids (HPW, HPMo, and HSiW) employed in the present work with nitrogen dioxide two processes occur. A portion of the NO_2 is sorbed (chemisorbed and/or physisorbed) into the solid and some fraction of this sorbed NO_2 is converted to O_2, NO and HNO_3, which are observed in the effluent. No quantities of N_2 were observed under any of the conditions employed in the present work with the parent acids.

Multiple pulses of NO_2 were employed to provide information on the capacities and behaviour of the solid acids with NO_2.

The quantity of NO_2 removed from the gas phase by each of the three catalysts at 150°C after pretreatment at 150°C is reported for a number of pulses (Fig.3.1). These data reflect both the NO_2 sorbed by the catalysts and that converted to the aforementioned products.

As is evident in Figure 3.1, the composition of the anion has a substantial effect on the results. However the nature of the peripheral metal atoms has considerably more influence than that of the central atom since the results for HPW and HSiW are approximately the same. The quantities of NO_2 sorbed or converted with HPW from each pulse are nearly constant at 90% for the first five pulses while with HPMo only 10% of the NO_2 is sorbed and/or converted. After eight pulses a sharp drop in the fraction of NO_2 lost from the gas phase is evident with both HPW and HSiW. After the eighth pulse, the solid acids are saturated with NO_2.

The maximum quantities of nitrogen-containing (N) species held on the catalysts after exposure to repeated pulses of NO_2 at 150°C expressed as the number of NO_2 molecules per anion are, for HPW and HSiW equal to approximately 3, not too dissimilar from the number of protons, 3 and 4, respectively per anion (Table 3.1). However, after pretreatment with He and exposure to NO_2 at 300°C, these numbers are considerably reduced. The values obtained for HPMo are vanishingly small at both temperatures.

Exposure of the catalysts after pretreatment at 300°C to pulses of NO_2 at the same temperature produces results remarkably dissimilar to those obtained at 150°C. (Fig.3.2). While the fraction of NO_2 sorbed or converted on HPW is relatively large for the first pulse, this quantity diminishes substantially with each successive pulse. In contrast to the results at 150°C, HSiW and HPMo now show similar results with both catalysts showing sorption and conversion of NO_2 amounting to 20% or less after the first pulse. All three catalysts show relatively low values of sorption and conversion after two pulses.

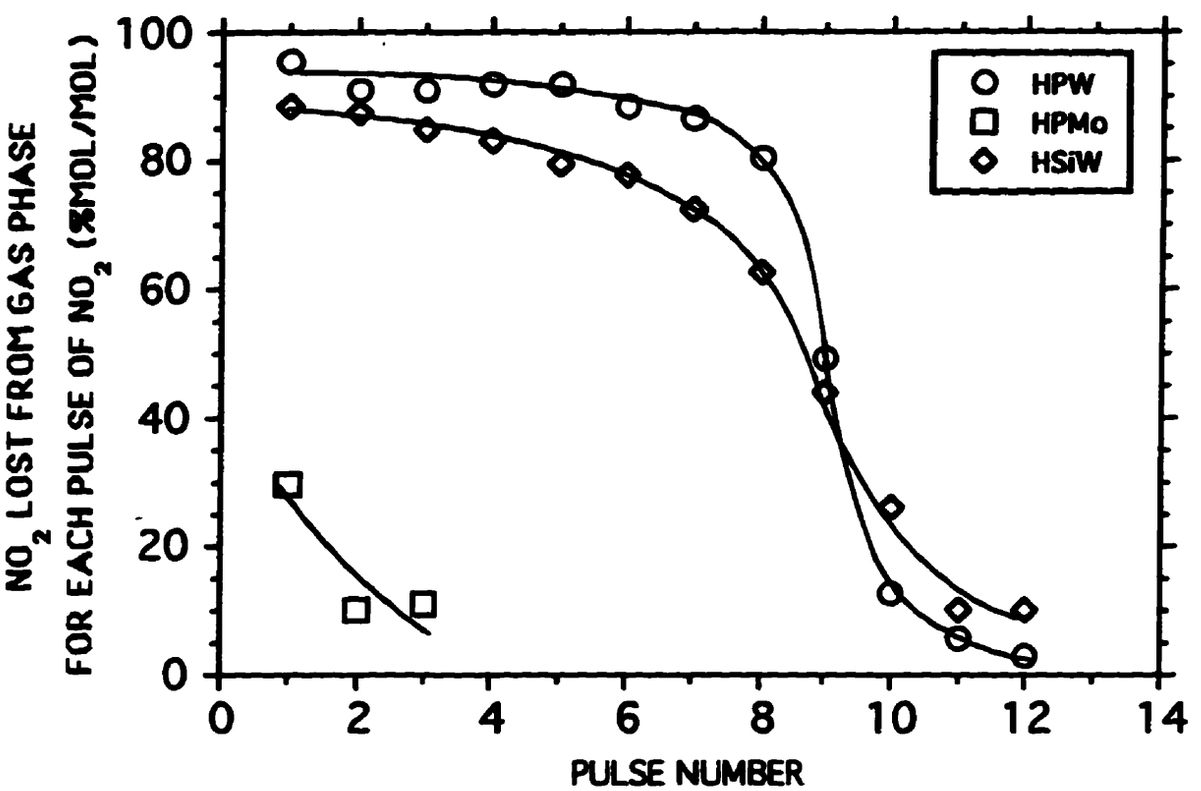

Fig. 3.1 NO_2 removed from the gas phase in a sequence of pulses of NO_2 on HPW, HPMo, and HSiW. Pretreatment and reactor temperature of 150°C. Mass of solid in reactor, 0.075g (26.0μmoles HPW, 41.1μmoles HPMo, 26.1μmoles HSiW); pulse size, 17.0 μmoles NO_2.

TABLE 3.1

MAXIMUM QUANTITY OF SORBED NO_2[a]

Catalysts	150°C[b]	300°C[b]
HPW	2.9	0.8
HPMo	0.1	0.0
HSiW	2.5	0.3

a NO_2 per anion
b Pretreatment (Helium 1 hr) and sorption temperatures.

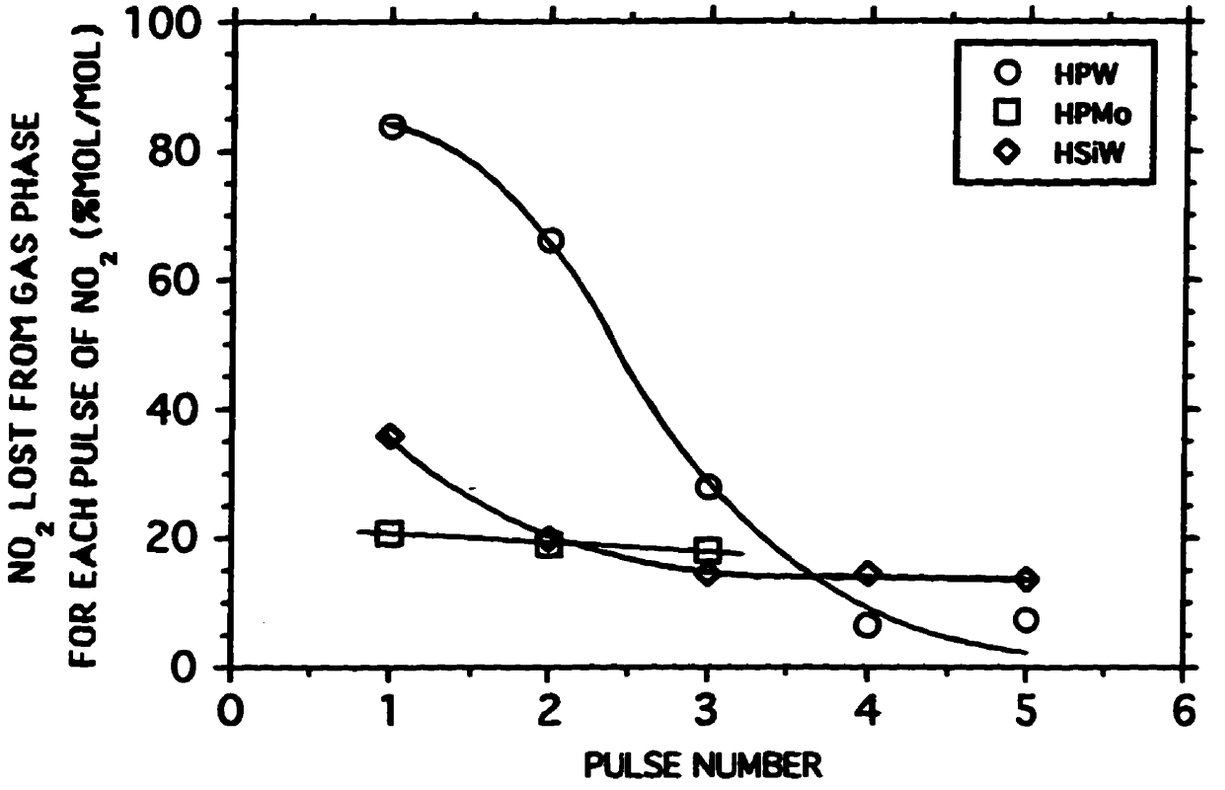

Fig. 3.2 Losses of NO_2 from the gas phase in a sequence of pulses of NO_2 on HPW, HPMo, and HSiW. Pretreatment and reactor temperature of 300°C. Mass of solid in reactor, 0.075g (26.0μmoles HPW, 41.1μmoles HPMo, 26.1μmoles HSiW); pulse size, 17.0 μmoles NO_2.

The quantity of NO_2 lost from the gas phase, as stated above, is representative of the quantity sorbed on the solid acids plus any products of reaction or decomposition exiting from the reactor. The total quantity of nitrogen-containing materials (NO, NO_2, and HNO_3) found in the effluent, expressed as moles N per moles NO_2 injected for each pulse are shown in Figure 3.3. For all the solid acids studied in the present work, the nitrogen remaining on the solids (in whatever form) at 150°C is maximum at the first pulse. As before, the two tungsten-containing acids behave similarly and show a markedly higher sorption than HPMo. The temperature dependence of the first pulse on HPW is shown in Table 3.2. The quantities of NO_2 sorbed reach a maximum at 150-300°C and become insignificant at temperatures in excess of 500°C.

The predominant gaseous products emerging from the catalysts during exposure to a pulse of NO_2 are HNO_3, O_2, and vanishingly small quantities of NO. With HPW pretreated at 150°C and exposed to NO_2 at the same temperature the fraction of the NO_2 converted to HNO_3 increases monotonically with the number of pulses up to seven and then decreases markedly, while that with HSiW increases up to three pulses and then begins to decrease (Fig.3.4). With both catalysts the HNO_3 vanishes from the effluent after ten pulses. With HPMo the fraction of NO_2 converted to HNO_3 is relatively small and is reduced significantly after one pulse. After pretreatment at 300°C and exposure to NO_2 at the same temperature, the quantity of HNO_3 produced with HPW passes through a maximum during the second pulse and vanishes after four pulses. With HSiW and HPMo at this temperature, the conversion of NO_2 to HNO_3 is very small for each pulse of NO_2. The quantities of oxygen found in the gas phase after exposure of the catalyst to various pulses of NO_2 are less than 1% and 10% for HPW and HSiW at 150°C and 300°C, respectively, and vanishingly small for HPMo at either temperature (Fig.3.5).

Adsorption-desorption measurements for NO (Fig.3.6) on HPW at room temperature produced isotherms displaying an absence of reversibility similar to that observed with zeolites some years ago (Ref.3.1). Little NO was sorbed on HPW pretreated at 250°C. When HPW was exposed to NO_2 prior to the NO adsorption-desorption measurement, greater quantities of NO was irreversibly adsorbed.

Adsorption-desorption measurements for NO_2 (Fig.3.7) on HPW at 25°C also produced isotherms displaying an absence of reversibility. However, more than 5 NO_2 per anion were sorbed up to atmospheric pressure. Upon evacuation the number of sorbed molecules would remain to about 3 to 3.5 NO_2/KU.

In comparison with the quantity of NO_2 sorbed and/or reacted on HPW, that of NO is minimal (Fig.3.8). The data reported in Figure 3.8 is expressed in terms of the increase in the number of moles of atomic nitrogen found on the solid as a result of exposure to a flow of NO as a function of the quantity of NO_2 previously taken up by the solid. In the absence of previously

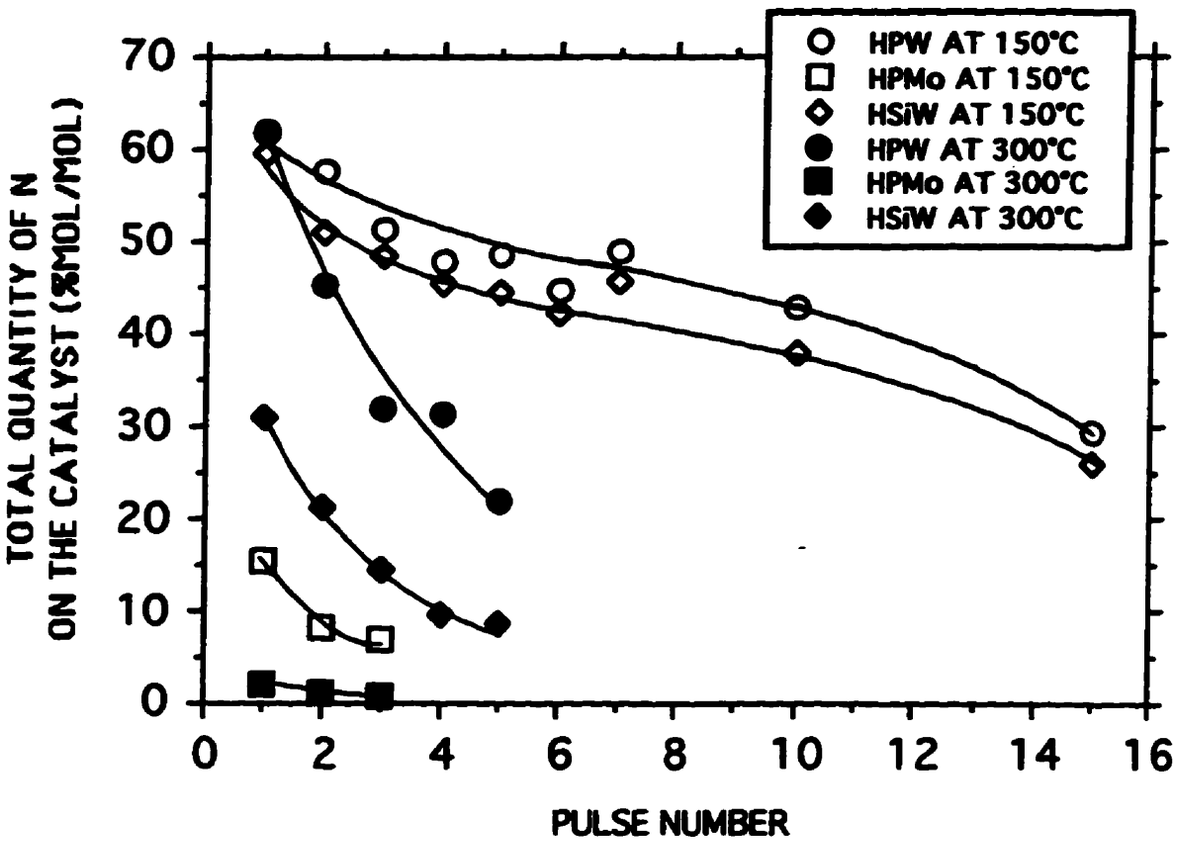

Fig. 3.3 Total amount of nitrogen-containing compounds (NO, NO_2, and HNO_3) sorbed on HPW, HPMo, and HSiW (total sorption of NO_2). Pretreatment and reactor temperature of (empty) 150°C; and (filled) 300°C. Each datum is obtained on a fresh sample. Mass of solid in reactor, 0.075g (26.0μmoles HPW, 41.1μmoles HPMo, 26.1μmoles HSiW); pulse size, 17.0 μmoles NO_2.

TABLE 3.2

SORPTION OF NO_2 ON HPW

Temperature[a] (°C)	Total Sorbed[b] (μmol nitrogen-atoms)	Nitrogen-atom per Keggin Unit
25	4.5	0.17
150[c]	6.0	0.23
150	10.5	0.40
300	10.5	0.40
400	3.9	0.15
500	0.5	0.02
600	0.1	0.004

a Pretreatment and sorption temperature.

b Quantity of nitrogen-atom-containing materials remaining on the catalyst after exposure of catalyst (0.075g or 26.0μmoles) to a pulse of 17.0 μmol NO_2 (in helium flow 60 mL/min at temperature shown).

c This sample of HPW was pretreated at 400°C in helium flow (60 mL/min) prior to the injection of NO_2 at 150°C.

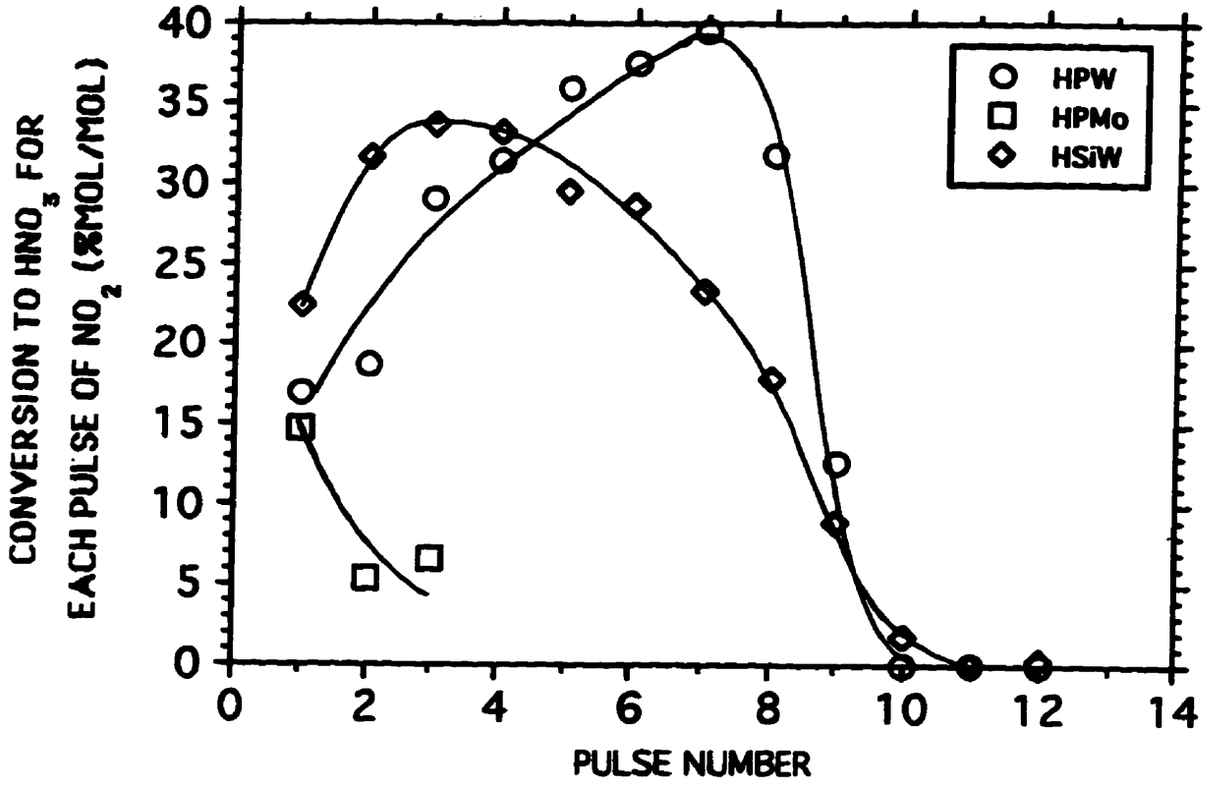

Fig. 3.4 Conversion of NO_2 to HNO_3 in a sequence of pulses of NO_2 on HPW, HPMo, and HSiW. Pretreatment and reactor temperature of 150°C. Mass of solid in reactor, 0.075g (26.0μmoles HPW, 41.1μmoles HPMo, 26.1μmoles HSiW); pulse size, 17.0 μmoles NO_2.

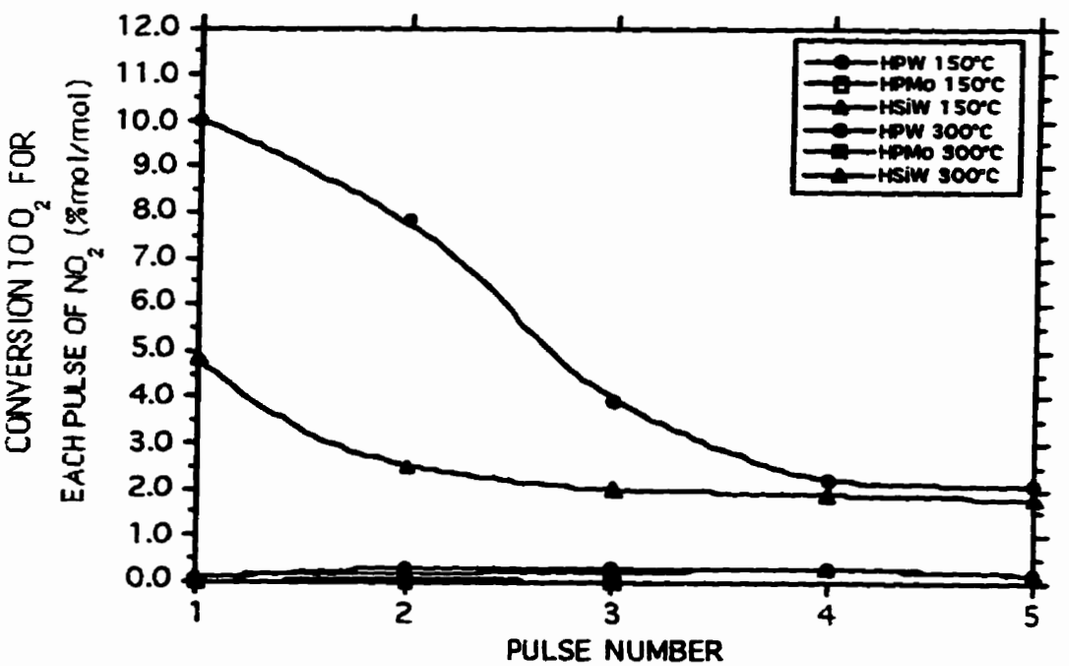

Fig. 3.5 Conversion of NO_2 to O_2 in a sequence of pulses of NO_2 on HPW, HPMo, and HSiW. Pretreatment and reactor temperature of (empty) 150°C; and (filled) 300°C. Mass of solid in reactor, 0.075g (26.0μmoles HPW, 41.1μmoles HPMo, 26.1μmoles HSiW); pulse size, 17.0 μmoles NO_2.

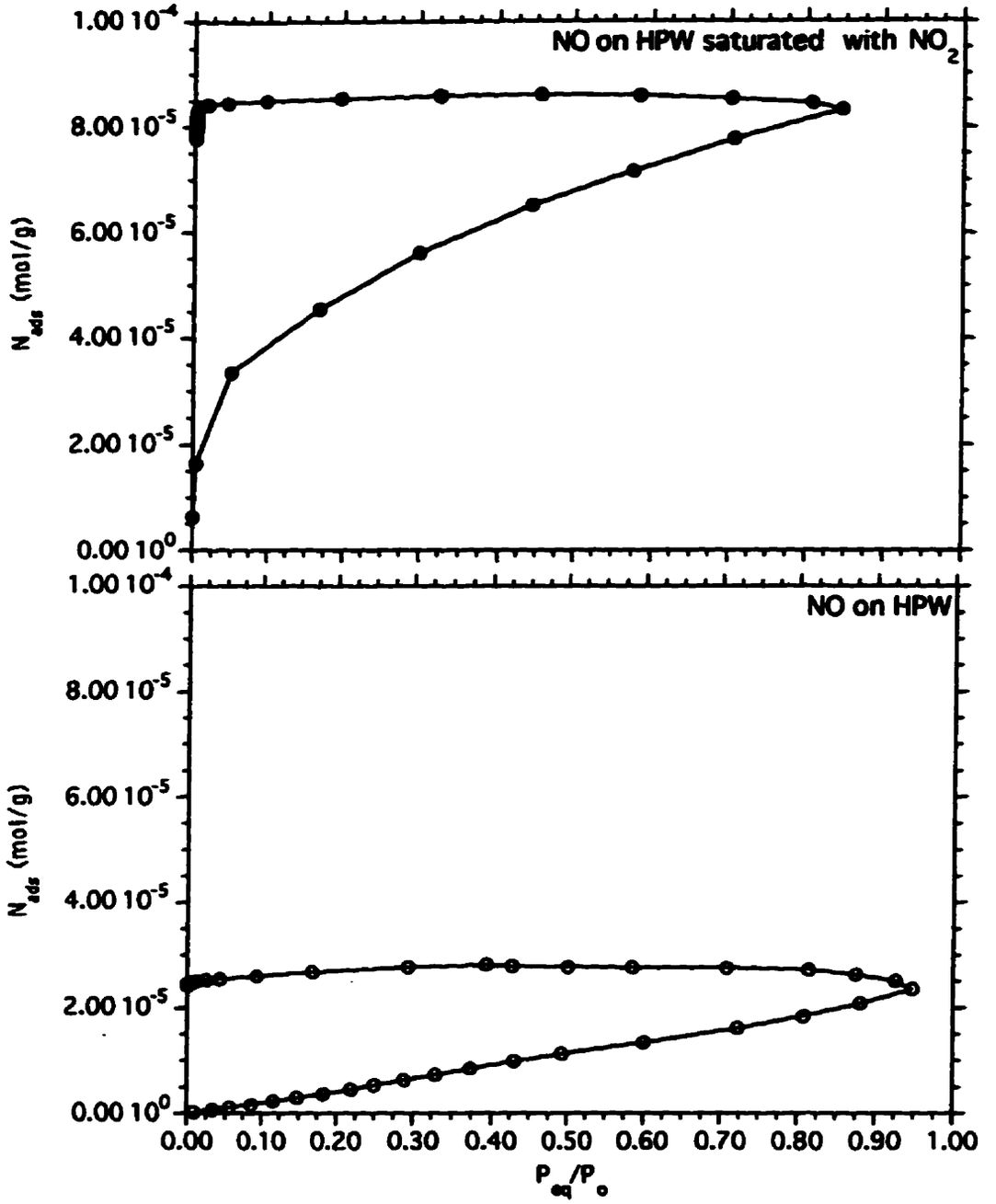

Fig. 3.6 Adsorption-desorption isotherm of NO on HPW and NO on NO_2-saturated HPW at 25°C. Each sample of HPW (3.1g or 1.1mmole) was pretreated in air at 250°C and exposed to the NOx at 25°C.

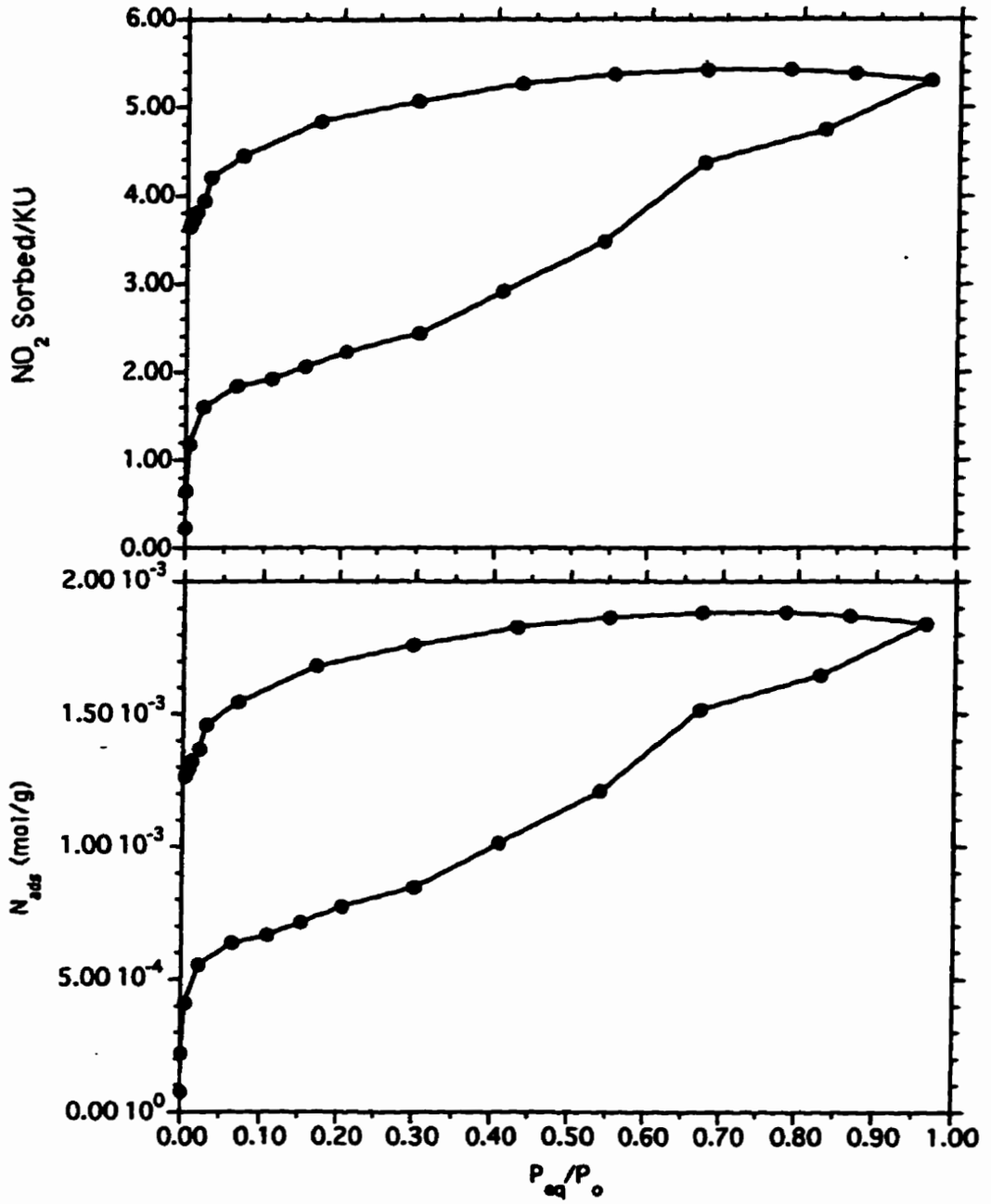

Fig. 3.7 Adsorption-desorption isotherm of NO_2 on HPW at 25°C. The sample of HPW (0.19g or 66.0μmoles) was pretreated in helium at 150°C.

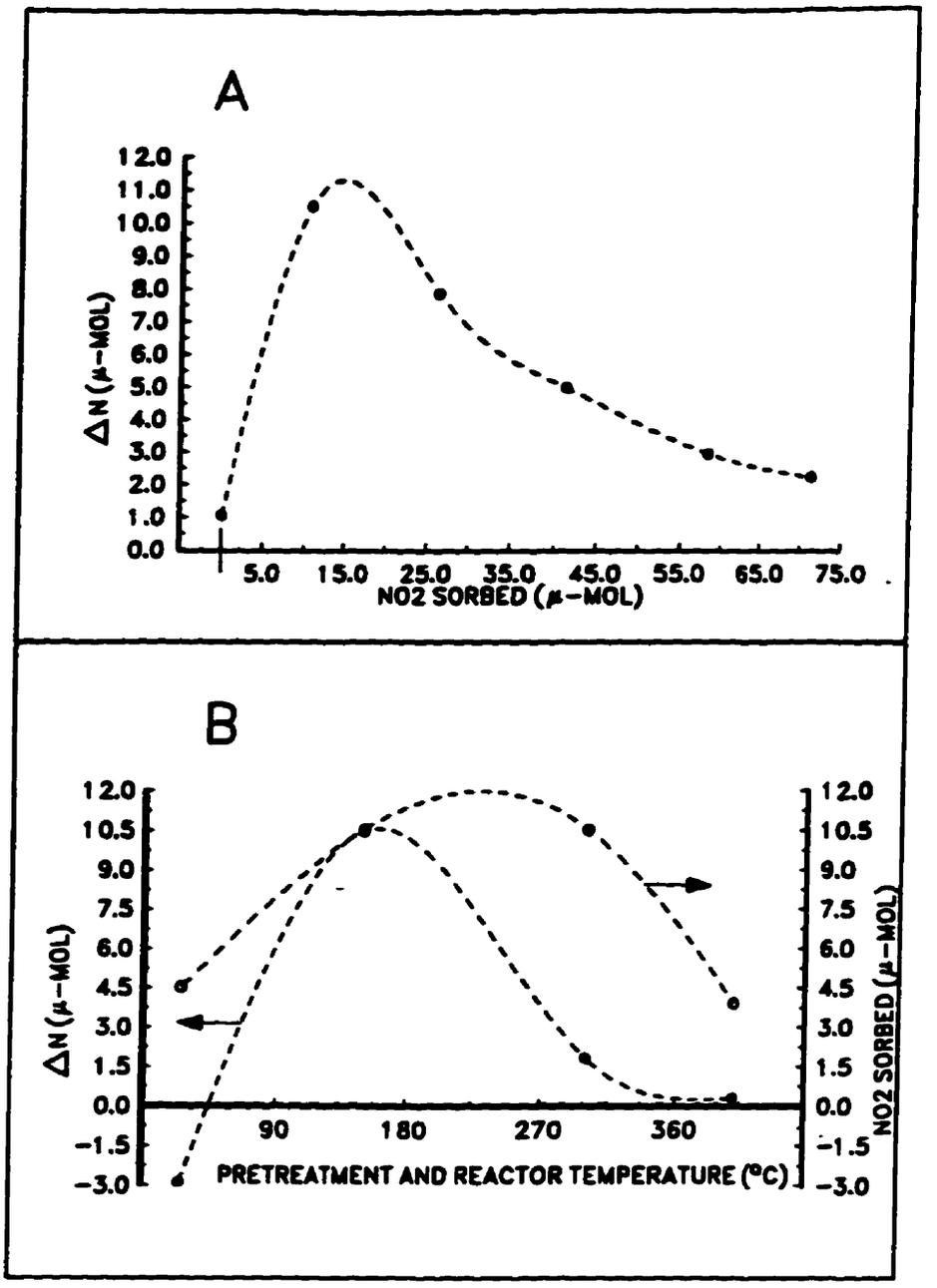

Fig. 3.8 Sorption of NO on NO_2-exposed HPW; (A) as a function of the quantity of NO_2 sorbed previously at 150°C, and (B) as a function of pretreatment and reactor temperature when 1 pulse of NO_2 (17.0 μmol NO_2) was previously injected. Each point is obtained with a fresh aliquot. Four pulses of NO (10.0 μmoles each) were injected prior to the determination of total nitrogen on the catalyst. Mass of solid in reactor, 0.075g (26.0μmoles).

sorbed NO_2 the sorption of NO is almost insignificant. However after prior sorption of NO_2 the quantity of NO taken up increases, passes through a maximum, and decreases. The maximum quantities of NO taken up by the solid are approximately equal to those of NO_2.

The sorption of NO on HPW containing previously sorbed NO_2 increases with temperature, reaching a maximum at approximately 150°C and decreases as the temperature continues to increase, ultimately becoming insignificant at 360°C.

The TPD patterns for HPW, pretreated for 1 hour at 150°C in a flow of helium (60 mL/min), display two peaks, one at approximately 300°C and the other at 500°C, both produced by water, the former resulting from the evolution of water molecules hydrogen-bonded to the protons and anionic oxygen atoms, the latter from water resulting from the extraction of the latter by the former (Fig.3.9A) (Ref.3.2). After exposure to NO at 30°C for 5 min, little or no change was observed in the TPD peaks (Fig.3.9B). However after exposure to NO_2 at 30°C for 5 min, a shoulder is now evident at approximately 200°C and the peak at 500°C has increased and shifted to a somewhat higher temperature (Fig.3.9C). It should also be noted that the 300°C peak has slightly diminished. The latter peak is now found to result from the desorption of both water and NO_2. Finally, the catalyst was exposed to NO_2 at 30°C for 5 min and subsequently to NO at 30°C for 5 min (Fig.3.9D). The low temperature (approximately 150°C) peak has increased in magnitude, the 300°C peak has decreased still further and the highest temperature peak has further increased in magnitude and shifted to a higher temperature.

The effect of exposing HPW pretreated in helium at 150°C for 1 hour to various numbers of pulses of NO_2 at 150°C can be seen in the TPD patterns of Figure 3.10. As the number of pulses of NO_2 increases from 1 to 7 the shoulder at 150-200°C due to water increases, then decreases. While the water peak at 300°C increases to a maximum (at the second pulse) (Fig.3.11), the quantity of NO_2 desorbing at 500°C increases sharply and levels off at approximately the same value of the dosage of NO_2 as observed for the maximum with water (after the second pulse of NO_2 introduced).

TPD of HSiW shows somewhat similar results to those found with HPW but with some differences. As with HPW the peak due to water appearing at approximately 300°C decreases in size with increasing number of pulses of NO_2 while that at 500°C increases (Fig.3.12). An additional small shoulder is evident on the 500°C peak. This has previously been seen with HSiW not exposed to NO_2 (Ref.3.2).

Information on the source of the TPD peaks is available from Figure 3.13 which shows the comparative results for all three solid acids pretreated and saturated with NO_2 at 150°C. The numbers found above the curves, representative of each species (see legend) are positioned at the maximum intensity detected for the specific ion. The presence of a peak attributed to oxygen at

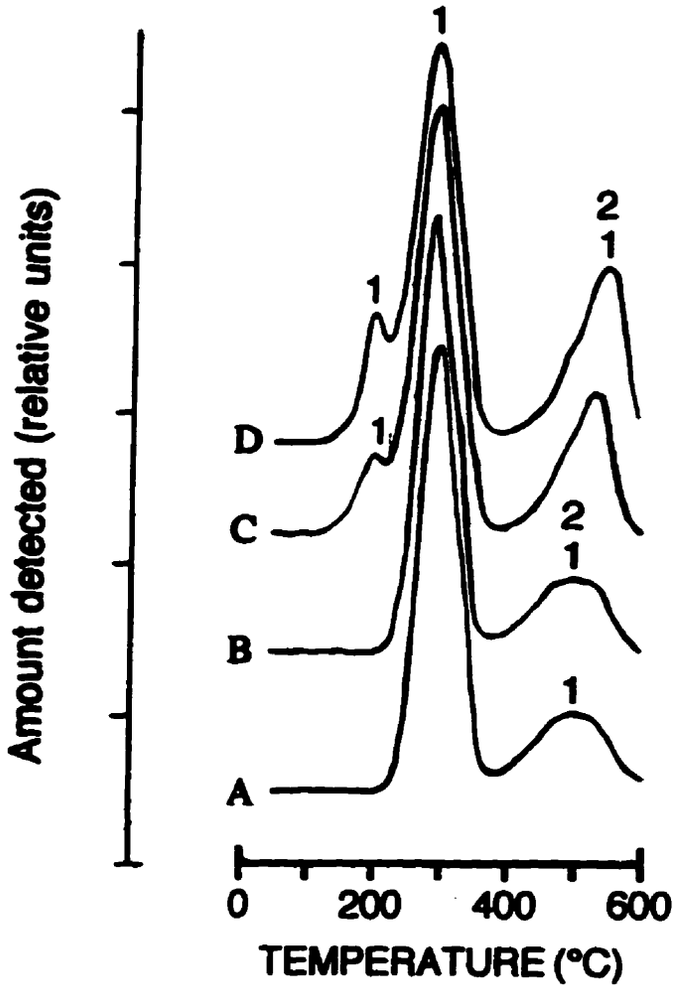

Fig. 3.9 TPD of HPW pretreated in helium at 150°C for 1 hr and exposed to flow of (A) helium at 30°C; (B) NO at 30°C; (C) NO_2 at 30°C; and (D) first to NO_2 at 30°C and then with NO at 30°C. Helium flow rate, 45.0 mL/min; temperature rate, 60°C/min; mass of solid in reactor, 0.150g (52.1μmoles); sorbing gas flow rate, 30.0 mL/min at 1 atm. LEGEND: 1, H_2O; 2, NO_2.

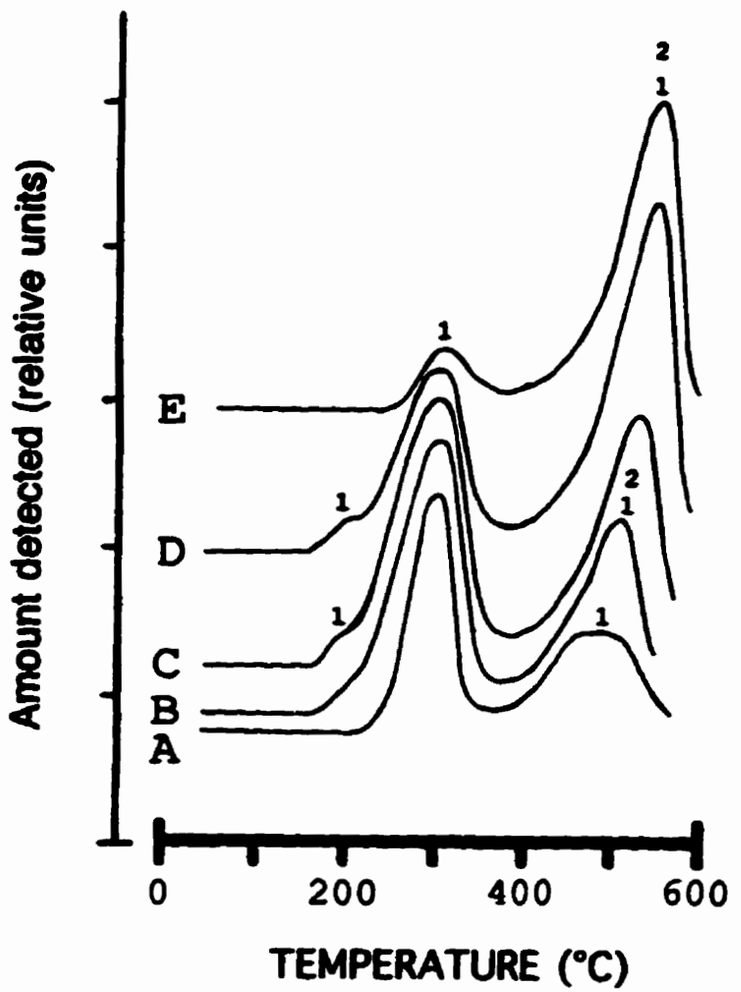

Fig. 3.10 TPD of HPW pretreated in helium at 150°C for 1 hr, (A), and exposed, at 150°C to (B) 1 pulse of NO_2; (C) 2 pulses of NO_2; (D) 4 pulses of NO_2; and (E) 7 pulses of NO_2. Helium flow rate, 45.0 mL/min; temperature rate, 60°C/min; mass of solid in reactor, 0.165g (57.3μmoles); pulse size, 17.0 μmoles NO_2. LEGEND: 1, H_2O; 2, NO_2.

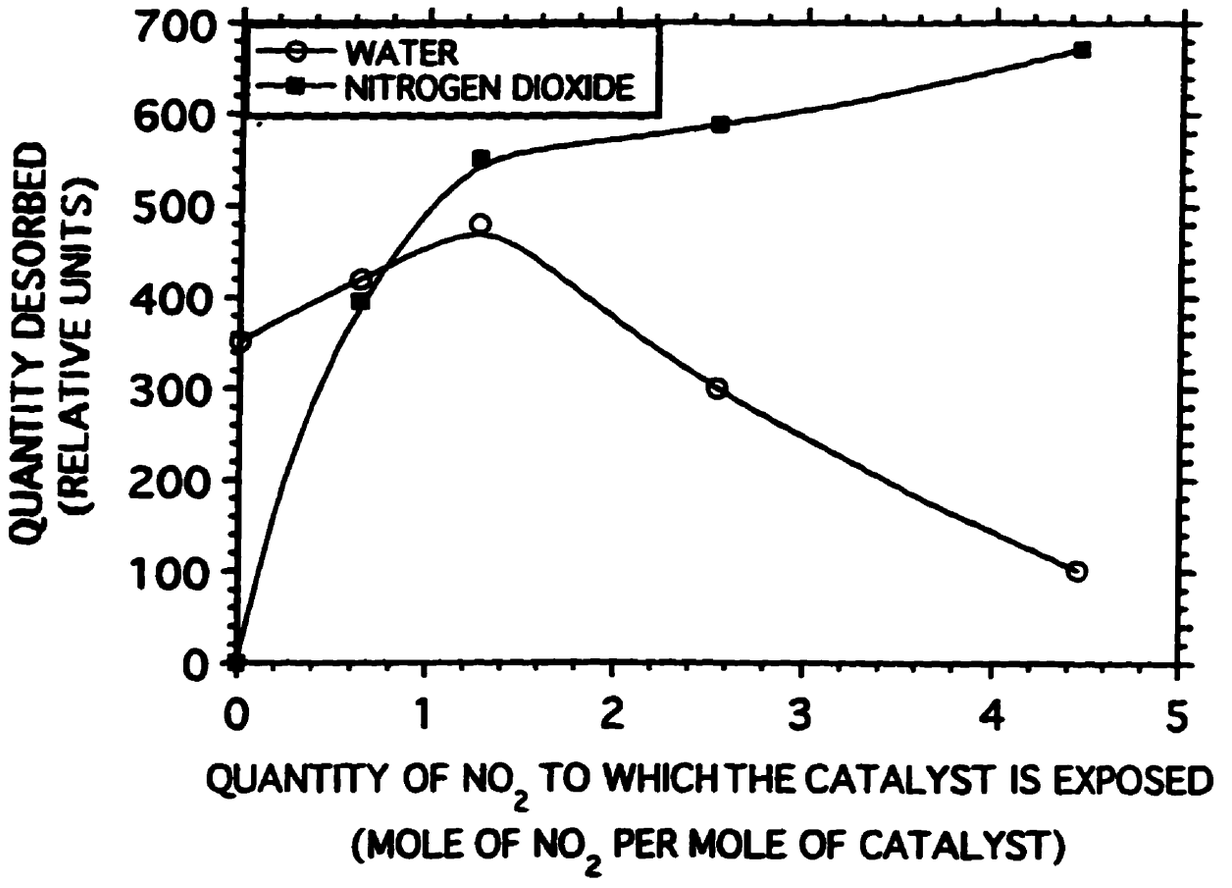

Fig. 3.11 H_2O and NO_2 desorbed at 300°C and 500°C, repectively for increasing quantities of sorbed NO_2 as measured from TPD of Figure 3.8.

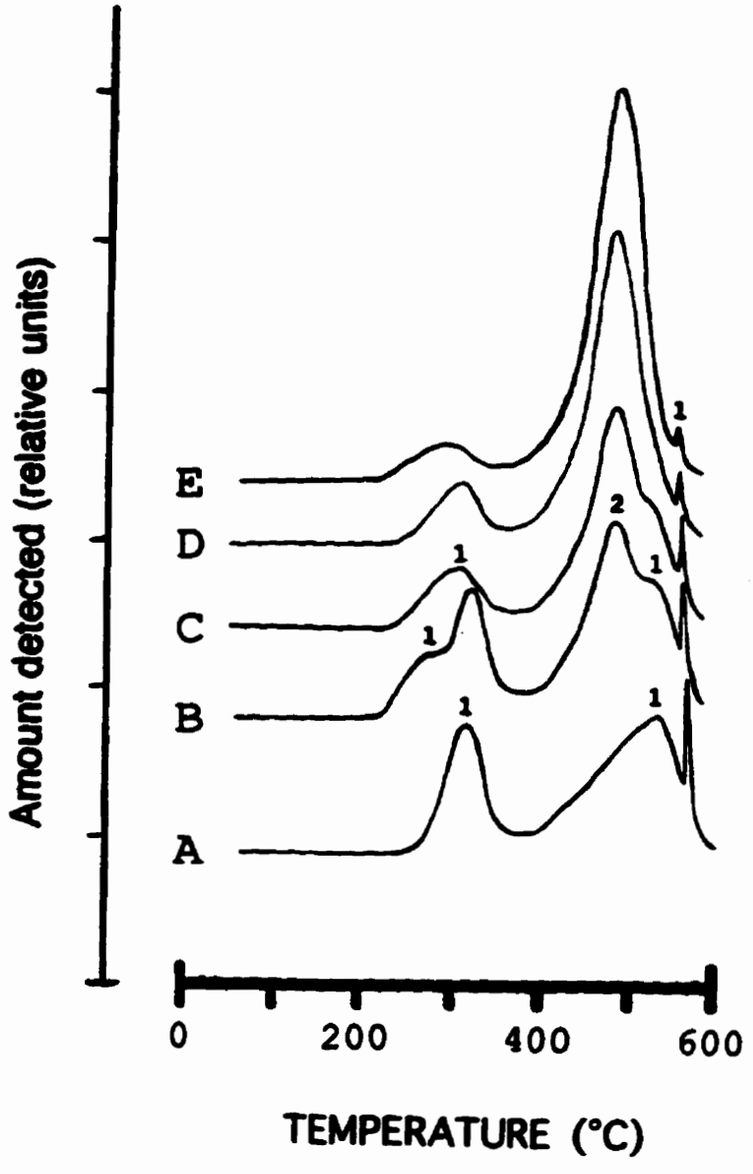

Fig. 3.12 TPD of HSiW pretreated in helium at 150°C for 1 hr, (A), and exposed, at 150°C to (B) 1 pulse of NO_2; (C) 2 pulses of NO_2; (D) 4 pulses of NO_2; and (E) 7 pulses of NO_2. Helium flow rate, 45.0 mL/min; temperature rate, 60°C/min; mass of solid in reactor, 0.155g (53.8μmoles); pulse size, 17.0 μmoles NO_2. LEGEND: 1, H_2O; 2, NO_2.

350°C with the two tungsten-containing acids is particularly interesting. Evidently the TPD peak seen in Figure 3.13 at approximately 275°C results from the evolution of water and NO_2 while that at 550°C is produced primarily from NO_2 with a trace of water.

With HPMo, in the absence of NOx, a similar TPD spectra as observed with HPW and HSiW is seen, but at a temperature of 475°C HPMo begins to decompose. After exposure of HPMo, pretreated at 150°C for 1 hour in a flow of helium (60 mL/min), to NO_2 at 30°C, no definite TPD peak is observed. However with HPMo pretreated and exposed to NO_2 at 150°C, NO_2 desorbs at 300°C and the water peak at 450°C is not affected by the presence of NO_2.

Supplementary experiments show that HPW sorbs only a small quantity of HNO_3 (i.e. 2.3 μmoles at 150°C). A TPD of HPW soaked in concentrated HNO_3 shows that HNO_3 desorbs and decomposes with the main water peak (at 300°C) and there is no increase of the peak appearing at 500°C (Fig.3.14).

The results obtained by TGA on HPW (Fig.3.15) are similar to those from TPD, but the maxima are shifted to lower temperatures. At room temperature, and upon evacuation, the untreated HPW initially loses 107 mg/g of water (not shown in Fig.3.15). On heating from 25°C to 50°C approximately 13 mg/g of water is lost (as seen in Fig.3.15A). With NO_2-exposed (continuous flow of NO_2 at 30 mL/min and 1 atm) HPW (Fig.3.15B) and upon evacuation at 25°C, the weight remains constant. However, increase in the temperature results in a weight loss. For HPW treated with NO_2, the total mass desorbed (combined heat and evacuation) was 40 mg/g of catalyst, which corresponds to 2.5 NO_2/KU (assuming that all desorbing molecules are NO_2, and traces of water molecules). A relative maximum in the desorption occurs at 350°C in comparison to 550°C observed in the TPD experiments. For HSiW exposed to NO_2, the weight loss of 46 mg/g of catalyst is equivalent to 2.9 NO_2/KU.

As with HPW (treated with NO_2), HSiW did not show any decrease of weight upon evacuation at room temperature. With NO_2-saturated HPMo most of the loss in weight occurs on evacuation at room temperature.

The infrared spectra of HPW before and after saturation with NO_2 are shown in Figure 3.16. The bands in the region 800-1200 cm^{-1}, which are characteristic of the anion of Keggin structure, are clearly evident. After exposure of HPW to NO_2, a band at 2264 cm^{-1}, not seen in the presence of NO and the absence of NO_2, is evident in Figures 3.16B and 3.16C. The intensity of this band reaches a maximum after pretreatment of the sample at 150°C and saturation with NO_2 at the same temperature (Fig.3.16B). This band shifted to 2215 cm^{-1} when $^{15}NO_2$ was sorbed on HPW. The infrared spectra also show a diminution in the intensity of bands attributed to water and H_3O^+ as NO_2 is sorbed.

When HPW is exposed to NO after saturation with NO_2 (Fig.3.16D) a band, characteristic of N_2O_3, appears at 1304 cm^{-1}.

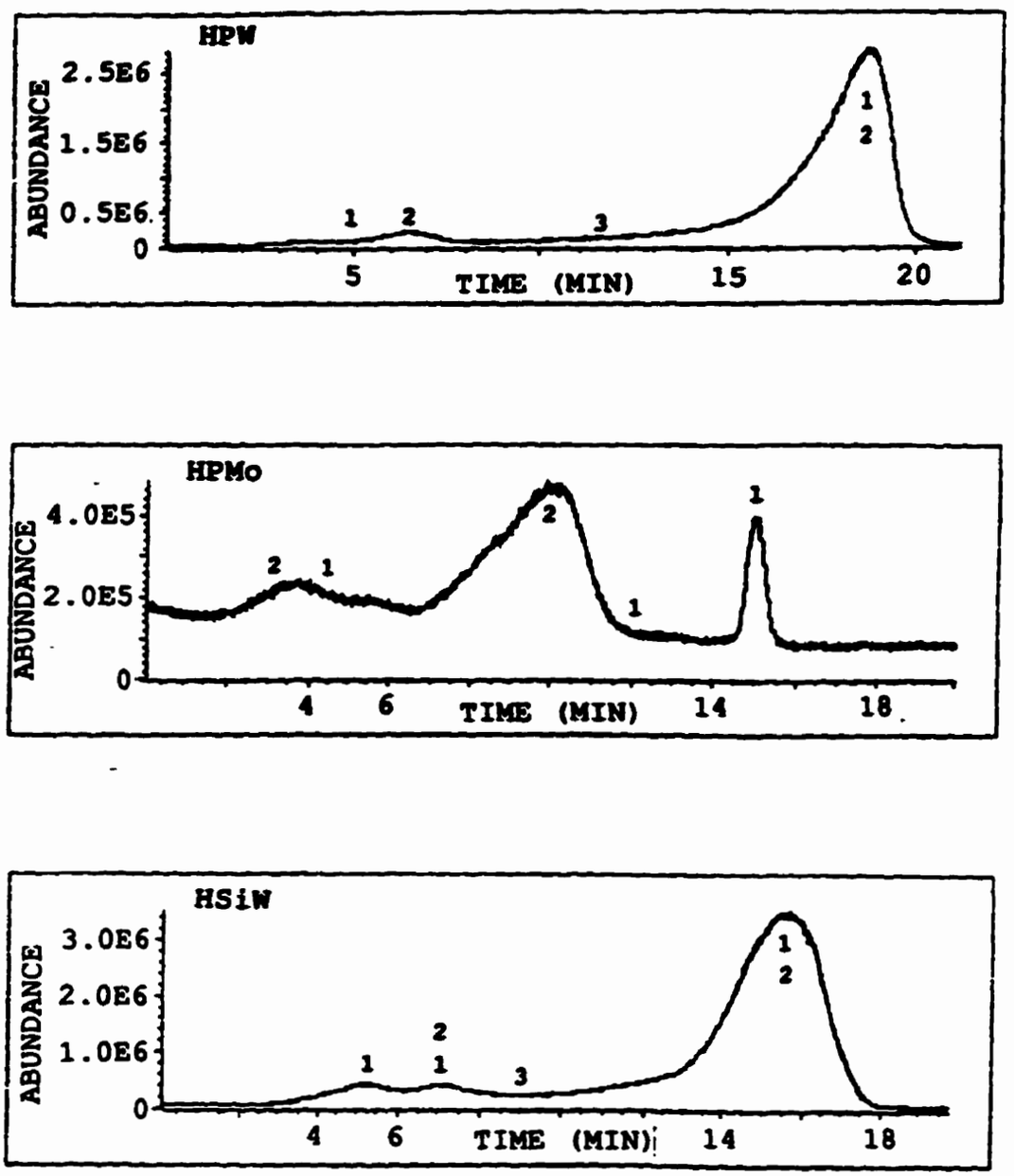

Fig. 3.13 Total ion TPD of HPW, HPMo, and HSiW pretreated (helium flow of 60 mL/min for 45 min) and then exposed to NO_2 (30 mL/min for 5 min) at 150°C. Mass of solid in reactor, 0.150g (52.1μmoles HPW, 82.2μmoles HPMo, 52.1μmoles HSiW); He flow rate, 10 mL/min; temperature range, 30 to 600°C; *dT/dt*, 30°C/min. LEGEND: 1, H_2O; 2, NO_2;and 3, O_2.

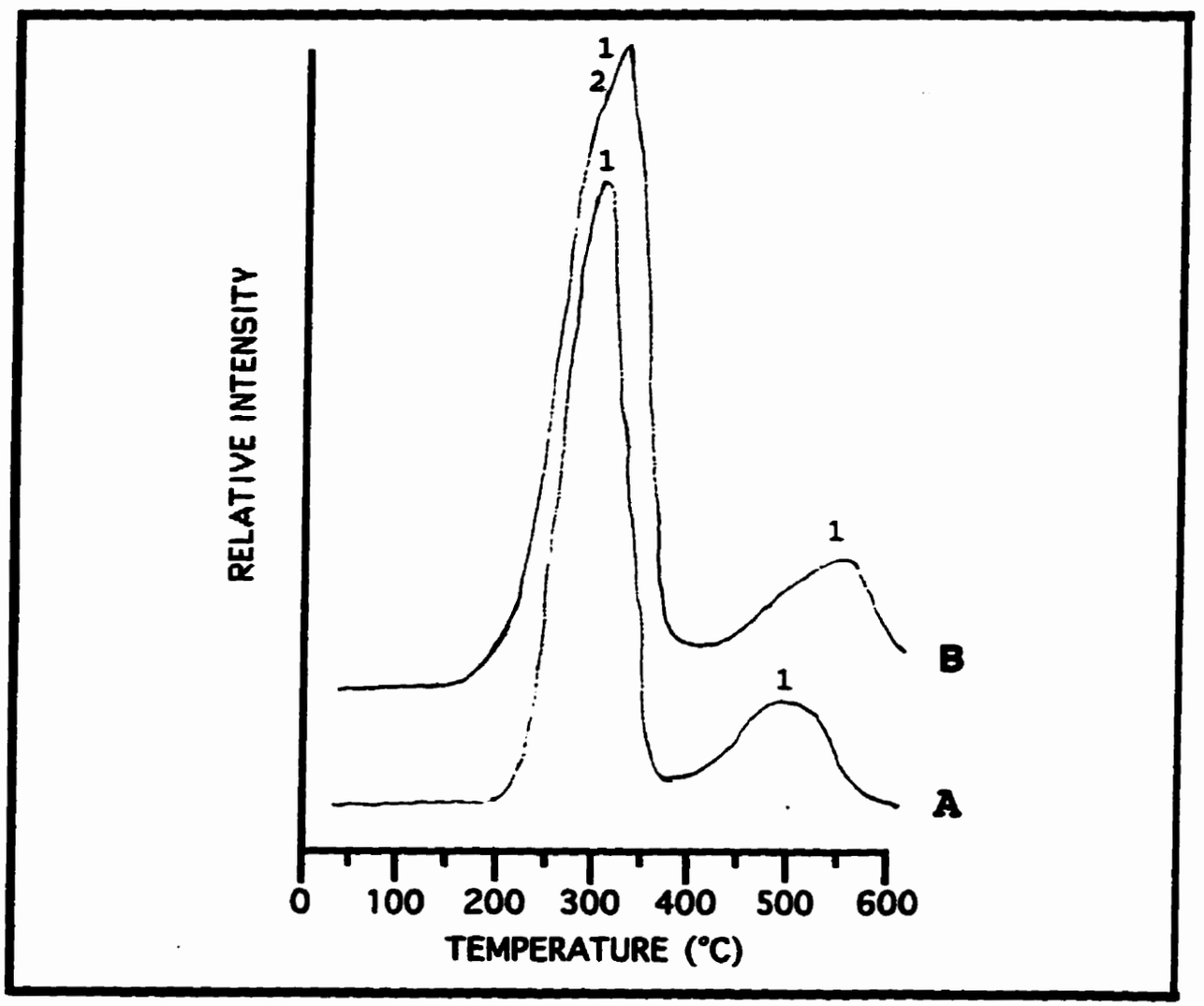

Fig. 3.14 TPD of HPW (A) pretreated in helium at 150°C for 1 hr, and (B) soaked in concentrated HNO_3, at 25°C. Helium flow rate, 45.0 mL/min; temperature rate, 60°C/min; mass of solid in reactor, 0.155g (53.1μmoles). LEGEND: 1, H_2O; 2, HNO_3.

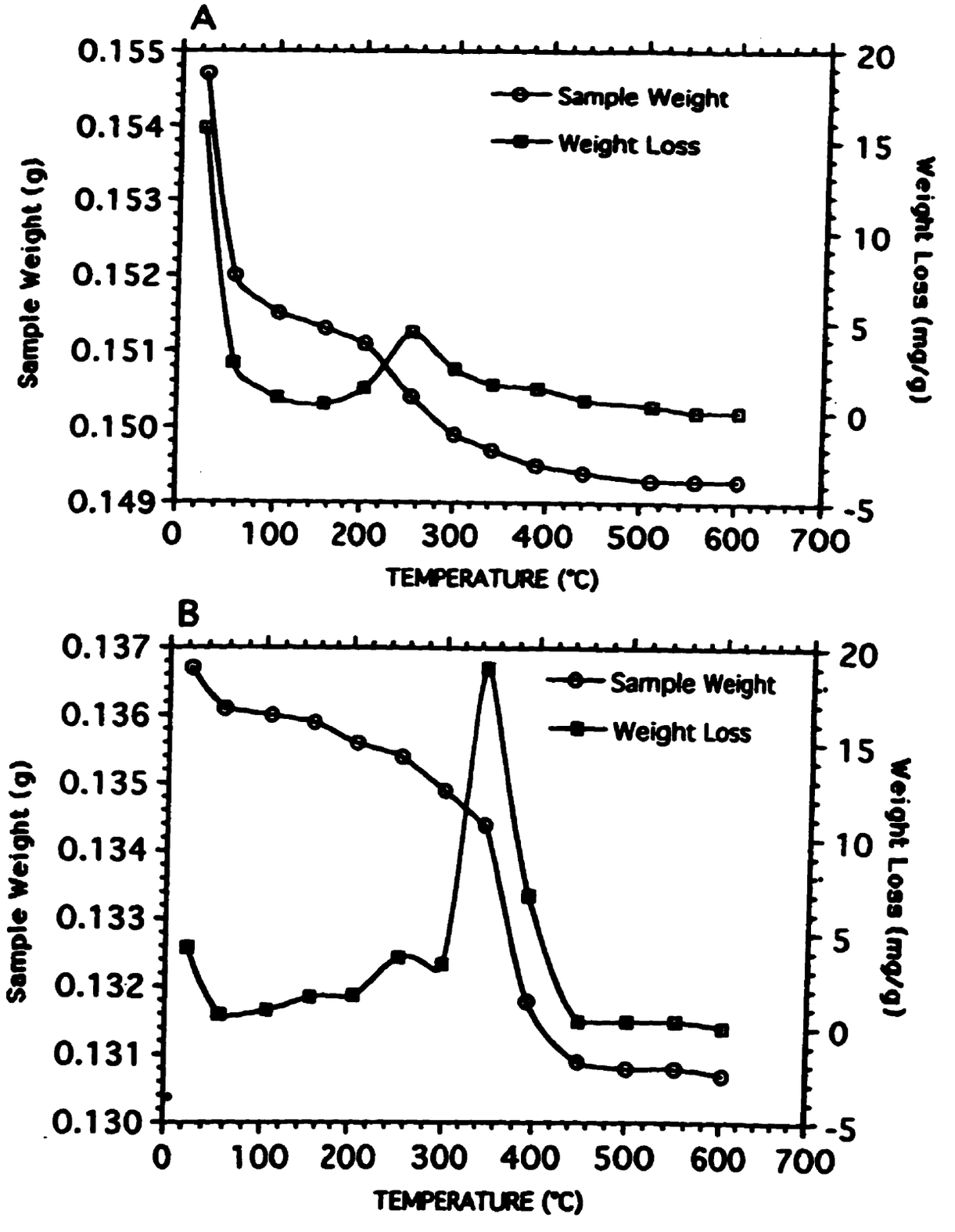

Fig. 3.15 TGA of (A) HPW as received; and (B) HPW pretreated in helium at 150°C and then exposed to flow of pure NO_2 (30mL/min at 1 atm) at 150°C. Mass of acid used: (A) 0.1733g (60.2μmoles), (B) 0.1366g (47.4μmoles).

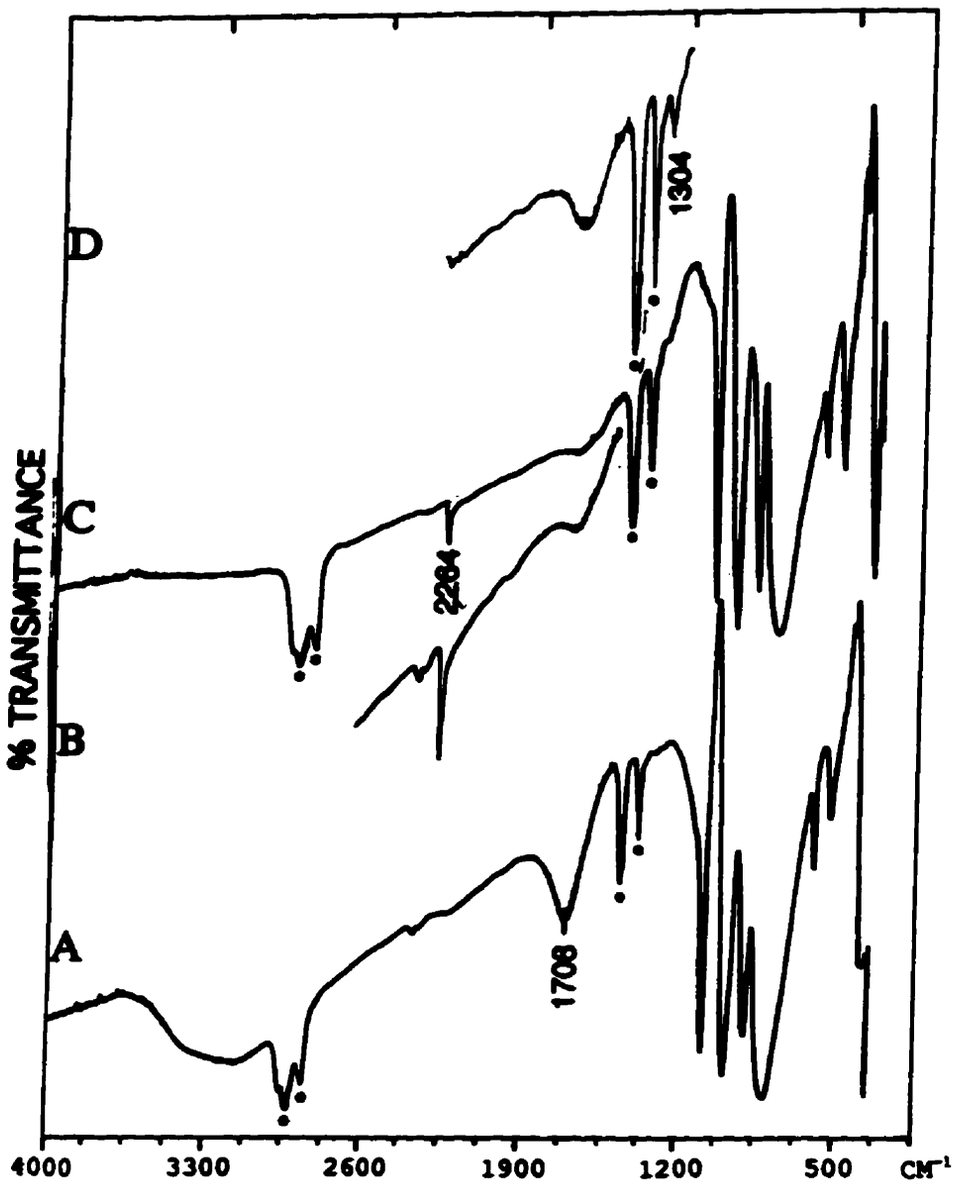

Fig. 3.16 Infrared spectra of HPW: (A) after pretreatment (200°C, 1 hr) in a flow of helium; (B) after pretreatment (150°C, 1 hr) in a flow of helium and then exposed to flow of pure NO_2 (30 mL/min at 1 atm) at 150°C; (C) pretreated as in (A) and then exposed to flow of pure NO_2 (30 mL/min at 1 atm) at 25°C; (D) pretreated as in (B) but after 1 pulse of 17.0 μmoles of NO_2 and then 1 pulse of 10.0 μmoles of NO at 25°C; *=NUJOL.

Similar spectra are found with HSiW, with the additional band at 2257 cm^{-1} (Fig.3.17). The molybdenum-containing acid did not show the aforementioned band in its infrared spectra after exposure to NO_2, or NO.

Powder X-ray diffraction patterns of HPW and HPW treated with NO_2 at 300°C (Fig.3.18) show that the crystallographic structure of the solid is retained, although new diffraction bands associated with the presence of NO_2 are evident. The acid was heated to 300°C to remove most of the water molecules which interfere with the diffraction pattern. It is clear from the infrared and X-ray diffraction results that the sorption of NO_2 on the acids does not change the basic structure of the Keggin Units.

The surface areas of HPW, pretreated at 150°C for 1 hour in a flow of helium (60 mL/min), before and after exposure to a continuous flow of NO_2 (30 mL/min at 1 atm) are similar (9.3 m^2/g) indicating that the sorption of NO_2 has little or no influence on the surface of the solid available to N_2.

To gather more information and help elucidate the infrared spectra of heteropoly acids exposed to NO_2, Raman spectra on samples of HSiW and HSiW exposed to $^{14}NO_2$ (Fig.3.19A, B, C), HPW and HPW exposed to $^{15}NO_2$ (Fig.3.20A,B,C,D), and HPW exposed to $^{14}NO_2$ (Fig.3.22A, B, C, D) were measured. All samples were measured from sealed capillary tubes to assure their dryness and avoid reaction with water from the atmosphere.

After exposure of HSiW to NO_2 at 150°C, the bands attributed to the Keggin anion remain unchanged from those observed prior to exposure to the oxide of nitrogen. However, a strong unpolarized new band at 2263 cm^{-1} is observed (Fig.3.19A). Furthermore, this new band is not symmetrical but has a shoulder situated at 2254 cm^{-1}. More detailed examination of the spectra (Figs.3.19B, C) suggests a new band at approximately 810 cm^{-1}. On HPW exposed to $^{15}NO_2$ (Fig.3.20), the new bands are found at 2226 cm^{-1} with a shoulder at 2209 cm^{-1}, 835 cm^{-1}, and 680 cm^{-1}, respectively, and are also unpolarized. When HPW was exposed to $^{14}NO_2$ (Fig.3.21), the new bands were found at 2267 cm^{-1} with a shoulder at 2250 cm^{-1}, 810 cm^{-1}, and 660 cm^{-1}, respectively. The band at 660 cm^{-1} seems to be related to the Keggin structure and not from one of the vibrational modes of the nitrogen species sorbed on the acid.

The ^1H MAS NMR spectra of HPW before and after exposure to NO_2 show that the protons are retained on the solid acid after contact with NO_2 (Fig.3.22). However, a small downfield chemical shift is seen after exposure to NO_2.

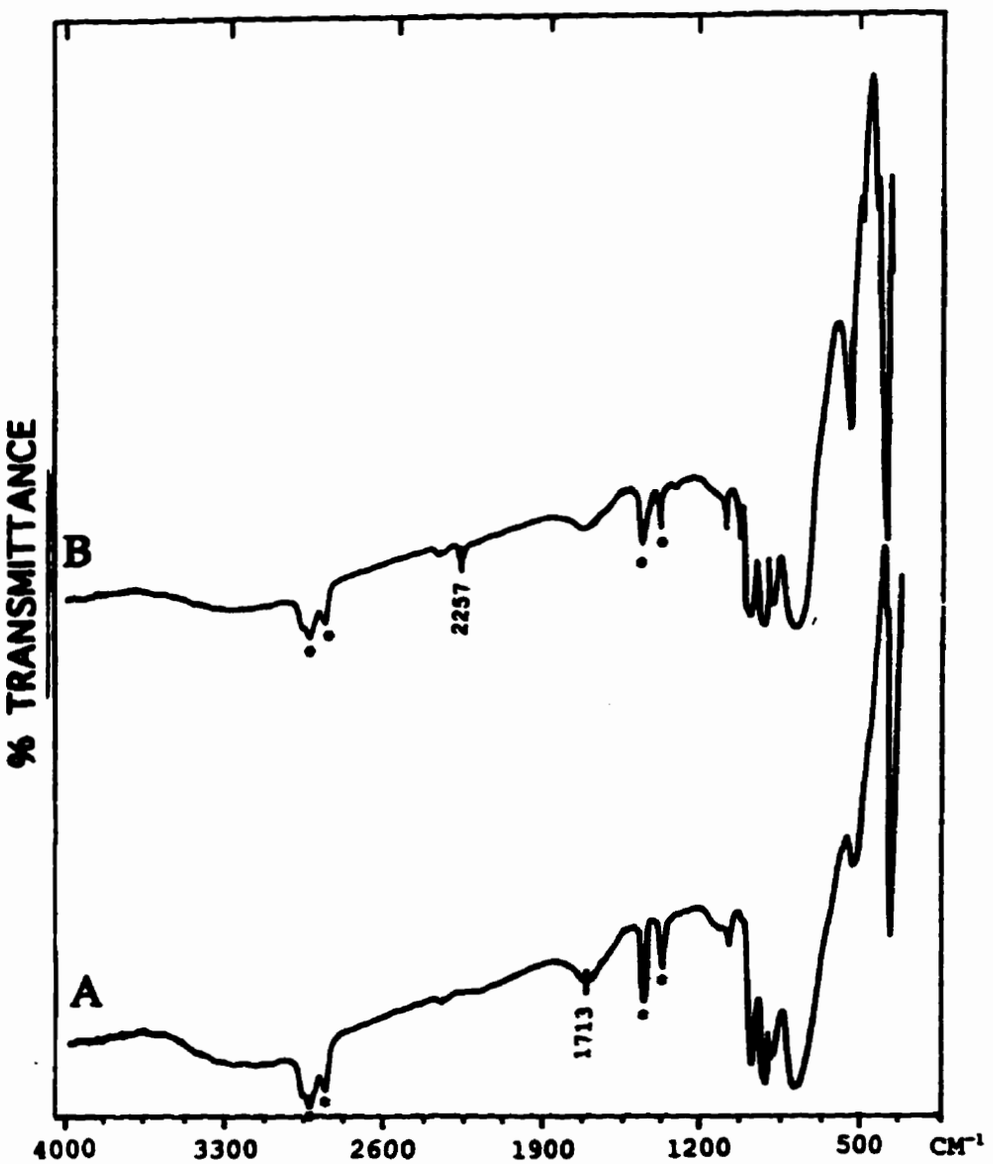

Fig. 3.17 Infrared spectra of HSiW: (A) after pretreatment (150°C, 1 hr, 60 mL/min) in a flow of helium; (B) after exposure to flow of pure NO_2 (30 mL/min at 1 atm) at 150°C; *=NUJOL.

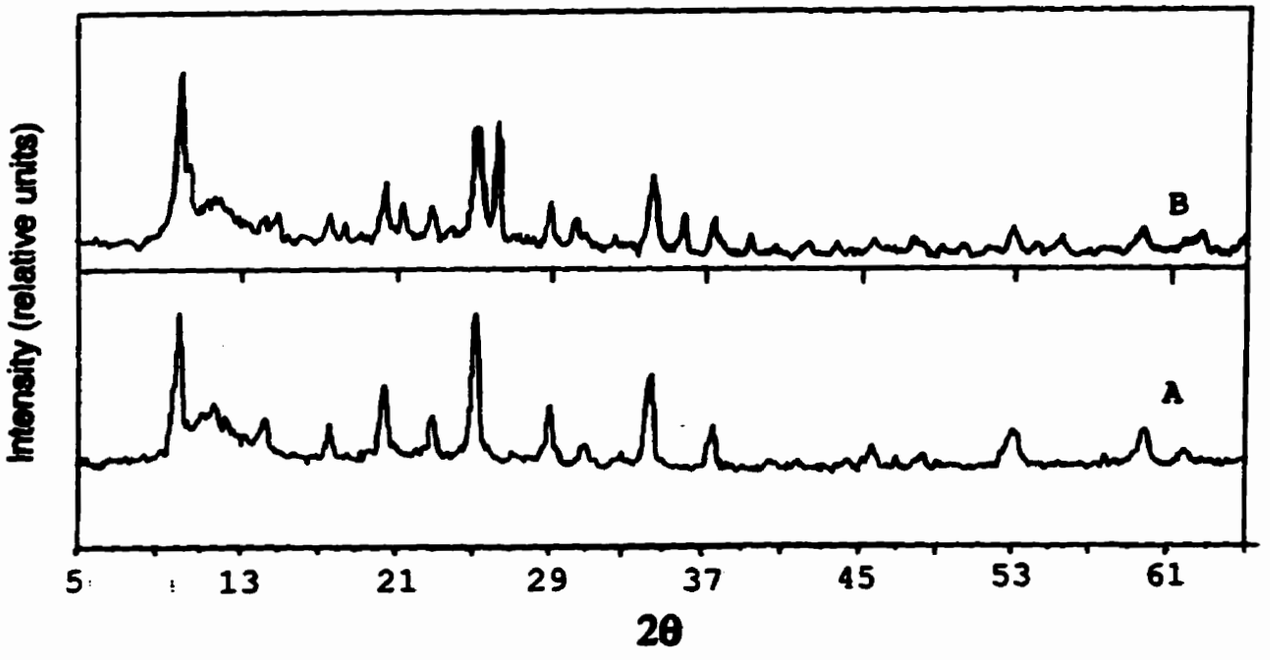

Fig. 3.18 X-ray diffraction spectra of HPW: (A) after pretreatment (300°C, 1 hr, 60 mL/min) in a flow of helium; (B) after exposure to flow of pure NO_2 (300°C, 5 hr, 30 mL/min, 1 atm).

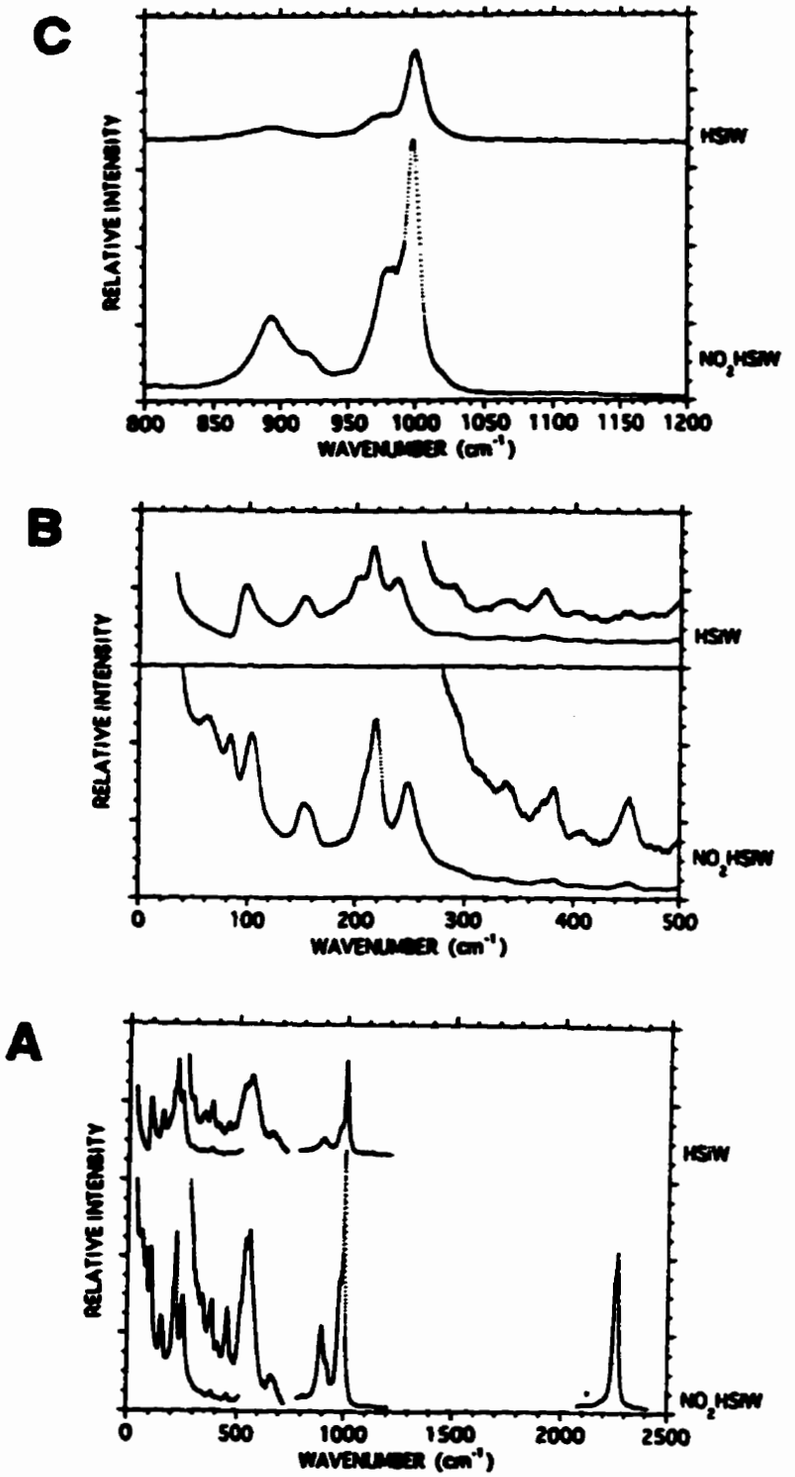

Fig. 3.19 Raman spectra of HSiW and HSiW exposed to $^{14}NO_2$ at 150°C. A) 0-2500 cm^{-1} range; B) 0-500 cm^{-1} range; C) 800-1200 cm^{-1} range.

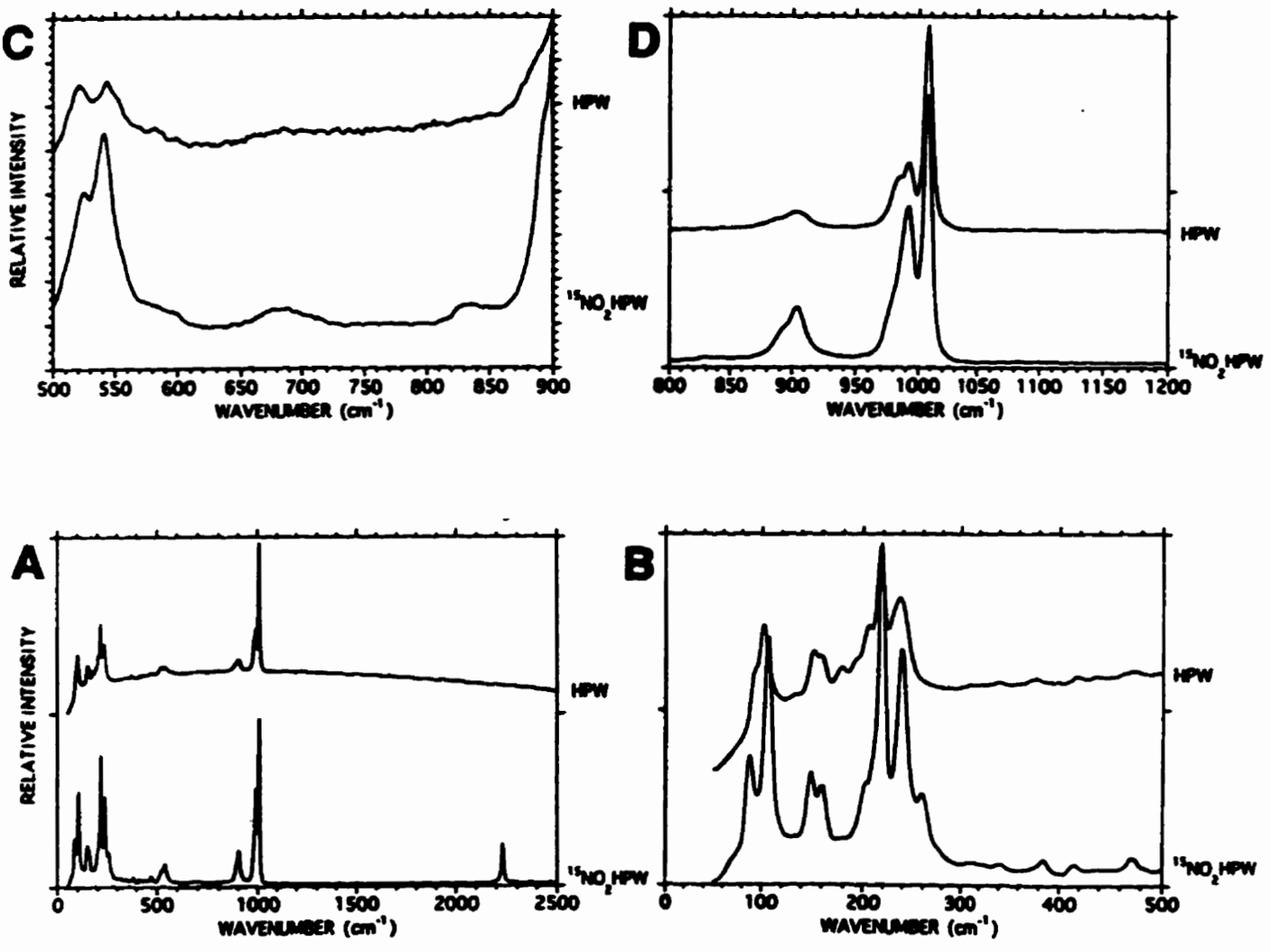

Fig. 3.20 Raman spectra of HPW and HPW exposed to $^{15}NO_2$ at 150°C. A) 0-2500 cm^{-1} range; B) 0-500 cm^{-1} range; C) 500-900 cm^{-1} range; D) 800-1200 cm^{-1} range.

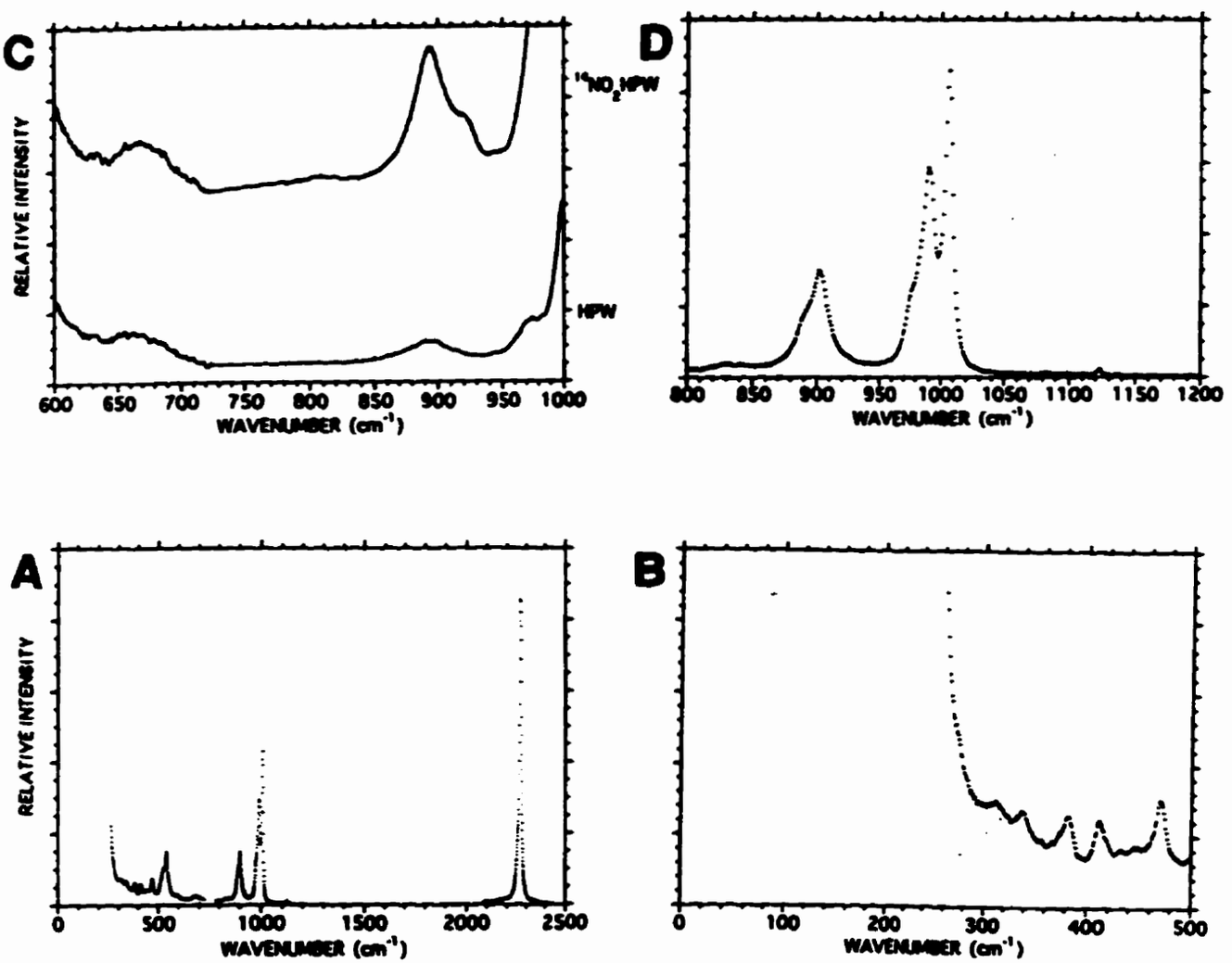

Fig. 3.21 Raman spectra of HPW exposed to $^{14}NO_2$ at 150°C. A) 0-2500 cm^{-1} range; B) 0-500 cm^{-1} range; C) 600-1000 cm^{-1} range; D) 800-1200 cm^{-1} range.

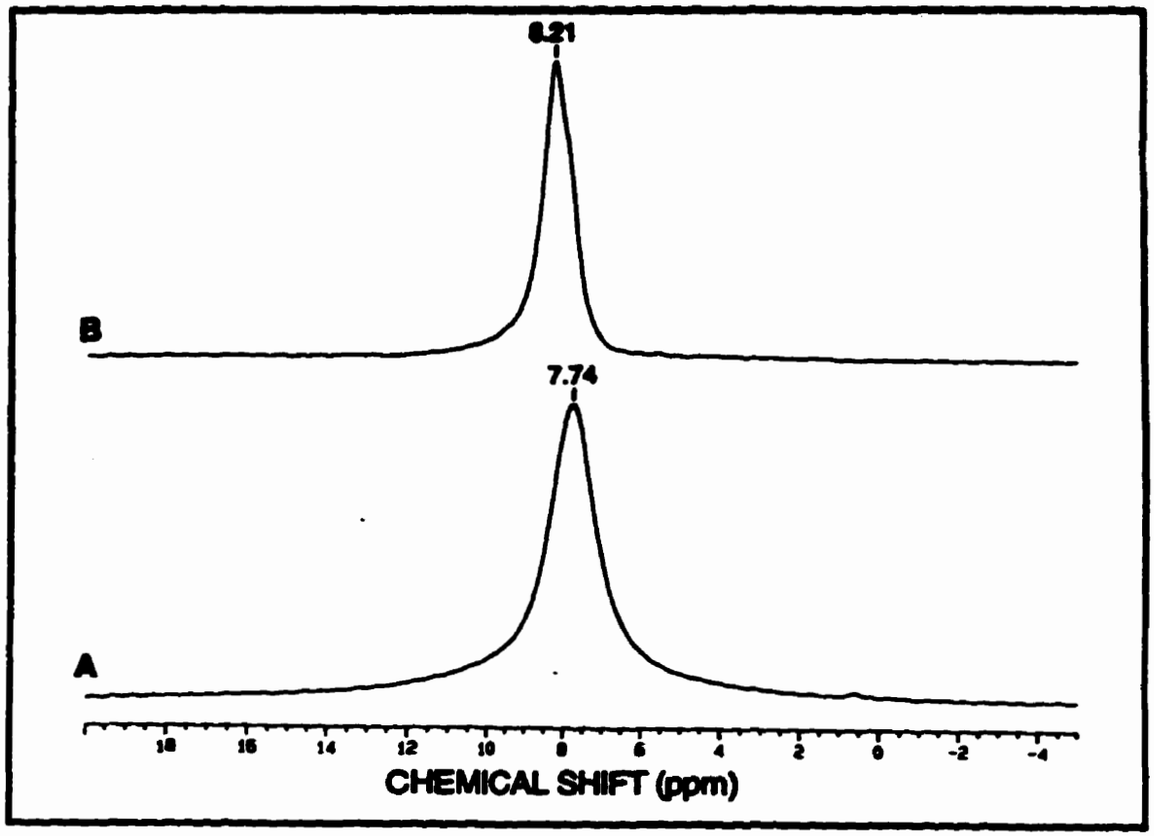

Fig. 3.22 ^{1}H MAS NMR of HPW, before (A), and after (B) exposure to NO_2.

Labelled ^{15}N proton-decoupled and ^{15}N MAS-NMR were used to provide information on the structure of $[HNO_2]^+$. An aliquot of HPW was pretreated at 150°C and exposed to pure $^{15}NO_2$ at 150°C. Enriched $^{15}NO_2$ was used since the natural abundance of ^{15}N is about 0.37% (Ref.3.3), which makes it difficult to detect using MAS-NMR spectroscopy. Both types of ^{15}N experiments showed a singlet at 4.14 ppm (Figs.3.23 and 3.24 for ^{15}N proton-decoupled (^{15}N $\{^1H\}$) and ^{15}N experiments, respectively).

B. Discussion

SORPTION AND CONVERSION OF NO_2 ON HETEROPOLY ACIDS

The amount of NO_2 sorbed and converted on the three heteropoly acids is evidently strongly dependent on the composition of the anion, but particularly on the nature of the peripheral metal atom. The two solid acids containing tungsten take up substantially larger quantities of NO_2 than that containing molybdenum. Earlier extended Hückel calculations have predicted that the protonic acidic strength of the solids containing tungsten would be higher than those containing molybdenum (Ref.3.4) and various experimental methods for the measurement of acidity have provided confirmation of this prediction (Refs.3.5 to 3.7). Evidently the acidity of these cluster compounds is dependent on their structure. More specifically, the acidity is dependent on the structure of the anion. Thus evidence exists for a relationship between the quantity of NO_2 taken up and the Brønsted acidity.

Since the surface areas of these solid acids are small (less than 10 m^2/g) the NO_2 which sorbs and reacts is evidently penetrating, as found with other polar molecules, into the bulk structure of the solid, that is, between the cations and anions. In a first step, in order to penetrate the bulk structure, NO_2 molecules react with the water molecules surrounding the protons to produce HNO_3 which desorbs into the gas phase. The stripping of the water molecules makes the protons available for NO_2 to interact and be held by them. It is of interest to note that the maximum quantity of NO_2 held on the 150°C-pretreated catalyst, as NO_2 or other nitrogen-containing molecules, corresponds (after evacuation), with HPW and HSiW, to approximately 3 molecules per Keggin Unit while with HPMo the value is only about 0.10. This provides evidence both for the bulk diffusion of NO_2 into the acids and the dependence of the interactive process between NO_2 and the acids on the acidic strength of the solids. Additionally, it was found in this study that the introduction of NO_2 does not change the structure of the Keggin Unit itself. It was also found that after exposure to NO_2 and its sorption on and into the bulk of the solid acids, the protons were largely retained within the structure.

Yang and Chen (Ref.3.8) introduced NO with O_2 on heteropoly acids and proposed that the water molecules surrounding the protons are substituted by NO with a stoichiometry of 3 NO per Keggin Unit. However, they noted that without added O_2, vanishingly small quantities of NO are sorbed. NO passed over the catalysts could only be sorbed after exposure for long period of time (days).

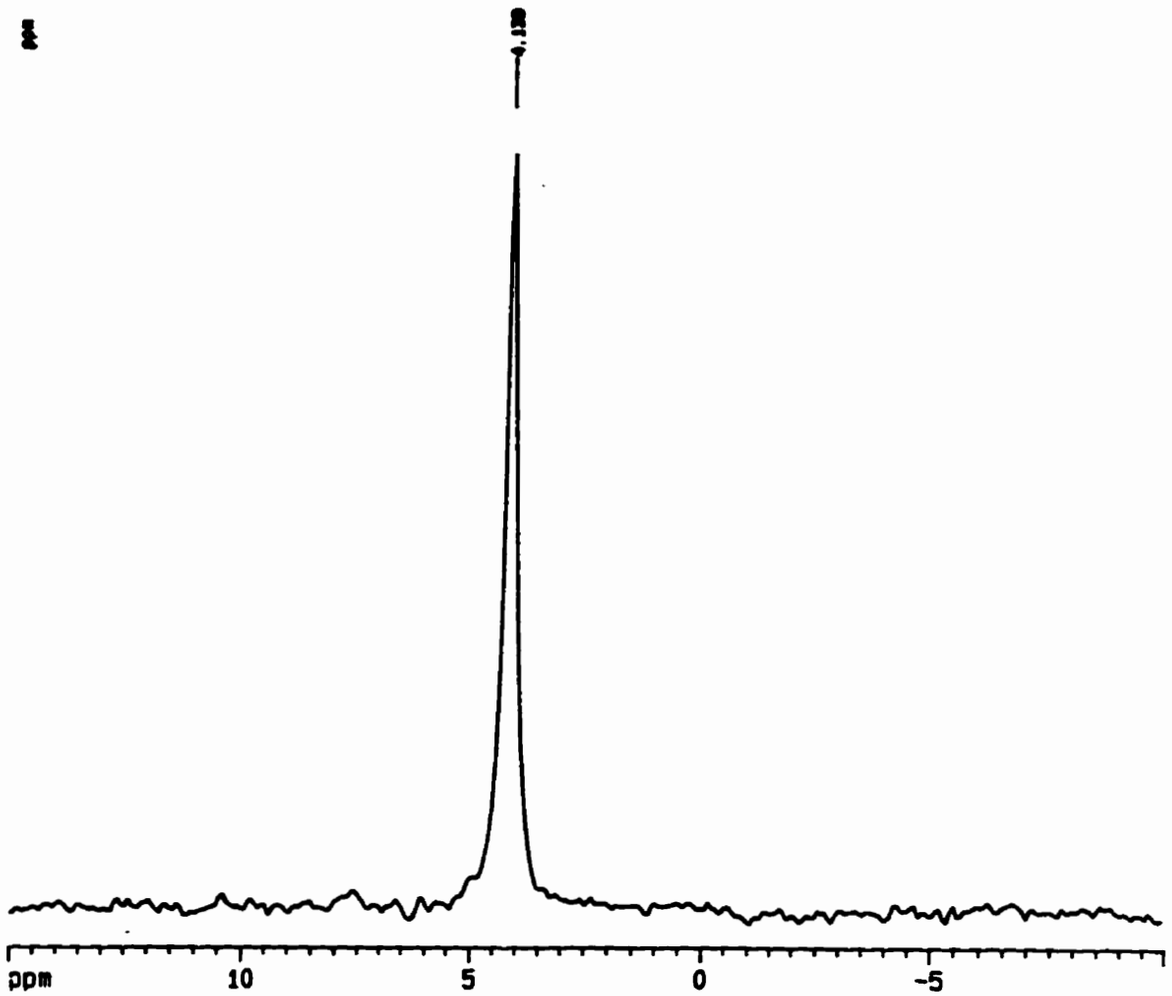

Fig. 3.23 ^{15}N {^{1}H} MAS-NMR of HPW exposed to $^{15}NO_2$ at 150°C.

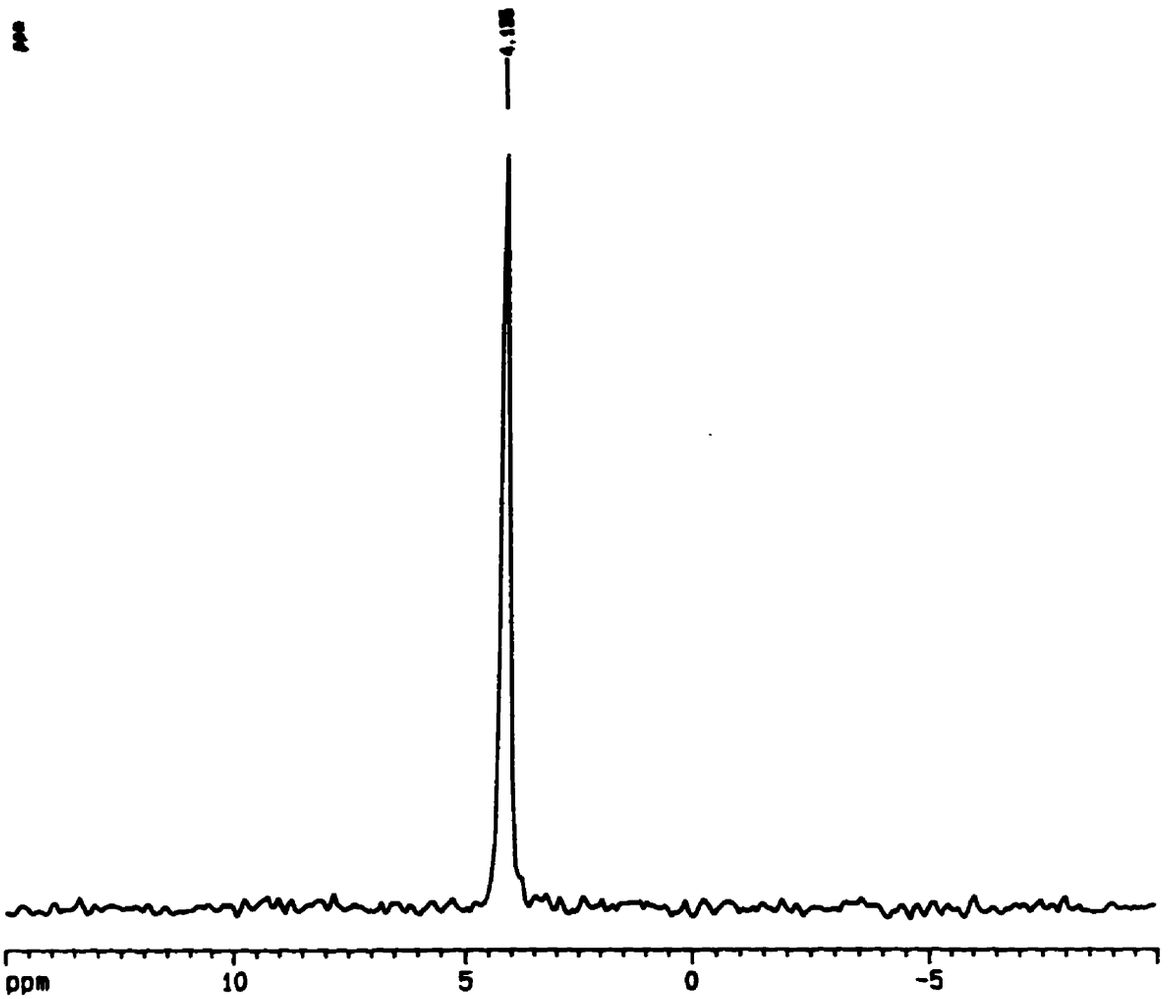

Fig. 3.24 ^{15}N MAS-NMR of HPW exposed to $^{15}NO_2$ at 150°C.

The results of Yang and Chen are not surprising since it is expected that NO will rapidly react with the added O_2 to form NO_2 (Ref.3.9).

The quantity of NO_2 sorbed is strongly dependent on the temperature to which the catalysts have previously been heated. For example HPW heated to 600°C sorbs relatively small quantities of NO_2. This suggests that the quantity of NO_2 sorbed may be related to the protons and/or water which is present on and in the solids as well as the presence of the Keggin structure. From TPD results, the quantity of water desorbed by the tungsten-containing acids at 300°C clearly decreases with increase in the amount of NO_2 which is sorbed. The desorption at this temperature has previously been shown to be associated with relatively low energies and thus to water existing on and in the solid in hydrogen-bonded form. There are two processes which are consistent with this observation: the hydrogen-bonded water may be displaced by and/or reacts with the added NO_2.

The higher temperature (approximately 550°C) TPD water peaks have previously been shown to be associated with relatively high energies and in magnitude with the approximate number of protons on and in the solid. This peak is observed to increase substantially in intensity as the amount of NO_2 contained in the solid increases. Thus the decrease of the lower temperature peak and the increase in the higher temperature peak can be rationalized through the process in which NO_2 reacts with water contained within the solid to produce nitric acid (HNO_3), nitric oxide (NO), and nitrous acid (HNO_2).

$$3\ NO_2 + H_2O \rightarrow 2\ HNO_3 + NO \qquad \text{(Eq.3.1)}$$

$$2\ NO_2 + H_2O \rightarrow HNO_3 + HNO_2 \qquad \text{(Eq.3.2)}$$

Substantial quantities of nitric acid were produced by the reaction of NO_2 with the water contained within the bulk of the acids. In the effluent, traces of NO and O_2 were detected along with the nitric acid and the excess NO_2. The NO may arise, in part, as a second product from the aforementioned reaction (Eq.3.1) while the O_2 may result from the decomposition of HNO_3. Experiments in which HNO_3 was passed over HPW at 300°C produced 48% mole O_2 per mole HNO_3 injected.

NO_2 can directly react with water to give nitric acid (Eqs.3.1 and 3.2). NO cannot react directly with water without the presence of a base (OH^-) to produce HNO_2 and N_2O. Under the present reaction conditions, nitrous acid would rapidly decompose to NO_2, NO and water (Ref.3.10).

$$4NO + H_2O \rightarrow 2HNO_2 + N_2O \qquad \text{(Eq.3.3)}$$

$$2HNO_2 \leftrightarrow NO_2 + NO + H_2O \qquad \text{(Eq.3.4)}$$

In the sorption experiments of NOx on the heteropoly acids, no nitrous oxide (N_2O) was detected.

Protonated nitric acid ($H_2NO_3^+$) is very unstable and readily dissociates into nitronium ion (NO_2^+) and water (Ref.3.10).

$$H_2NO_3^+ \rightarrow NO_2^+ + H_2O \qquad \text{(Eq.3.5)}$$

Nitric acid will act as a base when in contact with a stronger acid to give nitronium ions. A good example is the mixture of nitric acid and sulfuric acid (Ref.3.11). Sulfuric acid is a stronger acid than nitric acid and nitronium bisulfate is the predominant product found in solution.

$$HNO_3 + 2H_2SO_4 \leftrightarrow NO_2^+ + H_3O^+ + 2HSO_4^- \qquad \text{(Eq.3.6)}$$

The formation and existence of nitronium salts are well understood (Refs.3.11 to 3.19).

By comparison the formation of the nitrosonium ion (NO^+) is usually achieved by the ionization or protonation of liquid dinitrogen tetroxide (N_2O_4) (Ref.3.10).

$$N_2O_4 + H^+ \rightarrow HNO_3 + NO^+ \qquad \text{(Eq.3.7)}$$

If placed in sulfuric acid, dinitrogen dioxide will give equimolar quantities of NO^+ and NO_2^+ (Ref.3.20).

$$N_2O_4 + 3H_2SO_4 \leftrightarrow NO^+ + NO_2^+ + 3HSO_4^- + H_3O^+ \qquad \text{(Eq.3.8)}$$

A mixture of dinitrogen trioxide and sulfuric acid also produces mainly NO^+.

$$N_2O_3 + 3H_2SO_4 \leftrightarrow 2NO^+ + 3HSO_4^- + H_3O^+ \qquad \text{(Eq.3.9)}$$

Dinitrogen pentoxide placed in sulfuric acid, and also in nitric acid, will produce only NO_2^+ (Refs.3.19 and 3.21).

$$N_2O_5 + 3H_2SO_4 \leftrightarrow 2NO_2^+ + 3HSO_4^- + H_3O^+ \quad \text{(Eq.3.10)}$$

However, the presence of water will transform the nitronium and nitrosonium ions by converting them to nitric and nitrous acid, respectively (Ref.3.20).

$$NO_2^+ + 2HSO_4^- + H_3O^+ \leftrightarrow HNO_3 + 2H_2SO_4 \quad \text{(Eq.3.11)}$$

$$NO^+ + 2HSO_4^- + H_3O^+ \leftrightarrow HNO_2 + 2H_2SO_4 \quad \text{(Eq.3.12)}$$

Another route for the formation of the protonated nitronium ion is the direct association of the NO_2 with a proton as in Equation 3.13;

$$NO_2 + H^+ \rightarrow HNO_2^+ \quad \text{(Eq.3.13).}$$

As mentioned earlier, HNO_2 is a thermally unstable molecule and readily decomposes. However, the protonated nitronium ion, HNO_2^+, is thermally more stable than nitrous acid. The HNO_2^+ molecules will then decompose at approximately 550°C to give mainly NO_2 in the gas phase, and traces of water from the associative reaction of the residual protons and protruding oxygen atoms from the Keggin Units.

The chemical analysis of the strong desorption peak at approximately 500-550°C (see Figs.3.10 and 3.11) revealed that its composition was mainly NO_2. However due to thermal decomposition, quantities of NO and N_2 were detected.

Yang and Chen (Ref.3.8) also reported that the quantity of NO and N_2 in the effluent during the thermal desorption was strongly dependent on the heating rate. If NO^+ (or HNO^+) was the molecular species sorbed on the heteropoly acid, equimolar quantities of water and/or oxygen would be expected to desorb concomitantly with the N_2 from the reaction of the protons and the extra oxygen atoms provided by the oxide of nitrogen. Nitric oxide is thermodynamically unstable and undergoes disproportionation (Ref.3.10). The detection of N_2 without N_2O is surprising if NO (as NO^+ or HNO^+) is the species sorbed.

$$4NO \rightarrow N_2O_3 + N_2O \quad \text{(Eq.3.14)}$$

$$N_2O_3 \leftrightarrow NO + NO_2 \quad \text{(Eq.3.15)}$$

However, NO_2 would only be detected if species like NO_2^+ or HNO_2^+ were sorbed on the acids. The thermal desorption of NO_2, with minimum decomposition, is possible if done at slow heating rate. The formation of NO and N_2 would only be due to thermal decomposition in the gas phase. The formation of nitric acid, according to Equations 3.1 and 3.2, by injection of water on a NO_2-saturated sample would only be possible if species like NO_2, NO_2^+, or HNO_2^+ exist on the catalyst.

As mentioned earlier, Yang and Chen (Ref.3.8) reported the production of N_2 when the adsorption products on the catalyst HPW were thermally desorbing at 400°C. In the present work, nitrogen (N_2) was not detected as a desorption product, for any desorption temperature. They also reported the production of N_2 when HPW was exposed to NO. In the present work with the heteropoly acids, no nitrogen was detected in the gas phase after the sorption of NO_2 or NO on the three acids at both 150°C and 300°C. Furthermore, the detection of N_2 in the effluent may result from the detection method used. The injection of NO, NO_2, or HNO_3 in a mass spectrometer will give a signal at 28 amu. However, it was found in the present work that HPW was capable of sorbing very little NO (0.07 NO/KU as seen by adorption-desorption isotherm measurements) and much more if NO_2 was previously sorbed.

In view of the observations showing that the preponderance of the effluent gases from the catalysts on exposure to NO_2 is HNO_3 the interaction between NO_2 and H_2O appears to play a major role in the overall process. The change in the production of HNO_3 at 150°C can be rationalized from the stoichiometric Equations 3.1 and 3.2. The position of the maximum observed for the tungsten-containing acids is dependent on the quantity of water contained in and on the solid acids and moves to a higher pulse number when the water content is higher, reflecting a higher production of HNO_3. With a high water content, more NO_2 pulses will be needed to remove the water molecules (as H_2O and HNO_3) to eventually enter the cation cage. Even though the water content changes according to the pretreatment (temperature and pressure), the number of water molecule directly associated with the protons remains basically the same for low pretreatment temperature (100-300°C). Thus the production of HNO_3 will show approximately the same maximum value for a given acid. Hence, as it was found, the quantity of NO_2 stored in the secondary Keggin structure will be smaller for a water-stripped acid. This behaviour is not surprising if the NO_2 has to enter the bulk to associate with the proton as $[HNO_2]^+$ (either from the direct association of nitrogen dioxide or the protonation of nitric acid).

The H^+ sites were found to be regenerated by rehydrating the acid. A sequence of pulses of water injected at 150°C on HPW containing previously sorbed NO_2 showed that HNO_3 was desorbed in diminishing quantity with each pulse, while the quantity of NO_2 remaining on the catalyst also decreased with each pulse (Table 3.3). Thus the NO_2 in the

TABLE 3.3

REGENERATION AND PRODUCTION OF HNO_3 BY INJECTION OF WATER ON NO_2-SATURATED HPW AT 150°C

Water Introduced (μl)[a,b]	HNO_3 Detected in Effluent (μmol)
1	3.9
2	2.1
3	1.7
4	1.2
5	1.0
6	1.1
7	0.8
total	11.8[c,d]

a Injection of water (55.6μmoles/μL) on 0.075 g (26.0μmoles) of HPW pretreated in helium flow (60 mL/min) at 150°C for 45 min and then saturated with NO_2 (30 mL/min) for 5 min) at 150°C.

b 71.3 μmol of NO_2 were sorbed on HPW at 150°C (at saturation) (2.7 NO_2/KU).

c 59.9 μmol of NO_2 remained on HPW (2.3 NO_2/KU).

d The NO_2 removed from HPW as HNO_3 can be replaced by re-exposing HPW to NO_2.

secondary Keggin structure is also available for water molecules to react. The displaced NO_2 was readily replaced by again contacting the catalyst containing the residual NO_2 with additional quantities of NO_2. At low temperature, the production of HNO_3 and the sorption of NO_2 can be repeated indefinitely. It is also relevant to note that HPW has a relatively small capacity for HNO_3 with only 2.3 and 3.1 μmoles of HNO_3 (on 0.076 g or 26.0 μmoles HPW) sorbed at 150 and 300°C, respectively.

When NO_2 is injected on the solid acids, the production of nitric acid presumably follows Equations 3.1 and 3.2, one of which suggests that NO may be among the expected products. Nitric oxide was not seen in the gas phase with HPW and HSiW at held at 150°C. Obviously the NO produced, according to Equations 3.1, 3.2, and 3.4, sorbs or reacts with species on the catalysts. It is believed that NO would react with probably HNO_3 (or NO_3^-) according to Equation 3.16 or associates with NO_2 (as in Eq.3.17), and the nitrogen dioxide formed will react with water molecules and/or sorb.

$$NO + HNO_3 \leftrightarrow NO_2 + HNO_2 \qquad \text{(Eq.3.16)}$$

$$NO + NO_2 \leftrightarrow N_2O_3 \qquad \text{(Eq.3.17)}$$

Of course, if O_2 is produced (from the decomposition of HNO_3), NO could react with it to produce NO_2. The NO sorption is maximum at 150°C, for between 10 and 15 μmoles of NO_2 sorbed (in whatever form). As expected for pulse experiments, the adsorption of NO_2 in the reactor is not homogeneous but linear from the head to the foot of the catalyst bed. Furthermore, it is known from TPD measurements that HNO_3 desorbs with the water molecules and/or thermally decomposes. When NO_2 is injected on the solid acids, it sorbs and reacts with water molecules to produce HNO_3 and NO (as in Equation 3.1). Part of the HNO_3 produced will sorb (probably as NO_3^-) in a later position in the reactor (for T<300°C) and any NO produced (or injected) will react according to Equation 3.16 or 3.17. Furthermore, NO_2 would also displace HNO_3 from the solid to the gas phase, since increasing the amount of NO_2 on the catalyst decreases the amount of water on it and the amount of NO being pick-up when injected after NO_2 aliquots. Evidences for the formation of N_2O_3 were found by infrared spectroscopy (Fig.3.16) at 1304 cm^{-1} when the acid was saturated with NO_2 at 150°C first and then followed by NO at 25°C (Ref.3.22). Thermodynamically, and in reasonable amount, a direct association of NO with NO_2 is only possible at low temperature.

In view of the chemistry, the formation of nitronium and nitrosonium ions, and the present catalytic system, strong evidence exists for the protonation of nitrogen dioxide (or nitric

acid) and the formation of $[HNO_2]^+$. The route for the formation of $[HNO_2]^+$, with the injection of NO_2, is much more direct than the formation of NO^+ or $[HNO]^+$with injection of NOx on the heteropoly acids. However, the formation of quantities of NO^+ is not to be completely rejected.

INFRARED SPECTROSCOPY OF HETEROPOLY ACIDS

Although infrared spectroscopy is a useful tool for the investigation of sorbed molecules, overlap of bands may complicate the interpretation of results (Ref.3.23). Heteropoly oxometalates display large absorption bands in a region of the infrared spectrum where a large number of small molecules would show characteristic ir-bands.

After saturation of HPW with NO_2 a new, unsymmetrical, band appeared at 2264 cm^{-1}, and using difference spectrum, another band could be seen at 600 cm^{-1}. For NO_2-HSiW the former band was located at 2257 cm^{-1}. Although precautions were taken to minimize the loss of sorbed nitrogen species, the new band was, nevertheless, not intense. Possible new vibrational bands in the 500-1800 cm^{-1} region were most likely shadowed by the strong Keggin bands.

After saturation of HPW with $^{15}NO_2$, the aforementioned band shifted to 2215 cm^{-1}, while the remainder of the spectrum remained unchanged.

The active infrared bands of molecules of interest containing ^{14}N can be found in Table 3.4 (Ref.3.24). The ν, ν_1, ν_2, and ν_3 correspond to the stretching, symmetric stretching, bending, and antisymmetric stretching modes of vibration, respectively.

The normal stretching vibration of NO is found at 1876 cm^{-1}. However, one NO electron occupies the π^*-orbital. This electron is expected to be transferred to the metal during the formation of the bond, giving the nitrosonium ion NO^+ with a full triple bond (Ref.3.23). This alteration of the electron density in this antibonding orbital will change greatly the vibration frequency. Although the stretching frequency of NO^+ is found at approximately 2300 cm^{-1}, its magnitude will decrease with increase of the size of the anion (Refs.3.23 and 3.24). The highest stretching frequency is found with $(NO)_2GeF_6$ at 2391 cm^{-1}, and the lowest with $(NO)_2TiCl_6$ at 2165 cm^{-1}. Therefore, the sorption of NO, and formation of NO^+, as proposed by Yang and Chen (Ref.3.25), on 12-tungstophosphoric acid is expected to further decrease the stretching frequency of NO^+. The observation of a band at 2264 cm^{-1} would correspond approximately to the molecular radius of $CuCl_2$. Obviously the Keggin Units are much larger than copper (II) chloride. Another factor affecting the stretching frequency is the type of bond between NO (or NO^+) and a metal (Ref.3.23). For covalent, coordination, ionic, and ion-coordination bonds, the frequency ranges are found at approximately 1600-1800, 1700-1870, 1500-2400, and 1900-2100 cm^{-1}, respectively.

TABLE 3.4

INFRARED FREQUENCIES[a] OF MOLECULES OF INTEREST

Molecule:	NO[b]	NO^+[c]	NO_2[b]	NO_2^+[c]
Modes				
ν (stretch)	1876.0	2150-2400		
ν_1 (sym)			1320.0	Inactive
ν_2 (bend)			749.7	538-605
ν_3 (antisym)			1616.9	2360-2392
$\nu_2+\nu_3$			2355.2	

a cm^{-1}.
b Gas phase.
c Range for most inorganic salts.

Using the simple harmonic oscillator model for a normal and isotopic diatomic molecule gives a very good approximation for the ratio of the isotopic fundamental stretching frequencies of such real (anharmonic) molecules (Ref.3.26).

$$\nu^i/\nu = (\mu/\mu^i)^{1/2} \qquad \text{(Eq.3.18)}$$

Where ν^i and ν are the stretching frequencies for the isotopic and normal molecules, respectively, and μ and μ^i are the reduced masses for the normal and isotopic molecules, respectively. Using Equation 3.18, ν^i/ν for ^{15}NO and ^{14}NO can be calculated as 0.9989. Using the experimental values (2215 cm^{-1} and 2264 cm^{-1}, for ^{15}N and ^{14}N labelled molecules, respectively) we get, $\nu^i/\nu = 0.978 \pm 0.001$. These two values are significantly different. The number obtained from our results compares to that for NO_2 calculated from literature values (Ref.3.24); ν^i/ν for ^{14}NO, $^{15}NO = 0.9824$, and $\nu_3{}^i/\nu_3$ for $^{14}NO_2$, $^{15}NO_2 = 0.9785$.

The same calculation can be done for $^{15}NO_2$ and $^{14}NO_2$. However, since NO_2 is not a linear diatomic molecule, another equation must be used. For harmonic, non-linear, symmetrical labelled Y-X-Y molecules, Equation 3.19 (Ref.3.26) can be used:

$$(\omega^i_3/\omega_3)^2 = (m_X m_Y(m^i_X+2m^i_Y\sin^2\alpha))/(m^i_X m^i_Y(m_X+2m_Y\sin^2\alpha)) \qquad \text{(Eq.3.19)}$$

where ω_3 is the normal antisymmetric stretching frequency of the Y-X-Y molecule, m_X and m_Y are the atomic weights of its X and Y atoms, α is half the YXY angle, and the superscript i denotes quantities belonging to the respective labelled molecule. ω_3 has been used instead of ν_3 in order to emphasize that the formula holds strictly only for the zero-order frequencies (Ref.3.27). Using Equation 3.19 and a literature value of 134° for the O-N-O angle (Ref.3.9), we get $\omega^i_3/\omega_3 = 0.978$, which is exactly the ratio found with the experimental values. This result would suggest that the antisymmetric stretching frequency of NO_2 is responsible for the new infrared band. However, according to Table 3.4, the antisymmetric stretching frequency of NO_2 is normally found at 1616.9 cm^{-1}.

It is found that the angle in the triatomic molecule has little effect on the ratio ω^i_3/ω_3. For harmonic linear Y-X-Y molecules, the following expression (Ref.3.26) can be used to calculate ω^i_3/ω_3:

$$(\omega^i_3/\omega_3)^2 = (m_Y(1+2m^i_Y/m^i_X))/(m^i_Y(1+2m_Y/m_X)) \qquad \text{(Eq.3.20).}$$

Using Equation 3.20 for free NO_2^+, which is a linear molecule, we obtain a ratio ω^i_3/ω_3 of 0.977. If we compare this last result with the values from Table 3.4, the fact that NO_2^+ exists

sorbed on HPW (or HSiW), and the observation of a band at 2264 cm^{-1}, which is a little lower than the normal range found in Table 3.4, for $\nu_3 NO_2^+$, one can conclude that if it is NO_2^+, then the molecule must be bent and not purely linear.

It was also reported in the literature (Refs.3.9 and 3.24) that when NO_2 (as NO_2^+) is attached to a group (-Z), the antisymmetric stretching frequency of NO_2^+ will decrease with an increase in the electronegativity of the latter. For example, the NO_2^+ antisymmetric stretching frequency in FNO_2 is found at 1793 cm^{-1}, whereas in R_3CNO_2 (where R is any organic group) it is found at 1540 cm^{-1}. For the case where unbound, purely ionic, NO_2^+, the antisymmetric stretching frequency is found at approximately 2375 cm^{-1}.

The definite assignment of the additional infrared band is difficult because of the small intensity of the band and the screening effect of the Keggin Units on the infrared signal. Raman spectroscopy can provide supplementary information on the nature of the sorbed specie(s).

RAMAN SPECTROSCOPY OF HETEROPOLY ACIDS

Raman spectroscopy has been extensively used to study sorbed molecules at the surface of catalysts (Ref.3.28, and references therein). Improvements in the sampling techniques, excitation sources and detectors have made the technique extremely sensitive. Even molecules sorbed on optically opaque samples can be detected. It should be noted that Raman and infrared spectroscopy are complementary techniques to each other.

All Raman spectra of the acids present the usual Keggin bands between 0 and 1100 cm^{-1}. The assignments for these vibrational modes are found in Reference 3.29.

Yang and Chen, using only infrared spectroscopy, attributed the 2264 cm^{-1} infrared band to the stretching of NO^+ (Ref.3.25). This band could also, as explained previously, come from the ν_3 antisymmetric stretching mode. However, this mode is normally Raman inactive for $D_{\infty h}$ molecules. This mode would be Raman inactive if it was a purely NO_2^+ cation. The above observations and calculations would suggest that the angle in NO_2^+ is less than 180° when the molecule is sorbed on the acids, thus ν_3 of NO_2^+ (now of C_{2v} symmetry) would now become Raman active. Further, the symmetrical stretching (ν_1) band is expected to be polarized. The experimental results suggest that this band is the antisymmetrical stretching, ν_3.

The Raman activity of ν_3 for NO_2^+ was observed and quantified for solid nitronium salts by Barbes and Vast (Ref.3.30). The Raman activity of $\nu_3 NO_2^+$ was caused by the non-linearity of the molecule due to anion-cation interactions in the solid salts. The partial covalent bond between the anion and the cation would be responsible for the change in the symmetry of the molecule. The authors quantified the NO_2^+ bands for a series of salts (from totally covalent to totally ionic bondings) using infrared and Raman spectroscopy, relating the shift of frequency to

the angle of NO_2^+. From their calculations, the angle of NO_2^+ on the heteropoly acids would be between 160 and 170°. In gaseous NO_2, the angle O-N-O is 134° (Ref.3.9).

If the molecular specie was NO^+, no other band would appear in the Raman spectrum. The observation of a second band at approximately 610 cm^{-1}, assigned to the bending mode of NO_2^+ (ν_2), strongly suggests that NO (or NO^+) is not the sorbed molecular specie. For most nitronium salts ν_2 is found between approximately 500 cm^{-1} and 800 cm^{-1}. Although the heteropoly acids are not porous materials and thus do not contain micropores, it is expected, however, that since NO_2 is penetrating into the bulk and associates with the proton, the high value found for $\nu_2NO_2^+$ on heteropoly acids could then be explained by the presence of the proton and the surrounding Keggin Units. The shoulder on the band above 2200 cm^{-1} would also suggest that $[HNO_2]^+$ exists in different sites with a slightly smaller angle. It is possible that the NO_2 molecules bonded to the surface protons (compared to bulk protons) could be responsible for this shoulder on the band.

^{15}N-MAS-NMR OF HETEROPOLY ACIDS

Since the aforementioned observations provide evidence for the association of NO_2 molecules with the protons contained on and in the heteropoly acids but provide little or no information on the geometrical configuration of $[HNO_2]^+$ species, the application of NMR spectroscopy appeared both interesting and relevant.

While the chemical shift in NMR spectroscopy gives only a crude indication of the environment of individual nuclei, nitrogen NMR is very sensitive to the environment of the nuclei. It was observed that, for simple molecules containing nitrogen, the shielding of the nitrogen was proportional to the angle -N- (Ref.3.31). Thus, NO_3^- is more deshielded than NO_2^-, which is more deshielded than NO or NO_2^+.

Two different techniques are used in the present work; proton-decoupling (^1H-decoupled) and heteroatom coupling experiments. The proton-decoupling NMR experiment is the measurement of the spin-nuclei itself, where the spin-coupling of the protons are removed. Since only one NO_2 is apparently associated with each proton, a singlet is expected. Since only one peak at 4.14 ppm (Fig.3.23) was detected, the presence of a single monomer ^{15}N was confirmed by the experiment. Gaseous or liquid NO_2 cannot be measured by NMR because of its doublet state. NO_2^+, which is linear, is expected to have a chemical shift between -100 ppm and -150 ppm, whereas NO^+ and NO_3^- are expected to show a chemical shift of approximately -50 and -10 ppm, respectively. Further, all ^{15}N have the same environment since the single peak is symmetrical in shape. A chemical shift of 4.14 ppm corresponds approximately to a bent and charged O-N-O molecule bonded to a proton and an oxygen of the anion.

Heteroatom-proton coupling experiments consist in measuring the coupling between the spin of the heteroatom, here ^{15}N, and the spin of proton(s). For our system, $[HNO_2]^+$, a single peak is expected if the proton is situated far from the ^{15}N. However, if the proton is "bonded" to the ^{15}N, a doublet would be seen because of spin-coupling between the two nucleii. Figure 3.24 shows the ^{15}N-^1H coupling experimental result. Only a single peak is observed also at 4.14 ppm. This suggests that the proton is associated with the oxygen atom and not the nitrogen atom of NO_2.

C. Conclusions

NO_2 has been shown to diffuse into the bulk structure of heteropoly acids, particularly those containing tungsten, where reaction occurs with the water contained therein, producing HNO_3, which is readily desorbed. The bared protons are then available to sorb a NO_2 molecule (1 NO_2 per proton). Residual quantities of water are held within the solids apparently in association with the protons.

Although relatively small quantities of NO are sorbed on any of the present solid acids, prior sorption of NO_2, on HPW and HSiW, significantly increases the sorption of NO. The previously sorbed NO_2 facilitates the formation of N_2O_3 on addition of NO at 25°C.

The differences seen with changes of the temperature of the reactor is believe to come only from changes in the rates rather than changes in the mechanisms since no new products were observed in the gas phase with changes of the temperature. However, increasing the pretreatment temperature will change the amount of HNO_3 produced as well as (to a certain extent) the quantity of NO_2 pick-up.

The tungsten-containing acids show a much higher capacity for storing NOx than those containing molybdenum. This behaviour is found to be consistent with the Brønsted acidity of these compounds. It was also found that the number of NO_2 molecules on the acids was approximately that of the protons per anion on the acids, suggesting a one-to-one association of NO_2 molecules with protons. However, the NO_2 bonded to the protons may cause a change in the charge distribution inside the Keggin Unit itself, which could result in a stronger bond for the protons (those which are not associated with NO_2) left within the solid acids. In the case of HSiW, this is even more convincing since approximately $3NO_2$ are distributed around the Keggin Unit, leaving one proton without NO_2. The acidic strength of this last proton could be significantly reduced, preventing the protonation of a fourth NO_2.

From the observations of the sorption of NO_2 by the heteropoly acids, and most especially the infrared and Raman observations and calculations, it is evident that $[HNO_2]^+$ exists on these acids (HPW and HSiW). Moreover, the results suggest that the NO_2 is bonded to the proton causing the O-N-O in $[HNO_2]^+$ to be bent. This in turn would cause the

antisymmetric stretching mode to be Raman active. NO^+ (or $[HNO]^+$) as a possible species is rejected because the expected shift of the NO^+ stretching frequency, caused by the size of the anions, does not support the present observations, and the fact that another band, from O-N-O bending mode, was observed with Raman spectroscopy.

From the NMR results, the NO_2 is associating with the proton via one of the oxygen atoms. The positive charge is believed to be on the proton and is responsible for the increase of the angle of NO_2 from 134° to approximately 165°.

The $[HONO]^+$ formed is accountable for the spectroscopic results. The protonation of NO_2 on the heteropoly acids is responsible for the formation of the new nitronium salt, $(HNO_2)_3PW_{12}O_{40}$.

With the exception of the Raman spectra, the ^{15}N NMR results, and the infrared calculations with $^{15}NO_2$, the results presented in this section were published in References 3.32, 3.33, and 3.34.

REFERENCES

3.1 Addison, W.E., and Barrer, R.M., *J.Chem.Soc.*, **757** (1955).

3.2 Hodnett, B.K., and Moffat, J.B., *J.Catal.*, **88**, 253 (1984).

3.3 Weast, R.C., and Astle, M.J., *CRC Handbook of Chemistry and Physics 62nd Edition*, CRC Press Inc., Boca Raton, 1981.

3.4 Moffat, J.B., *J.Mol.Catal.*, **26**, 385 (1984).

3.5 Gosh, A.K., and Moffat, J.B., *J.Catal.*, **101**, 238 (1986).

3.6 Nayak, V.S., and Moffat, J.B., *Appl.Catal.*, **47**, 97 (1989).

3.7 Jozefowicz, L.C., Karge, H.G., Vasilyeva, E., and Moffat, J.B., *Microporous Mater.*, **1**, 313 (1993).

3.8 Yang, R.T., and Chen, N., *Ind.Eng.Chem.*, **33**, 825 (1994).

3.9 Jolly, W.L., *The Inorganic Chemistry of Nitrogen*, W.A. Benjamin, Inc., New York, 1964.

3.10 Lagowski, J.J., *Modern Inorganic Chemistry*, Marcel Dekker, Inc., New York, 1973.

3.11 Bennet, G.M., Brand, J.C.D., and Williams, G., *J.Chem.Soc.*, 869 (1946).

3.12 Goddard, D.R., Hughes, E.D., and Ingold, C.K., *Nature*, **158**, 480 (1946).

3.13 Qureshi, A.M., Carter, H.A., and Aubke, F., *Can.J. of Chem.*, **49**, 35 (1971).

3.14 Nebgen, J.W., McElroy, A.D., and Klodowski, H.F., *Inorg.Chem.*, **4**, 1796 (1965).

3.15 Truter, M.R., Cruickshank, D.W.J., and Jeffrey, G.A., *Acta Cryst.*, **13**, 855 (1960).

3.16 Goddard, D.R., Hughes, E.D., and Ingold, C.K., *J.Chem.Soc.*, 2559 (1950).

3.17 Ingold, C.K., Millen, D.J., and Poole, H.G., *J.Chem.Soc.*, 2576 (1950).

3.18 Millen, D.J., *J.Chem.Soc.*, 2589 (1950).

3.19 Millen, D.J., *J.Chem.Soc.*, 2606 (1950).

3.20 Millen, D.J., *J.Chem.Soc.*, 2600 (1950).

3.21 Ingold, C.K., and Millen, D.J., *J.Chem.Soc.*, 2612 (1950).

3.22 Simon, A., Horakh, J., Obermayer, A., and Borrmann, H., *Angew.Chem.Int.Ed.Engl.*, **31**, 301 (1992).

3.23 Davydov, A.A., *Infrared Spectroscopy of Adsorbed Species on the Surface of Transition Metal Oxides*, John Wiley & Sons, England, 1984.

3.24 Lippard, S.J., *Progress in Inorganic Chemistry; Volume 27*, John Wiley & Sons, New York, 1980.

3.25 Chen, N., Yang, R.T., *J.Catal.*, **157**, 76 (1995).

3.26 Pinchas, S., and Laulicht, I., *Infrared Spectra of Labelled Compounds*, Academic Press, London, 1971.

3.27 Herzberg, G., *Molecular Spectra and Molecular Structure, II. Infrared and Raman Spectra of Polyatomic Molecules*, D.Van Nostrand Co., New Jersey, 1968.

3.28 Stencel, J.M., *Raman Spectroscopy for Catalysis*, Van Nostrand Reinhold, New York, 1990.

3.29 Rocchiccioli-Deltcheff, C., Thouvenot, R., et Franck, R., *Spectrochimica Acta*, **32A**, 587 (1976).

3.30 Barbes, H., et Vast, P., *Revue de Chimie Minérale*, **8**, 851 (1971).

3.31 Mason, J., *Multinuclear NMR*, Pleneum Press, New York, 1987.

3.32 Belanger, R., and Moffat, J.B., *J.Catal.*, **152**, 179 (1995).

3.33 Belanger, R., and Moffat, J.B., *Environm. Sci. and Tech.*, **29**, 1681 (1995).

3.34 Belanger, R., and Moffat, J.B., *Catal. Letters*, **32**, 371 (1995).

CHAPTER IV

SORPTION AND REACTION OF NO AND NO_2 ON AMMONIUM 12-TUNGSTOPHOSPHATE (NH_4PW)

A. Results

On exposure of NH_4PW to NO_2 at 150°C the principal product in the effluent is, initially, N_2 (Fig.4.1). However, with continued addition of pulses of NO_2 the selectivity to N_2 decreases, becoming vanishingly small after approximately 100 μmoles have been injected. The selectivity to NO is relatively high for the first injection of NO_2 and decreases as the number of pulses increases. The selectivity to N_2O and O_2 remains insignificant for all injections.

In addition to the products found in the reactor effluent, quantities of unreacted NO_2 are also present. In the first pulse, the quantity corresponds to approximately 29% of the NO_2 injected. The NO_2 detected in the effluent increases rapidly with increase in the number of pulses and reaches a plateau at the third pulse.

The quantities of the various products as well as NO_2 found in the effluent after exposure of NH_4PW to various pulses of NO_2 at 300°C are summarized in Figure 4.2. With the first pulse of NO_2 the selectivity to N_2 is now high while the quantity of NO_2 found in the effluent is very low. With subsequent pulses the quantities of N_2 and NO_2 decrease and increase, respectively, until after approximately 100 μmoles of NO_2 have been added, the selectivity to N_2 is vanishingly small and the quantity of NO_2 continues to increase. At 300°C, the selectivity to N_2O is comparable to N_2 for the first injection and decreases almost linearly with increasing injection number to reach vanishingly small quantities at high pulse number. Concomitantly with these changes the selectivity to O_2 increases, passes through a maximum and decreases while that of NO remains relatively small.

In the ammonium salt prepared as stoichiometric, at room temperature approximately 3 ammonium cation per Keggin Unit are contained within the structure (Fig.4.3). However, with an increase of pretreatment temperature, and without any introduction of NOx, approximately one molecule of ammonia per Keggin Unit is lost from the catalyst at temperatures up to 450°C. Above 450°C, more ammonia desorbs and from 500°C the remaining ammonia molecules are desorbing as well as releasing water molecules from the association of the protons and some of the protruding oxygen atoms of the anions. After thermal decomposition, the salt does not sorb any quantities of ammonia either from the gas phase or aqueous solution.

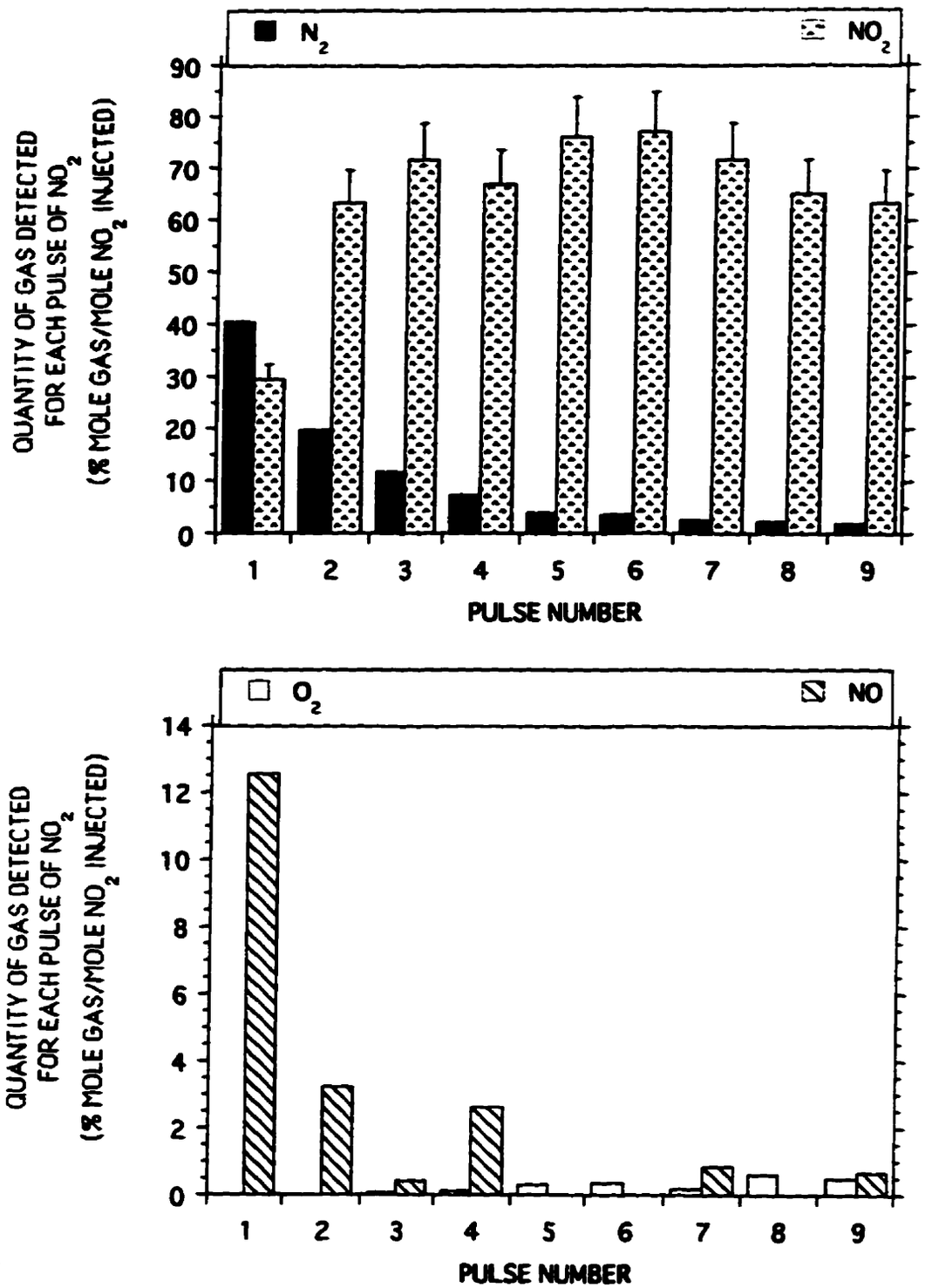

Fig. 4.1 Concentration of N_2, NO_2, N_2O, O_2, and NO, for each pulse of NO_2, in the effluent of a microreactor containing stoichiometric NH_4PW held at 150°C. Mass in reactor = 0.075g (38.8μmoles). Pulse size = 17 μmol NO_2. Helium flow = 15 mL/min.

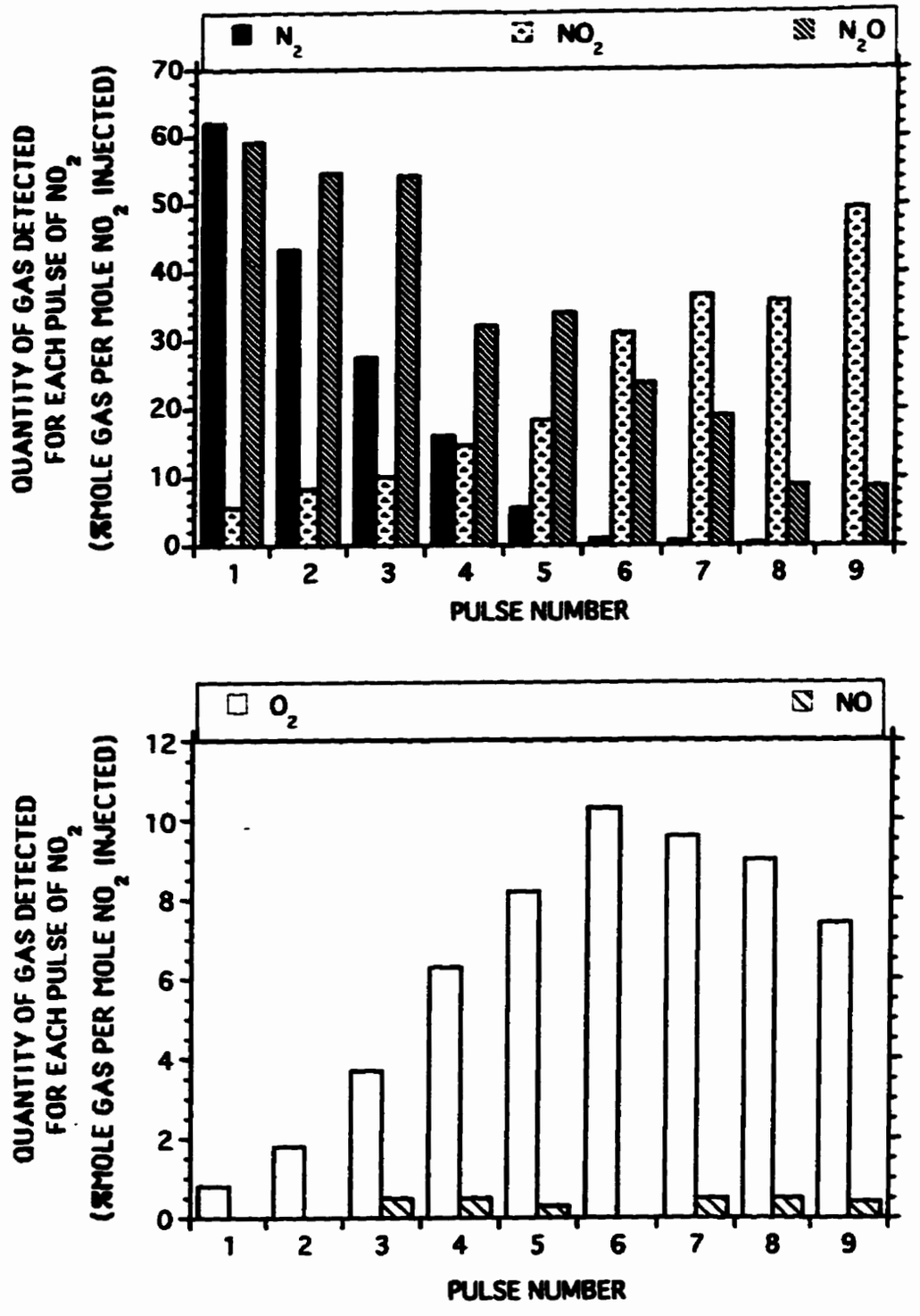

Fig. 4.2 Concentration of N_2, NO_2, N_2O, O_2, and NO, for each pulse of NO_2, in the effluent of a microreactor containing stoichiometric NH_4PW held at 300°C. Mass in reactor = 0.075g (38.8μmoles). Pulse size = 17 μmol NO_2. Helium flow = 15 mL/min.

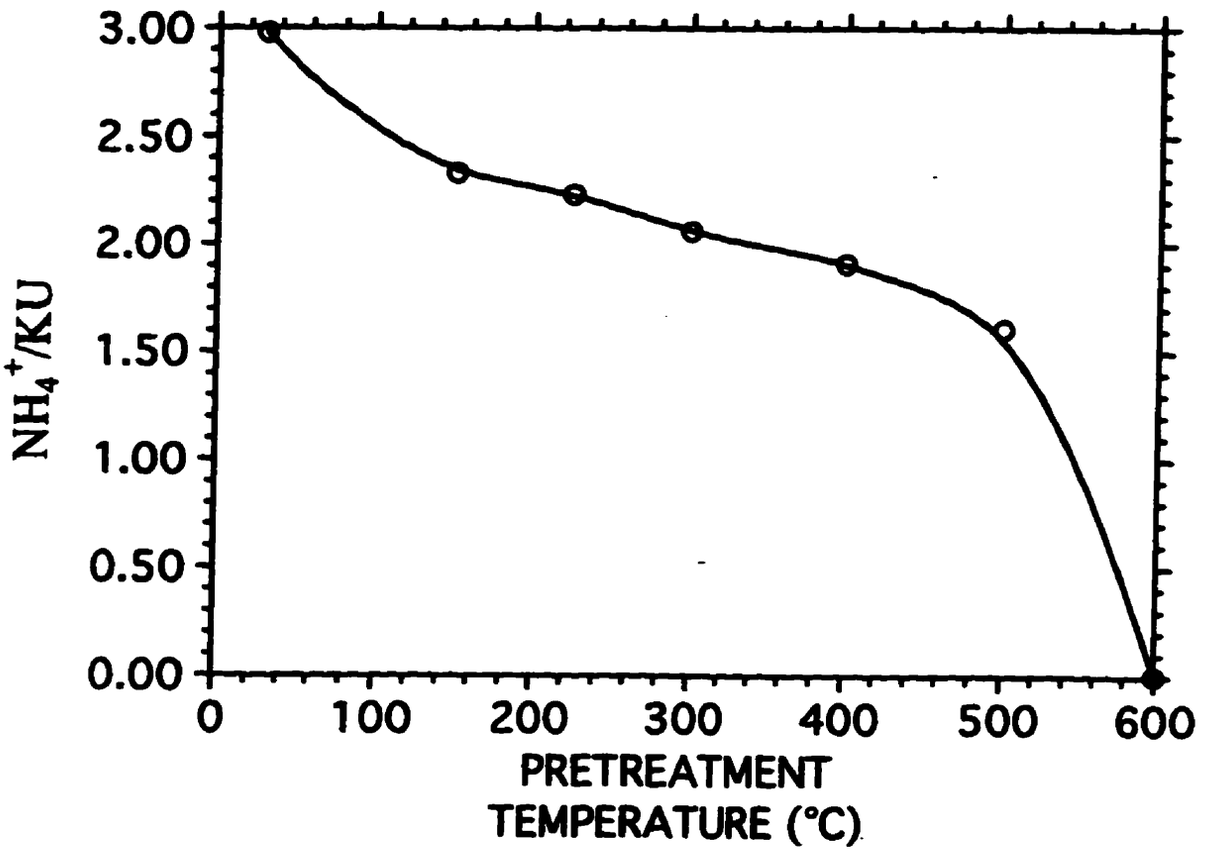

Fig. 4.3 Effect of pretreatment temperature on the quantity of ammonium cation per Keggin Unit contained within the stoichiometric ammonium 12-tungstophosphate pretreated in helium. Mass in reactor = 0.075g (38.8μmoles). Helium flow = 15 mL/min.

The influence of the reaction temperature is illustrated in Figures 4.4 to 4.6. With the first pulse yields of N_2, although nil at 25°C, are substantial at all temperatures presented in Figure 4.4. However the yields of N_2 at these temperatures decrease with the quantities of NO_2 added and have become insignificant after 100 μmoles of NO_2 have been injected. Although the yield of N_2 is higher at 300°C at the first pulse, the yield of N_2 at 150°C decreases less rapidly than the other temperatures studied.

The selectivity to N_2O is sensitive to the temperature of the reactor. At temperatures lower than 200°C, the selectivity remains vanishingly small (Fig.4.5). However, above 200°C, the selectivity is relatively high. From 200°C to 250°C the selectivity increases by a factor of 5, and from 250°C to 300°C the selectivity increases by a factor of 2. This suggests that the production of N_2O is initiated at approximately 200°C.

Selectivities to NO are significantly high at 25 and 150°C, but virtually nonexistent from 200°C and above for the first pulse (Fig.4.6). Furthermore, from 150°C and up, the selectivity to N_2 remains higher than that of all other species in the effluent although at 300°C the selectivity to N_2O is similar to that of N_2. A relatively small quantity of oxygen (O_2) is detected at 300°C with the first pulse but none is detected at 25 and 150°C except for a small amount after the 4th pulse for 150°C. With increase in NO_2, the selectivity to oxygen is greater at 300°C than at 150°C (see later).

In the synthesis of the microporous ammonium salts, it is possible to obtain salts with different stoichiometry relating to the ammonium content. In Figures 4.7 to 4.11 are presented the results of the injection of NO_2 at 300°C on salts having different ammonium content: 15% excess ammonium, stoichiometric, and 15% deficit ammonium, NH_4PW (+15%), NH_4PW, and NH_4PW (-15%), respectively.

The quantity of N_2 found in the reactor effluent from the injection of NO_2 is maximum for the first pulse for all stoichiometries. However, for the first pulse, the stoichiometric salt yields the maximum N_2, followed by +15% and -15% respectively. From the maximum value found for all stoichiometries, the quantity of N_2 in the effluent decreases rapidly to vanishingly small quantities at the 6^{th} pulse. However, the production of N_2O (Fig.4.8) is higher for the salt having an excess of NH_4^+ and increases to a maximum of 68% at the second pulse of NO_2 and decreases linearly for additional pulses. The stoichiometric and ammonium-deficient salts show no maximum in the quantity of N_2O produced, but the linear decline in this quantity commences with the first pulse. The ammonium-deficient salt shows a smaller yield of N_2O.

NO was observed from the first pulse with the ammonium-deficient catalyst, but no NO was detected in the reactor effluent stream under similar conditions with the ammonium-excess and stoichiometric salts (Fig.4.9). However, significant quantities of NO were found from the second pulse of NO_2 with all three catalysts. With the ammonium-excess and stoichiometric

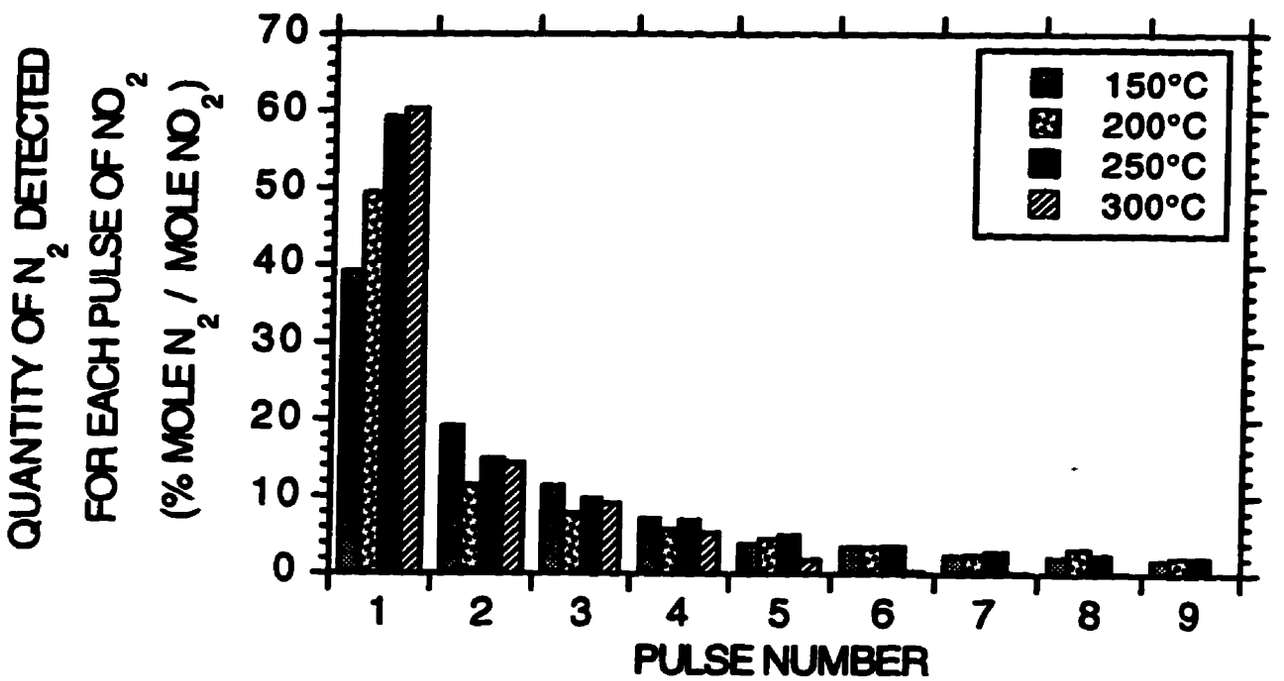

Fig. 4.4 Concentration of nitrogen (N_2) for each pulse of NO_2 introduced, for reactors containing stoichiometric NH_4PW held at different temperatures. Mass in reactor = 0.075g (38.8μmoles). Pulse size = 17 μmol NO_2. Helium flow = 15 mL/min.

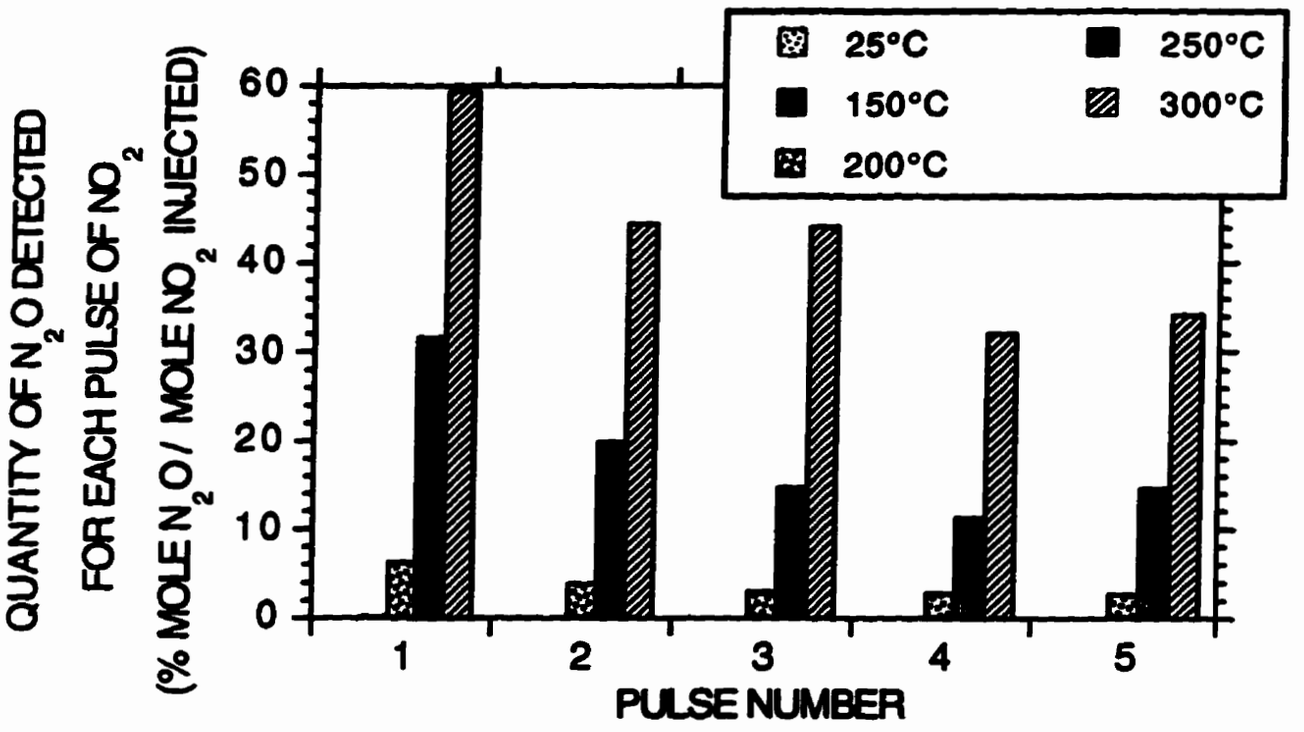

Fig. 4.5 Concentration of nitrous oxide (N_2O) for each pulse of NO_2 introduced, for reactors containing stoichiometric NH_4PW held at different temperatures. Mass in reactor = 0.075g (38.8μmoles). Pulse size = 17 μmol NO_2. Helium flow = 15 mL/min.

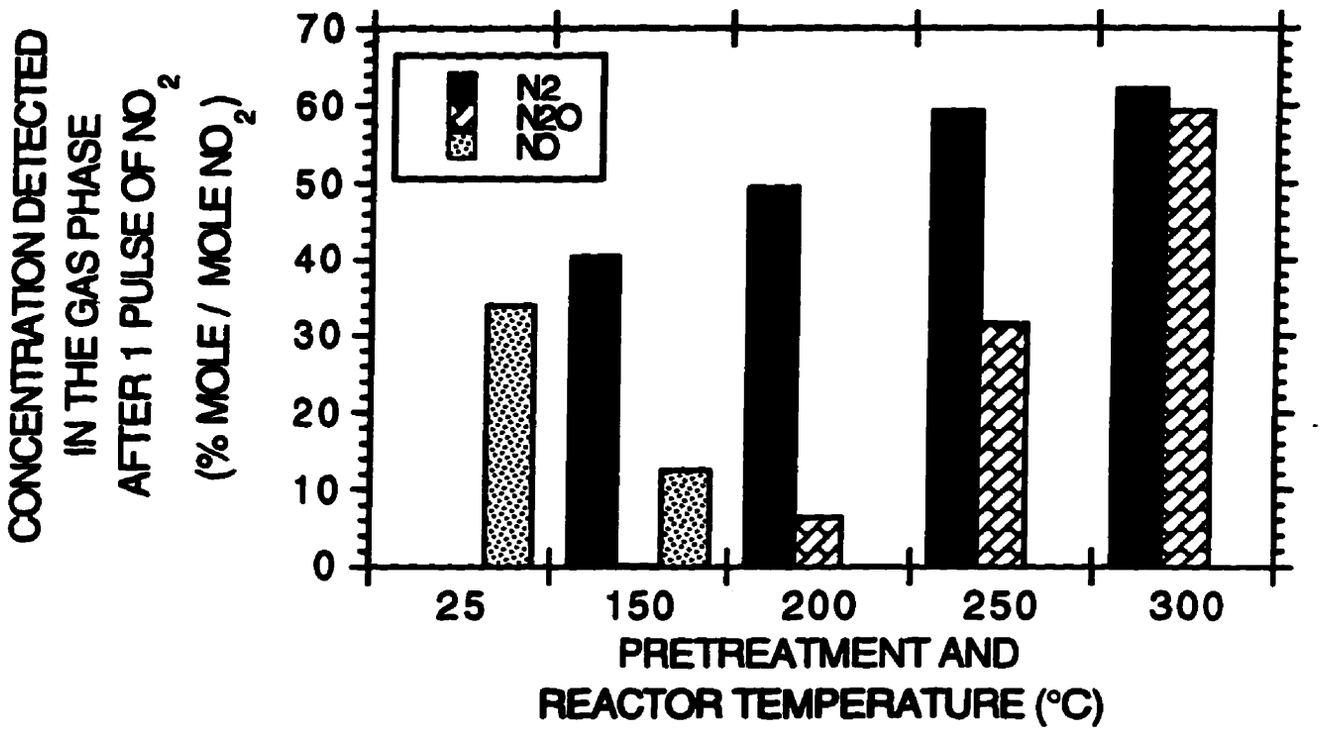

Fig. 4.6 Quantity of N_2, N_2O and NO, found in the effluent of a reactor containing stoichiometric NH_4PW, when only 1 pulse of NO_2 is injected for different temperatures. Mass in reactor = 0.075g (38.8μmoles). Pulse size = 17 μmol NO_2. Helium flow = 15 mL/min.

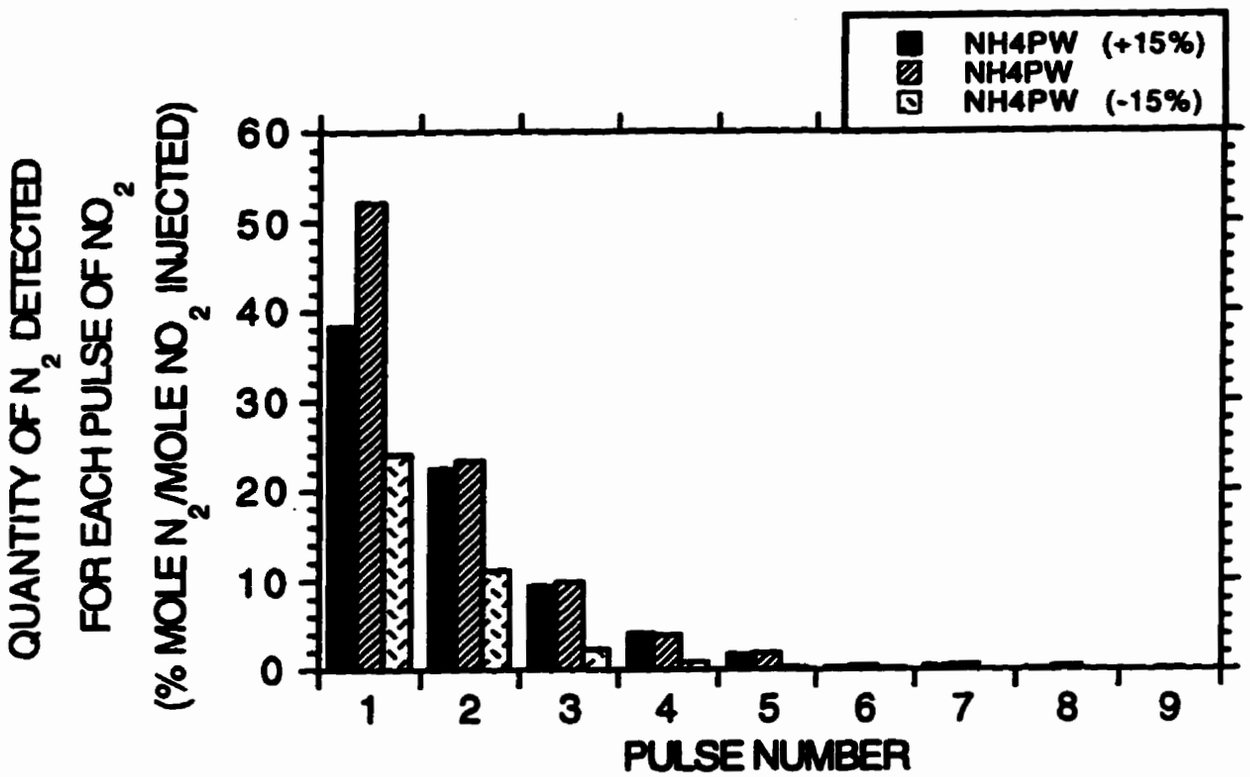

Fig. 4.7 N_2 detected in the gas phase for each pulse of NO_2 on stoichiometric and non-stoichiometric NH_4PW, for pretreatment and reactor temperatures of 300°C. Mass in reactor = 0.050g. Pulse size = 17 μmol NO_2. Helium flow = 15 mL/min.

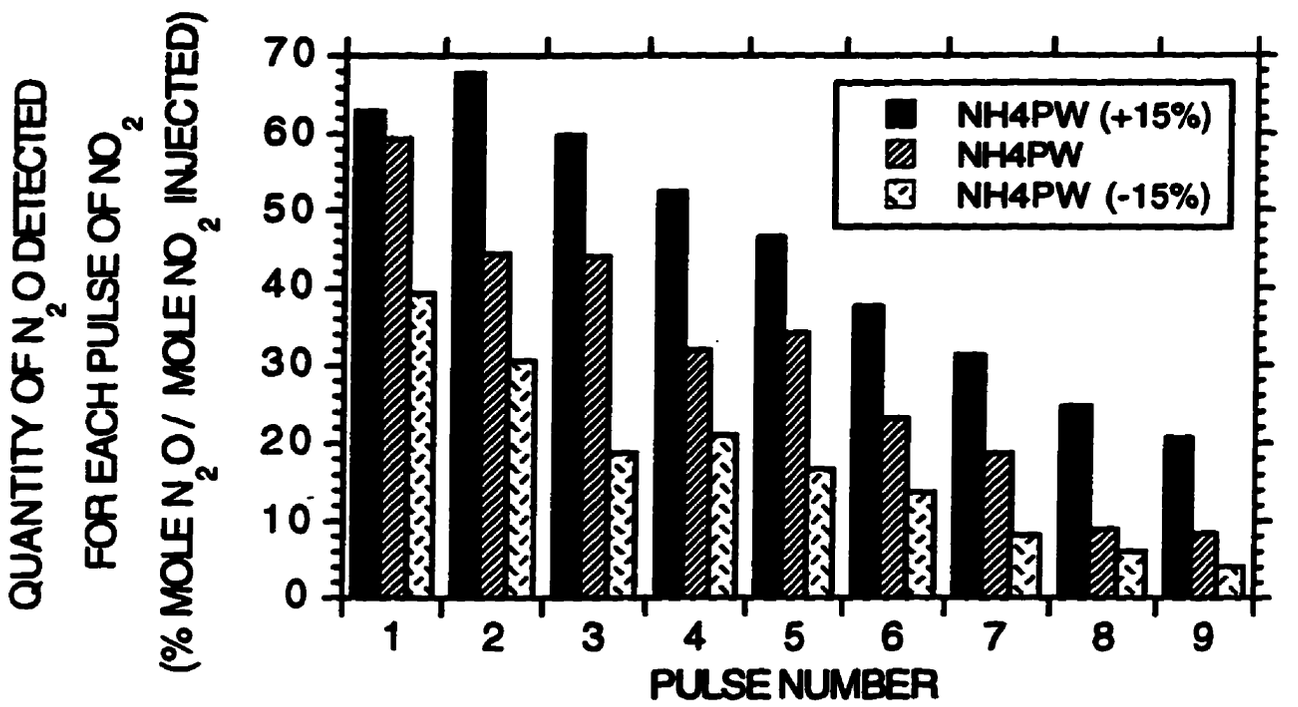

Fig. 4.8 N_2O detected in the gas phase for each pulse of NO_2 on stoichiometric and non-stoichiometric NH_4PW, for pretreatment and reactor temperatures of 300°C. Mass in reactor = 0.075g. Pulse size = 17 μmol NO_2. Helium flow = 15 mL/min.

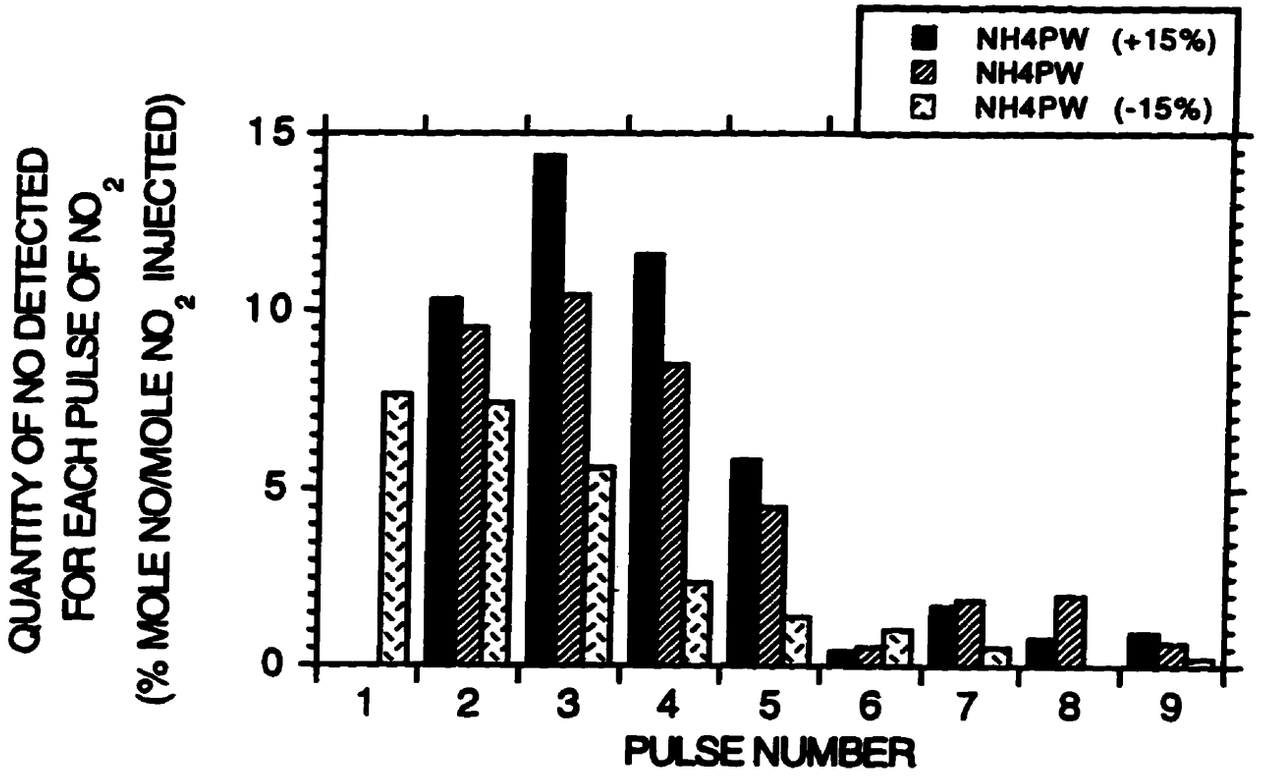

Fig. 4.9 NO detected in the gas phase for each pulse of NO_2 on stoichiometric and non-stoichiometric NH_4PW, for pretreatment and reactor temperatures of 300°C. Mass in reactor = 0.050g. Pulse size = 17 μmol NO_2. Helium flow = 15 mL/min.

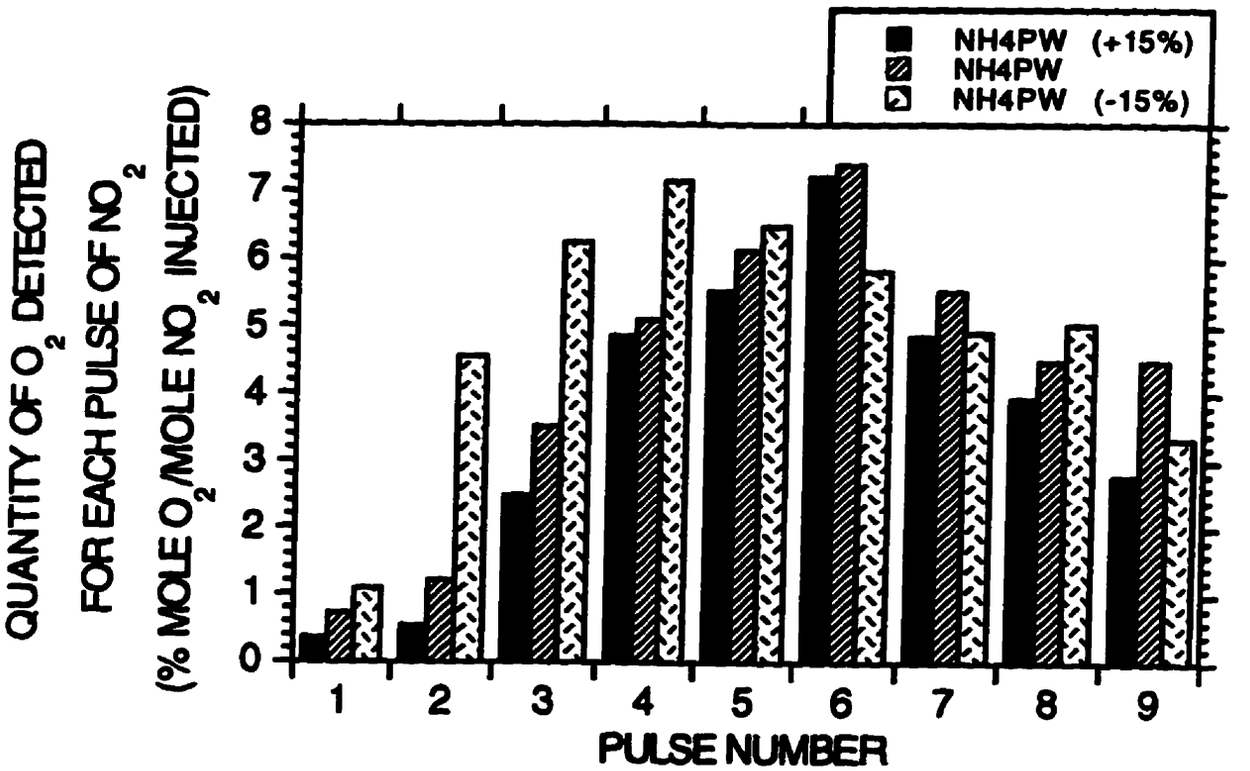

Fig. 4.10 O_2 detected in the gas phase for each pulse of NO_2 on stoichiometric and non-stoichiometric NH_4PW, for pretreatment and reactor temperatures of 300°C. Mass in reactor = 0.050g. Pulse size = 17 μmol NO_2. Helium flow = 15 mL/min.

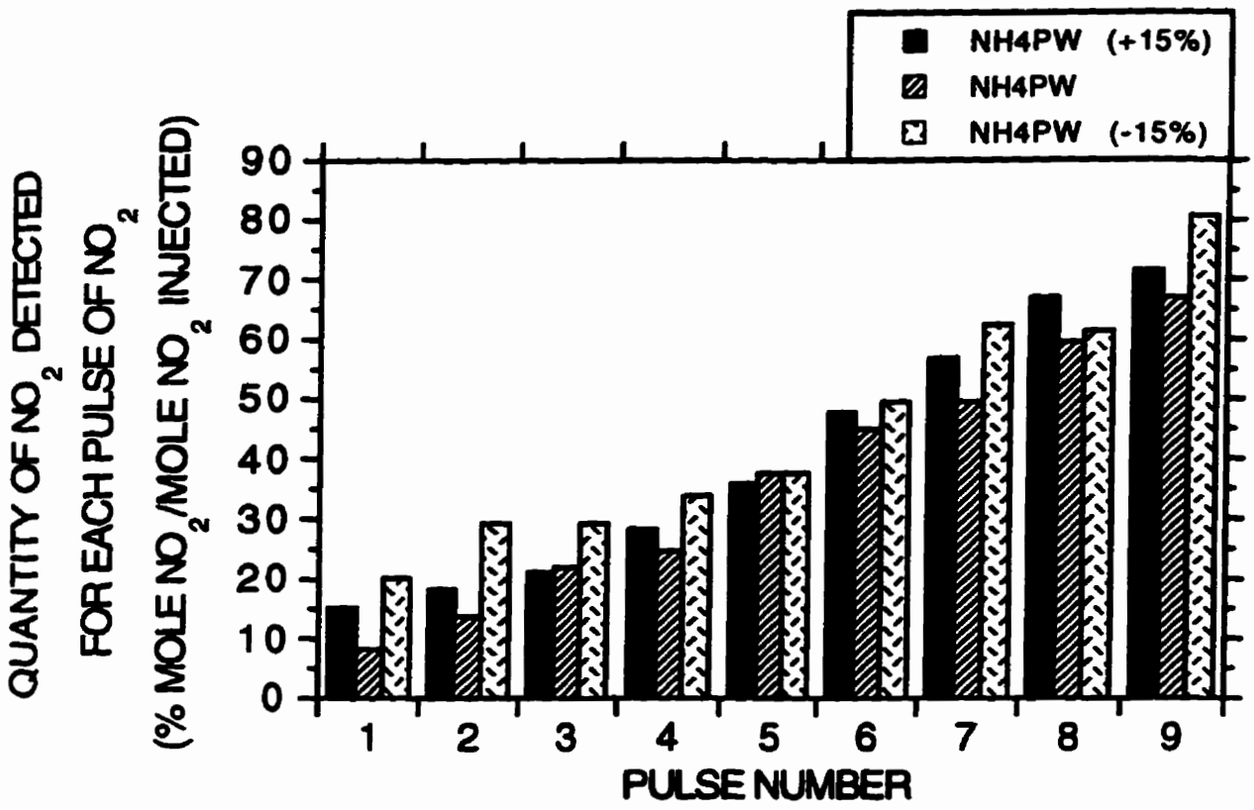

Fig. 4.11 NO_2 detected in the gas phase for each pulse of NO_2 on stoichiometric and non-stoichiometric NH_4PW, for pretreatment and reactor temperatures of 300°C. Mass in reactor = 0.050g. Pulse size = 17 μmol NO_2. Helium flow = 15 mL/min.

salts the production of NO reached a maximum at the third pulse while with the ammonium-deficient salt a steady decline in the amount of NO generated was observed after the second pulse.

The amount of O_2 (Fig.4.10) in the gas at the exit of the reactor, for all stoichiometries, increased to a maximum with increasing amount of NO_2 introduced into the reactor. However, the maximum is found at the 4^{th} and 6^{th} pulse of NO_2, for the deficient and for the excess and stoichiometric salts, respectively. The amount of NO_2 found in the reactor effluent is shown on Figure 4.11. For all stoichiometries studied, the quantity of NO_2 increases with the pulse number. However, the stoichiometric salt sorbs and converts more NO_2 for each pulse.

Temperature-programmed reaction (TPR) of NO_2 on labelled $^{15}NH_4PW$ (Fig.4.12) shows that NO_2 is reduced at temperature as low as 100°C. As the temperature of reaction is increased, the formation of molecular nitrogen, as NN and ^{15}NN, increases and reaches a maximum at 210°C for normal N_2 and at 360°C for labelled N_2. However, at temperatures above 440°C, no molecular nitrogen could be detected. A great quantity of water is detected with the reduction of NO_2. The concentrations of NO_2 and NO reach a minimum at 360°C. However at 360°C the concentration of N_2O, as NNO and ^{15}NNO reaches a maximum. The formation of N_2O can be observed from 190°C for both isotopes. The formation of ^{15}NNO is insignificant at temperatures above 440°C, but small quantities of NNO are still detectable above that temperature. The formation of labelled ^{15}NO remains at trace concentration throughout the TPR experiment.

The results of temperature programmed desorption experiments are recorded in Figures 4.13 to 4.16. The stoichiometric washed (SW) catalyst pretreated in helium at 30°C and 150°C for 1 hour (Fig.4.13A and D, respectively) shows only small peaks at approximately 175°C for desorbed water. It is to be noted however that, with the catalyst pretreated at 150°C the water peak has slightly shifted to a somewhat higher temperature. After saturation with NO or NO_2 at 30°C (Fig.4.13B and C, respectively), the peak at 175°C due to desorbed water has increased markedly, particularly after introduction of NO_2. The SW catalyst, after pretreatment at 150°C and exposure to NO at the same temperature displays an enlarged water peak at 175°C in addition to several overlapping peaks at temperatures ranging from 300-500°C (Fig.4.13E). In contrast the SW catalyst pretreated at 300°C and saturated with NO at the same temperature shows a large peak whose maximum occurs at approximately 475°C (Fig.4.13F) while after saturation with NO_2 the latter peak is similar in magnitude but the water peak at 200°C is significantly enlarged (Fig.4.13G).

The TPD pattern for NH_4PW prepared from a 15% deficit of the ammonium ion shows two relatively large overlapping peaks between 100 and 350°C with a smaller peak at 475°C (Fig.4.14A). After exposure to NO_2 the three peaks observed in the absence of NO_2 remain but

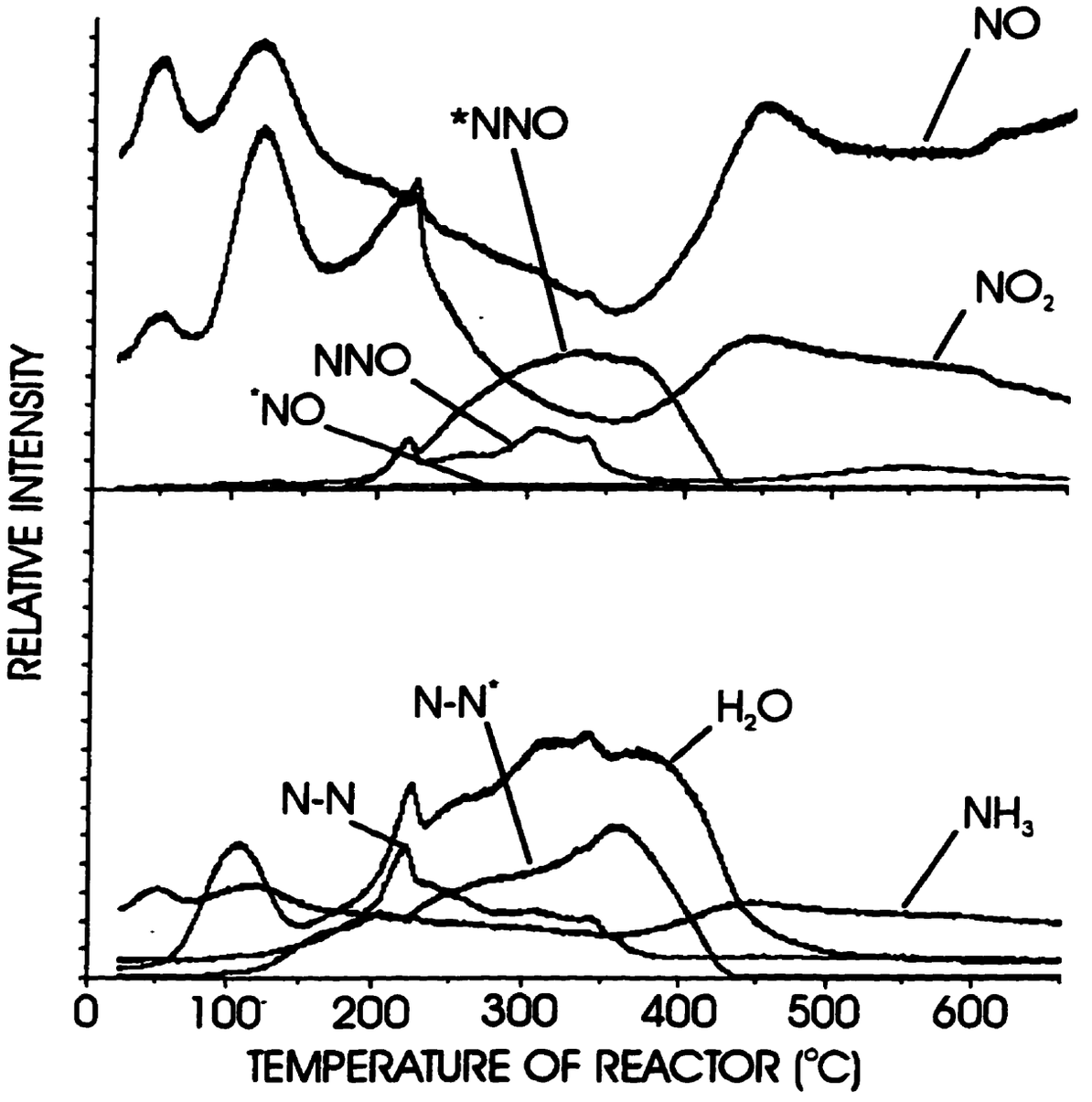

Fig. 4.12 Higher resolution temperature-programmed reaction of 0.075g (38.7μmoles) of $^{15}NH_4PW$ exposed to a continuous flow of 4960 ppm of NO_2. Heating rate = 10°C/min and Flow rate = 20 mL/min. * = Isotope 15.

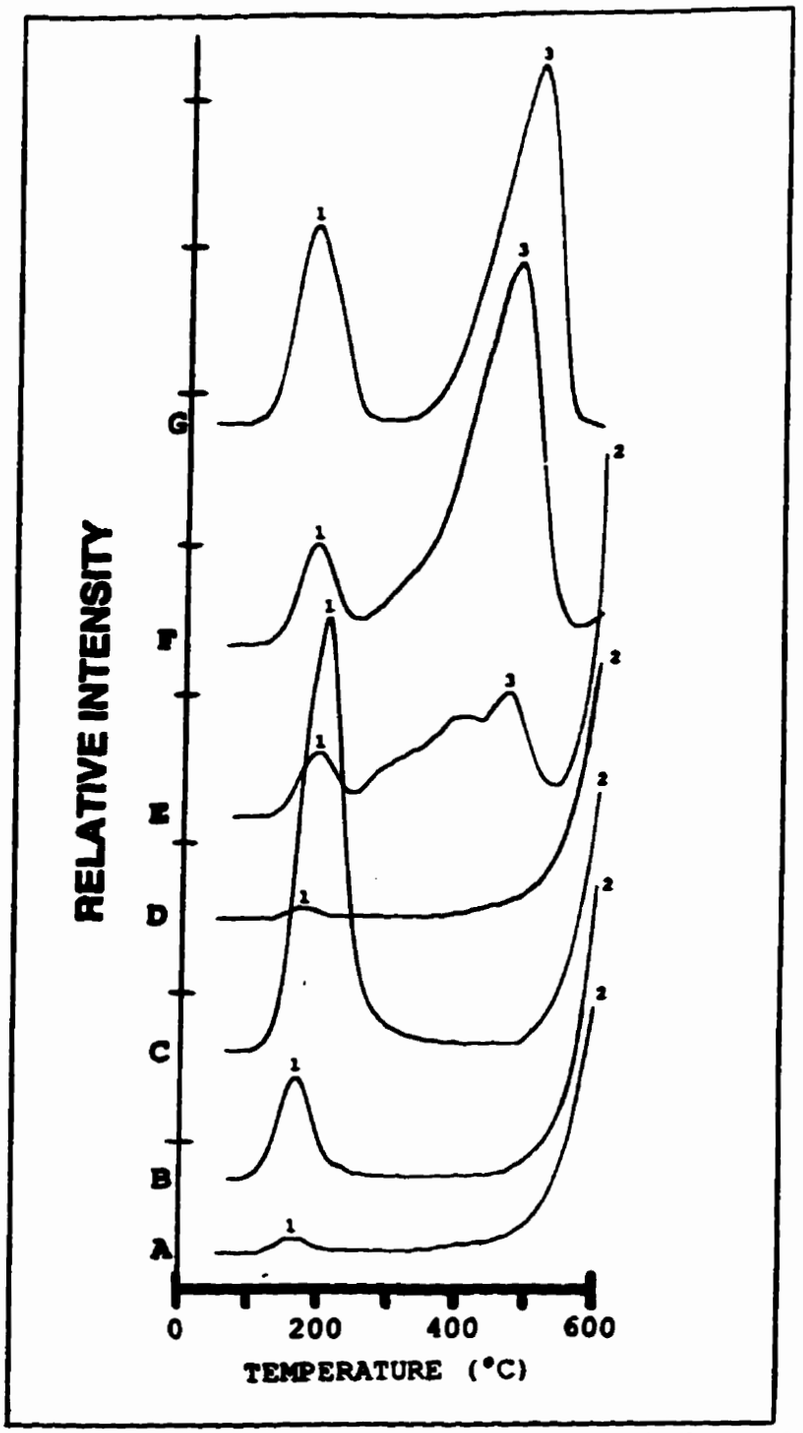

Fig. 4.13 TPD of NH_4PW{stoichiometric-washed} (A) pretreated in helium at 30°C for 1 hour; then (B) saturated with NO at 30°C for 1 hour; (C) same pretreatment as in (A) but saturated with NO_2 at 30°C for 1 hour; (D) NH_4PW{stoichiometric-washed} pretreated at 150°C for 1 hour; then (E) saturated with NO at 150°C for 1 hour; (F) NH_4PW{stoichiometric-washed} pretreated at 300°C for 1 hour, then saturated with NO at 300°C for hour; (G) same pretreatment as in (D) but saturated with NO_2 at 150°C for 1 hour. Mass of solid in reactor = 0.075g (38.8μmoles). Pulse size = 17 μmol of NO_2. Helium flow rate = 45 mL/min. Temperature rate = 60°C/min. LEGEND: 1) H_2O; 2) NH_3; 3) NO_2; 4) N_2O.

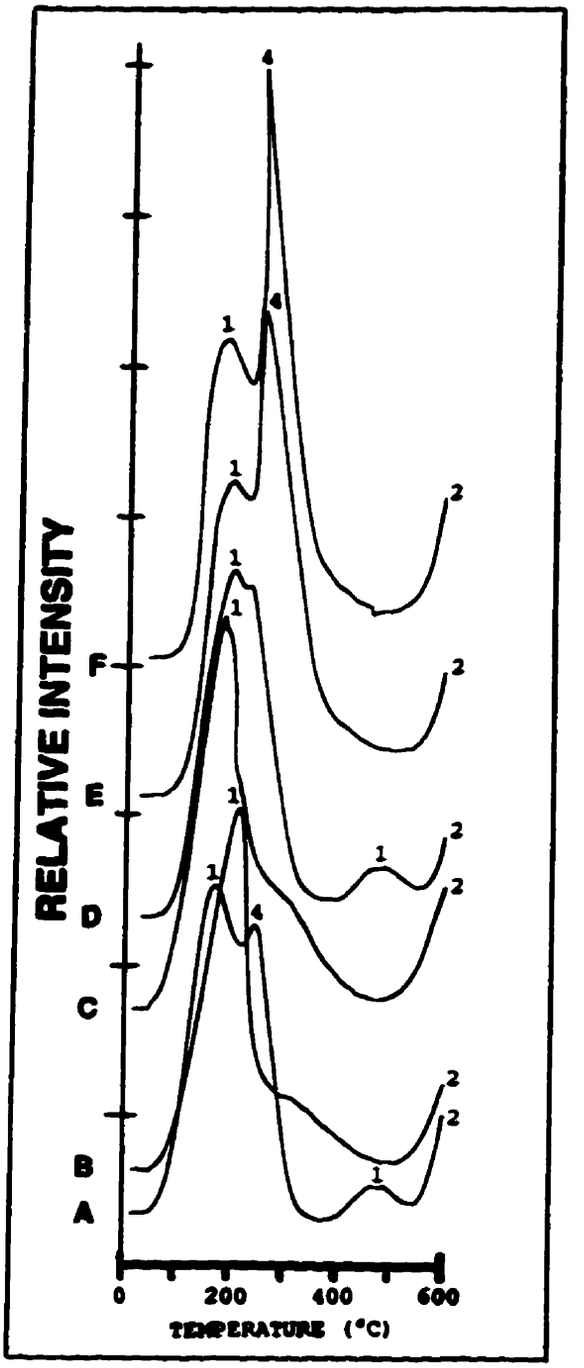

Fig. 4.14 TPD of $NH_4PW\{-15\%NH_4\}$ (A) pretreated in helium at 30°C for 15 min; then (D) exposed to 25 pulses of NO_2 at 30°C; TPD of $NH_4PW\{$stoichiometric-unwashed$\}$ (B) pretreated in helium at 30°C for 15 min; then (E) exposed to 25 pulses of NO_2 at 30°C; TPD of $NH_4PW\{+15\%NH_4\}$ (C) pretreated in helium at 30°C for 15 min; then (F) exposed to 25 pulses of NO_2 at 30°C. Mass of solid in reactor = 0.075g. Pulse size = 17 μmol of NO_2. Helium flow rate = 45 mL/min. Temperature rate = 60°C/min. LEGEND: 1) H_2O; 2) NH_3; 3) NO_2; 4) N_2O.

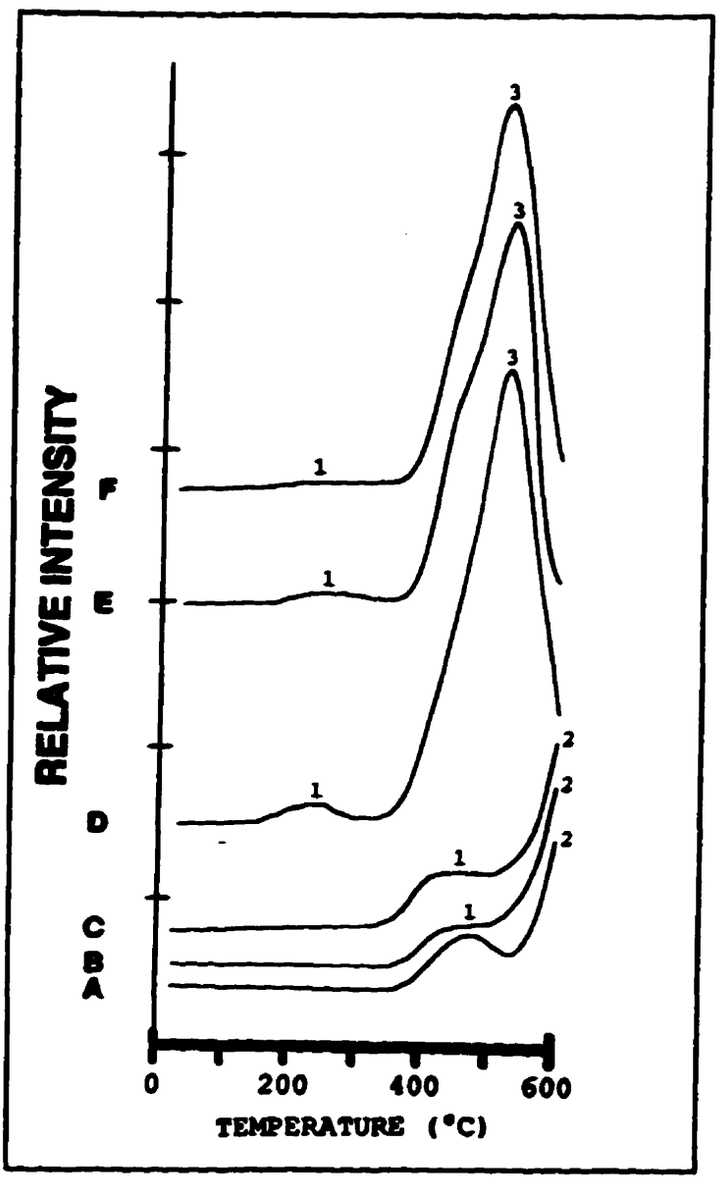

Fig. 4.15 TPD of $NH_4PW\{-15\%NH_4\}$ (A) pretreated in helium at 300°C for 15 min; then (D) exposed to 25 pulses of NO_2 at 300°C; TPD of $NH_4PW\{$stoichiometric-unwashed) (B) pretreated in helium at 300°C for 15 min; then (E) exposed to 25 pulses of NO_2 at 300°C; TPD of $NH_4PW\{+15\%NH_4\}$ (C) pretreated in helium at 300°C for 15 min; then (F) exposed to 25 pulses of NO_2 at 300°C. Mass of solid in reactor = 0.075g. Pulse size = 17 μmol of NO_2. Helium flow rate = 45 mL/min. Temperature rate = 60°C/min. LEGEND: 1) H_2O; 2) NH_3; 3) NO_2; 4) N_2O.

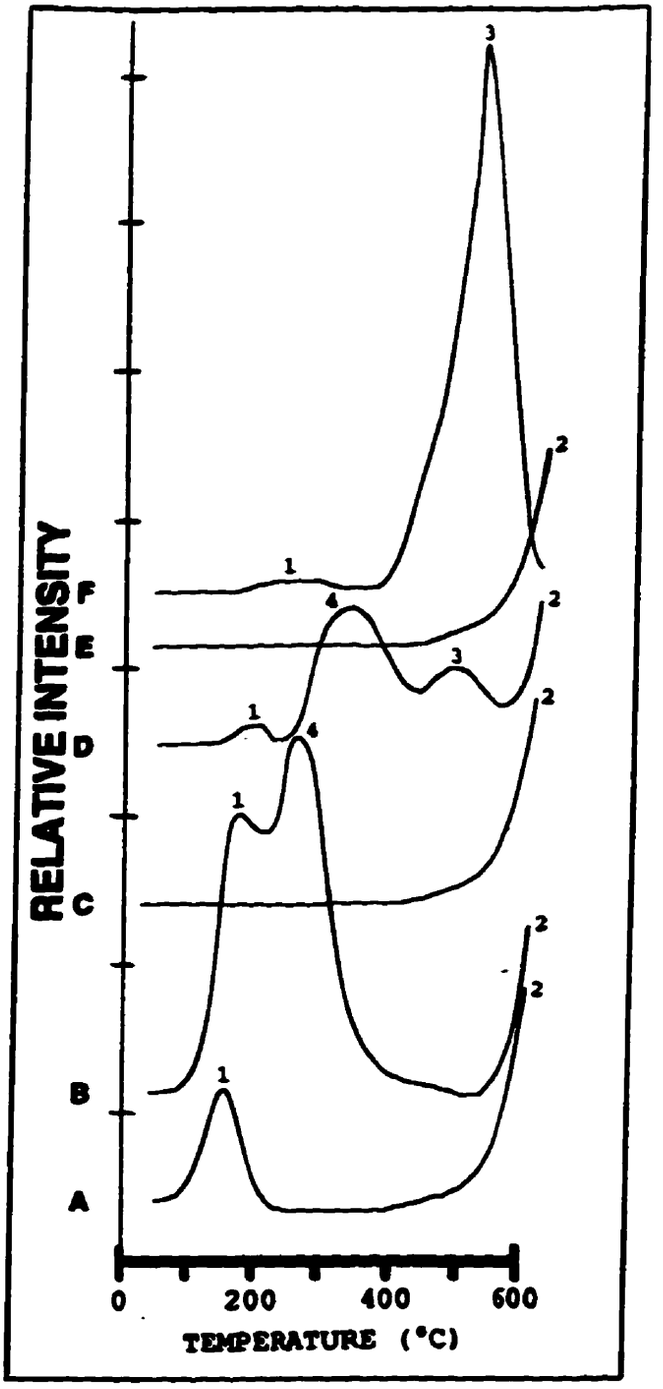

Fig. 4.16 TPD of NH_4PW{stoichiometric-washed} (A) pretreated in helium at 30°C for 15 min; then (B) exposed to 25 pulses of NO_2 at 30°C; TPD of NH_4PW{stoichiometric-washed} (C) pretreated in helium at 150°C for 15 min; then (D) exposed to 25 pulses of NO_2 at 150°C; TPD of NH_4PW{stoichiometric-washed} (E) pretreated in helium at 300°C for 15 min; then (F) exposed to 25 pulses of NO_2 at 300°C. Mass of solid in reactor = 0.075g (38.8μmoles). Pulse size = 17 μmol of NO_2. Helium flow rate = 45 mL/min. Temperature rate = 60°C/min. LEGEND: 1) H_2O; 2) NH_3; 3) NO_2; 4) N_2O.

the higher of the two overlapping peaks is more substantial (Fig.4.14D). Stoichiometric NH_4PW also displays the two overlapping peaks noted above, but in contrast, that at the higher temperature is considerably lower in intensity than that at the lower temperatures. No peak at 475°C is evident. After exposure of this catalyst to NO_2 the higher temperature peak of the two similarly overlapping peaks has enlarged considerably (Fig.4.14E). The TPD spectra of the NH_4PW sample prepared from a 15% excess of the ammonium ion also shows the two similarly overlapping peaks between 100 and 350°C, but of these, the peak at the higher temperature is now reduced to a shoulder (Fig.4.14C). After exposure to NO_2 this shoulder has been transformed to a significantly large peak (Fig.4.14F).

The TPD patterns for the aforementioned three samples pretreated at a higher temperature of 300°C show drastic differences as compared with those pretreated at 30°C (Fig.4.15). The ammonium ion deficient sample displays one relatively small peak at 475°C (Fig.4.15A) which, after exposure of the sample to NO_2, has grown significantly in intensity (Fig.4.15D). The stoichiometric and excess ammonium samples both before and after exposure to NO_2 show similar behavior.

Temperature-programmed desorption (TPD) of the stoichiometric-washed sample after exposure to NO_2 showed two overlapping peaks at 175 and 250°C (Fig.4.16B). After pretreatment at 150°C followed by exposure to NO_2 at the same temperature three peaks at 175, 300 and 500°C are evident by all substantially smaller that those observed after 30°C pretreatment and exposure (Fig.4.16D). With pretreatment and exposure to NO_2 at 300°C only a large peak at 500°C remains. It was shown by TPD that when the salts were saturated with NO_2 at 300°C, the only product of desorption was NO_2. The determination of this NO_2 on all salts used is found in Figure 4.17 and represented as nitrogen (N) per Keggin Unit. The nitrogen found corresponds to the approximate stoichiometry calculated.

Temperature-programmed desorption experiments, using MS detection, show that NH_3 does not begin to desorb from $^{15}NH_4PW$ until 400°C and the greater portion of the evolution takes place at temperatures higher than 550°C (Fig.4.18A). After exposure to NO_2 at 150°C for 2 hours, TPD (Fig.4.18B) shows that H_2O is desorbed from 110 to 650°C, along with small quantities of N_2O between 150 and 650°C. Smaller quantities of NO_2 are detected at 110 and 410°C. However, significant quantities of N_2 (as ^{15}NN) with maxima at 340 and 400°C desorb between 100 and 500°C with small quantities of ^{15}NN at 590°C. NO can be seen between 30 and 500°C with maxima at 110, 410, and 590°C. Finally, a small quantity of NH_3 above 550°C is seen desorbing from the catalyst. $^{15}NH_4PW$ pretreated and exposed to NO_2 at 300°C displays a small water peak at 200°C followed a broader peak between 350°C and 600°C. This later evolution of water is accompanied by a substantial evolution of NO and NO_2 at 500°C. No labelled nitrogen compound was sorbed (Fig.4.18C). It was found that most of the

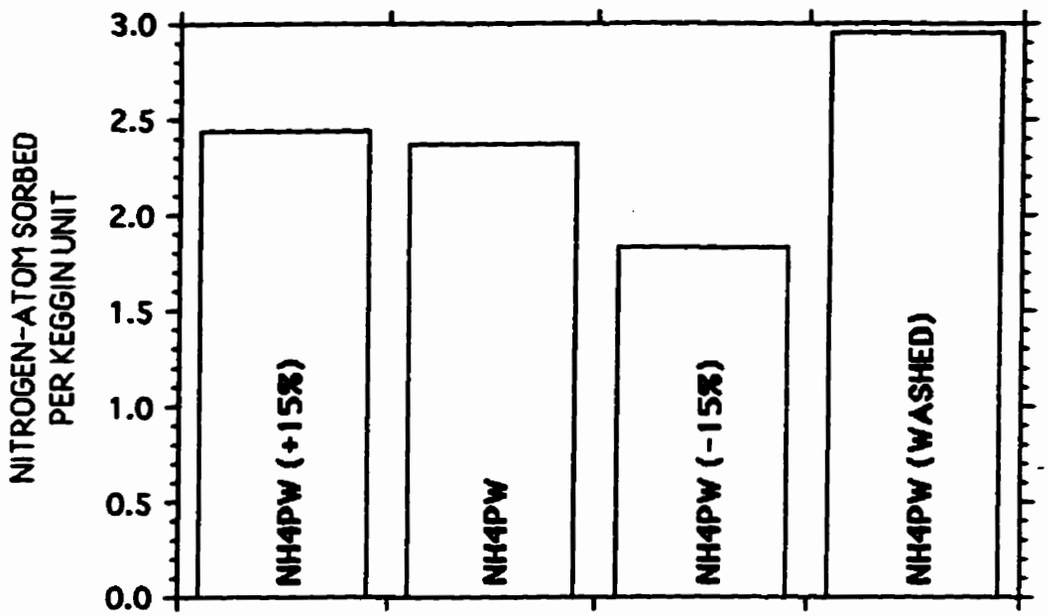

Fig. 4.17 Quantity of nitrogen atoms sorbed per Keggin Unit with the variation in the stoichiometry and preparation method after pretreatment and saturation with NO_2 at 300°C.

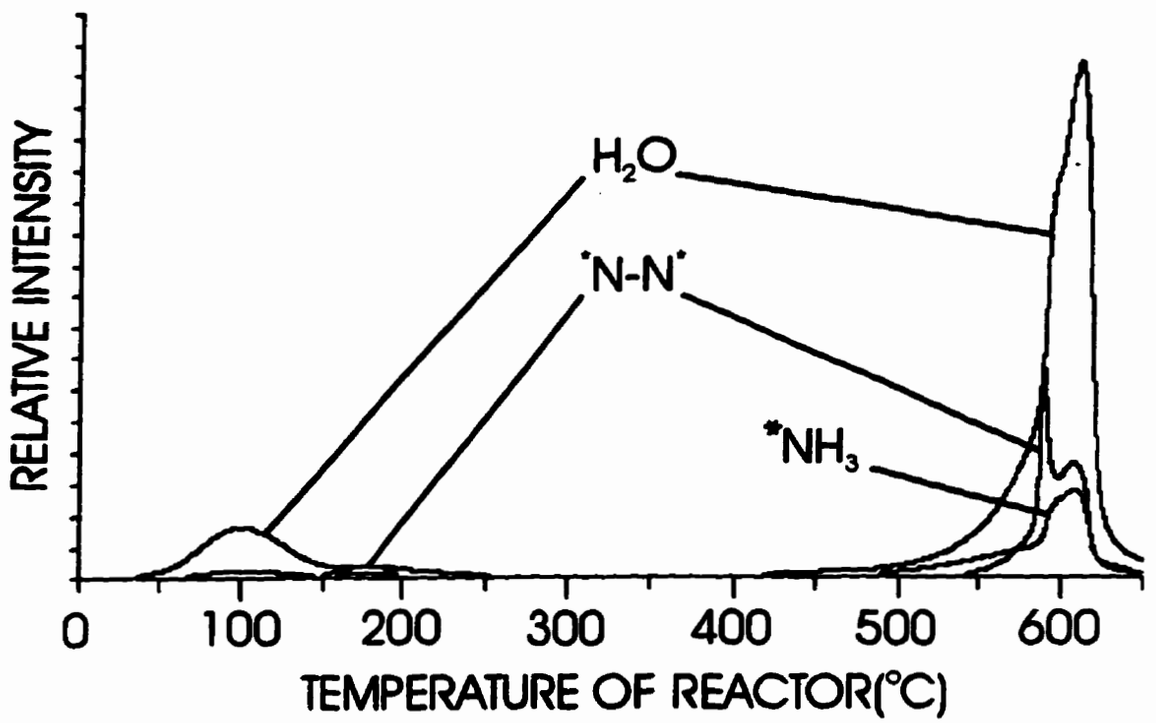

Fig. 4.18A Temperature-programmed desorption of 0.050g (25.8μmoles) of $^{15}NH_4PW$ as prepared. Helium flow = 20 mL/min. Heating rate = 10°C/min. * = Isotope 15.

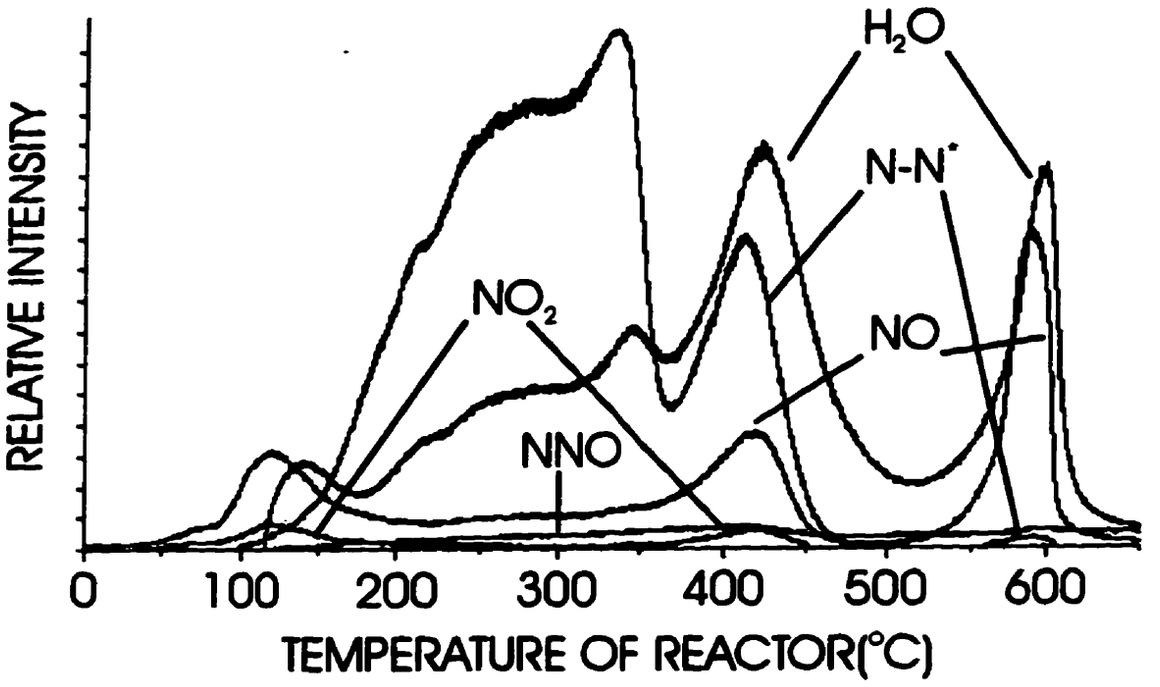

Fig. 4.18B Temperature-programmed desorption of 0.075g (38.7μmoles) of $^{15}NH_4PW$ pretreated with 4960 ppm NO_2 flow(20 mL/min) for 2 hours at 150°C. Helium flow = 20mL/min. Heating rate = 10°C/min. * = Isotope 15.

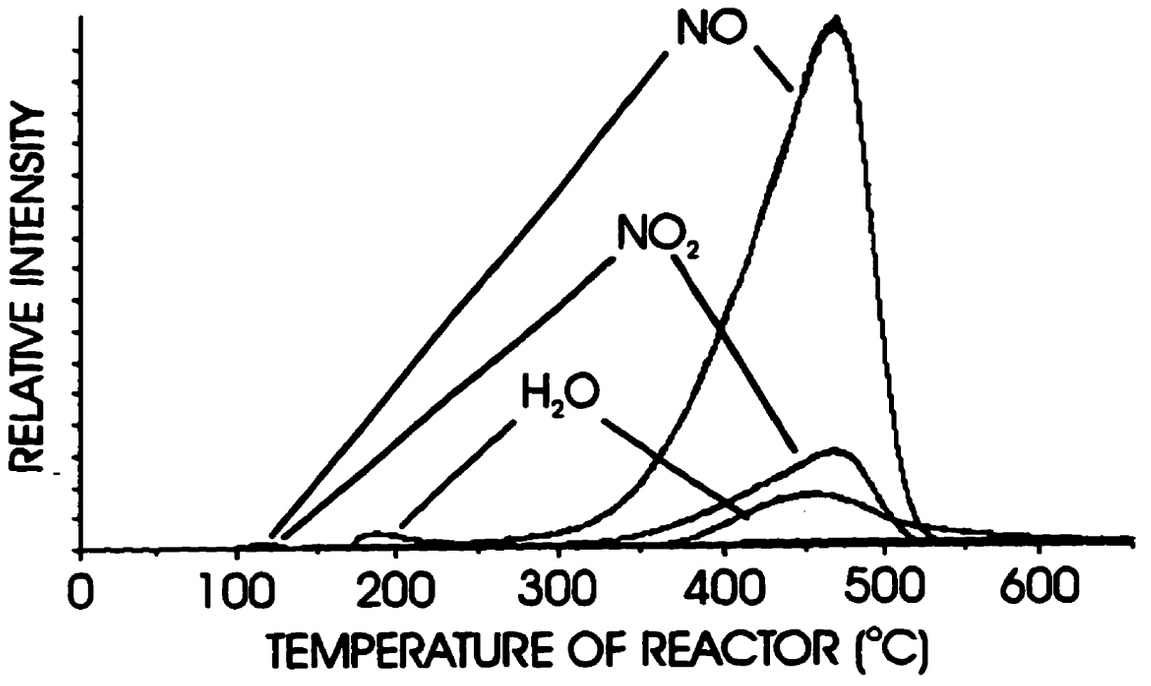

Fig. 4.18C Temperature-programmed desorption of 0.075g (38.7μmoles) of $^{15}NH_4PW$ pretreated with 4960 ppm NO_2 flow(20 mL/min) for 2 hours at 300°C. Helium flow = 20mL/min. Heating rate = 10°C/min.

peak at 450°C is due to NO_2 but because of the temperature rate used most of the NO_2 is thermally decomposed to NO. At higher temperature rates, the concentration of NO_2, compared to NO, was more important.

At 150°C, although N_2 is produced and rapidly desorbed, less than the stoichiometric quantity of NH_3 is consumed and subsequently the residual NH_3 is desorbed at elevated temperatures. The formation of N_2 seems to originate from two separate mechanisms; by reaction of NO_2 and NH_3, and from the auto-reduction of NO_2. The water desorbed results from the reaction of NH_3 and NO_2. The N_2O may be formed from the thermal decomposition of NH_4NO_3, the latter resulting from added NO_2. After exposure of the ammonium salt to NO_2 for two hours the unreacted NO_2 reacted with the ammonia to give N_2 as the temperature of the reactor was raised.

At the higher temperature of 300°C, virtually all of the NH_3 has been consumed by NO_2 and the unconverted NO_2 can remain sorbed on the catalyst. No NH_3 or N_2O desorption was observed.

Isothermal continuous reaction (ICR) experiments of NO_2 with $^{15}NH_4PW$ (Fig.4.19) show that the quantity of ^{15}NN and H_2O produced is smaller at 150°C than that at 300°C. However when the reaction is conducted at 300°C the reduction to ^{15}NN is vanishingly small after 90 minutes but continues to occur at 150°C. The concentration of N_2O (as ^{15}NNO and NNO) is very small at 150°C but important at 300°C.

The quantities of the different molecules found in the gas phase, for the first hour of reaction, are presented in Table 4.1. These values are corrected to take into consideration the fragmentation due to the MS detector. The results also follow the observations from TPR.

The stoichiometric-washed NH_4PW shows, as expected, the characteristic infrared bands of the Keggin anion in the 800-1200 cm^{-1} region, as well as bands at 3200 and 1421 cm^{-1} attributed to the ammonium ion (Fig.4.20A). After exposure to NO_2 at 150°C the former and latter bands remain, although the latter are somewhat decreased in intensity (Fig.4.20B) and, in addition, a small band appears at 2263 cm^{-1}, which is intensified in the spectra of the sample pretreated and exposed to NO_2 at 300°C.

The unwashed stoichiometric and non-stoichiometric samples display similar spectra before exposure to NO_2 (Fig.4.21).

After exposure to NO_2 the band at 2263 cm^{-1} is clearly evident particularly with the stoichiometric and the excess ammonium samples (Fig.4.21E, D, F). Interestingly the three overlapping bands between 1400 and 1500 cm^{-1} in the NO_2-free samples are converted to two distinct bands in the same region after exposure to NO_2 at 300°C, with the band due to the ammonium ion having vanished.

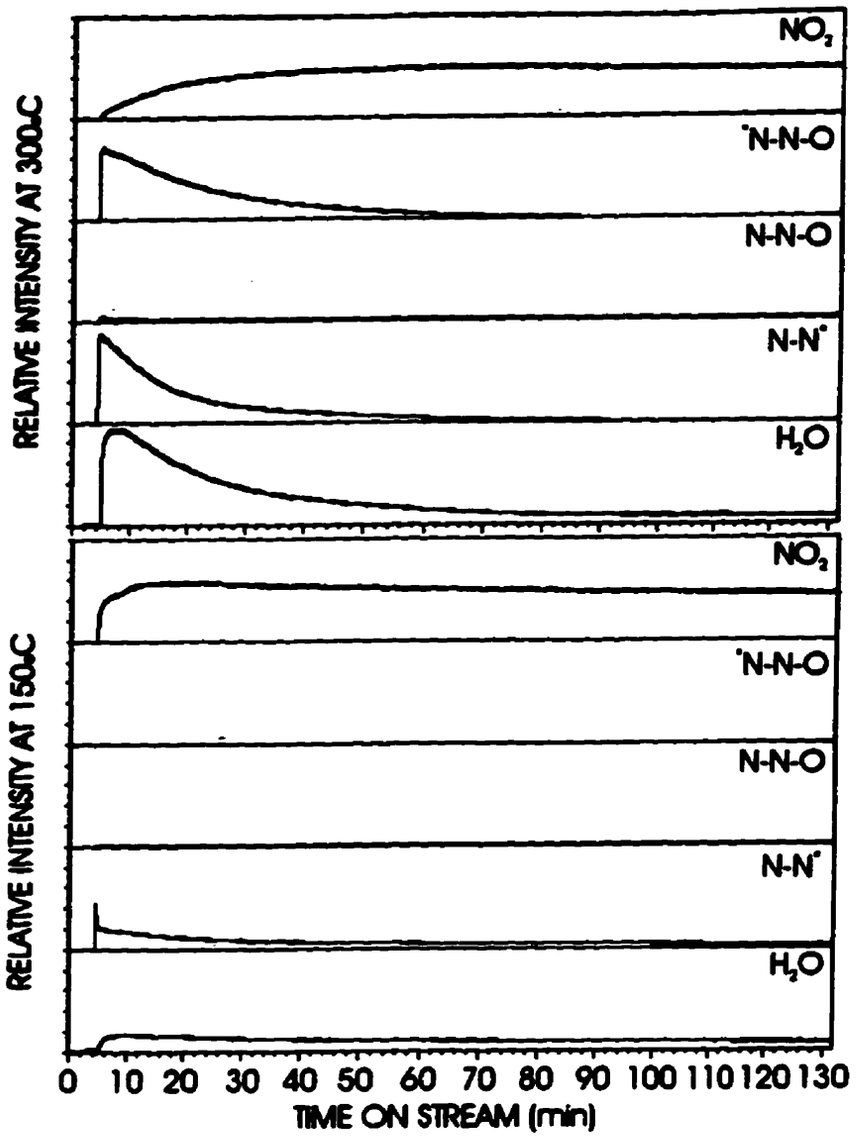

Fig. 4.19 Isothermal continuous reactions of 0.075g (38.7μmoles) $^{15}NH_4PW$ and 4960 ppm NO_2 flow(20 mL/min) at 150 and 300°C. * = Isotope 15.

TABLE 4.1

INTEGRATED AREA FOR THE ISOTHERMAL CONTINUOUS REACTION OF $^{15}NH_4PW$ AND NO_2

ICR 0.075g (38.7μmoles) $^{15}NH_4PW$ + 4960 ppm NO_2

Masses	Molecules	%mole detected/mole NO_2 injected[a]	
		150°C	300°C
18	HOH	5.5	16.7
28	NN	0.0	0.1
29	^{15}NN	3.9	8.7
30	NO	12.3	11.0
31	^{15}NO	0.1	0.4
44	NNO	0.4	0.6
45	^{15}NNO	0.0	9.5
46	ONO	50.9	42.2

a % mole detected corrected per Total Ion of NO_2 injected for 60 min integration of Fig.4.19.

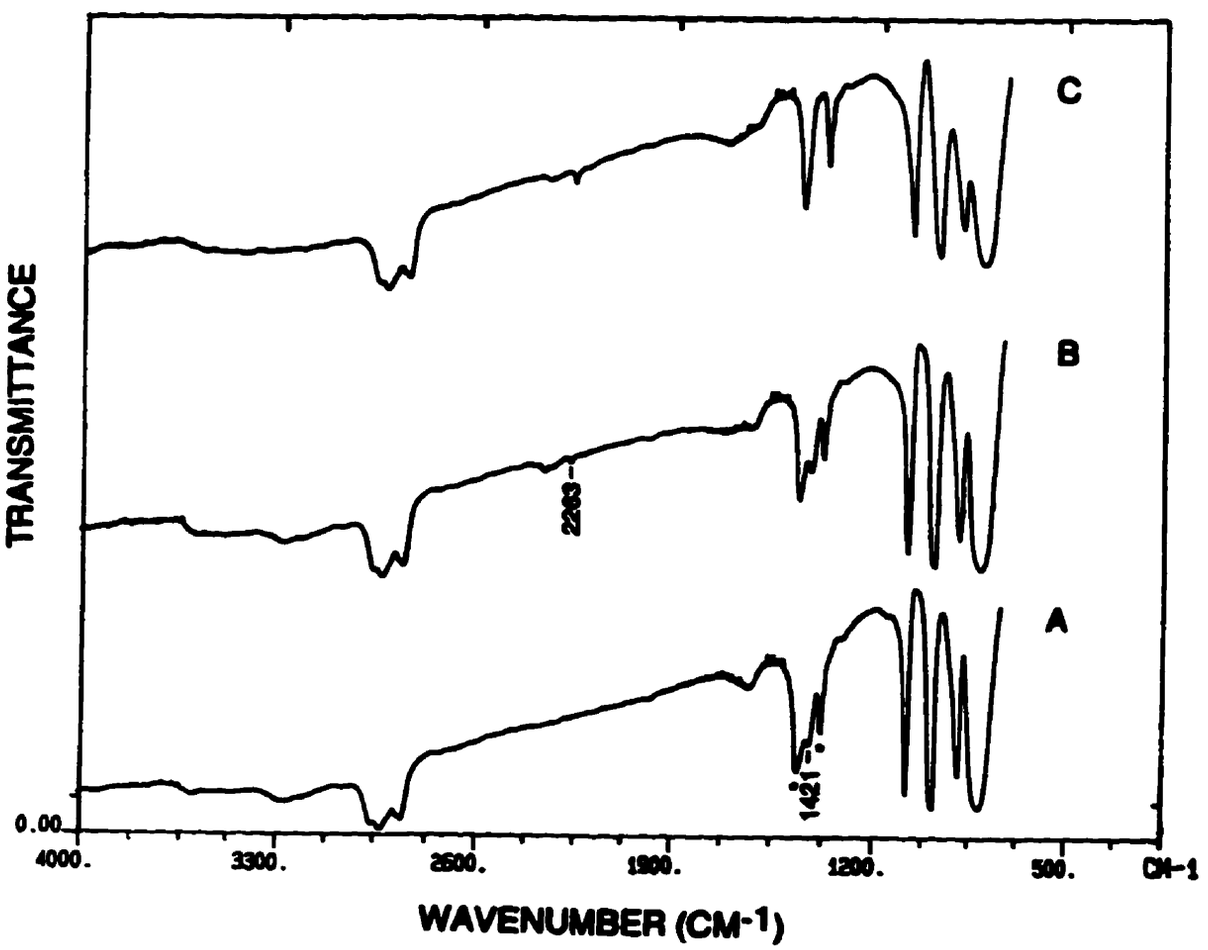

Fig. 4.20 Infrared spectra of (A) stoichiometric-washed NH_4PW at 25°C, then (B) pretreated and exposed to 20 pulses of NO_2 at 150°C. Same salt as in (A) but (C) pretreated and exposed to 14 pulses of NO_2 at 300°C. * = NUJOL bands.

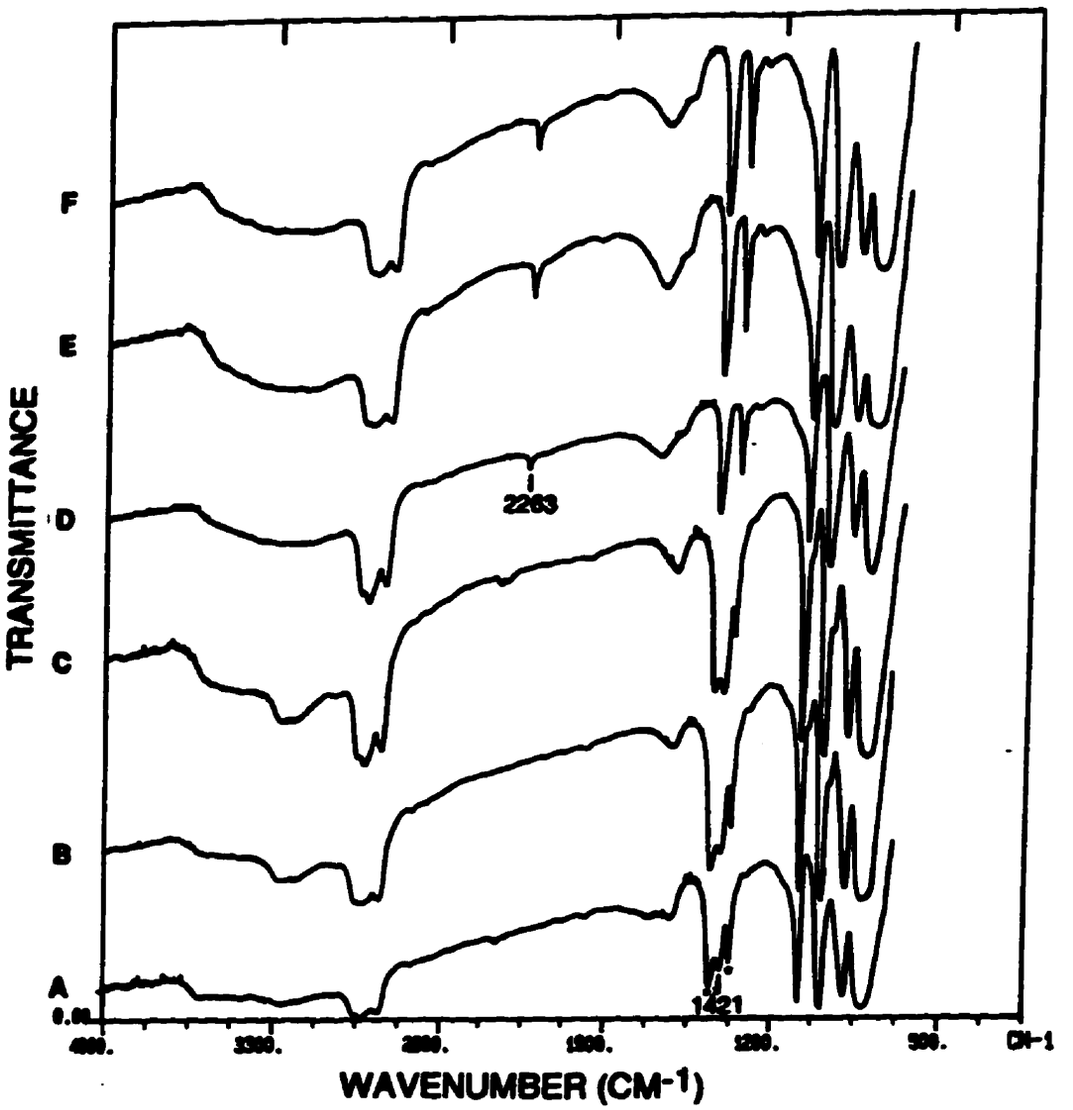

Fig. 4.21 Infrared spectra of (A) $NH_4PW\{-15\%NH_4\}$ at 25°C, then (D) pretreated and saturated with NO_2 at 300°C; (B) $NH_4PW\{$stoichiometric-unwashed$\}$ at 25°C, then (E) pretreated and saturated with NO_2 at 300°C; (C) $NH_4PW\{+15\%NH_4\}$ at 25°C, then (F) pretreated and saturated with NO_2 at 300°C. * = NUJOL bands.

The powder X-ray diffraction patterns of washed NH_4PW before and after exposure to NO_2 (Fig.4.22A and B, respectively) show that the crystallinity of the sample is essentially retained although the 2θ values are shifted after exposure to NO_2.

Further information on the interaction of NO_2 with the parent acid (HPW) and the ammonium salt (NH_4PW) can be obtained from ^1H NMR spectra (Fig.4.23). Pretreatment of HPW in helium at 150°C followed by saturation with NO_2 at the same temperature produces an increase in the chemical shifts but no diminution in the intensity of the protium peaks (Fig.4.23A1 and A2).

In contrast the spectra for stoichiometric NH_4PW pretreated in helium at 300°C contains four peaks, the most prominent appearing at 4.85 ppm but, after saturation with NO_2 at 300°C only one peak remains at 7.89 ppm, similar to that found with HPW (Fig.4.23B1 and B2). The effect of deficiencies and excesses of the ammonium ion can be seen from Figure 4.23C1 and C2 in which the former solid displays two prominent peaks while the latter shows one prominent peak with three subsidiary peaks.

The effect of the introduction of NO_2 on the surface areas of the NH_4PW samples is shown in Table 4.2. It is clear that, regardless of the nature of the NH_4PW, exposure to NO_2 reduces the surface areas by approximately 50%.

However the surface areas, after contact of the samples with NO_2, remain substantially higher than those of the parent acid (HPW).

On increase of the mass of the ammonium salt contained in the reactor held at 150°C NO_2 was essentially completely reduced with little or no NO contained in the effluent (Table 4.3). No trace of N_2O was found in the effluent after each injection of NO_2.

Little interaction was observed when NO was injected on the ammonium salt, NH_4PW. It was also observed that NO did not interact with the parent acid, HPW, except when NO_2 was previously injected.

Temperature-programmed reaction of NO on the labelled $^{15}NH_4PW$ reveals that NO is not reduced to N_2 at temperatures below 400°C (Fig.4.24). However, traces of NO_2 were observed at 100°C, as well as some ^{15}NN which is consistent with the reduction of NO_2 on NH_4PW. At temperatures above 400°C, NO is reduced to ^{15}NN with only traces of ^{15}NNO in the effluent of the reactor.

In order to separate the signal for H_2O and $^{15}NH_3$, both found at 18 amu, the experiment was repeated on microporous ND_3HPW, prepared from ND_4Cl and HPW (Fig.4.25). The observations for the reduction of NO to N_2 are comparable, but ammonia was only partially consumed during the process.

Figures 4.24 and 4.25 reveal that NO was not reduced at 150°C when injected on the NH_4PW. However, when nitric acid or NO_2 was injected onto the NH_4PW prior to the

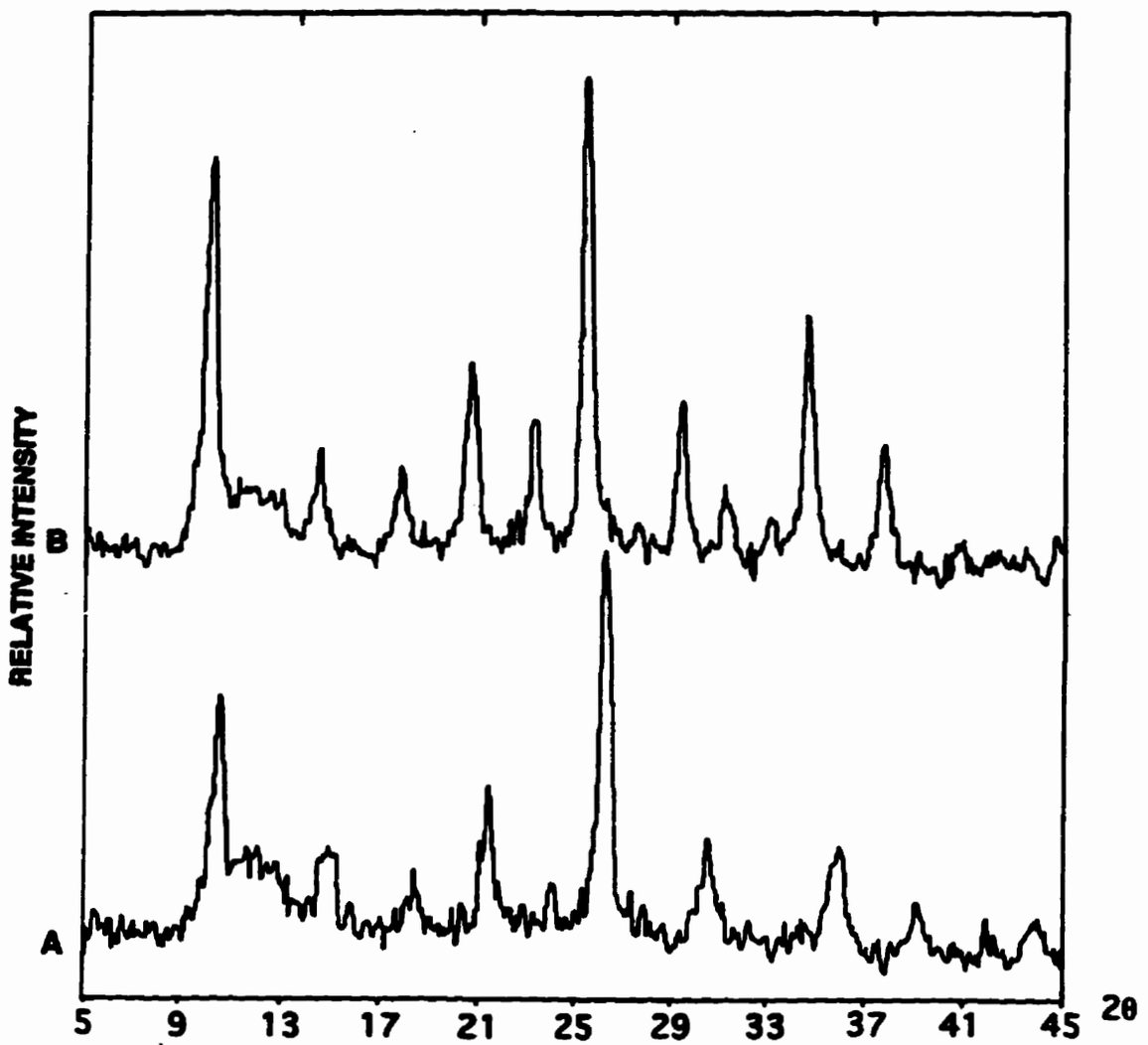

Fig. 4.22 X-ray diffraction patterns of (A) washed-NH_4PW at 25°C, then (B) pretreated and saturated with NO_2 at 300°C.

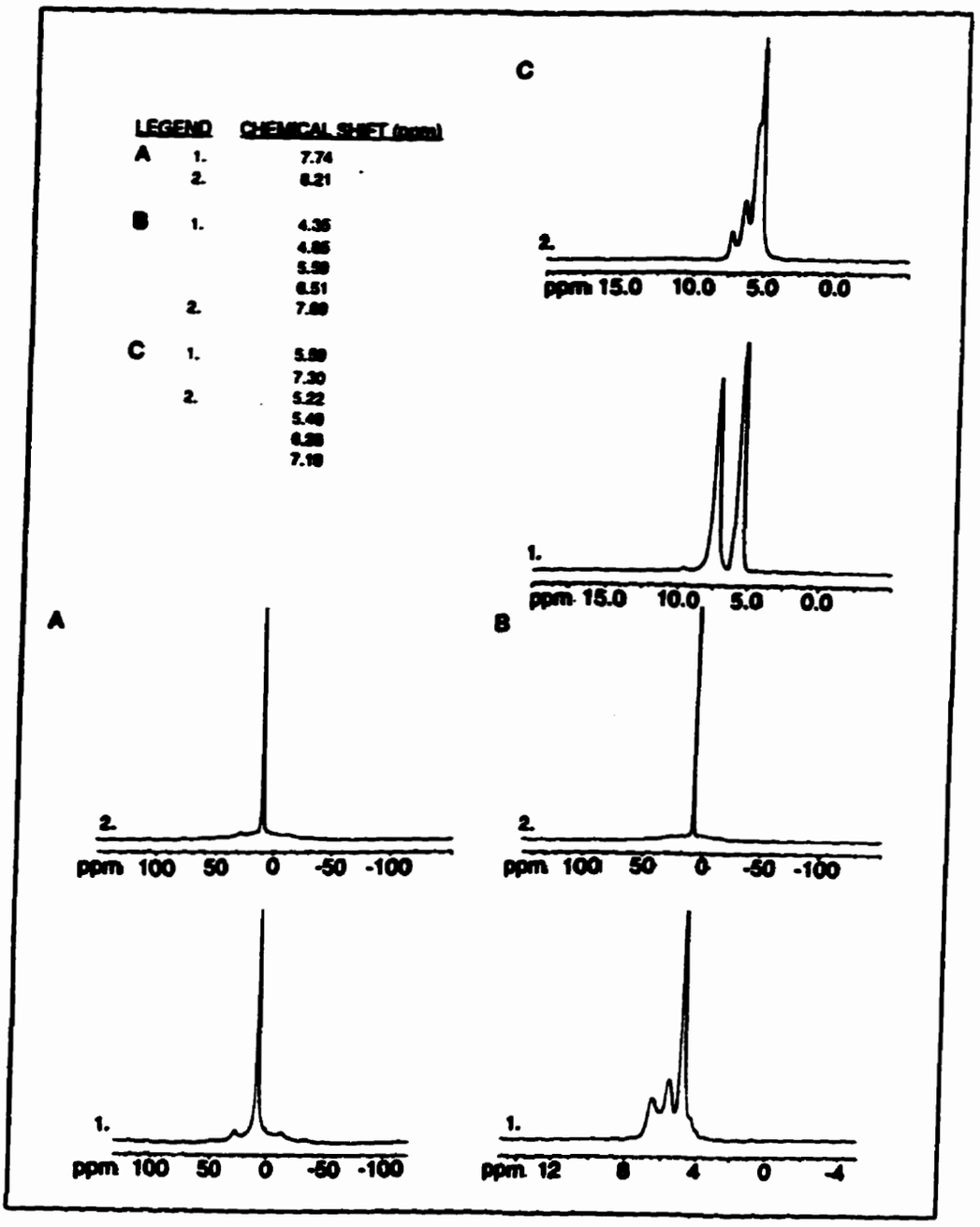

Fig. 4.23 ^{1}H MAS NMR of (A) 1. HPW pretreated at 150°C, 2. HPW pretreated and saturated with NO_2 at 150°C; (B) 1. stoichiometric-washed NH_4PW pretreated at 300°C, 2. stoichiometric-washed NH_4PW pretreated and saturated with NO_2 at 300°C; and (C) 1. NH_4PW (-15%) pretreated at 300°C, 2. NH_4PW (-15%) pretreated at 300°C.

TABLE 4.2

SURFACE AREAS

salt	temp[c] (°C)	sorption[d]	surface area[e] (m^2/g)
NH_4PW (+15%)[a]	300	He	92.1
NH_4PW (+15%)[a]	300	NO_2	52.9
NH_4PW (stoi)[b]	300	He	139.4
NH_4PW (stoi)[b]	300	NO_2	64.9
NH_4PW (stoi)[b]	300	NO_2-NH_3[f]	34.2
NH_4PW (stoi)[a]	300	He	104.8
NH_4PW (stoi)[a]	300	NO_2	63.8
NH_4PW (-15%)[a]	300	He	57.2
NH_4PW (-15%)[a]	300	NO_2	29.6

a Prepared by evaporation only.
b Purified by multiple washing.
c Pretreatment (30 min in He flow) and treatment (5 min in NO_2 flow) temperature.
d Sorption at 300°C.
e BET N_2 (78 K).
f Saturated first with NO_2, then with NH_3.

TABLE 4.3

EFFECT OF INCREASING THE MASS OF NH_4PW[a] HELD AT 150°C[b] ON THE REDUCTION OF NO_2

Mass (g)	Pulse Number[c]	N_2[d] (%mol/mol)	NO[d] (%mol/mol)	NO_2[d] (%mol/mol)
0.075	1	40.4	12.5	29.3
(38.8µmoles)	2	19.7	3.2	63.3
	3	11.7	0.4	66.9
0.500	1	58.0	0.4	0.0
(258µmoles)	2	56.7	0.0	0.0
	3	56.6	0.0	0.0

a Stoichiometric-washed NH_4PW.

b Pretreatment and injection temperature.

c 1 pulse = 17 µmoles of NO_2.

d % mole of N per mole of NO_2 injected in one pulse.

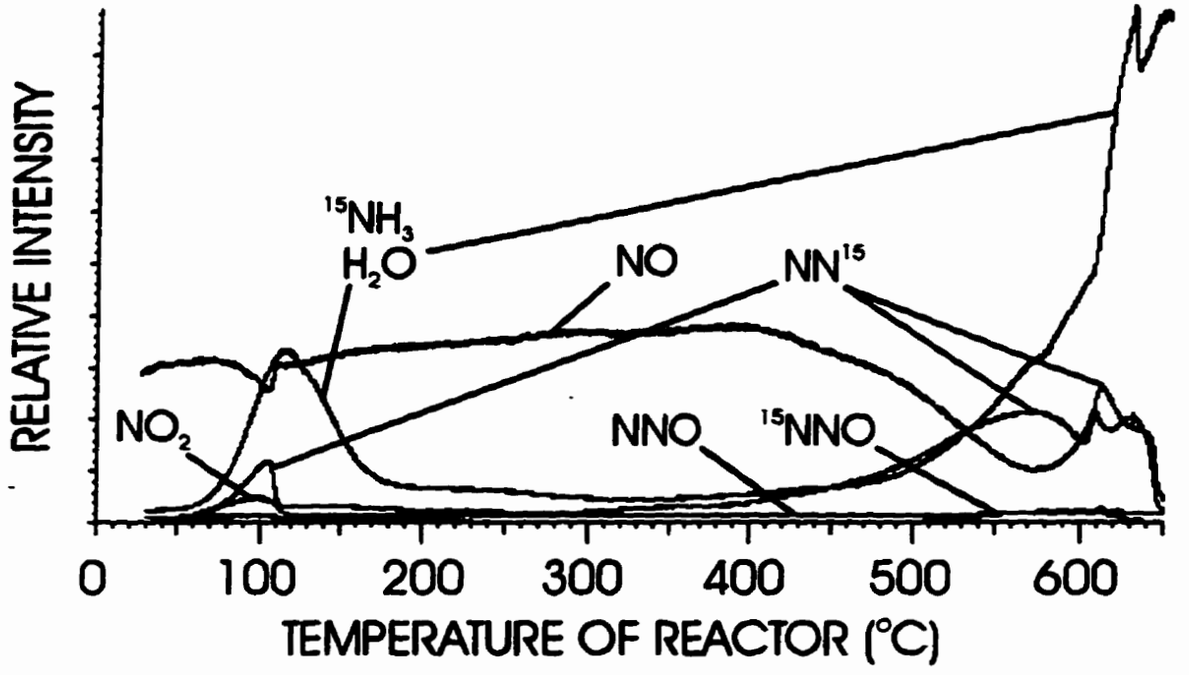

Fig. 4.24 TPR of 0.075g (38.7μmoles) of $^{15}NH_4PW$ exposed to flow(15.6 mL/min)of 4950 ppm NO.

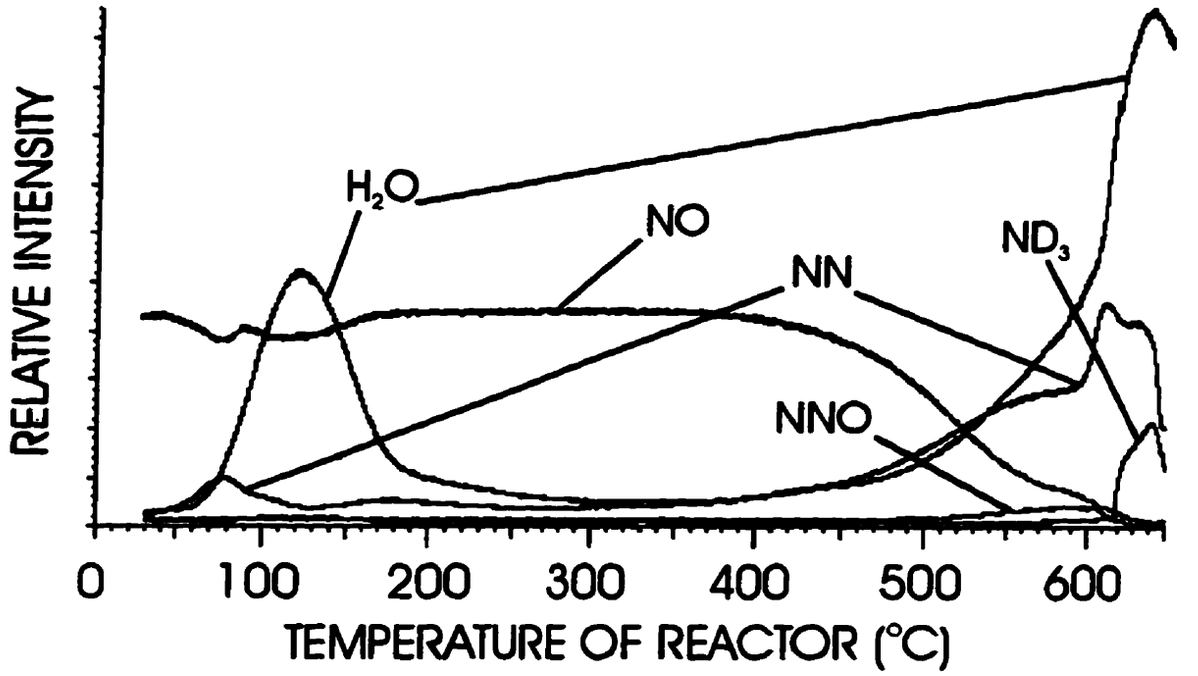

Fig. 4.25 TPR of 0.075g (25.5μmoles) of ND_3HPW exposed to flow(15.6 mL/min)of 4950 ppm NO.

introduction of NO into the reactor maintained at 150°C, NO is reduced to N_2 without the production of N_2O (Table 4.4).

B. Discussion

Nitrogen (N_2) is the predominant N-containing product resulting from the exposure of NH_4PW to NO_2 at temperatures above 150°C. Although O_2 and NO are found, the selectivities to these are relatively small, at least in the first several pulses. This is in sharp contrast with the observations for 12-tungstophosphoric acid, the precursor to the present catalyst, with which the principal gaseous product was HNO_3.

Since, with NH_4PW, it is evident that a reduction of NO_2 is occurring and since the quantity of N_2 produced decreases while that of NO_2 remaining in the effluent increases with increasing exposure of the catalyst to NO_2, it seems clear that the reductant is itself diminished as the process continues. Further, since no reduction process occurred with HPW whereas with NH_4PW such a process is clearly operative, the reductant is evidently the cation in the ammonium salt or, more particularly, ammonia. The elimination of the high-temperature TPD peak due to ammonia after saturation of NH_4PW with either NO or NO_2 (e.g. Figure 4.13) and the regeneration of the ^1H MAS NMR spectra of HPW after exposure of NH_4PW to NO_2 (Fig.4.23) provide tangible support for this contention and for the recovery of the parent solid acid.

Since the results of TPD experiments show that temperatures of 600°C or higher are required for the desorption of NH_3 from NH_4PW, it is evident that, in order for a reaction to proceed between the ammonium cation and NO_2, at temperatures lower than 600°C, the latter molecular species must enter the bulk of the solid. Earlier photoacoustic FTIR experiments have provided direct evidence for the ability of polar molecules such as ammonia, pyridine, and methanol to penetrate into the bulk structure of HPW, that is between the cations and anions, (Refs. 4.1 to 4.3) and in chapter III it has been shown that NO_2 interacts with both surface and interior protons.

Further, since NH_4PW possesses a high, relative to HPW, surface area, resulting primarily from the existence of a microporous structure, the interaction of NO_2 with the NH_3 contained within the bulk of the solid will be further facilitated.

A wide variety of catalysts and reactor systems has been studied for the selective catalytic reduction of NOx, (Refs.4.4 to 4.6, and 4.7). In addition various gases including NH_3, CO, H_2, and CH_4 have been tested as reductants for these nitrogen oxides (Ref.4.7). Since the catalyst employed in the present work is an ammonium compound, discussion will be limited here to NH_3 as a reductant.

TABLE 4.4

REDUCTION OF NO ON NH_4PW AT 150°C

Mass (mg)	Pretreatment[a]	NO Pulse[b] (pulse #)	N_2[c] (%mol/mol)	NO[c] (%mol/mol)
74 (38.2μmoles)	17μmol NO_2	1	98.4	39.8
		2	9.5	91.8
101 (52.2μmoles)	2μL HNO_3	1	130.5	0.0
		2	115.8	7.6
		3	57.0	54.1
		4	8.4	87.0

a Injection of HNO_3 and NO_2 directly on the NH_4PW contained in the reactor held at 150°C prior to the injection of NO pulses.

b 1 pulse = 10 μmoles of NO.

c % mole of nitrogen atoms per mole of NO injected.

A number of reactions have been suggested as relevant to the selective catalytic reduction (SCR) of NOx by NH_3 (Ref.4.8).

$$NO_2 + NH_3 \rightarrow N_2 + 3/2H_2O + 1/4O_2 \qquad \text{(Eq. 4.1)}$$

$$6NO_2 + 8NH_3 \rightarrow 7N_2 + 12H_2O \qquad \text{(Eq. 4.2)}$$

$$NO + NH_3 + 1/4O_2 \rightarrow N_2 + 3/2H_2O \qquad \text{(Eq. 4.3)}$$

$$NO + NO_2 + 2NH_3 \rightarrow 2N_2 + 3H_2O \qquad \text{(Eq. 4.4)}$$

For the analogous non-catalytic reduction (SNCR) developed by Exxon (Ref.4.9) which operates at 850-1050°C, the overall reactions have been found to be

$$6NO + 4NH_3 \rightarrow 5N_2 + 6H_2O \qquad \text{(Eq. 4.5)}$$

$$6NO_2 + 8NH_3 \rightarrow 7N_2 + 12H_2O \qquad \text{(Eq. 4.2)}$$

and a side reaction

$$4NH_3 + 3O_2 \rightarrow 2N_2 + 6H_2O \qquad \text{(Eq. 4.6)}$$

Although it is evident from TPD and infrared results that NO_2 can penetrate the bulk and be sorbed onto the catalyst bulk structure, where reduction occurs, the nature of the participation of the catalyst in the reduction of NO by NH_3 on supported and unsupported vanadium oxide has suggested that the process is associated with the conversion of V=O to V-OH groups with the latter reoxidized by oxygen from underlying layers (Refs. 4.10 to 4.17). Bosch and co-workers (Ref.4.18) suggested that the V=O groups may also be reduced to elemental vanadium by ammonia itself. Janssen et al. (Ref.4.19) proposed a more detailed reaction scheme in which N_2O, which begins to form at 300°C, is included.

Two features of the present catalyst appear to be relevant to the present discussion. Firstly, the catalyst is prepared by an acid-base reaction in which the desired product precipitates from aqueous solution. A surplus of protons will remain if the base (ammonia in the form of an ammonium salt) is added in less than the stoichiometric amount. In fact photoacoustic FTIR experiments have shown that NH_4PW prepared from stoichiometric quantities of the reactants is non-stoichiometric, with residual protons present (Ref.4.1). Secondly, the anion of NH_4PW

possesses two types of accessible oxygen atoms, those bridging the peripheral metal atoms, in the present system, tungsten, and terminal oxygen atoms (W=O) which protrude from the anion. Earlier work from this laboratory suggested that, at least in the catalysis of oxidation processes, the terminal oxygen atoms are more likely to be involved (Ref.4.20), and more recent work has provided support for the contention (Ref.4.21).

The results from the present work strongly suggest that the protons play an active role in the reduction process. Although the nature of the participation of protons in the decomposition or reduction of NO and/or NO_2 is as yet unclear (Ref.4.22), Kantcheva et al. in their studies of the interaction of NO_2 and NH_3 on anatase have suggested that the protons are required for the formation of the ammonium ion, which is claimed to be an integral feature of the reduction process (Ref.4.23). Parenthetically, it may be noted that protons have been shown to play a role, albeit indirect, in the partial oxidation of methane on the heteropoly acids, by generating oxygen vacancies in the heteropoly anion (Ref.4.24).

$$W{=}O + 2H^+ \rightarrow 2W\square + H_2O \qquad \text{(Eq. 4.7)}$$

Duffy et al. have proposed that oxygen vacancies are participants in the NO/NH_3 process on vanadia-titania catalysts (Ref.4.25).

A mechanism analogous to that proposed by Kantcheva et al. (Ref.4.23) may be suggested:

$$W^{5+}\text{-}O\text{-}NO_2NH_4^+ \rightarrow W^{6+}\text{--}O^\circ + [NH_4NO_2] \rightarrow$$
$$N_2 + 2H_2O + WO^\circ \qquad \text{(Eq. 4.8)}$$

Although it is evident, particularly from the results of TPD experiments, that water is a product of the reduction process, oxygen is also formed, but the quantity of the latter increases with each pulse of NO_2 while that of N_2 decreases. A number of possible explanations for these observations may be proposed. Any oxygen formed from the first pulses of NO_2 may be employed, at least in part, in the oxidation of a portion of the NH_3, which exists as NH_4^+ in the present catalyst, through a stoichiometry such as that in Equation 4.6, as proposed by various authors (Refs. 4.23, 4.26, and 4.27). Oxygen may also be involved in the reoxidation of a reduced site on the anion, as has been proposed for vanadia-titania (Ref.4.25) and anastase (Ref.4.23), although NH_3 may also affect this process (Ref.4.23). The maximum in the production of oxygen on apparent depletion of the reductant source may tentatively be related to the dissociation of the water formed during the reduction process and held in the catalyst and/or its reaction with NO_2 (Chapter III).

Although the mechanism proposed for the NO_2/NH_3 reaction on anatase postulates the formation of ammonium nitrite as an intermediate, the production of ammonium nitrate may also be occurring (Ref.4.23). It is well-known that nitrous oxide is prepared industrially from the controlled decomposition of NH_4NO_3 as

$$NH_4NO_3 \rightarrow N_2O + 2H_2O \qquad \text{(Eq. 4.9)}$$

which process begins at approximately 200°C (Ref.4.28). However since the parent acid of NH_4PW, 12-tungstophosphoric acid, has been shown to produce HNO_3 from NO_2, the reaction in which NH_4^+ is oxidized by nitric acid may also be occurring (Ref.4.29).

$$NH_4^+ + HNO_3 \rightarrow H_2O + H_3O^+ + N_2O \qquad \text{(Eq. 4.10)}$$

It is pertinent to note that, in the present work, appreciable quantities of N_2O do not begin to form until 200°C is reached.

It was seen that NO was not reduced or sorbed on the parent acid, HPW (Chapter III). However, if NO_2 was injected first onto HPW then a substantial quantity of NO could be sorbed.

When NO was injected on a fresh sample of NH_4PW, very little sorption and reduction were observed at relatively low temperatures. Although NO is produced at low temperature from the injection of NO_2 on NH_4PW, its reduction to N_2 was only observed at high temperature. Moreover, at low temperature (150°C), nitric oxide can be reduced successfully to N_2 if a promoter (NO_2 or HNO_3) is added or formed prior to its injection on the NH_4PW.

The injection of reactants promoting the formation of ammonium nitrate enhances the reduction of NO to N_2. The mechanisms presented in Equations 4.3, 4.4, and 4.5 are possible but were observed for very high temperatures. At very high temperature it is also believed that NO could extract an oxygen atom from the Keggin Unit to form NO_2, which can be reduced as seen above.

The association of NO with the NO_3^-, as seen in Chapter III, is a possible mechanism leading to the reduction of NO. From the reaction NO with NO_3^-, two molecules of NO_2 would form and then react with the NH_4^+ to give N_2. From this simple, yet plausible mechanism, it would appear that NH_4PW can only reduce NO_2. It is thus possible to reduce NO, but only if NO is oxidized first to NO_2.

The present catalyst thus appears to be dependent for its advantageous reduction properties on three features: its Brønsted acidity, which permits the generation of ammonium ions; its microporosity, which permits NOx to penetrate easily in the structure and react with NH_4^+; and its possession of relatively labile anionic oxygen atoms together with peripheral metal

atoms which, while capable of existing in several oxidation states, have relatively facile transformations between them.

The spent catalyst can be regenerated via precipitation from aqueous solution or injection of gaseous ammonia. Table 4.5 shows the reduction of NO_2 after subsequent regeneration cycles. The decrease in N_2 selectivity can be explained in part by the build-up of ammonium nitrate, which can be removed by heating the catalyst above 200°C.

C. Conclusions

The 12-tungstophosphoric ammonium salt can be used to reduce NO_2 efficiently. Since the "ammonia" is contained within the solid itself, no loss is expected in contrast with standard SCR processes where the reducing agent is injected directly into the gas phase upstream from the catalyst. The present catalyst offers the possibility of reducing the loss of ammonia, thus potentially diminishing or eliminating ammonia slip.

The reaction of NO_2 and NH_4^+ is dependent on the accessibility of the cation inside the bulk of the salt to NO_2. The reaction is more efficient if the impurities contained in the solid catalyst are removed by washing it with water. Furthermore, the reaction for the reduction of NO_2 with NH_4PW is more efficient at relatively high temperature. The effective temperature corresponds to that used in SCR processes for the reduction of NOx.

The direct reduction of NO by NH_4PW was found to be slow and inefficient (i.e. more than one hour for the solid to be saturated when exposed to a continuous flow of pure NO). However the ammonium 12-tungstophosphate is more effective for the reduction of NO_2.

After saturation with NO_2 and consumption of the ammonia contained within the ammonium salt, the parent solid acid (HPW) is recovered and displays the properties discussed in Chapter III. The ammonium salt can then be produced, as before, by precipitation from aqueous solution or by the exposure of the solid acid to gaseous ammonia.

The results presented in this section were recently published in References 4.30 and 4.31.

TABLE 4.5

EFFECT OF GAS PHASE REGENERATION WITH NH_3 AT 150°C

Regeneration Cycles[a]	N_2 (%)[b]	NO (%)[b]
Original salt	41.1	12.3
1st Cycle	52.9	0.0
2nd Cycle	28.7	0.0
3rd Cycle[c]	34.4	0.0

a 0.075g (38.8μmoles) NH_4PW pretreated in helium (15 mL/min) for 30 min. A regeneration cycle consists of injection of 10 mL (NTP) of NH_3, flushing in helium flow for 30 min, and then followed by 1 pulse NO_2 (17 μmoles).

b mole N_2 per mole NO_2 injected.

c Between the second and third cycle, the sample was heated at 300°C for 30 min and then cooled back to 150°C and then exposed to 10 mL NH_3.

REFERENCES

4.1 Highfield, J.G., Moffat, J.B. *J.Catal.*, **88**, 177 (1984).

4.2 Highfield, J.G., Moffat, J.B. *J.Catal.*, **89**, 185 (1984).

4.3 Highfield, J.G., Moffat, J.B. *J.Catal.*, **95**, 108 (1985).

4.4 See, for example, various papers in: Environmental Catalysis; ACS Symposium Series 552; American Chemical Society: Washington, DC, 1994; Emerging Technologies.

4.5 Brandin, J.G.M., Anderson, L.A.H., Odenbrand, C.U.I. *Catal. Today*, **4**, 186 (1989).

4.6 See, for example, Adelman, B.J., Lei, G.-D., Sachtler, W.M.H. *Catal. Lett.*, **28**, 119 (1994) and references therein.

4.7 Bosch, H., Jansson, F. *Catal. Today*, **2**, 369 (1988).

4.8 Matsuda, S., Kato, A. *Appl.Catal.*, **8**, 149 (1983).

4.9 Lyon, R.N. *Int.J.Chem.Kinet.*, **3**, 315 (1976).

4.10 Miyamoto, A., Yamazaki, Y., Inomata, M., Murakami, Y. *J.Phys.Chem.*, **85**, 2366 (1981).

4.11 Inomata, M., Mori, K., Miyamoto, A., Ui, T., Murakami, Y. *J.Phys.Chem.*, **87**, 754 (1983).

4.12 Inamata, M., Miyamoto, A., Murakami, Y. *J.Phys.Chem.*, **85**, 2372 (1981).

4.13 Inamoto, M., Mori, K., Miyamoto, A., Murakami, Y. *J.Phys.Chem.*, **87**, 761 (1983).

4.14 Miyamoto, A., Yamazak, Y., Inomata, M., Murakam, Y. *Chem.Lett.*, 1355 (1978).

4.15 Inomata, M., Miyamoto, A., Murakami, Y. *J.Chem.Soc., Chem.Commun.*, 1009 (1979).

4.16 Miyamoto, A., Hattori, A., Murakami, Y. *J.Solid State Chem.*, **47**, 373 (1983).

4.17 Mori, K., Miyamoto, A., Murakami, Y. *J.Catal.*, **95**, 482 (1985).

4.18 Bosch, H., Janssen, F.J.J.G., Oldenziel, J., van den Kerkhof, F.M.G., van Ommen, J.G., Ross, J.R.H. *Appl.Catal.*, **25**, 239 (1986).

4.19 Janssen, F.J.J.G., van der Kerkhof, F.M.G., Bosch, H., Ross, J.H.R. *J.Phys.Chem.*, **91**, 5921 (1987). Part 2: *J.Phys.Chem.*, in press.

4.20 Moffat, J.B. *J.Mol.Catal.*, **26**, 385 (1984).

4.21 Kozhevnikov, I.V., Sinnema, A., Jansen, R.J.J., Vanbekkum, H. *Catal.Lett.*, **27**, 187 (1994).

4.22 Satsuma, A., Yamada, K., Mori, T., Niwa, M., Hattori, T., Murakami, K. *Catal.Lett.*, **31**, 367 (1995).

4.23 Kantcheva, M., Busheva, V., Klissurski, D. *J.Catal.*, **145**, 96 (1994).

4.24 Kasztelan, S., McGarvey, G.B., Moffat, J.B. In *New Frontiers in Catalysis*; Guczi, L., Solymosi, F., Tétényi, P., Eds.; Elsevier: Amsterdam, 1993; p.1105.

4.25 Duffy, B.L., Curry-Hyde, H.E., Cant, N.W., Nelson, P.F. *Catal.Lett.*, **28**, 167 (1994).

4.26 Odriozola, J.A., Heinmann, H., Somorjai, G.A., Garcia de la Banda, J.F., Pereira, P. *J.Catal.*, **119**, 71 (1989).

4.27 Bosch, H., Janssen, F.J.J.G., van der Kerkhof, F.M., Oldenziel, J., van Ommen, J.G., Ross, J.R.H. *Appl.Catal.*, **25**, 239 (1986).

4.28 Jones, K. The Chemistry of Nitrogen; Pergamon Press: Oxford, 1975.

4.29 Rubtsov, Yu.I., Strizhevskii, I.L., Kazakov, A.I., Andrienko, L.P., Moshkovish, E.B. *Zh.Prikl.Khin. (S.-Peterburg)*, **62**, 2017 (1989).

4.30 Belanger, R., and Moffat, J.B., *Appl. Catal. B: Environm.*,(Accepted Nov.1, 1996).

4.31 Belanger, R., and Moffat, J.B., *Langmuir*, **12**, 2230 (1996).

CHAPTER V

SORPTION AND REACTION OF NO AND NO_2 ON AMMONIUM 12-MOLYBDOPHOSPHATE (NH_4PMo)

A. Results

Three temperatures (150, 300, and 400°C) were selected for investigation of the sorption and reaction of NO and NO_2 on ammonium 12-molybdophosphate.

Upon the injection of pulses of NO_2 on samples of NH_4PMo, the concentration of NO_2 in the effluent of the reactor is negligible for temperatures of 300°C or higher for catalysts A and B, which are prepared using ammonium nitrate and ammonium carbonate, respectively, mixed with stoichiometric amounts of HPMo (Fig.5.1). Salts A and B were further purified by multiple washings with distilled water.

At 150°C, the concentration of NO_2 in the gas phase remains at approximately 100% NO_2. At 300°C, catalysts A and B show the same behavior and the concentration in NO_2 is small for the first two pulses (first 34 μmoles NO_2) but reaches a plateau at 60% with the 8th pulse. However, with NH_4PMo-A at 400°C, the concentration of NO_2 in the effluent remains insignificant for the first five pulses (85 μmoles) and then rises sharply to a plateau of 80-85% at the 8th pulse.

The predominant product from the reduction of NO_2 is N_2 (Fig.5.2). The formation of N_2 is strongly related to the temperature of the reactor. For the first pulse at 150°C, catalysts A and B generate 75 and 20% N (as N_2), respectively. At 300°C, the reduction is found to yield approximately 130% N (as N_2) for the three catalysts. The concentration of N (as N_2) decreases slowly to vanishingly small quantities at these former temperatures as the number of pulses increases. However, at 400°C the first pulse of NO_2 produces approximately 200% N (as N_2). At this temperature the production of N_2 remains high until the fifth pulse for catalyst B and C (salt C was prepared from stoichiometric amounts of ammonium nitrate and HPMo, without further purification), breaks abruptly to reach vanishingly small quantities at the 6-7th pulse number. The conversion to N_2 on catalyst A decreases quasi-linearly from the first pulse to vanishingly small quantities at the 8th pulse.

At temperatures above 300°C, N_2O is also found in the gas phase from the injection of NO_2 on NH_4PMo (Fig.5.3). At 150°C, the quantity of N (as N_2O) is vanishingly small. Catalyst A and B do not show any N_2O produced, and only catalyst C displays selectivity to N_2O. Further, at 300°C, the injection of NO_2 produces greater quantities (>100%) of N (as N_2O) for the first pulse, for each of the three catalysts, and the selectivities decrease gradually to about 20% at the seventh pulse. However, the quantity of N (as N_2O) found in the effluent is lower at 400 than at 300°C. At 400°C, only NH_4PMo-A shows a significant production of

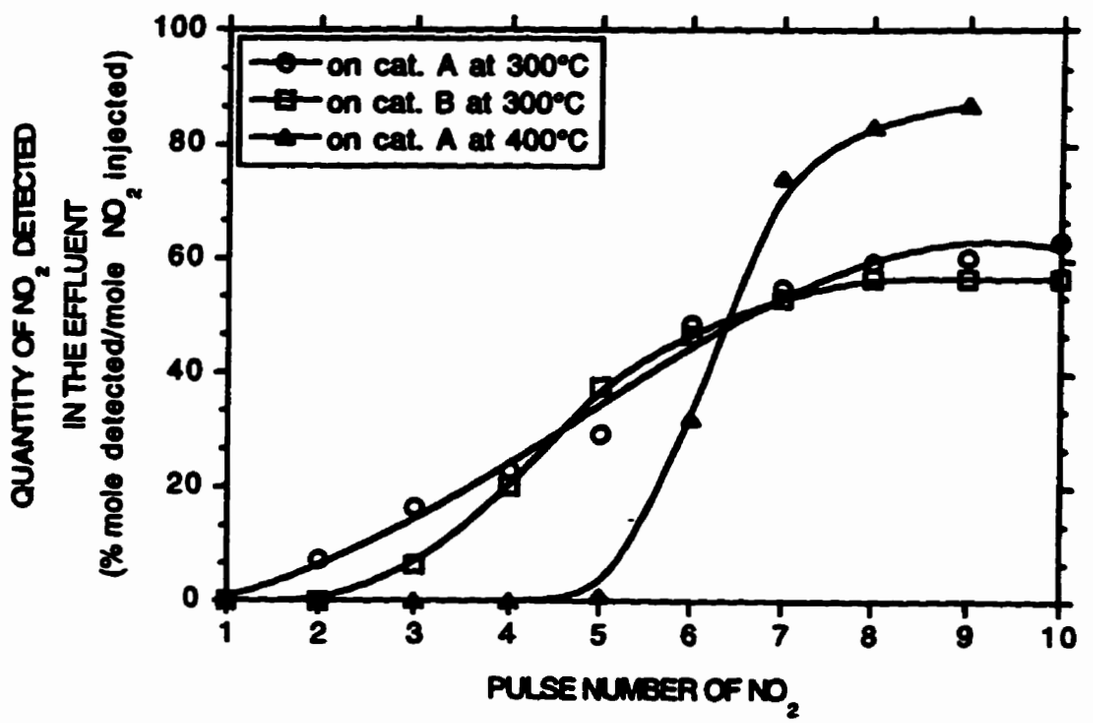

Fig. 5.1 Quantity of NO_2 detected in the effluent for each pulse of NO_2 introduced on catalysts A and B at different pretreatment and reactor temperatures. Mass in reactor = 0.075g (40.0μmoles). Pulse size = 17 μmol NO_2. Helium flow = 15 mL/min.

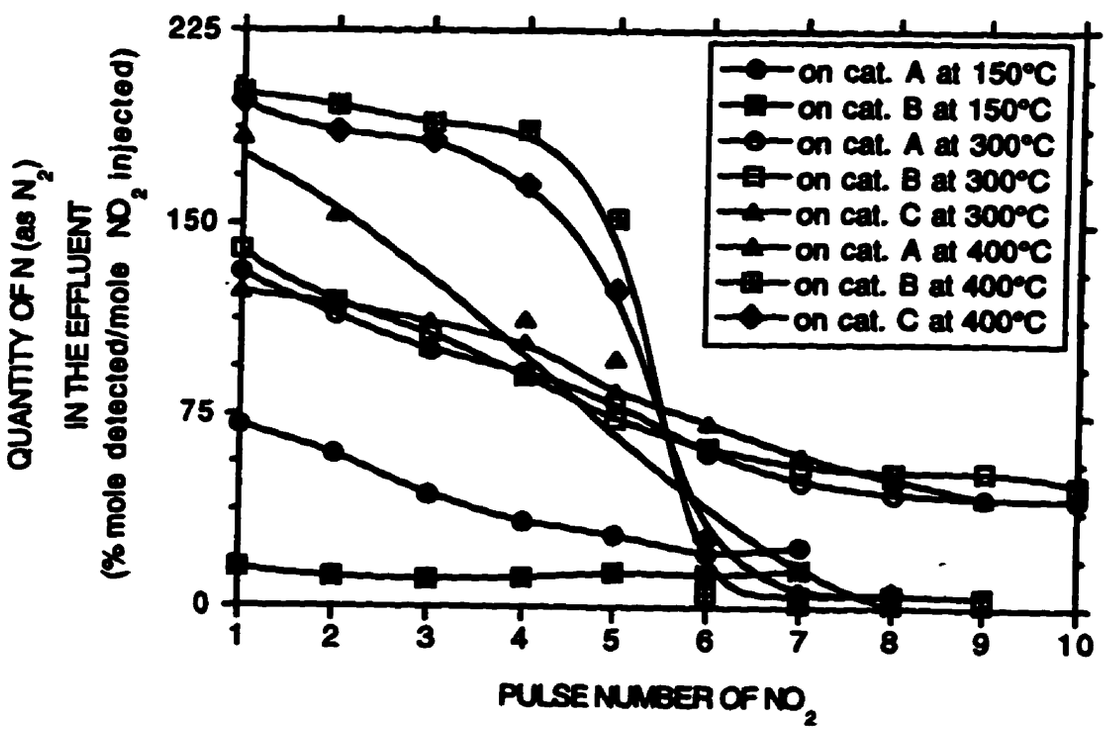

Fig. 5.2 Quantity of N (as N_2) detected in the effluent for each pulse of NO_2 introduced on catalysts A, B and C at different pretreatment and reactor temperatures. Mass in reactor = 0.075g (40.0μmoles). Pulse size = 17 μmol NO_2. Helium flow = 15 mL/min.

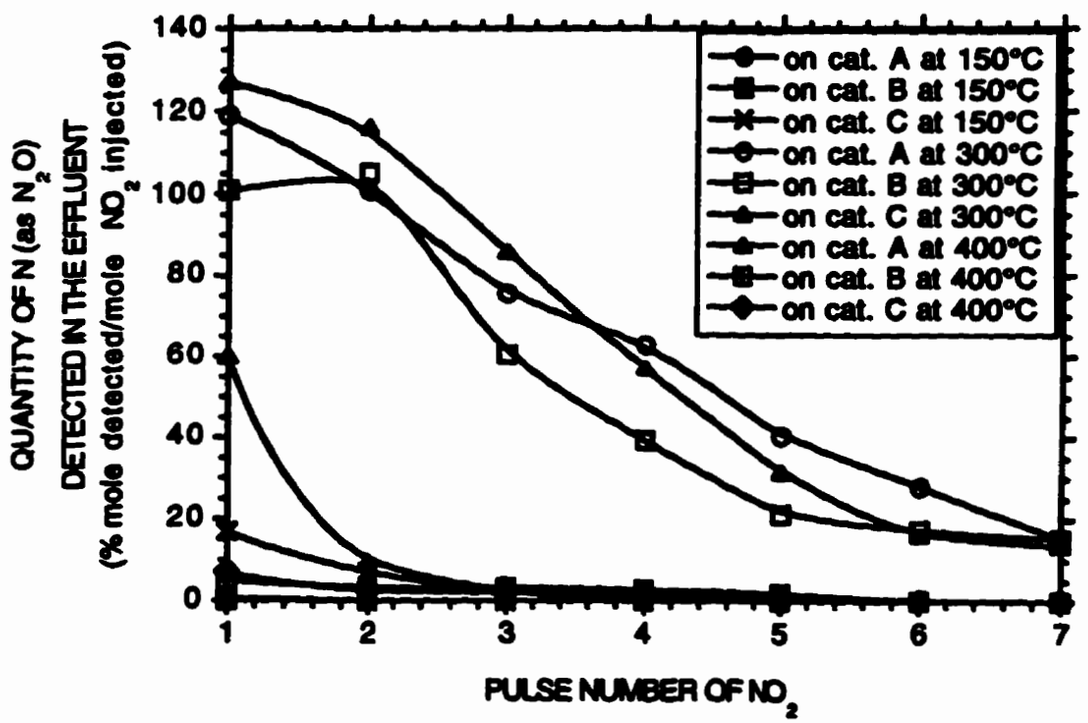

Fig. 5.3 Quantity of N (as N_2O) detected in the effluent for each pulse of NO_2 introduced on catalysts A, B and C at different pretreatment and reactor temperatures. Mass in reactor = 0.075g (40.0μmoles). Pulse size = 17 μmol NO_2. Helium flow = 15 mL/min.

N_2O in the first pulse, but for the two other catalysts the quantities in the effluent are smaller than 10% N (as N_2O) for all pulses.

NO is also produced from the reduction of NO_2 on NH_4PMo (Fig.5.4). For the injection of one pulse of NO_2, catalysts A and B, held at 150°C, produce 10 and 30% of NO, respectively. At 300 and 400°C, all NH_4PMo catalysts show little or no nitric oxide in the gas phase for the first pulse. At 150°C, catalyst A shows an increase in the selectivity to NO, to a maximum of 18% at the 3rd pulse, decreasing to vanishingly small quantities at the 7th pulse. Catalyst B, held at 150°C, shows a maximum production of 30% at the first pulse, decreasing rapidly, reaching 5% at the 4th pulse and then decreasing slowly.

At 300°C, the production of NO remains vanishingly small for all catalysts until the 4th pulse of NO_2, at which catalyst C shows an increase to a maximum of 10% at the 8th pulse while for the remaining two catalysts the quantity of NO remains vanishingly small for all pulses.

When NO_2 is injected on NH_4PMo samples held at 400°C, all three catalysts show a maximum in the quantity of NO in the effluent. For catalyst A, a maximum of 48% is found at the 3rd pulse, and for B and C their maxima of 24 and 14%, respectively, are found at the 6th pulse.

The reduction of NO_2 on NH_4PMo also produces small quantities of O_2 (Fig.5.5). With catalysts A and B held at 300°C, the selectivity to O_2 rises slowly from the first pulse to approximately 2% from the 3rd pulse. However, catalyst C held at 300°C, behaves similarly to all three catalysts held at 400°C, with vanishingly small selectivities to O_2 until the 5-6th pulse, at which the selectivities increase sharply to approximately 1.5-2%.

As is evident from the aforementioned results, the conversion of NO_2 and the selectivities, are dependent on the temperature of the reactor. Figure 5.6 summarizes the selectivities for the first pulse of NO_2 introduced in the reactor, as a function of the temperature, for all three catalysts. The conversion of NO_2 (with maximum N_2 and minimum N_2O) is at its maximum at 400°C.

Nitric oxide can also be reduced on NH_4PMo (Fig.5.7). The monitoring of the effluent shows that at 300°C, approximately 60% of NO is found in the gas phase for the first pulse on catalyst A. The concentration of NO increases very slowly for the subsequent pulses. At 400°C, the conversion of NO is very different. Approximately 100% of NO is removed from the gas phase in the first pulse of NO, on catalysts A and C, and about 87% with catalyst B. The quantity of NO in the effluent rises rapidly to high concentrations at the 4th pulse. With catalyst A, approximately 100% of NO injected is detected from the 4th and subsequent pulses. For catalyst B, the quantity of NO detected in the gas phase is much lower, approximately 80% at the 4th pulse, and then rises slowly. With catalyst C, the quantity of NO remaining in the effluent

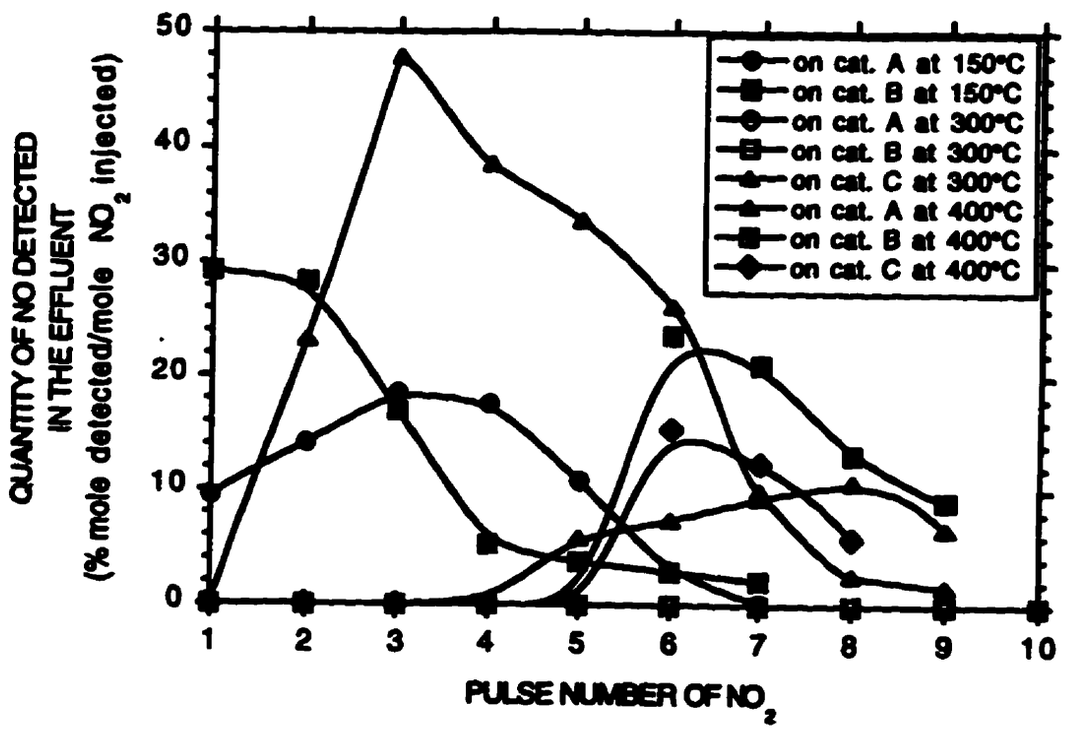

Fig. 5.4 Quantity of NO detected in the effluent for each pulse of NO_2 introduced on catalysts A, B and C at different pretreatment and reactor temperatures. Mass in reactor = 0.075g (40.0μmoles). Pulse size = 17 μmol NO_2. Helium flow = 15 mL/min.

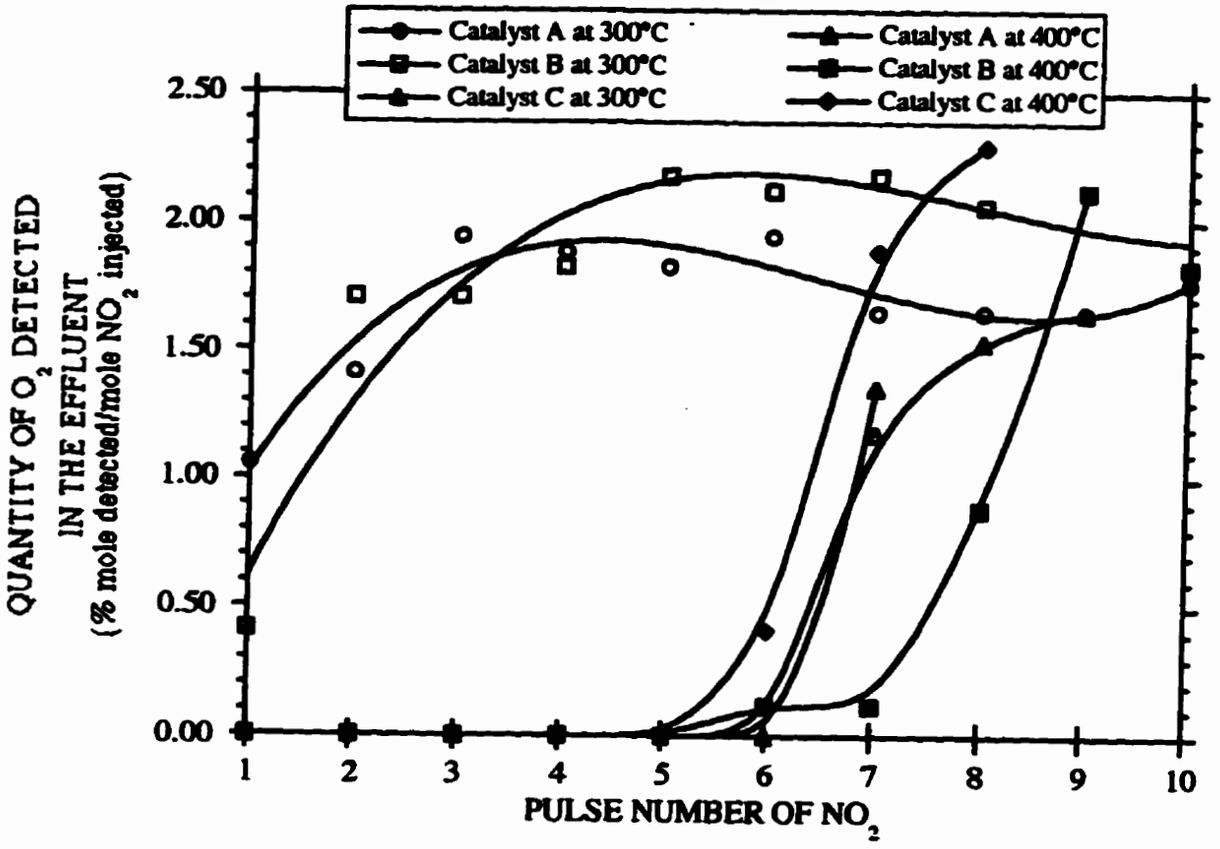

Fig. 5.5 Quantity of O_2 detected in the effluent for each pulse of NO_2 introduced on catalysts A, B and C at different pretreatment and reactor temperatures. Mass in reactor = 0.075g (40.0μmoles). Pulse size = 17 μmol NO_2. Helium flow = 15 mL/min.

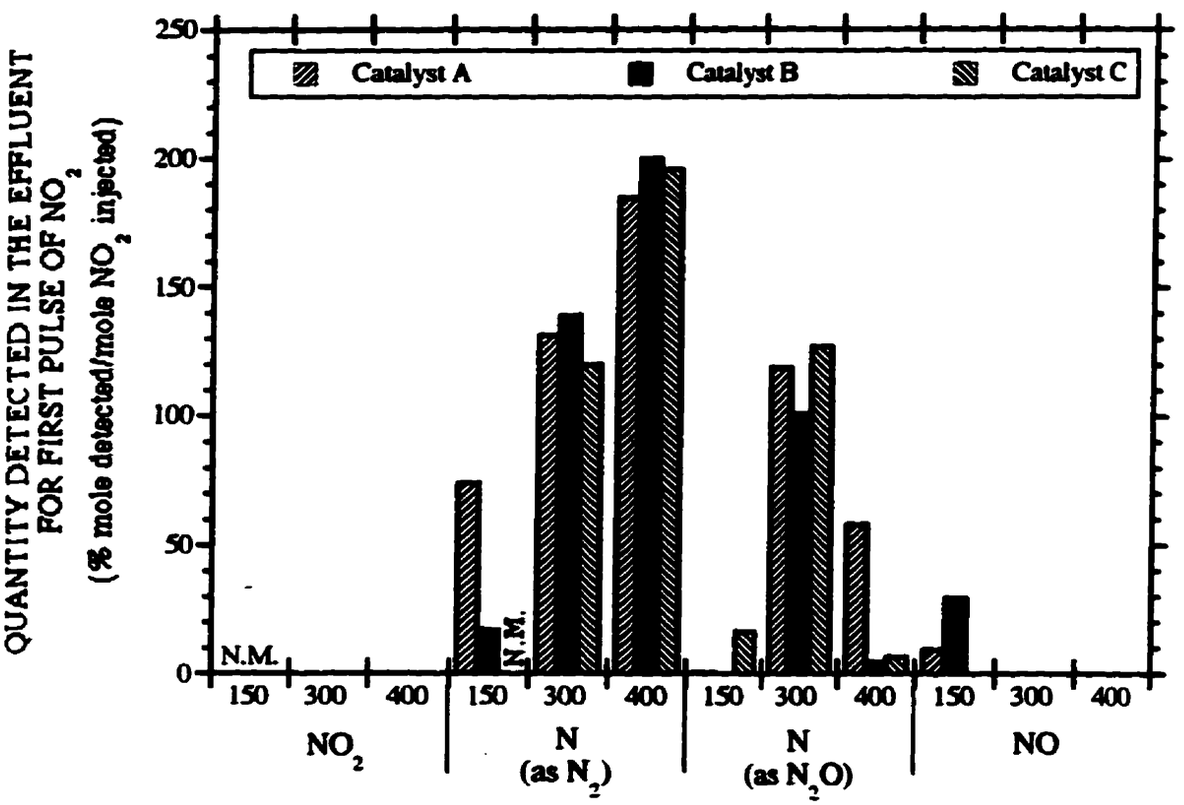

Fig. 5.6 Quantity of NO_2, N (as N_2), N (as N_2O), and NO detected in the effluent for the first pulse of NO_2 introduced on catalysts A, B and C at different pretreatment and reactor temperatures. Mass in reactor = 0.075g (40.0μmoles). Pulse size = 17 μmol NO_2. Helium flow = 15 mL/min.

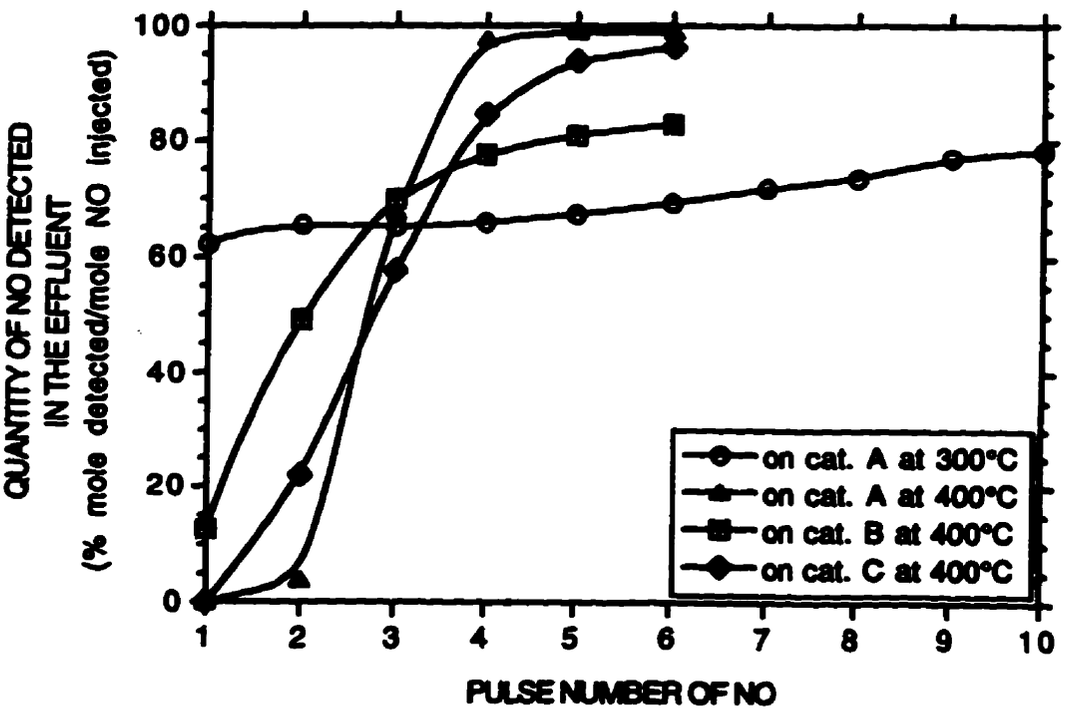

Fig. 5.7 Quantity of NO detected in the effluent for each pulse of NO introduced on catalysts A, B and C at different pretreatment and reactor temperatures. Mass in reactor = 0.075g (40.0μmoles). Pulse size = 10 μmol NO. Helium flow = 15 mL/min.

increases sharply with the number of pulses reaching 80% at the 4th pulse and, with further injections, increasing to values near 100%.

The principal product found in the effluent from the reduction of NO on NH_4PMo is N_2 (Fig.5.8). As expected from Figure 5.7, the production of N_2 generally decreases with increase in the number of pulses. Figure 5.8 is almost a horizontal mirror image of Figure 5.7. When NO is injected at 400°C, the selectivities to N (as N_2) are high, approximately 200% N (as N_2), for all three catalysts. However, when nitric oxide is injected on catalyst A at 300°C, the selectivity to N (as N_2) corresponds to approximately 100%. The concentration of N (as N_2) decreases slowly with the pulse number.

While the injection of NO_2 produces a relatively high selectivity to N_2O, the reaction of NO on NH_4PMo generates much smaller selectivities to this oxide of nitogen (Fig.5.9). With catalyst A exposed to nitric oxide at 300°C, the selectivity to N (as N_2O) remains constant at 5% for three pulses of NO, which is smaller than that obtained from the injection of NO_2. At 400°C, the selectivity to N_2O varies similarly to that from the injection of NO_2 on NH_4PMo but the quantities are smaller. The maximum N (as N_2O) produced is less than 20% of the NO injected. For all catalysts held at 400°C, the selectivities to N_2O produced decrease rapidly from their highest values, at the first pulse, to a plateau.

Little or no selectivity to O_2 was observed from the injection of NO on the catalysts at both 300 and 400°C.

The conversion of NO as well as the selectivities, are dependent on the temperature of the reactor. Figure 5.10 summarizes the selectivities for the first pulse of NO introduced in the reactor, as a function of the temperature, for all three catalysts. The conversion of NO (with maximum N_2 and minimum N_2O) is at its maximum at 400°C.

Isothermal continuous reaction (ICR) experiments of NO_2 on $^{15}NH_4PMo$, for the first hour of reaction, are presented in Table 5.1. These values are corrected to take into consideration the fragmentation due to the MS detector. The values show that the selectivities to ^{15}NN and H_2O increase with temperature, passing through maxima at 300°C.

The selectivity to NO in the effluent decreases as the temperature of the reaction is increased, and since no labelled NO is detected this oxide of nitrogen must originate solely from NO_2 without any apparent participation of the NH_3 contained within the catalyst. The conversion of NO_2 to NO is expected to increase with temperature, but, as it was seen, the NO itself is reduced at higher temperatures. The concentration of N_2O (as ^{15}NNO and NNO) is very small at 150°C, but significant at 300°C and at 425°C.

The analysis of the effluent from a NO_2/He feedstream passed continuously over ^{15}N-ammonium 12-molybdophosphate, heated at 10°C/min from room temperature to 650°C, is shown in Figure 5.11. The results reveal that NO_2 is reduced to N_2 at temperatures as low as

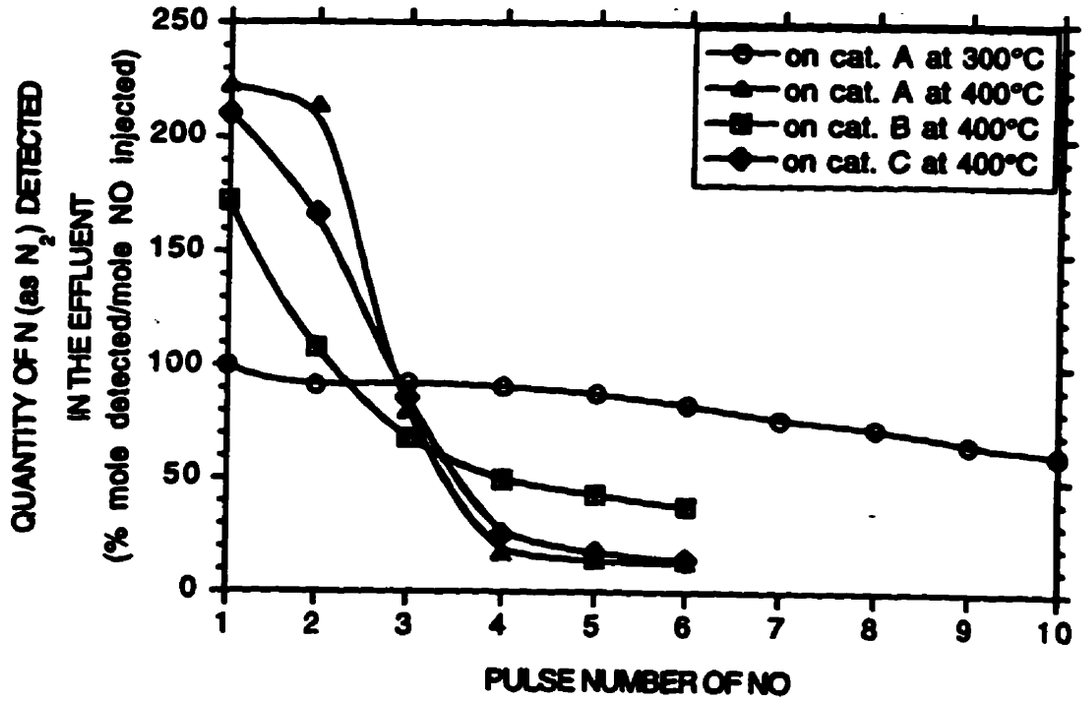

Fig. 5.8 Quantity of N (as N_2) detected in the effluent for each pulse of NO introduced on catalysts A, B and C at different pretreatment and reactor temperatures. Mass in reactor = 0.075g (40.0μmoles). Pulse size = 10 μmol NO. Helium flow = 15 mL/min.

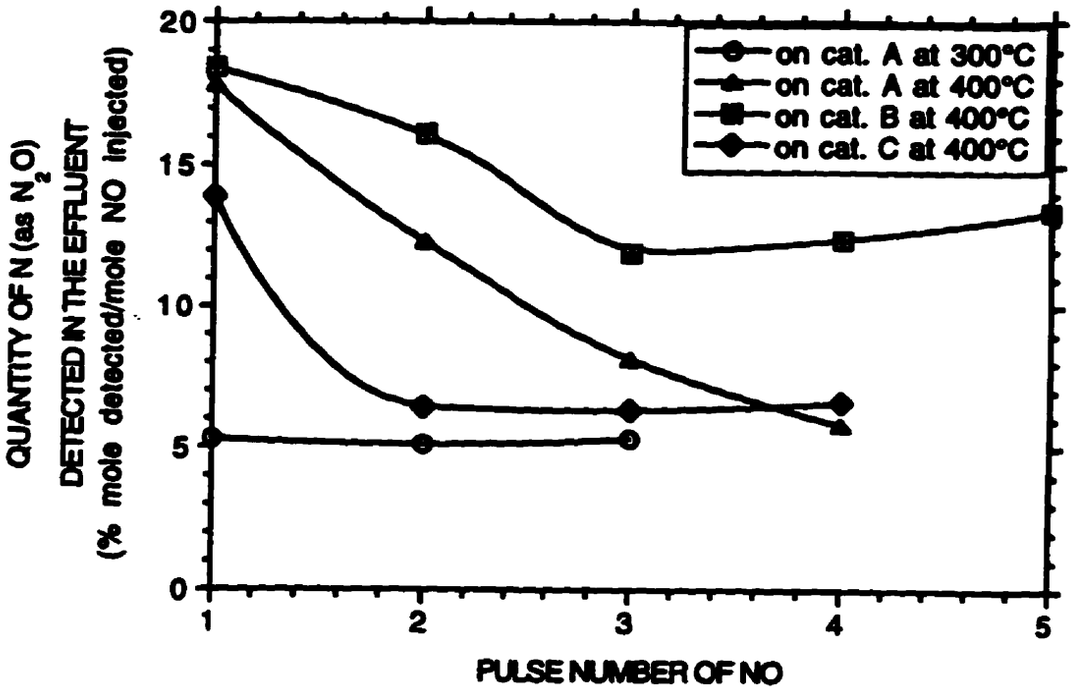

Fig. 5.9 Quantity of N (as N_2O) detected in the effluent for each pulse of NO introduced on catalysts A, B and C at different pretreatment and reactor temperatures. Mass in reactor = 0.075g (40.0μmoles). Pulse size = 10 μmol NO. Helium flow = 15 mL/min.

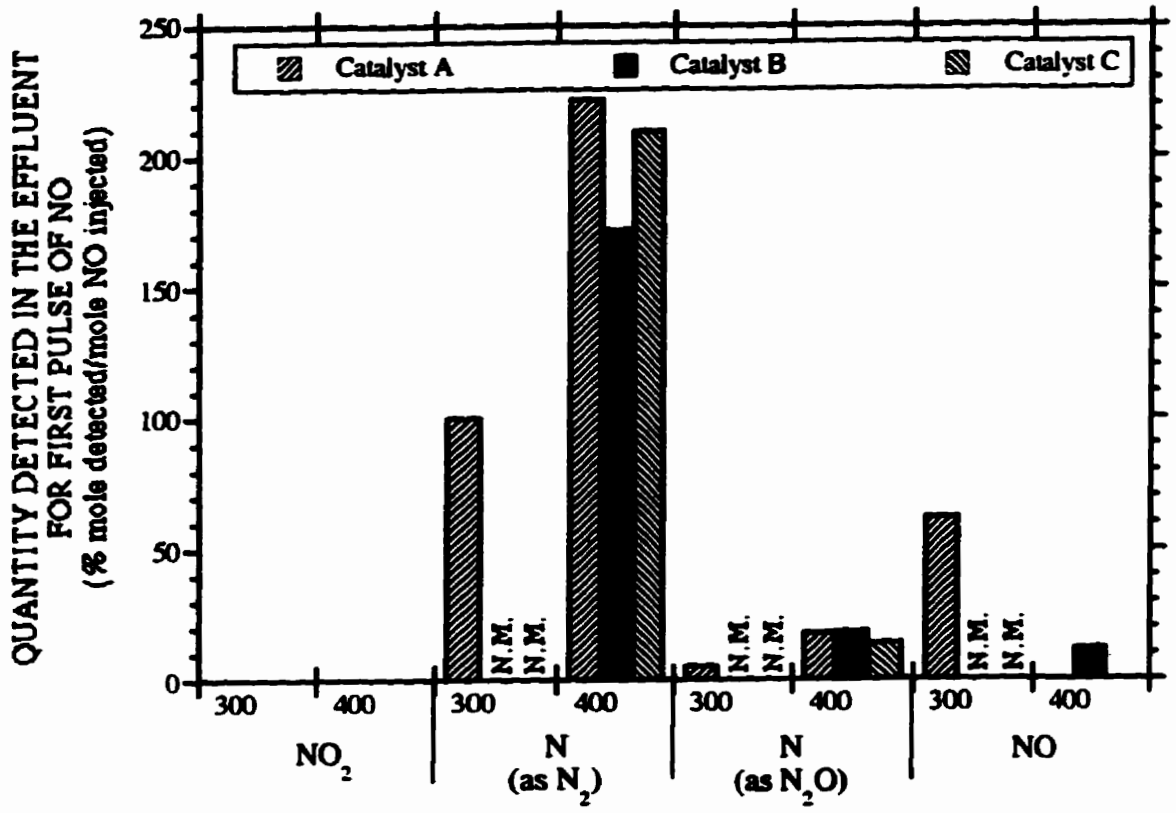

Fig. 5.10 Quantity of NO_2, N (as N_2), N (as N_2O), and NO detected in the effluent for the first pulse of NO introduced on catalysts A, B and C at different pretreatment and reactor temperatures. Mass in reactor = 0.075g (40.0μmoles). Pulse size = 10 μmol NO. Helium flow = 15 mL/min.

TABLE 5.1

INTEGRATED AREA FOR THE ISOTHERMAL CONTINUOUS REACTION OF $^{15}NH_4PMo$ AND NO_2

ICR 0.075g (39.9μmoles) $^{15}NH_4PMo$ + 4960 ppm NO_2

Masses	Molecules	%mole detected/mole NO_2 injected[a]		
		150°C	300°C	425°C
18	HOH	5.0	9.4	3.5
28	NN	0.0	0.0	0.0
29	^{15}NN	3.8	7.0	1.9
30	NO	9.6	5.9	4.2
31	^{15}NO	0.0	0.0	0.0
44	NNO	0.6	0.3	0.1
45	^{15}NNO	0.0	3.8	0.6
46	ONO	38.4	24.4	15.0

[a] % mole detected corrected per Total Ion of NO_2 injected for 60 min integration time.

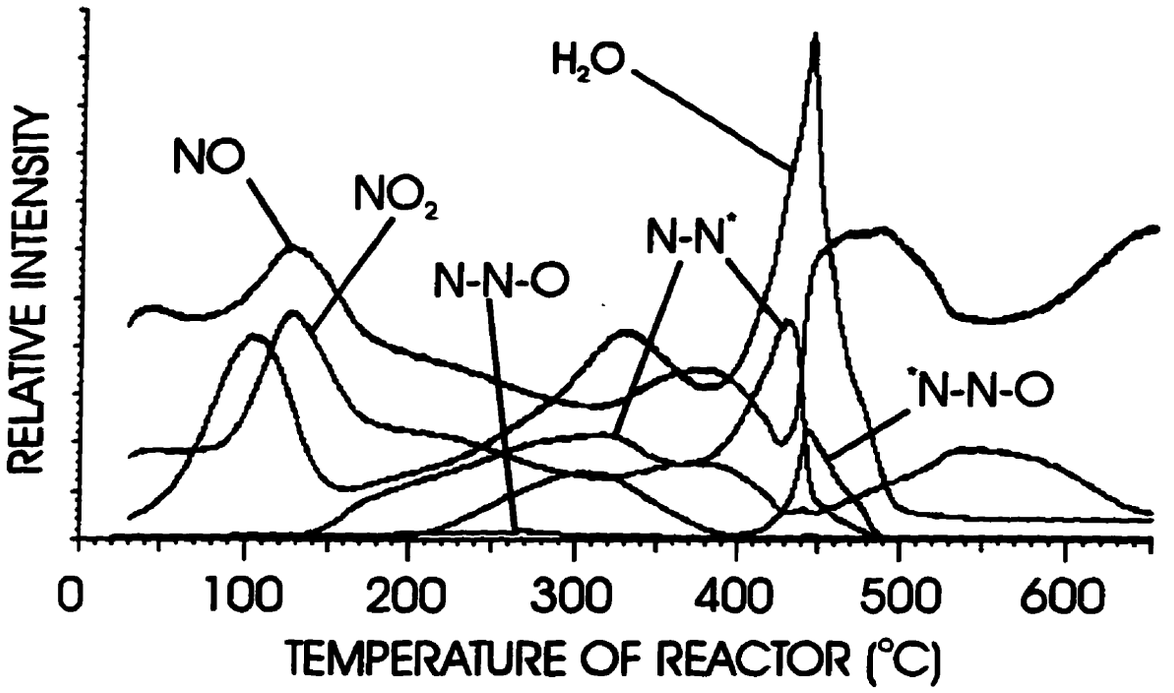

Fig. 5.11 Temperature-programmed reaction of 0.075g (39.9μmoles) of $^{15}NH_4PMo$ exposed to a continuous flow of 4960 ppm of NO_2. Heating rate=10°C/min and Flow rate=20 mL/min.* = Isotope 15.

80°C and up to 500°C, with maxima at 300 and 420°C, the latter being higher than the former. H_2O, NO, and N_2O form concomitantly with N_2 at 420°C. As will be shown later, with TPD results, the water peaks observed at 100 and 430°C result from hydrogen bonded and associatively desorbed water molecules, respectively. Although the variation of the relative intensity of N_2O with temperature is similar to that of N_2, a null point exists for the former species between 380 and 410°C. The concentration of NO, which is higher than expected because of the fragmentation in the MS detector, shows a maximum between 430 and 530°C. This production of NO occurs at a higher temperature than that at which the maxima appear for H_2O, N_2, and N_2O. However, this maximum in the NO concentration corresponds to a minimum in the quantity of NO_2 in the gas phase.

Temperature-programmed reaction of the labelled ^{15}N-ammonium 12-molybdophosphate exposed to a continuous flow of NO also shows the reduction of NO to mainly N_2 (Fig.5.12). Nitrogen molecules formed from the ammonia (as NH_4^+) contained within the catalyst and the NO from the gas phase are produced in relatively small quantities at 100°C, but much greater quantities are formed between 220 and 520°C with a maximum at 360°C. The maximum in the formation of N_2 is concomitant with the formation of water and the minimum in the concentration of NO in the effluent. However, at temperatures lower than 380°C, no N_2O was detected in the gas phase. Small quantities of N_2O are formed between 380 and 530°C with a maximum at 430°C. The concentration of NO_2 was negligible for the whole range of temperature except for vanishingly small quantities at 100°C (not shown).

Temperature-programmed desorption curves for the four salts of NH_4PMo as prepared are found in Figures 5.13 to 5.16. The fourth salt was prepared from ^{15}N-ammonium nitrate ($^{15}NH_4NO_3$) and HPMo. Catalyst A shows the expected TPD profile for an ammonium salt of a heteropoly oxometalate (Fig.5.13). Physisorbed (or hydrogen-bonded), water molecules contained at the surface and within the bulk of the salt desorb approximately at 100°C, as well as traces of ammonia. The peak which emerges between 400 and 550°C is due to associatively desorbed water resulting from the extraction of oxygen atoms from the anions by at least a portion of the protons. The latter peak is accompanied by the desorption of ammonia, from the ammonium cations, and N_2, apparently produced from the oxidation of NH_3. Two maxima are observed for the desorption of N_2. The first maximum, at 440°C, is observed concomitantly with the desorption of water and ammonia, while a second peak for N_2 can be seen at 600°C.

Catalyst B, prepared from ammonium carbonate, shows significant differences (Fig.5.14). This salt contains relatively small numbers of weakly bound, physisorbed, water molecules capable of desorbing at low temperature. Instead, two peaks due to ammonia desorption from the salt are seen. The main peak for ammonia appears at 280°C, immediately followed by a first water peak at 310°C. No nitrogen is observed with the first ammonia peak.

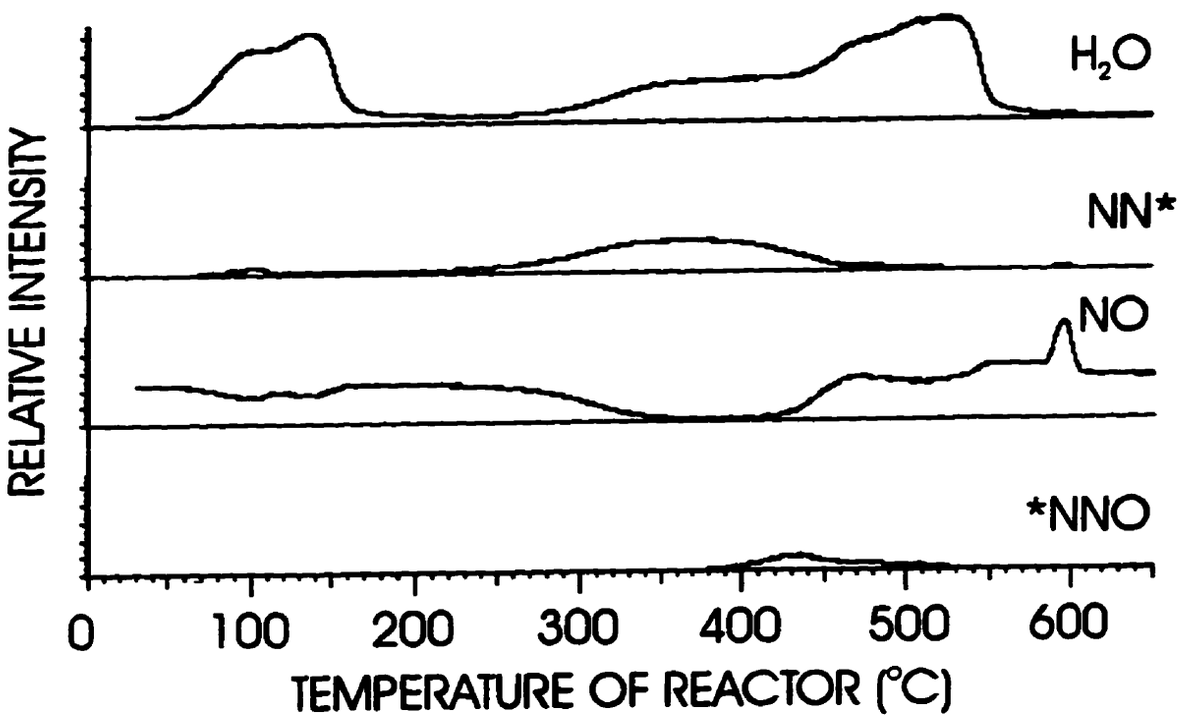

Fig. 5.12 Temperature-programmed reaction of 0.075g (39.9μmoles) of $^{15}NH_4PMo$ exposed to a continuous flow of 4950 ppm of NO. Heating rate=10°C/min and Flow rate=20 mL/min.* = Isotope 15.

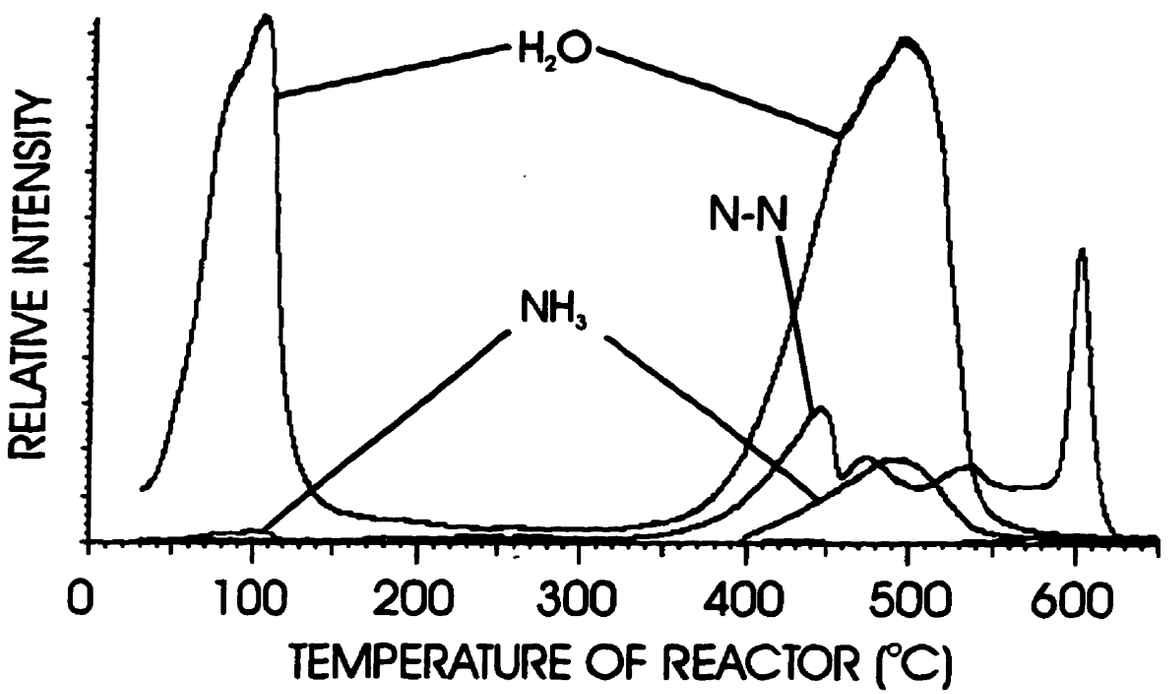

Fig. 5.13 Temperature-programmed desorption of 0.075g (40.0μmoles) of NH_4PMo-A as prepared. Heating rate=10°C/min and Flow rate=20 mL/min.

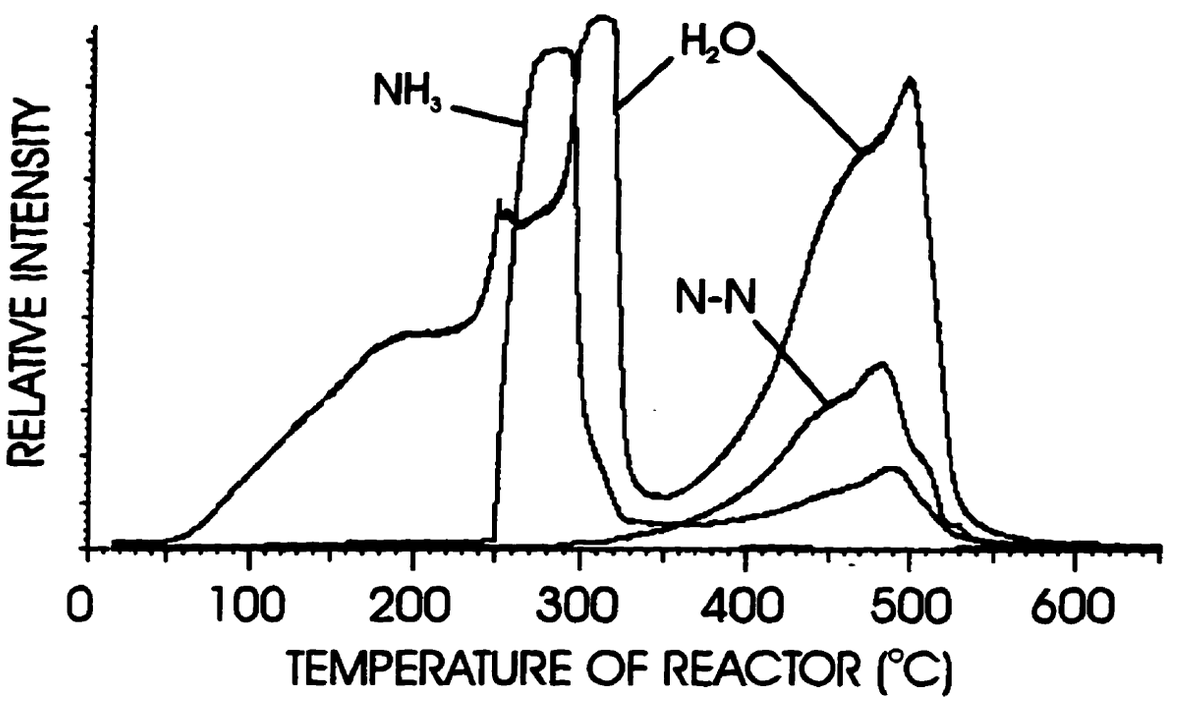

Fig. 5.14 Temperature-programmed desorption of 0.075g (40.0μmoles) of NH_4PMo-B as prepared. Heating rate=10°C/min and Flow rate=20 mL/min.

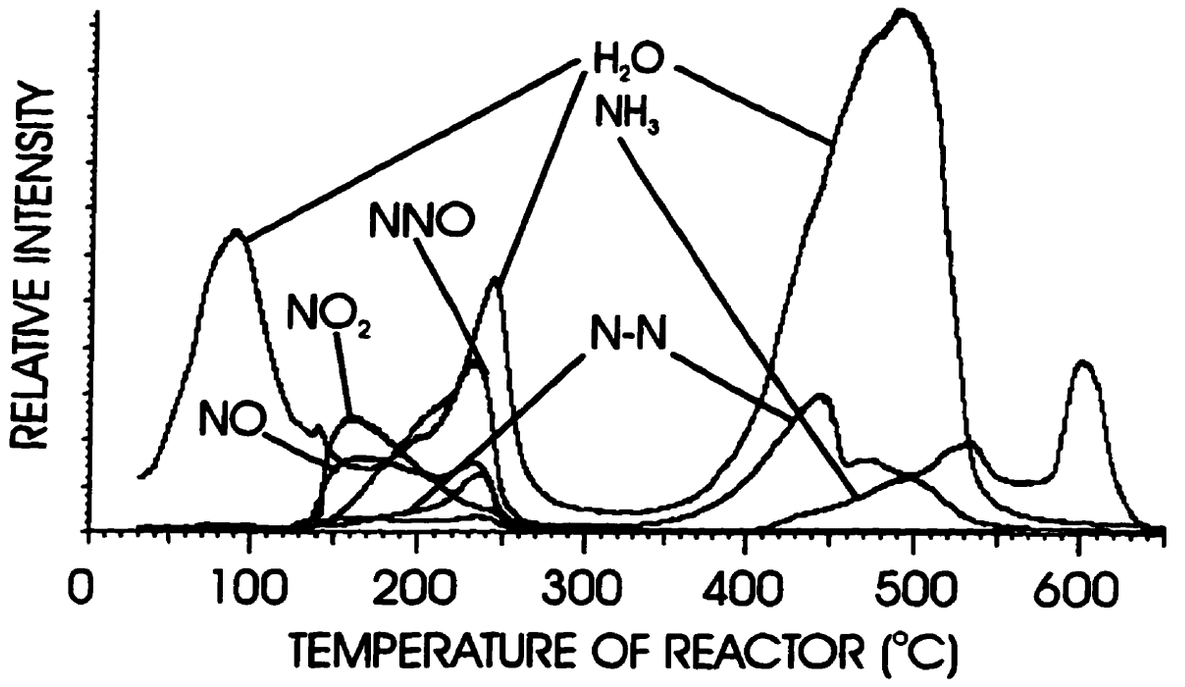

Fig. 5.15 Temperature-programmed desorption of 0.075g (40.0μmoles) of NH_4PMo-C as prepared. Heating rate=10°C/min and Flow rate=20 mL/min.

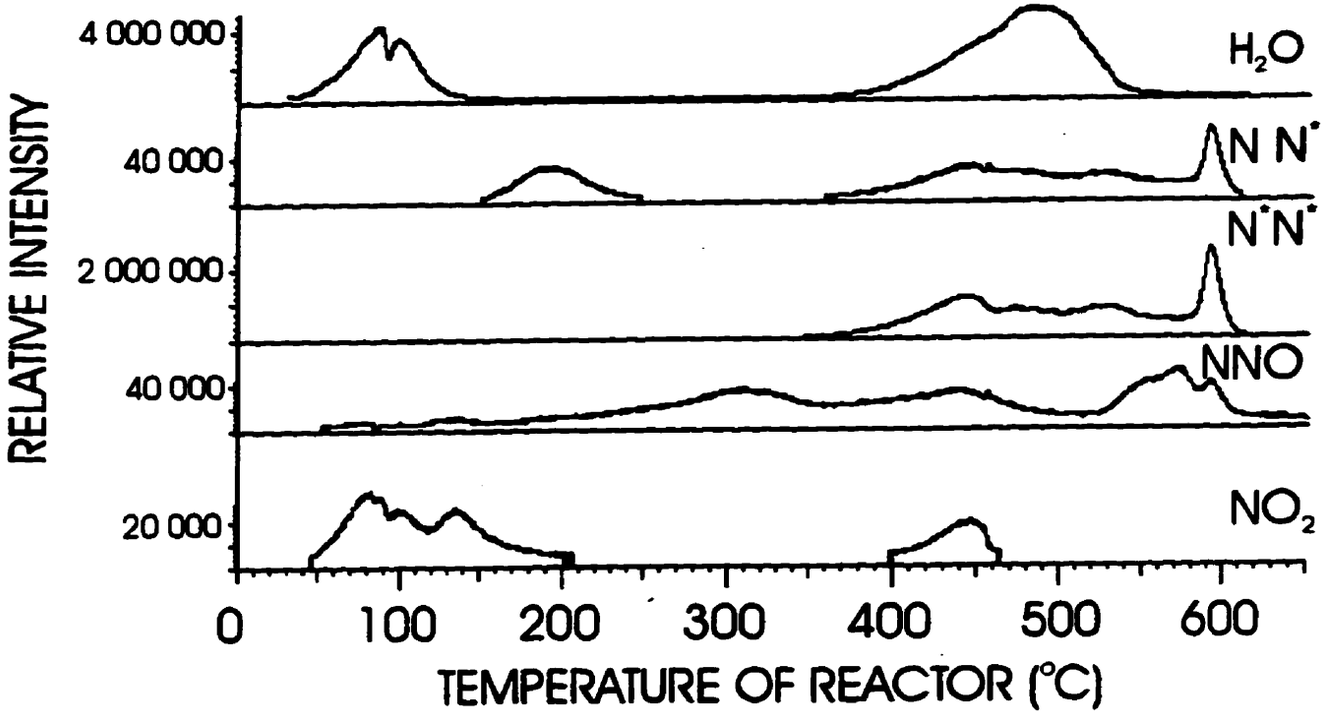

Fig. 5.16 Temperature-programmed desorption of 0.075g (39.9μmoles) of $^{15}NH_4PMo$ as prepared. Heating rate=10°C/min and Flow rate=20 mL/min. * = Isotope 15.

A second peak for the ammonia can be observed at 490°C, concomitantly with a second water peak and one due to N_2. This maximum corresponds, both quantitatively and qualitatively, to the same type of ammonium found in catalyst A, but the high temperature peak for the desorption of nitrogen, at 600°C, as observed for catalyst A, is not found for this ammonium salt.

The TPD observed for the catalyst C, which was also prepared from ammonium nitrate, however unwashed, shows a similar TPD as observed for catalyst A (Fig.5.15). However, the impurities (mainly unreacted ammonium nitrate) also desorb from the catalyst at temperatures below 280°C, as NO, NO_2, and N_2O. Very small quantities of ammonia also desorb in this temperature range. Further, the high temperature nitrogen peak, found at 600°C, is also observed for this salt.

The ^{15}N-ammonium 12-molybdophosphate catalyst also shows the same type of TPD recorded for catalyst C (Fig.5.16). The impurities remaining on the catalyst, as well as the physisorbed water, desorb at low temperature. This is followed by associatively desorbed water, concomitantly with ammonia (also with amu of 18) and N_2. The high temperature (600°C) nitrogen peak is also observed from the TPD. Further, one labelled nitrogen forms part of this molecular nitrogen, but this molecule is found at very little concentration (see relative intensity). Similarly to catalysts A and C, the peak observed at 600°C is the doubly-labelled nitrogen ($^{15}N^{15}N$) from the autooxidation of $^{15}NH_3$ (from $^{15}NH_4^+$).

Nitrogen dioxide was introduced into the reactor containing ^{15}N-ammonium 12-molybdophosphate pretreated and held at three different temperatures, 150, 300 and 425°C (Figs.5.17 to 5.19), respectively.

The temperature-programmed desorption analysis of $^{15}NH_4PMo$, pretreated and exposed to NO_2 at 150°C (Fig.5.17), shows small quantities of water desorbing from 200 to 420°C, at which temperature a significant desorption peak is observed. This desorption peak possesses two maxima observed at 450 and 500°C. The desorption of water, at 200°C, is concomitant with the desorption of ^{15}NN and traces of NO and NO_2. However, quantities of NO, and traces of NO_2, desorb concomitantly with the major peak of water observed at high temperature. No significant amount of N_2O (or ^{15}NNO) was detected throughout the TPD.

For a pretreatment and exposure to NO_2 at 300°C, significant differences are observed (Fig.5.18). The intensity of the signal can be seen from an evaluation of the signal/noise ratio (s/n) of the trace. Very small quantities of water were detected with a maximum at 410°C. Nitric oxide was detected in the effluent without a definite maximum. Traces of NO_2 were observed desorbing from the catalyst at 70°C and above 610°C. No detectable quantity of ^{15}NN could be observed in the effluent.

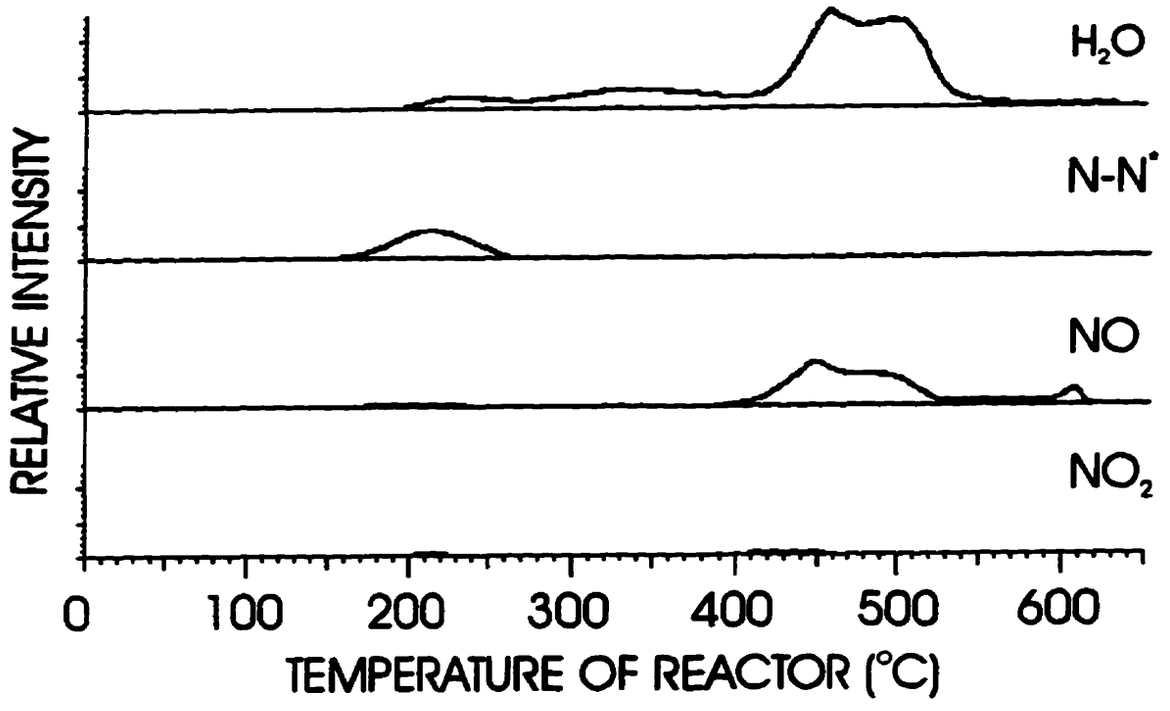

Fig. 5.17 Temperature-programmed desorption of 0.075g (39.9μmoles) of $^{15}NH_4PMo$ pretreated and exposed to flow of 4960ppm NO_2 at 150°C. Heating rate=10°C/min and NO_2, He Flow rate=20 mL/min. * = Isotope 15.

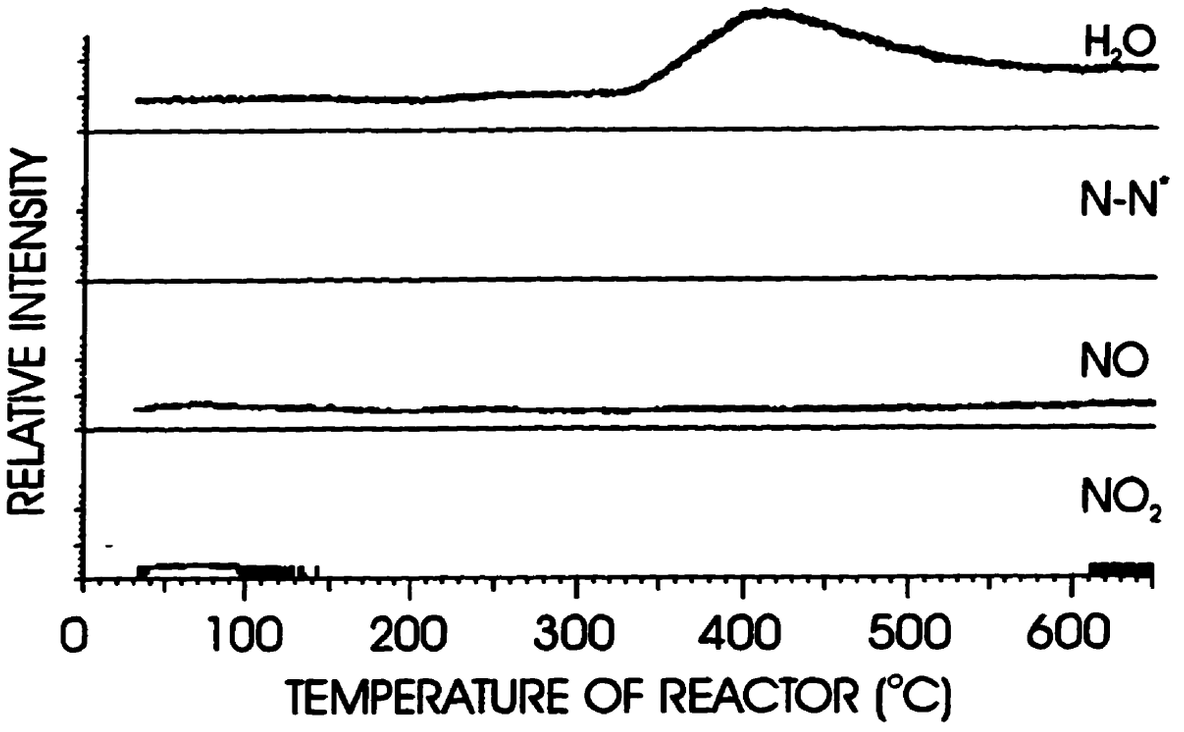

Fig. 5.18 Temperature-programmed desorption of 0.075g (39.9μmoles) of $^{15}NH_4PMo$ pretreated and exposed to flow of 4960ppm NO_2 at 300°C. Heating rate=10°C/min and NO_2, He Flow rate=20 mL/min. * = Isotope 15.

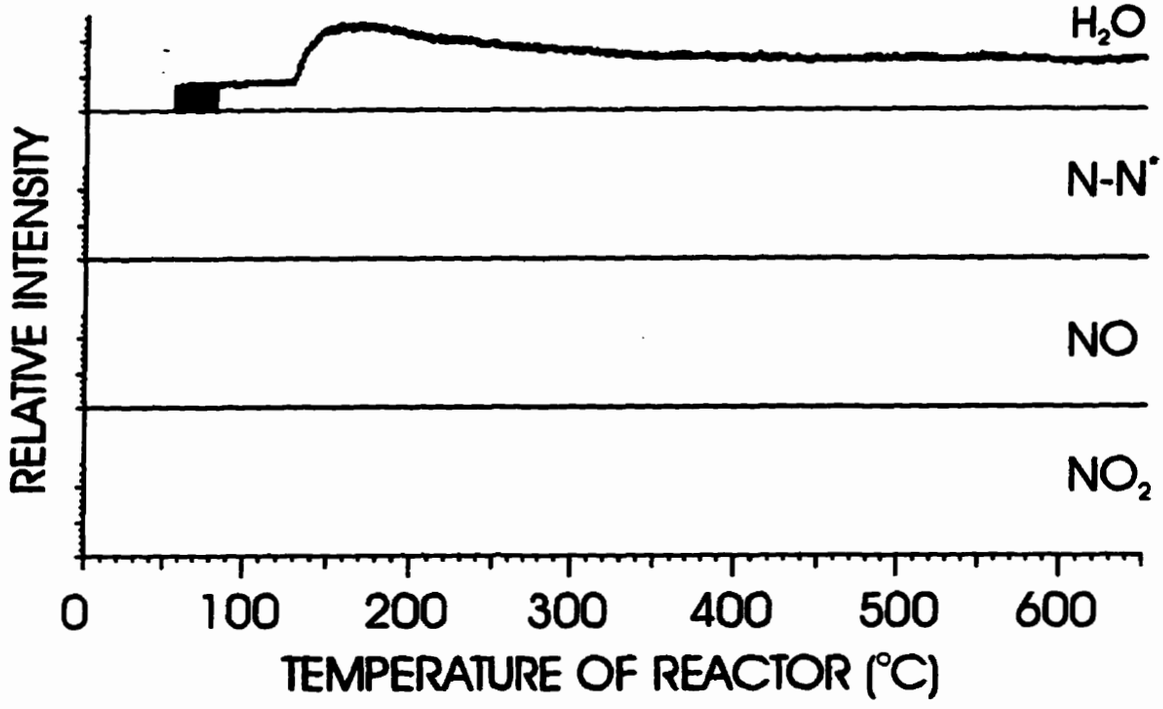

Fig. 5.19 Temperature-programmed desorption of 0.075g (39.9μmoles) of $^{15}NH_4PMo$ pretreated and exposed to flow of 4960ppm NO_2 at 425°C. Heating rate=10°C/min and NO_2, He Flow rate=20 mL/min. * = Isotope 15.

When the labelled catalyst was pretreated and exposed to NO_2 at 425°C (Fig.5.19), very small quantities of water could be observed desorbing from the solid. The s/n is lower than that of Figure 5.18. The salt appears to be decomposed after exposure to NO_2 at this high temperature, as observed using infrared spectroscopy (see later).

The surface areas of ammonium 12-molybdophosphate B (Fig.5.20), pretreated at 25, 300 and 400°C, are 4, 68 and 170 m^2/g, respectively. Such differences may be attributed to the loss of water at 250-350°C (see Fig.5.14). After exposure to NO_2 at 300 and 400°C, the surface areas decreased to 27 and 5 m^2/g, respectively. The reduction of NO on NH_4PMo at 400°C also results in the diminution of the surface area to 10 m^2/g.

Infrared spectra of NH_4PMo, with and without exposure to NOx, provide useful ancillary information on the nature of the interaction between NOx and the catalysts. Normalized (with P-O stretching at 1063.3 cm^{-1}) infrared spectra show that heat pretreatment in helium does not change the spectroscopic features of NH_4PMo of type A. In Figure 5.21, the band for ammonium seen at 1407.8 cm^{-1} (for symmetrical H-N stretching), after pretreatment at 25°C, shifted to 1409.3 and 1413.6 cm^{-1} after pretreatment at 300°C and 400°C, respectively, although the intensity remained unchanged. The remaining bands were insignificantly influenced by the thermal pretreatment.

The injection of NO_2 on NH_4PMo-A at 300°C results in the elimination of the ammonium band at 1409.3 cm^{-1} (Fig.5.22), and the band for P-O stretching at 1063.3 cm^{-1} shifted to 1064.5 cm^{-1}. The Mo-O_t stretching (terminal oxygen) at 965.8 cm^{-1} shifted to 962.9 cm^{-1}, and is of the same intensity as the reference pretreated at 300°C. No significant shifts can be seen in the symmetric and antisymmetric Mo-O-Mo vibrations found at 866 cm^{-1} and 798 cm^{-1}, respectively, but only a small decrease in intensity.

When NO is the saturating gas, the Mo-O_t band shifted to 964.9 cm^{-1} and is slightly more intense then when NO_2 is used. Further, the ammonium band is reduced by approximately 24 % (relative to the reference).

As with the parent acid, HPMo, no band was observed in the 1800-4000 cm^{-1} region which would be expected for NO_2^+. The band due to H_3O^+ (observed at 1600 cm^{-1}) is, apparently, not affected by the pretreatment temperature or the exposure to NOx.

Similar results were found for NH_4PMo exposed to NOx with injection at 400°C, but with some differences. At this temperature (Fig.5.23), the ammonium band vanishes with NO_2, but remains intact with NO. After injection of NO at 400°C, the Mo-O_t band at shifted to 981.3 cm^{-1} and increased in intensity. As before, the two Mo-O-Mo vibrations, as well as the other bands, are not significantly shifted. However, the intensity of absorbance from the Keggin Units is affected by the reduction of NOx at 400°C. With the exposure to NO or NO_2, the

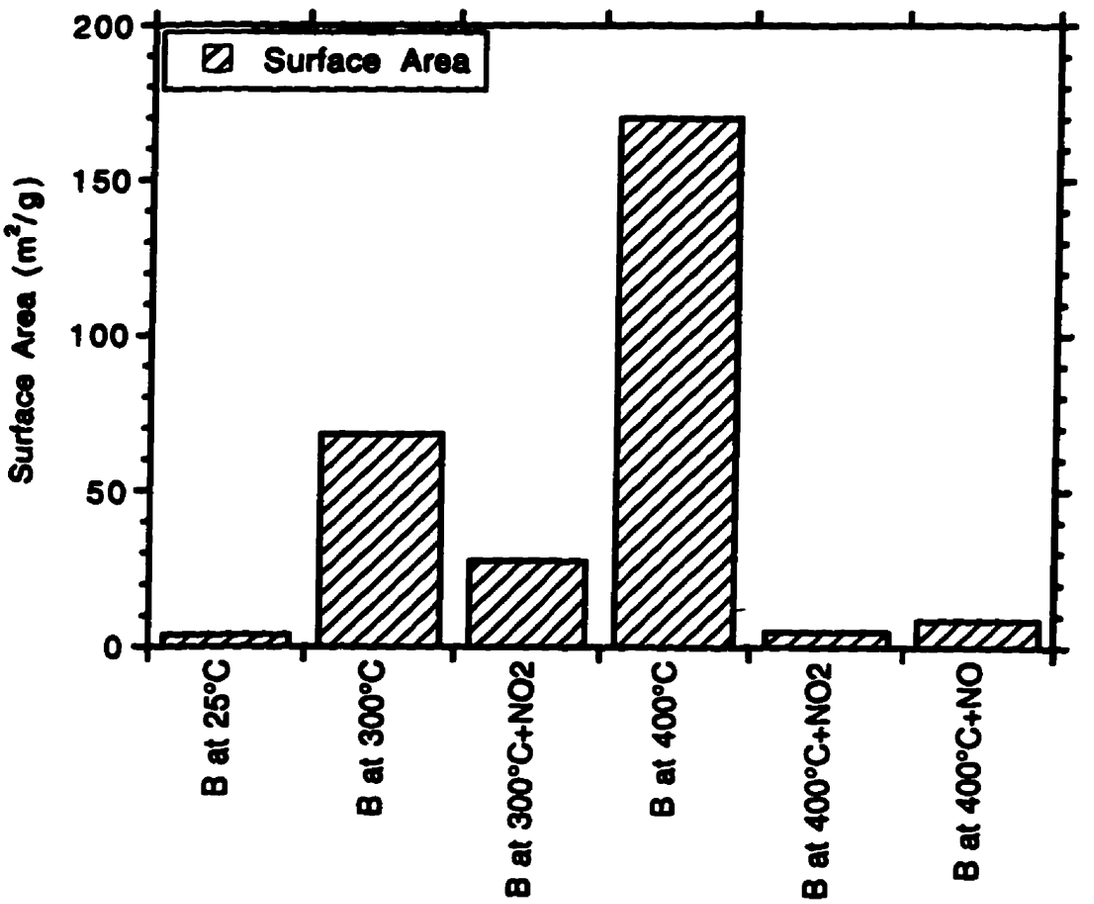

Fig. 5.20 Surface area of catalyst B under different treatment temperatures and gases. Each sample was pretreated at the respective temperature prior to saturation with appropriate gas at the same temperature.

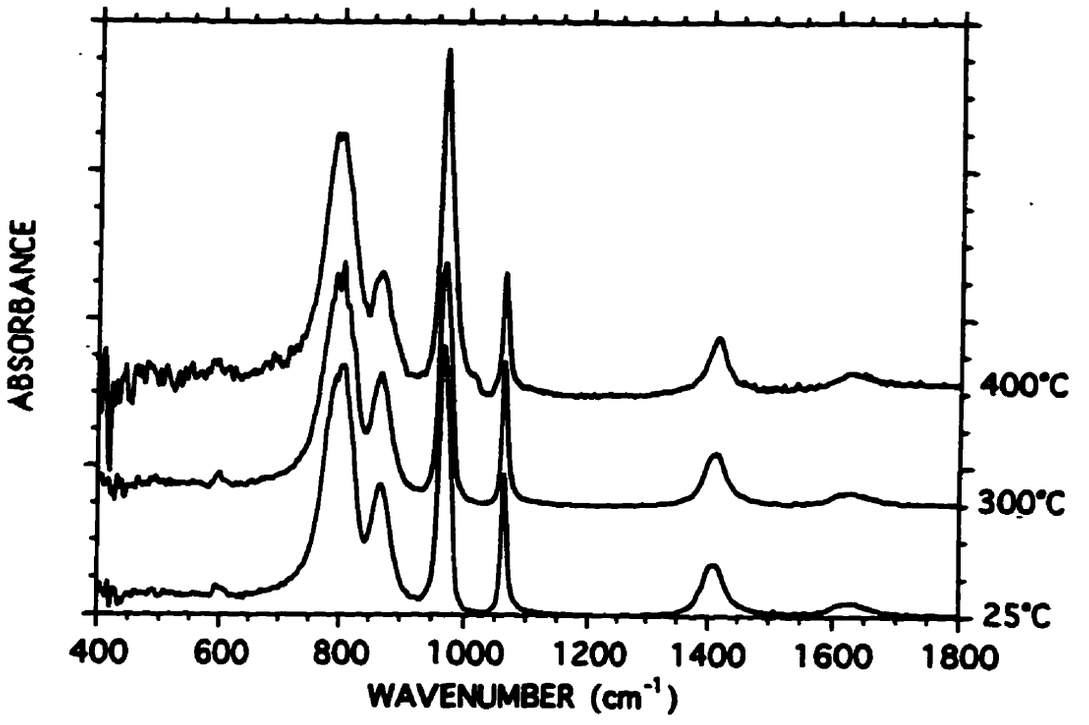

Fig. 5.21 Normalized infrared spectra of catalyst A after different pretreatment temperatures.

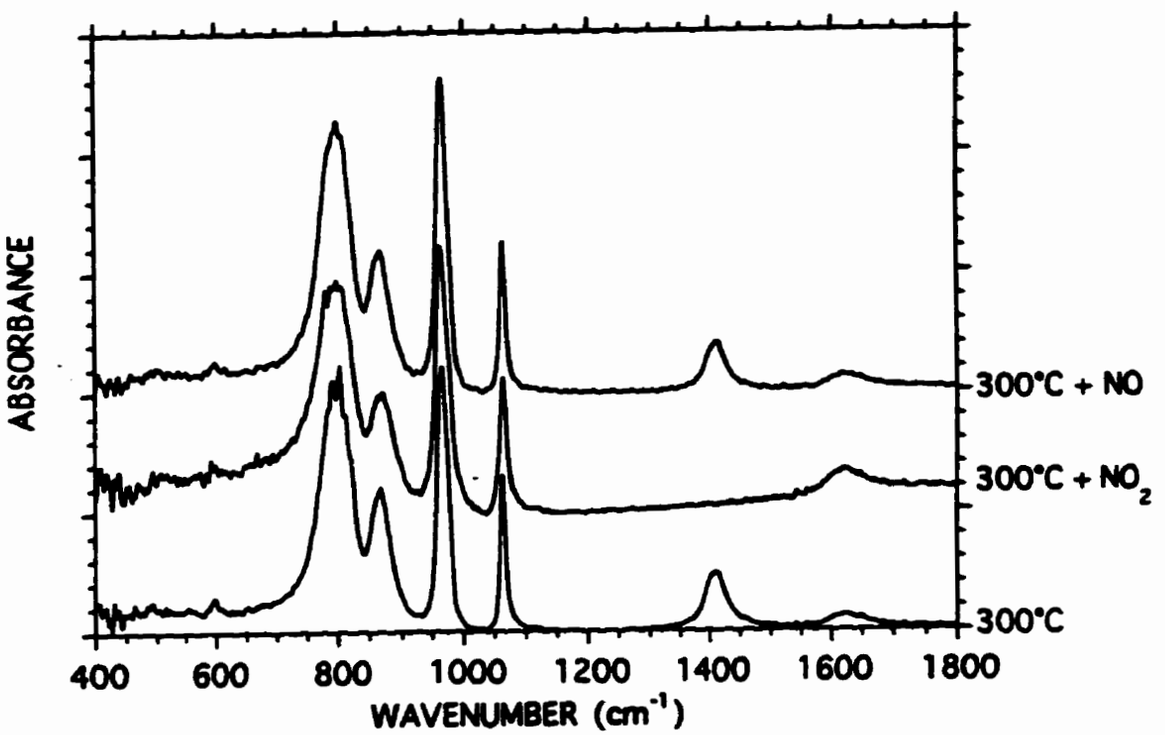

Fig. 5.22 Normalized infrared spectra of catalyst A after pretreatment and saturation with NO_2 and NO at 300°C.

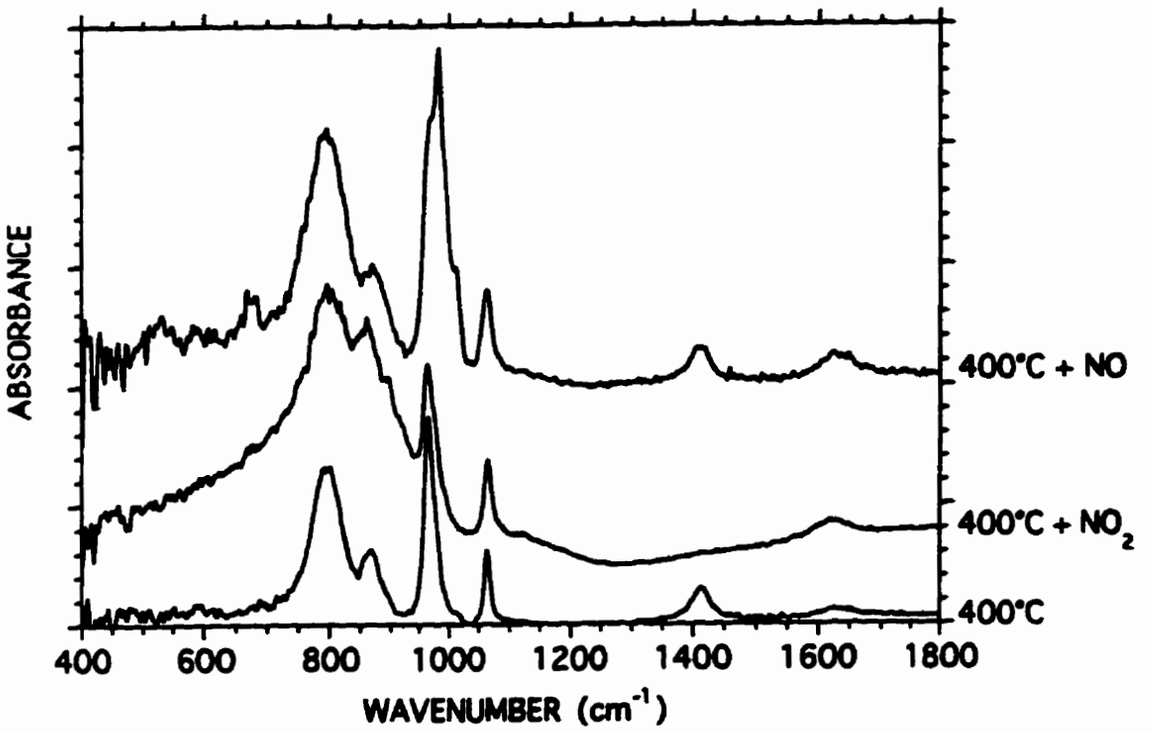

Fig. 5.23 Normalized infrared spectra of catalyst A after pretreatment and saturation with NO_2 and NO at 400°C.

intensity increased significantly for both symmetric and antisymmetric Mo-O-Mo vibrations, relative to the reference sample pretreated at 400°C in helium.

The vibrational spectra for catalysts of type B (Figs.5.24 and 5.25) and C (Figs.5.26 and 5.27), pretreated and treated, were measured. The same spectroscopic features (as those found for catalyst A) were observed for these two catalysts before and after treatment with NOx at 300 and 400°C. For both NH_4PMo-B and C, it can be seen, from their respective spectra, that the Keggin structure infrared signature is greatly affected after exposure to NO_2 at 400°C. Nevertheless, exposure of catalyst B and C to NO has the same effect as that on catalyst A.

These changes in the structure of the salts can also be seen from X-ray diffraction patterns (Fig.5.28). The X-ray diffraction pattern of NH_4PMo-A, as prepared, shows many diffraction lines (Fig.5.28A). It is also evident that the structure of NH_4PMo prepared with the ammonium carbonate (B) leads to a salt having a slightly different structure (Fig.5.28B), although, this difference is not evident in the infrared spectra. When the salt A is exposed to NO_2 at 400°C, it is obvious from the diffraction pattern (Fig.5.28C) that the structure has been altered. Most of the original lines of the unexposed salt disappeared upon saturation with NO_2. However, with the injection of NO at 400°C, the intensities of most lines decreased without any substantial changes in the structure.

The history of the protons of NH_4PMo-A can be seen with ^1H MAS NMR (Fig.5.29). The spectrum for the pretreated salt shows a single peak of high intensity at 5.7 ppm for the protons of the NH_4^+ cations (Fig.5.29A). This result shows that all protons are equivalent in ammonium 12-molybdophosphate. After saturation with NO_2 at 300°C (Fig.5.29B), the peak at 5.7 ppm shifted to 5.5 ppm and decreased in intensity. Further, a new band at 8.4 ppm is clearly visible and can be assigned to the protons of the parent acid, HPMo. However, when exposed to NO at the same temperature, this new band is not visible. The intensity of the ammonium band, at 6.2 ppm, has also decreased (Fig.5.29C). The same remarks apply to the exposure of the salt to NO at 400°C (Fig.5.29D). The ammonium protons are now found at 6.4 ppm. The absence of shifts assignable to protons provides evidence for the consumption of these when NO is injected on the salt either at 300°C or 400°C. In contrast, NO_2 injected at 300°C, reacts with the ammonia while the protons are retained to form the parent acid.

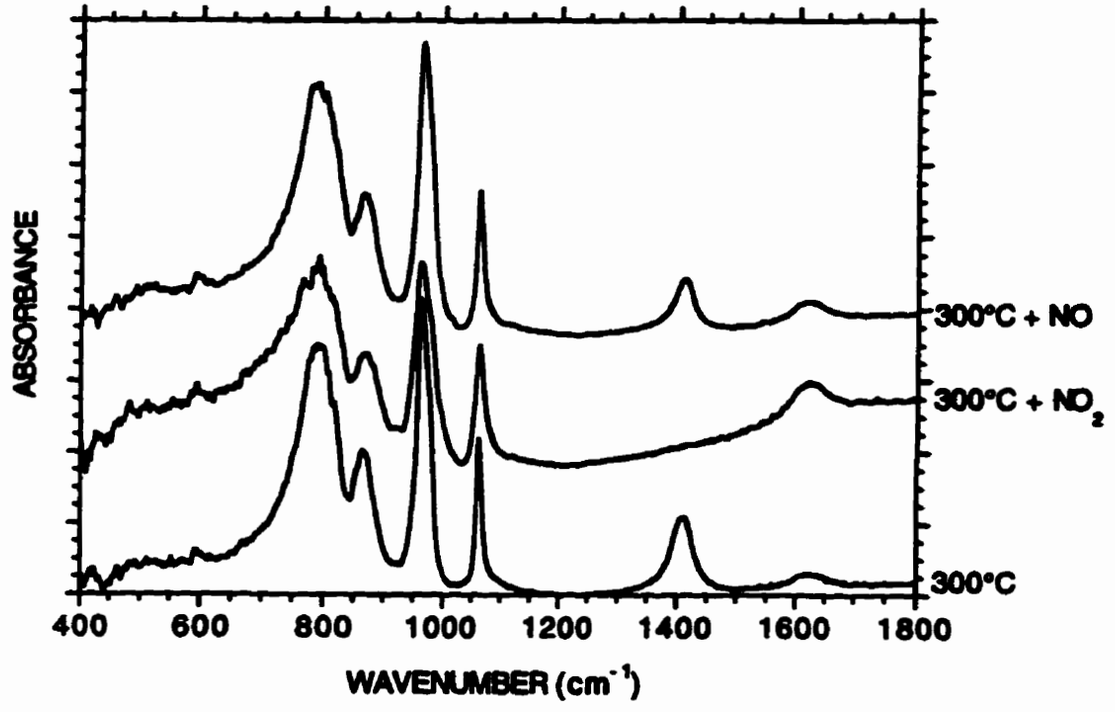

Fig. 5.24 Normalized infrared spectra of catalyst B after pretreatment and saturation with NO_2 and NO at 300°C.

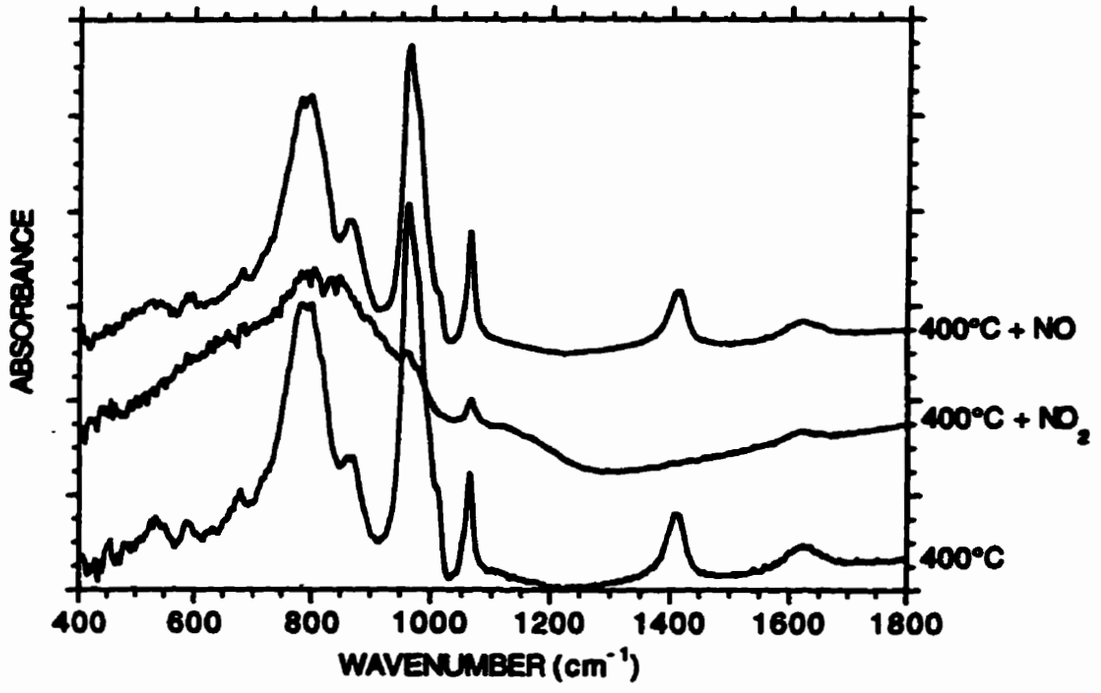

Fig. 5.25 Normalized infrared spectra of catalyst B after pretreatment and saturation with NO_2 and NO at 400°C.

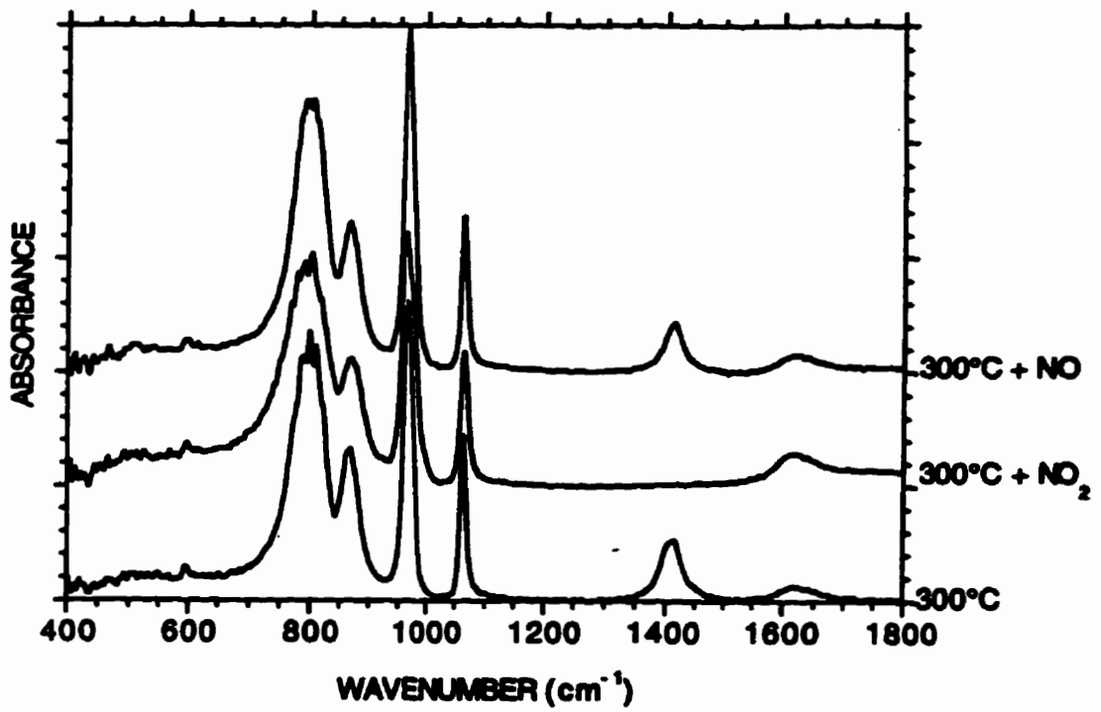

Fig. 5.26 Normalized infrared spectra of catalyst C after pretreatment and saturation with NO_2 and NO at 300°C.

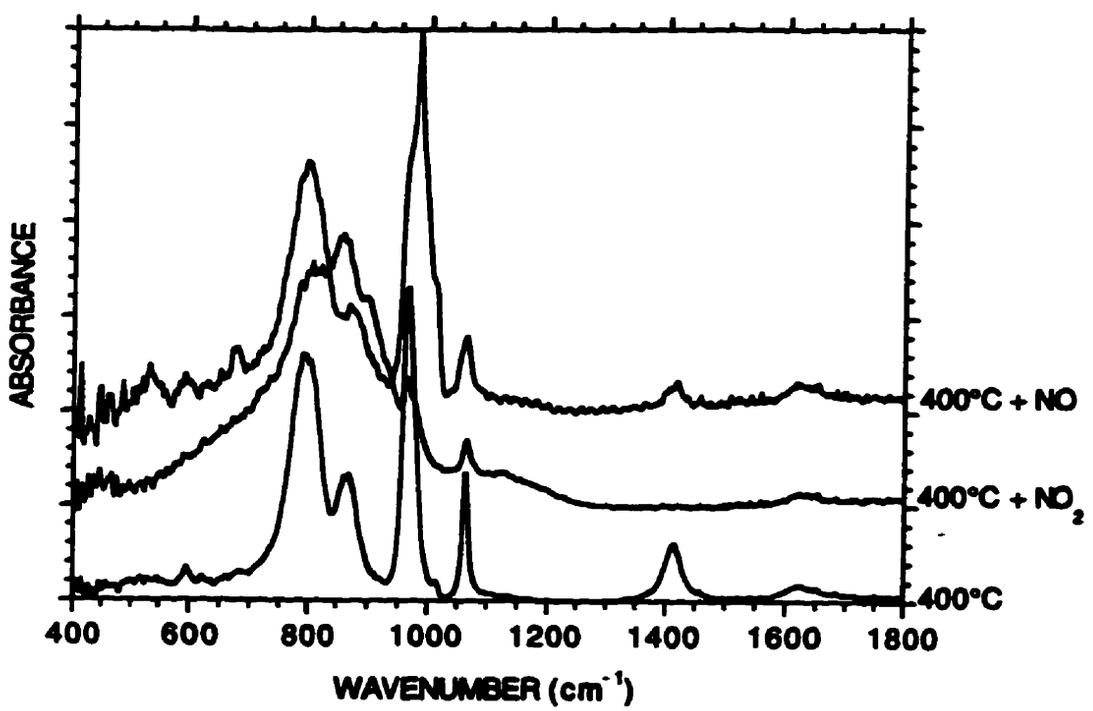

Fig. 5.27 Normalized infrared spectra of catalyst C after pretreatment and saturation with NO_2 and NO at 400°C.

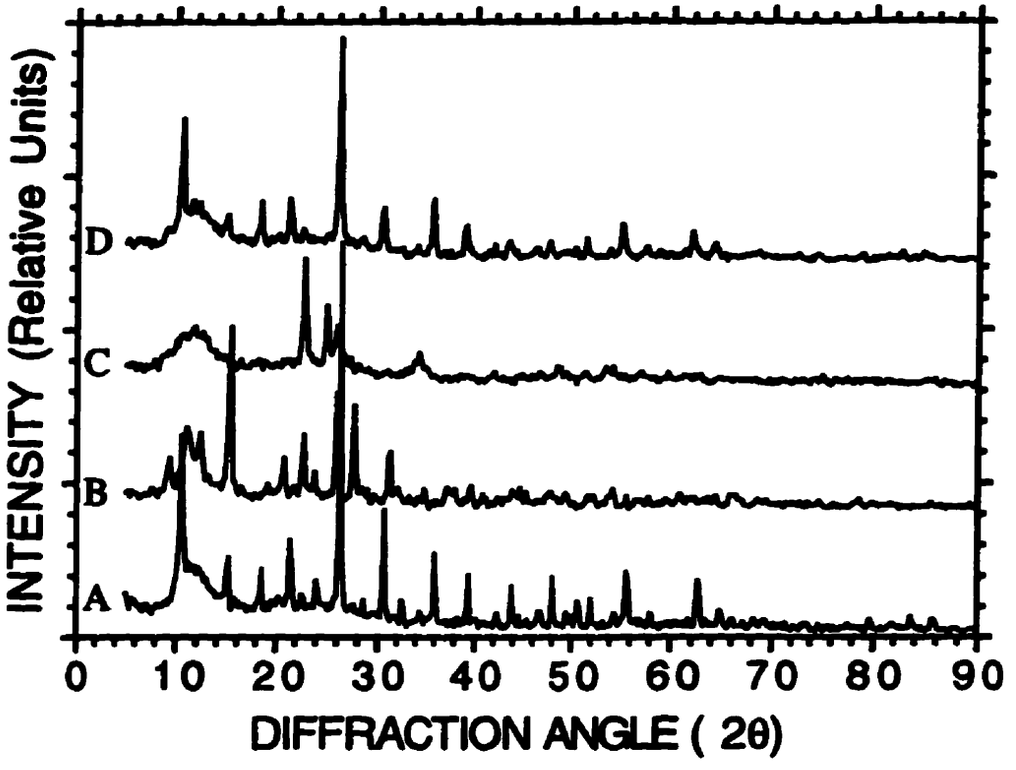

Fig. 5.28 X-ray diffraction patterns of (A) NH_4PMo-A as prepared; (B) NH_4PMo-B as prepared; (C) NH_4PMo-A pretreated at 400°C and then saturated with NO_2 at 400°C; (D) NH_4PMo-A pretreated at 400°C and then saturated with NO at 400°C.

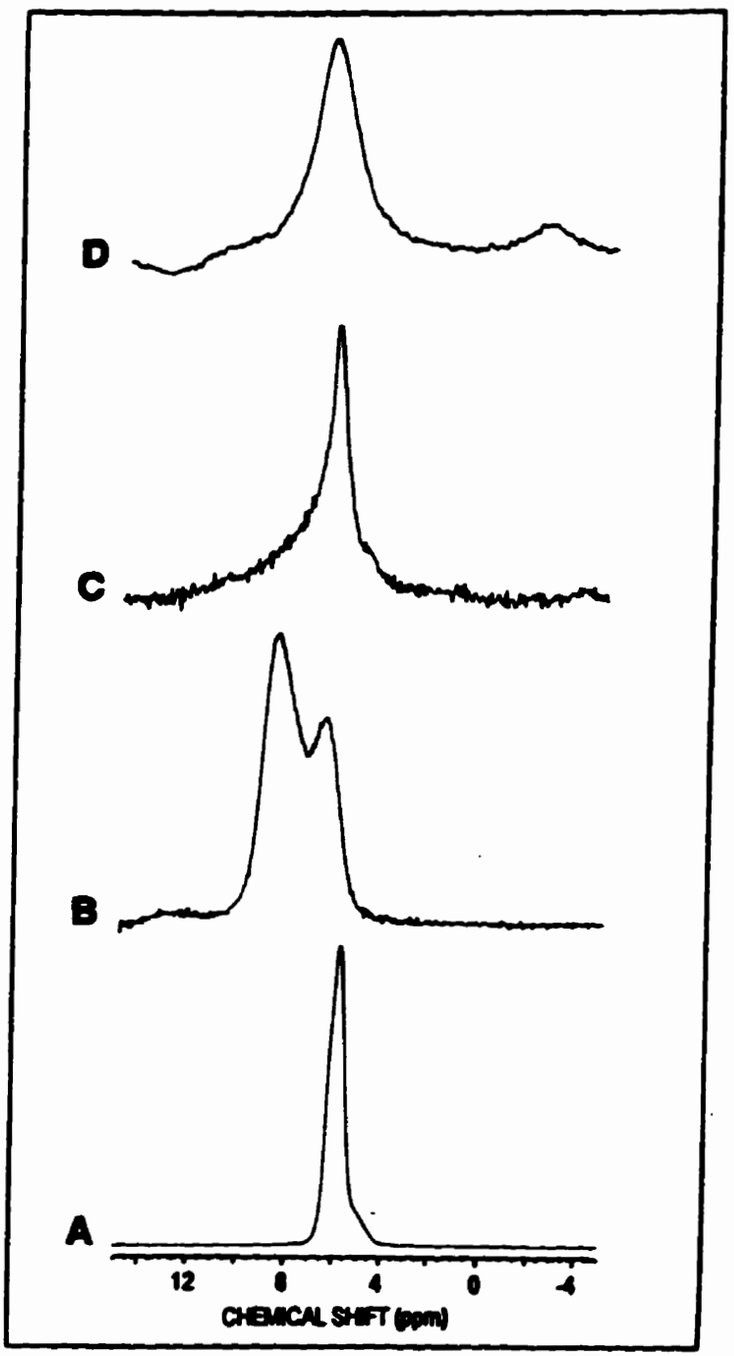

Fig. 5.29 ^{1}H MAS NMR of (A) NH_4PMo-A pretreated in helium at 300°C; (B) NH_4PMo-A pretreated at 300°C and then saturated with NO_2 at 300°C; (C) NH_4PMo-A pretreated at 300°C and then saturated with NO at 300°C; (D) NH_4PMo-A pretreated at 400°C and then saturated with NO at 400°C.

B. Discussion

Reduction of NO_2

The present results are qualitatively and quantitatively similar to those found with ammonium 12-tungstophosphate for the reduction of NO_2. The loss of NO_2 and the formation of N_2 at 300°C evidently results from the direct reaction of NO_2 and NH_3 (as NH_4^+) in the structure of ammonium 12-molybdophosphate. Most chemical reactions found in Chapter IV can apply to the present catalyst. The reduction of NO_2 is believed to follow Equation 5.1.

$$NO_2 + NH_4^+ \rightarrow N_2 + 3/2H_2O + 1/4O_2 + H^+ \qquad \text{(Eq. 5.1)}$$

The loss of NO_2 is directly related to the reaction with ammonia. Very little contribution to the consumption of NO_2 can be ascribed to the association of NO_2 with the protons of the resulting acid, after depletion of the ammonia molecules, as with the NH_4PW salts. This is consistent with the observation that 12-molybdophosphoric acid has a considerably smaller capacity for the retention of NO_2 than that observed with HPW because of the difference in acidic strength (Chapter III).

Increasing the temperature of the reactor also increases the efficiency of the reaction. The quantity of NO_2 removed from the gas phase is higher at 400°C than at 300°C, and the selectivity to N_2 is also higher at the former temperature. However, at 300°C, N_2O is formed in the reduction process, possibly from the decomposition of ammonium nitrate complex which may have formed from the reaction of excess NO_2 and water, the latter from the reduction process.

$$3NO_2 + H_2O \leftrightarrow 2HNO_3 + NO \qquad \text{(Eq. 5.2)}$$

$$HNO_3 + NH_4^+ \leftrightarrow [NH_4NO_3] + H^+ \qquad \text{(Eq. 5.3)}$$

$$[NH_4NO_3] \rightarrow N_2O + 2H_2O \qquad \text{(Eq. 5.4)}$$

The reaction in which NH_4^+ is directly oxidized by nitric acid,

$$NH_4^+ + HNO_3 \rightarrow 2H_2O + N_2O + H^+ \qquad \text{(Eq. 5.5)}$$

may also by occurring (Ref.5.1).

Apparently, under the present conditions, little or no N_2O can be formed from the direct gas phase reaction between NO_2 and NH_3. The reduction of the selectivity to N_2O at 400°C may be related to the relative instability of HNO_3 at the higher temperature.

Major structural changes are found within the salt when the reaction is performed at high temperature. The spectroscopic and the surface area results, clearly show that the Keggin units are strongly affected by the reduction of NO_2 at 400°C. However, the infrared spectra revealed that when the reduction is performed at 300°C, the structure of the anion is relatively unperturbed and the salt can be regenerated by wet or gaseous processes as with NH_4PW. At 300°C, the parent acid, HPMo, can be regenerated to form ammonium 12-molybdophosphate by addition of gaseous ammonia.

The source of the cations used in the preparation and the purity of the catalyst affect the selectivity to N_2. At low temperature (150°C) this difference is substantial. The catalyst prepared from ammonium nitrate (catalyst A) gives a higher yield than with that prepared from ammonium carbonate (catalyst B). Little or no difference in the N_2 selectivity can be seen at 300°C.

The effect of the preparation can be seen in the formation of the by-products when NO_2 is injected at 400°C. The washed catalyst (prepared with ammonium nitrate), held at 400°C, shows the highest selectivity to N_2O. This catalyst also shows the greatest overall selectivity to NO, for the same reaction temperature.

Other spectroscopic results clearly reveal that the structure of the anion of ammonium 12-molybdophosphate, prepared from the ammonium carbonate, is partially decomposed, although the selectivity to N_2 is not altered. The fact that the aforementioned catalyst undergoes structural changes could, however, affect the yield after the regeneration process. It is also known that 12-molybdophosphoric acid is thermally and chemically less stable than 12-tungstophosphoric acid (see TPD results). The acid containing molybdenum decomposes at a lower temperature than that containing tungsten. During the high temperature reactions, the terminal oxygen atoms are apparently extracted by the protons. For HPMo this happens at a lower temperature, showing that the terminal oxygen atoms are more labile than those contained in HPW (Ref.5.4).

Reduction of NO

It was first observed from the reduction of NO_2, that the selectivity to NO was changing as the conversion of NO_2 was increasing. In some cases no nitric oxide could be found in the effluent. NO was found to be directly reduced by ammonium 12-molybdophosphate with a selectivity to N_2 which increased with temperature. However, the Keggin anions were structurally affected by the reduction of NO and, as seen from ^1H MAS NMR, the protons were consumed in the process.

Under the present conditions, it is observed that gas phase reaction between ammonia and nitric oxide, without the addition of O_2, does not yield N_2. However, the stoichiometry of the reaction appears to follow the reaction for the reduction of NO_2, as written above. The first

pulse of NO shows approximately 100% selectivity to N_2. Further, the results from NO on the labelled ammonium salt suggest that the second nitrogen comes from the catalyst (^{15}NN), as well as in the formation of ^{15}NNO.

Infrared results show that after exposure to NO, the intensities of the bands were affected. That observation suggests that NO may be initially oxidized to NO_2, which is then subjected to the reduction by NH_3 (Eq.5.1).

$$NO + Mo{=}O_t{-}H^+ \rightarrow H^+NO_2 + Mo, \qquad \text{(Eq. 5.5)}$$

$$H^+NO_2 \rightarrow NO_2 + H^+ \qquad \text{(Eq. 5.6)}$$

The reaction is favored by higher temperatures at which the terminal oxygen atoms are more labile. The ^1H MAS NMR data suggest that the protons are being consumed.

Infrared results do not show a significant reduction of the band for the ammonium ion. However, ^1H MAS NMR shows a diminution of intensity of the peak for the ammonium protons. Apparently, the band at 1063.3 cm^{-1} is not purely from the P-O stretching vibration, but may be contaminated with the contribution of some other vibrational modes, as seen from a shift in the baseline, this in turn may enhance the NH_4^+ band. A mechanism excluding the use of the ammonium cation for the reduction of NO is, at this point, unclear.

The source of the cation and the purity of the salt affect the reduction process. The defects induced from the preparation of NH_4PMo-B, using ammonium carbonate, are responsible for the lesser selectivity to N_2, as well as the lesser lability of the protruding oxygen atoms. The impurities in NH_4PMo-C are apparently responsible for the smaller selectivity to N_2O.

C. Conclusions

The present results show that both NO and NO_2 can be removed successfully with ammonium 12-molybdophosphate. At low temperature (150°C), the reduction of NO is insignificant. Higher temperatures are needed for the total reduction of both NO and NO_2. As the temperature is increased the selectivity to N_2 increases, while the quantity of N_2O in the effluent passes through two maxima, from 200-350°C and at 450°C. The purity, as well as the source of the cation, has an effect on the results.

At 300°C, the selectivity to N_2 is lower than desired, although the salt can be regenerated, in contrast to the observations at 400°C at which temperature structural degradation occurs.

While it is clear that NH_4PMo is capable of reducing NO and NO_2, the detailed mechanism by which the heteropoly anion participates in the process is not yet known. However, the influence of the composition of the anion on the protonic acidic strength appears to play an important role in the process.

REFERENCES

5.1 Rubtsov, Yu.I., Strizhevskii, I.L., Kazakov, A.I., Andrienko, L.P., Moshkovish, E.B. *Zh.Prikl.Khin. (S.-Peterburg)*, **62**, 2017 (1989).

5.2 Moffat, J.B., *J.Mol.Catal.*, **26**, 385 (1984).

5.3 Jozefowicz, L.C., Hellmut, G.K., Vasilyeva, E., and Moffat, J.B., *Microporous Materials*, **1**, 313 (1993).

5.4 Kasztelan, S., and Moffat, J.B., *J.Catal.*, **106**, 512 (1987).

CHAPTER VI

SORPTION AND REACTION OF NO AND NO_2 ON SALTS OF GROUP IA AND THALLIUM SALT

A. Results

Temperature-programmed reaction experiments were carried out with NO_2 on different salts of HPW, and the results are compared with those for the parent acid, HPW.

The temperature-programmed reaction of NO_2 and HPW (Fig.6.1) shows the sorption of NO_2 at 200°C, concomitant with the desorption of substantial quantities of water. The desorption of NO_2 is observed at 240 and 530°C. The former NO_2 desorption peak results from the formation and desorption of HNO_3, the latter resulting from NO_2 chemisorbed within the bulk of the acid. Protons and anionic oxygen atoms are associatively desorbed as water at 450°C. The concentration of O_2 in the desorbate begins to increase at temperatures higher than 500°C. This production of oxygen is concomitant with the increase and decrease of gas phase NO and NO_2, respectively. Little or no N_2 or N_2O were produced from the interactions between NO_2 and the acid (HPW).

Figures 6.2 to 6.7 are the TPR of NO_2 and the salts of HPW, protons of which were replaced by elements from group IA (Li, Na, K, Rb, Cs), and thallium (Tl), respectively.

The first two salts, LiPW (Fig.6.2) and NaPW (Fig.6.3), show features which are similar to each other, but distinctly different from those obtained with HPW. As the temperature of the reactor is increased, the desorption of water can be observed with a maximum at 150°C. Quantities of NO and NO_2 in the gas phase remain relatively constant up to approximately 500°C. Molecular oxygen is produced at temperatures higher than 550°C for LiPW, and 500°C for NaPW with small increases and decreases in NO and NO_2, respectively. Little or no N_2 and N_2O were found in the effluent.

The remaining four salts, KPW (Fig.6.4), RbPW (Fig.6.5), CsPW (Fig.6.6), and TlPW (Fig.6.7), show similar characteristics in their respective NO_2-TPR. The physisorbed water molecules desorb with a maximum appearing at 90-100°C followed by the formation and desorption of HNO_3 (seen as NO_2 because of the fragmentation) at 110°C. The production of O_2 increases at temperatures higher than 500°C concomitant with the changes in NO and NO_2 concentrations as observed with the previous samples. No N_2 and N_2O were observed desorbing from the catalysts.

TPR experiments were also carried out with NO over the aforementioned salts, as well as with their parent acid, HPW.

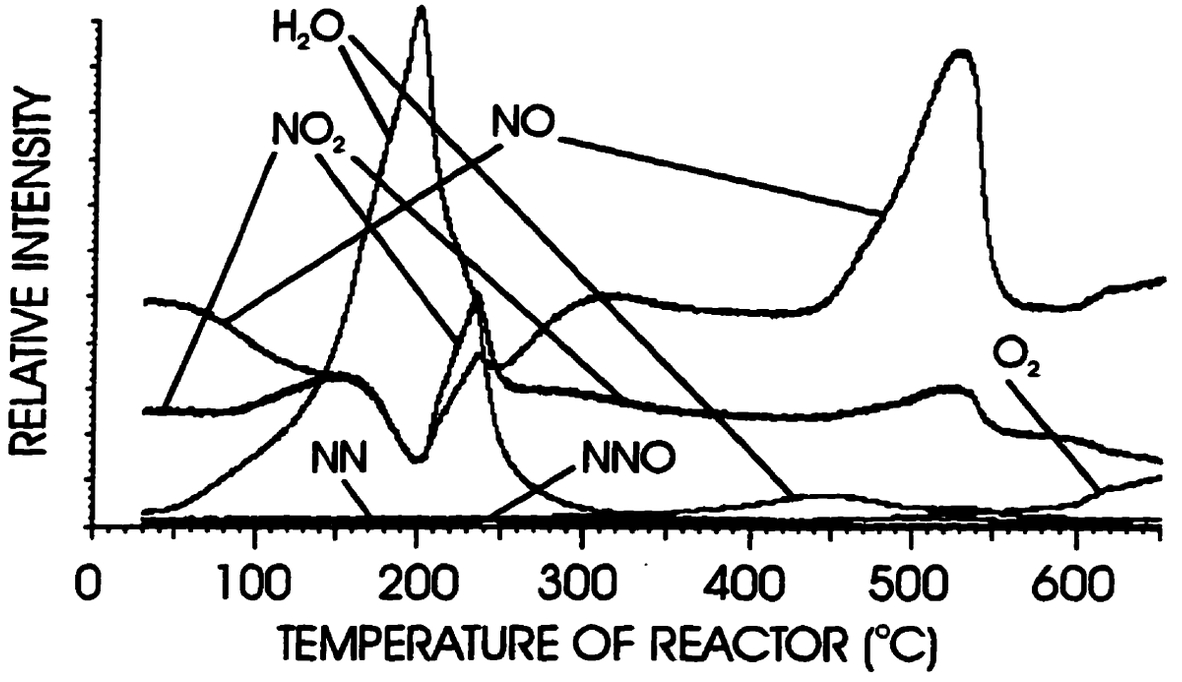

Fig.6.1 Temperature-programmed reaction of 0.075g (26.0μmoles) of HPW exposed to a continuous flow of 4960 ppm of NO_2. Heating rate=10°C/min and Flow rate=20 mL/min.

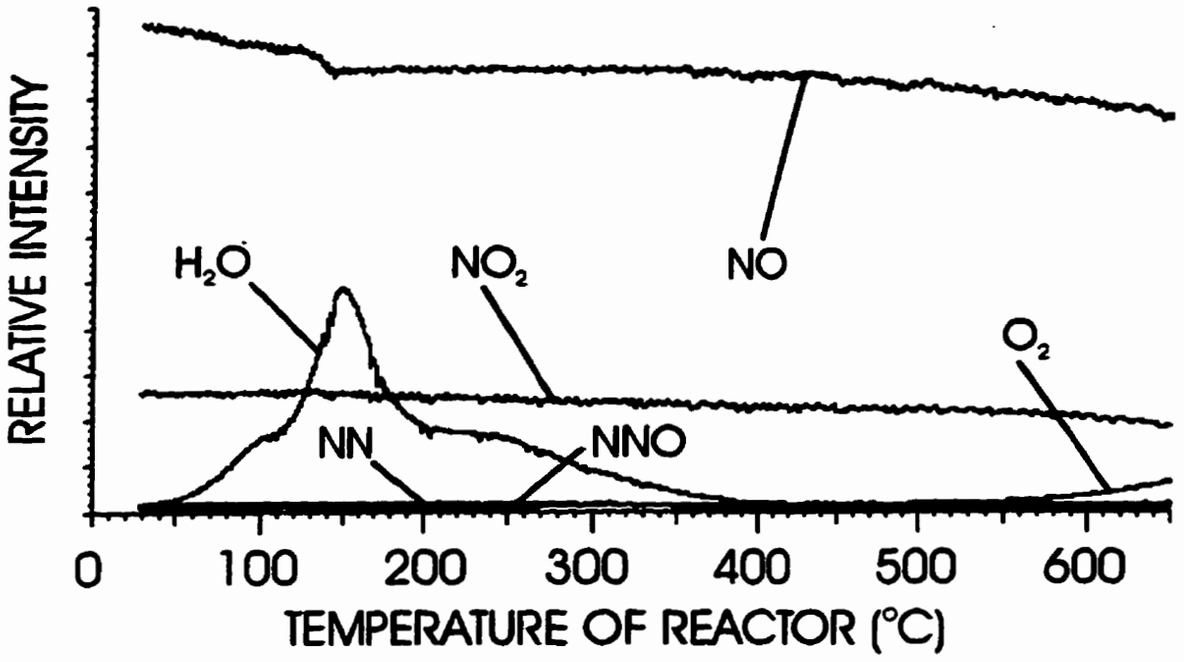

Fig.6.2 Temperature-programmed reaction of 0.075g (25.9μmoles) of LiPW exposed to a continuous flow of 4960 ppm of NO_2. Heating rate=10°C/min and Flow rate=20 mL/min.

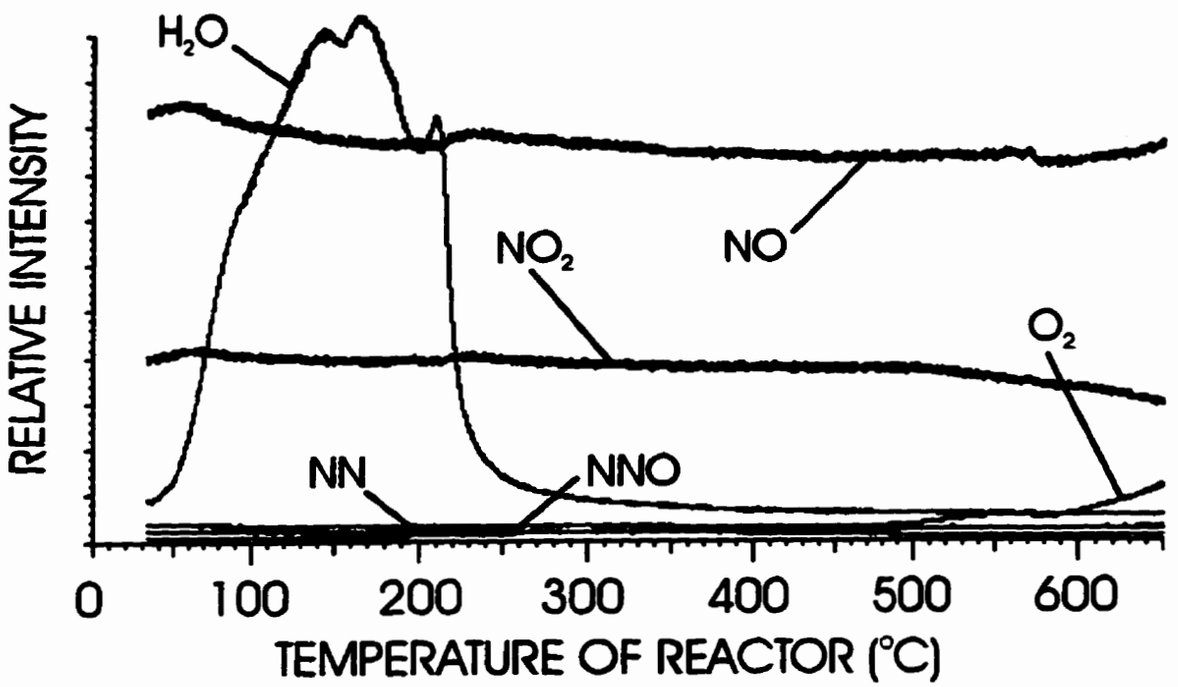

Fig.6.3 Temperature-programmed reaction of 0.075g (25.5μmoles) of NaPW exposed to a continuous flow of 4960 ppm of NO_2. Heating rate=10°C/min and Flow rate=20 mL/min.

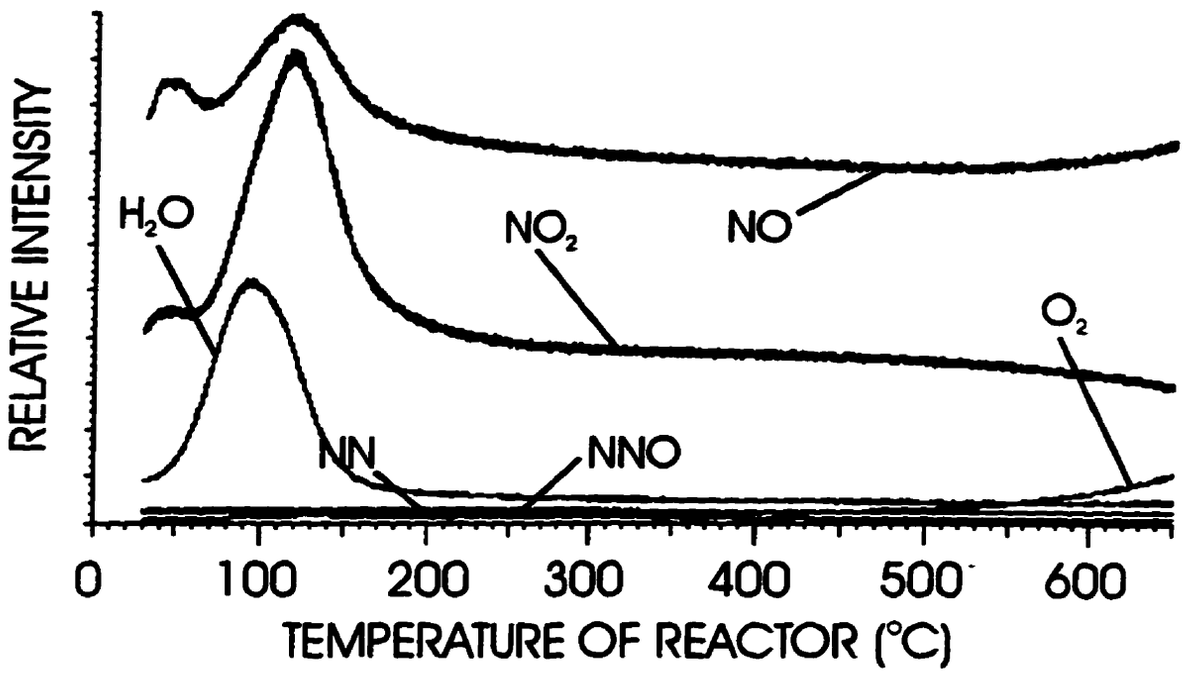

Fig.6.4 Temperature-programmed reaction of 0.075g (25.0μmoles) of KPW exposed to a continuous flow of 4960 ppm of NO_2. Heating rate=10°C/min and Flow rate=20 mL/min.

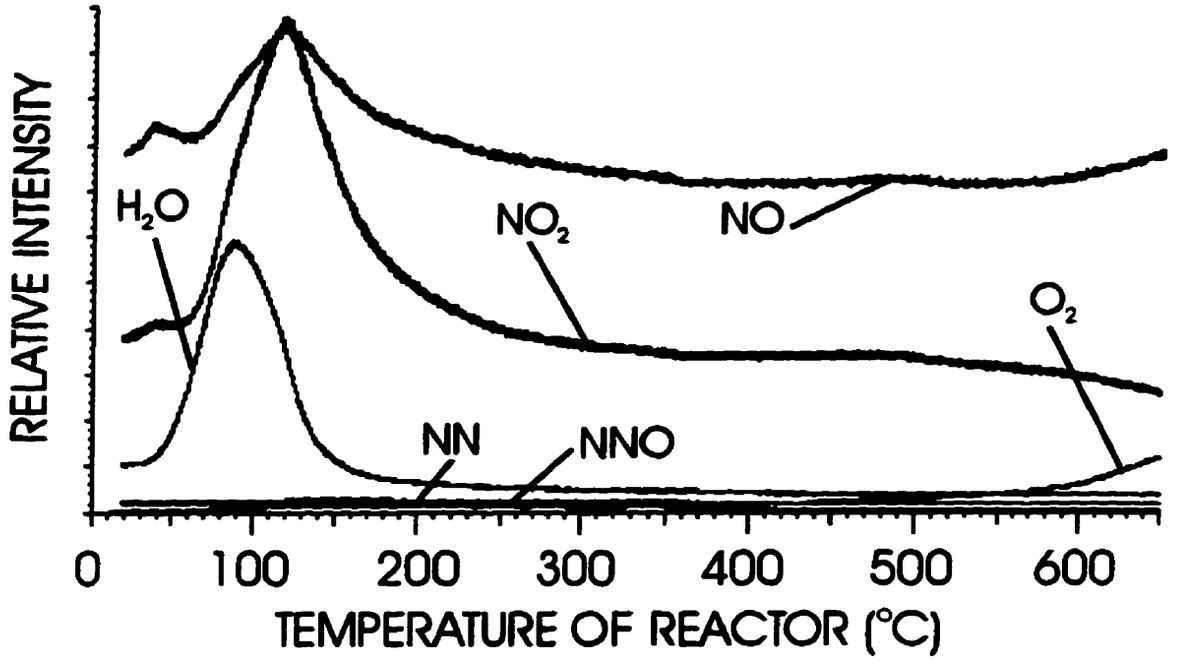

Fig.6.5 Temperature-programmed reaction of 0.075g (23.9μmoles) of RbPW exposed to a continuous flow of 4960 ppm of NO_2. Heating rate=10°C/min and Flow rate=20 mL/min.

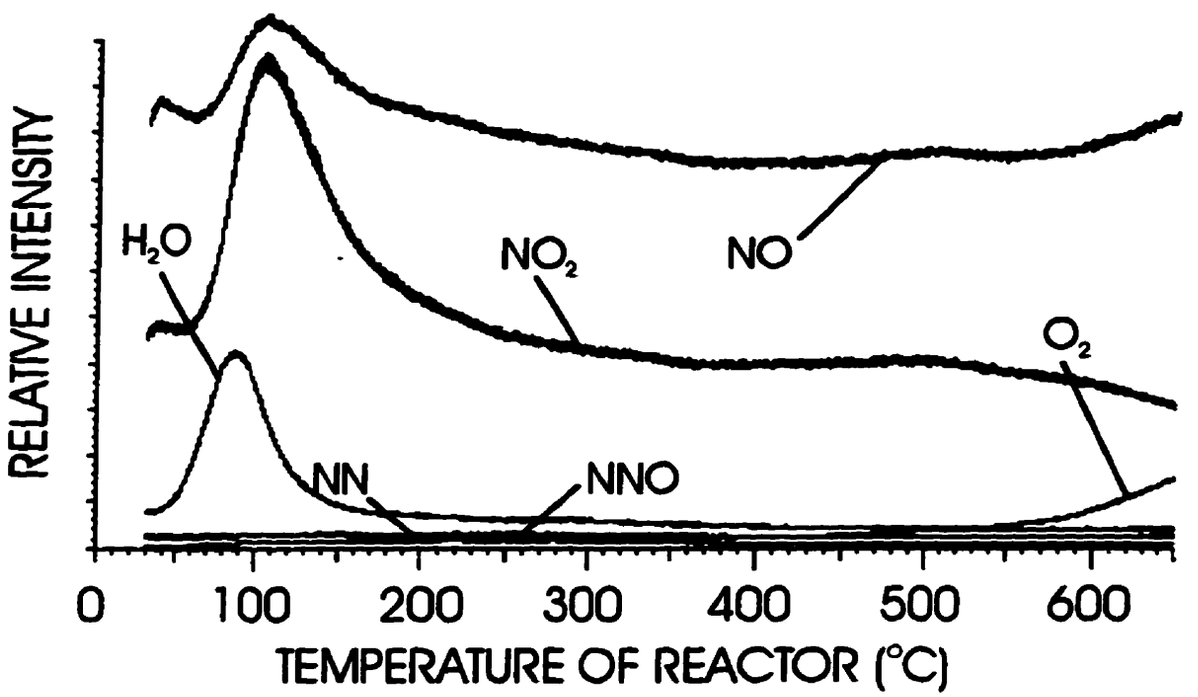

Fig.6.6 Temperature-programmed reaction of 0.075g (22.9μmoles) of CsPW exposed to a continuous flow of 4960 ppm of NO_2. Heating rate=10°C/min and Flow rate=20 mL/min.

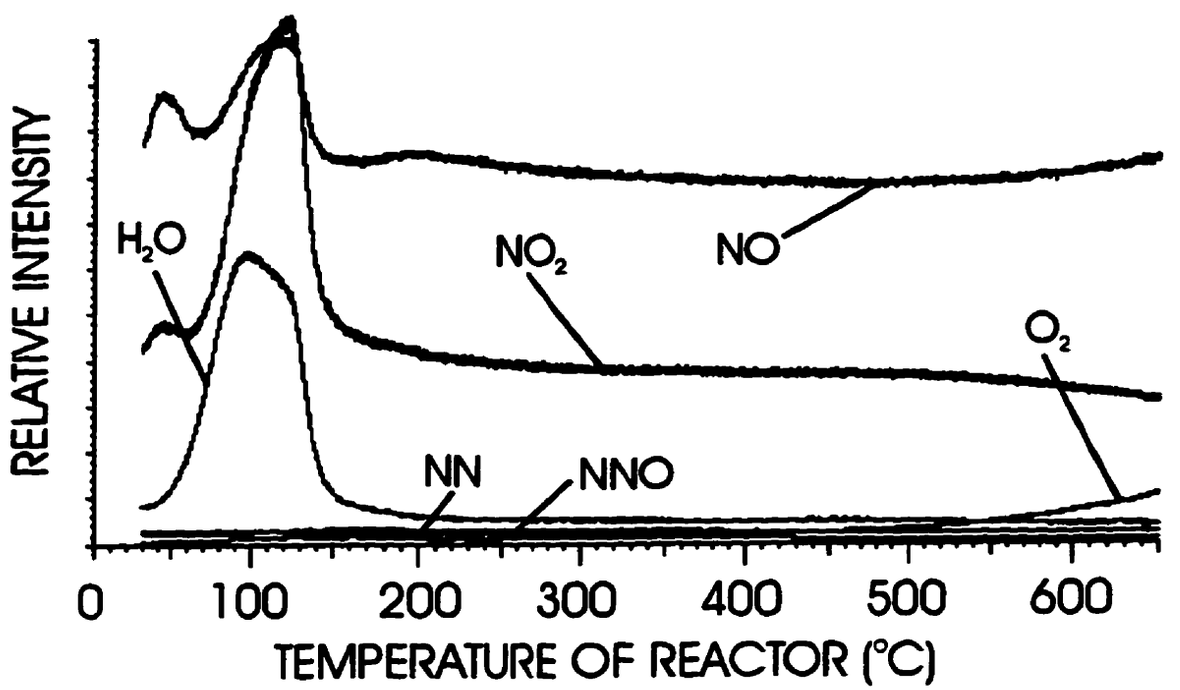

Fig.6.7 Temperature-programmed reaction of 0.075g (21.6μmoles) of TlPW exposed to a continuous flow of 4960 ppm of NO_2. Heating rate=10°C/min and Flow rate=20 mL/min.

TPR of NO over 12-tungstophosphoric acid (Fig.6.8) shows the characteristic desorption of water with maxima at 240 and 470°C, for the weakly bound and associatively desorbed water, respectively. A small quantity of NO_2 desorbs at 510°C. Little or no N_2 or N_2O were produced. Oxygen remained at negligible levels throughout the NO-TPR experiment.

The TPR results for LiPW and NaPW are shown in Figures 6.9 and 6.10, respectively. Both TPR show a large but single water peak with a maximum at about 200°C. Small quantities of NO_2 are found in the effluent at two different temperatures. For LiPW, the maxima for the NO_2 peaks are found at 230 and 580°C, but at 125 and 510°C with NaPW. Infinitesimal quantities of N_2 and N_2O were detected in the effluent of the reactor and O_2 remained at negligible levels.

The NO-TPR of KPW (Fig.6.11) shows significant differences from the former catalysts. The weakly bound water is desorbing with a narrow peak at 110-140°C along with small quantities of NO_2. As with the other catalysts exposed to NO, no O_2 was observed exiting the reactor.

Infrared spectra of HPW and the group IA derivatives pretreated in helium at 300°C are presented in Figure 6.12. The infrared spectrum of ammonium 12-tungstophosphate is also included in this figure for comparative purposes. These spectra were normalized with the P-O stretching band at 1063.3 cm^{-1}.

All spectra display the series of five or six bands between 600 and 1200 cm^{-1} which are characteristic of the Keggin structure and the band for H_3O^+ at 1625 cm^{-1}. The spectrum of NH_4PW shows an extra band at 1410 cm^{-1} characteristic of the ammonium cation.

Substantial differences exist from 950 to 1050 cm^{-1} (Fig.6.13), the region in which the band for the W-O_t stretch is found, the maximum for which is found at 983 cm^{-1} for HPW as well as for LiPW and NaPW. The relative infrared absorbances are similar for all the examined salts, with the exception of NH_4PW, the band of which has shifted to higher wavenumbers and whose relative infrared absorbances have increased. For NH_4PW, the maximum is found at the same wavenumber as with HPW, but the infrared absorbance of the shoulder at 995 cm^{-1} has increased as observed with KPW, RbPW, and CsPW.

After exposure of each of the aforementioned salts, held at 300°C, to 85 μmoles of NO_2, the infrared spectra display the same features as found in the absence of NO_2 (Fig.6.14). As noted in Chapter IV, the ammonium band at 1410 cm^{-1} from the NH_4PW spectrum is reduced in intensity after reaction. No infrared absorption band due to NO_2 (as $[HNO_2]^+$) was observed in the region between 1800 and 4000 cm^{-1} with any of the salts.

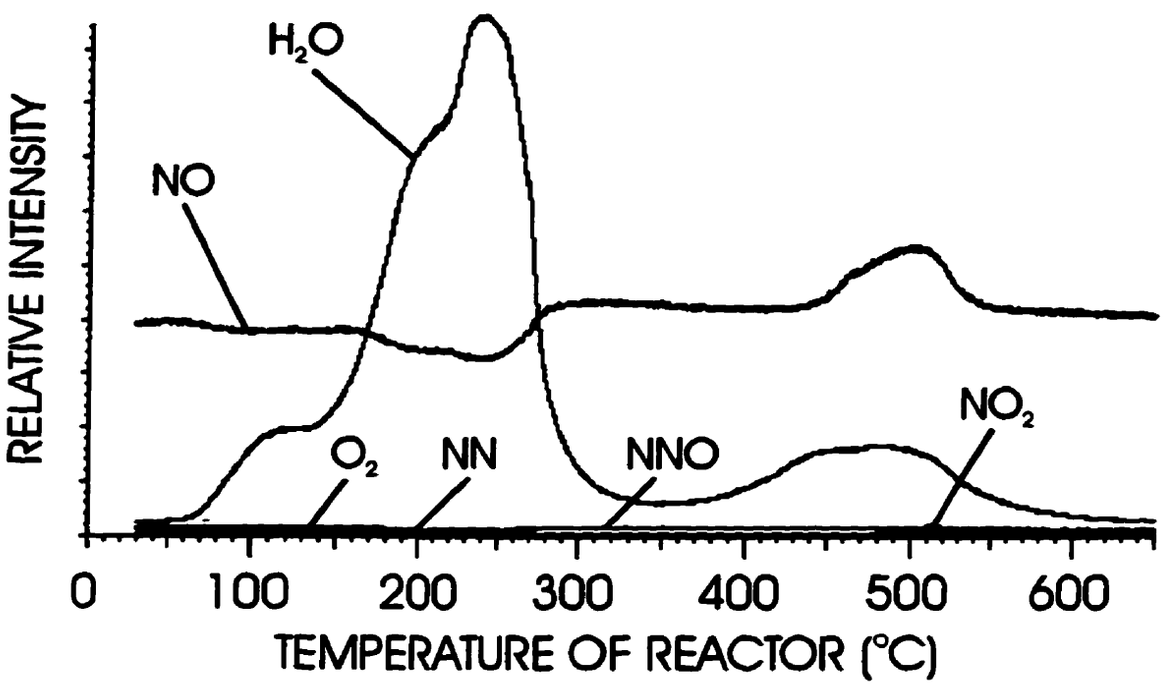

Fig.6.8 Temperature-programmed reaction of 0.075g (26.0μmoles) of HPW exposed to a continuous flow of 4950 ppm of NO. Heating rate=10°C/min and Flow rate=20 mL/min.

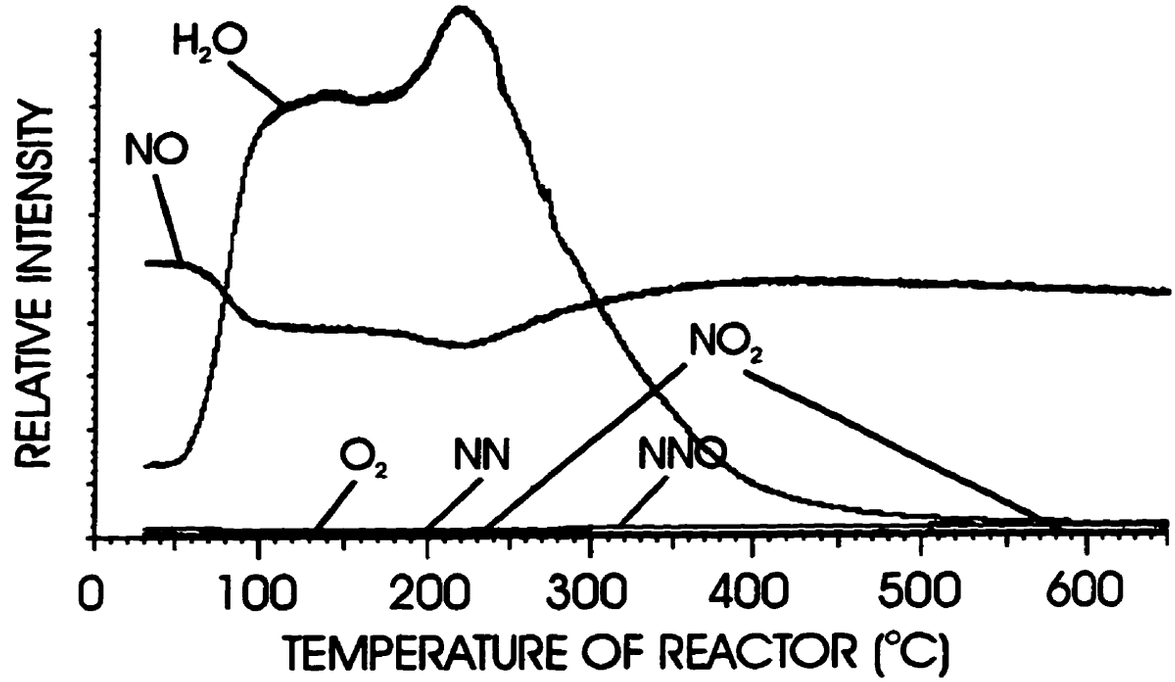

Fig.6.9 Temperature-programmed reaction of 0.075g (25.9μmoles) of LiPW exposed to a continuous flow of 4950 ppm of NO. Heating rate=10°C/min and Flow rate=20 mL/min.

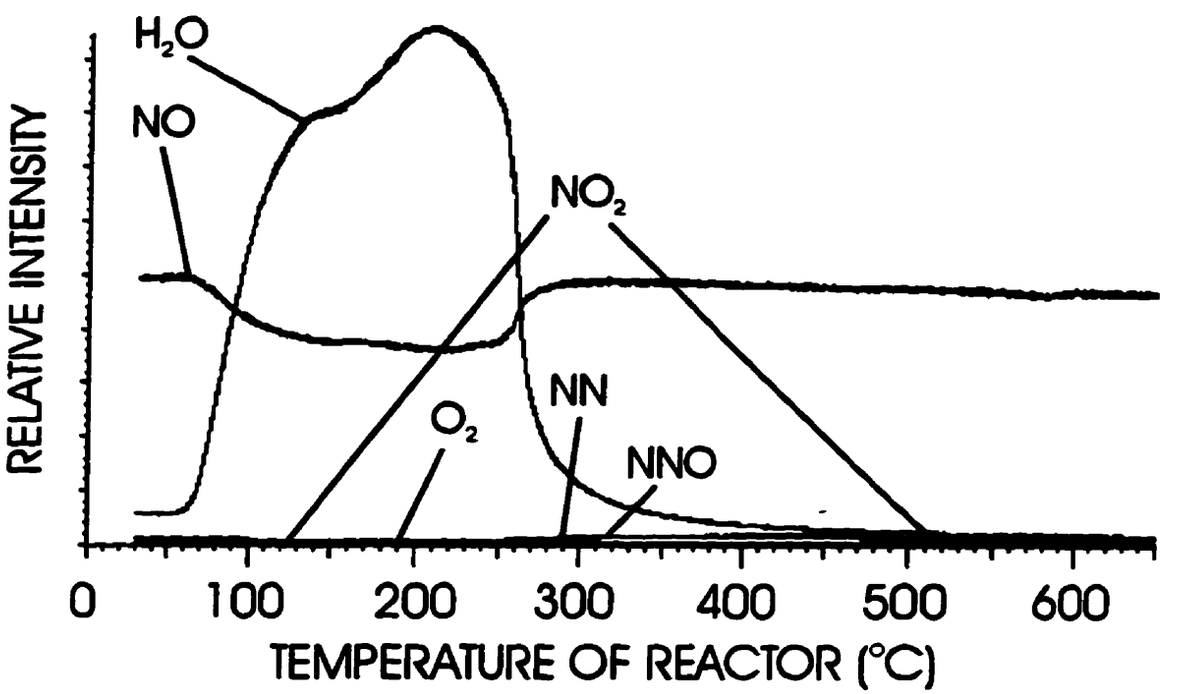

Fig.6.10 Temperature-programmed reaction of 0.075g (25.5μmoles) of NaPW exposed to a continuous flow of 4950 ppm of NO. Heating rate=10°C/min and Flow rate=20 mL/min.

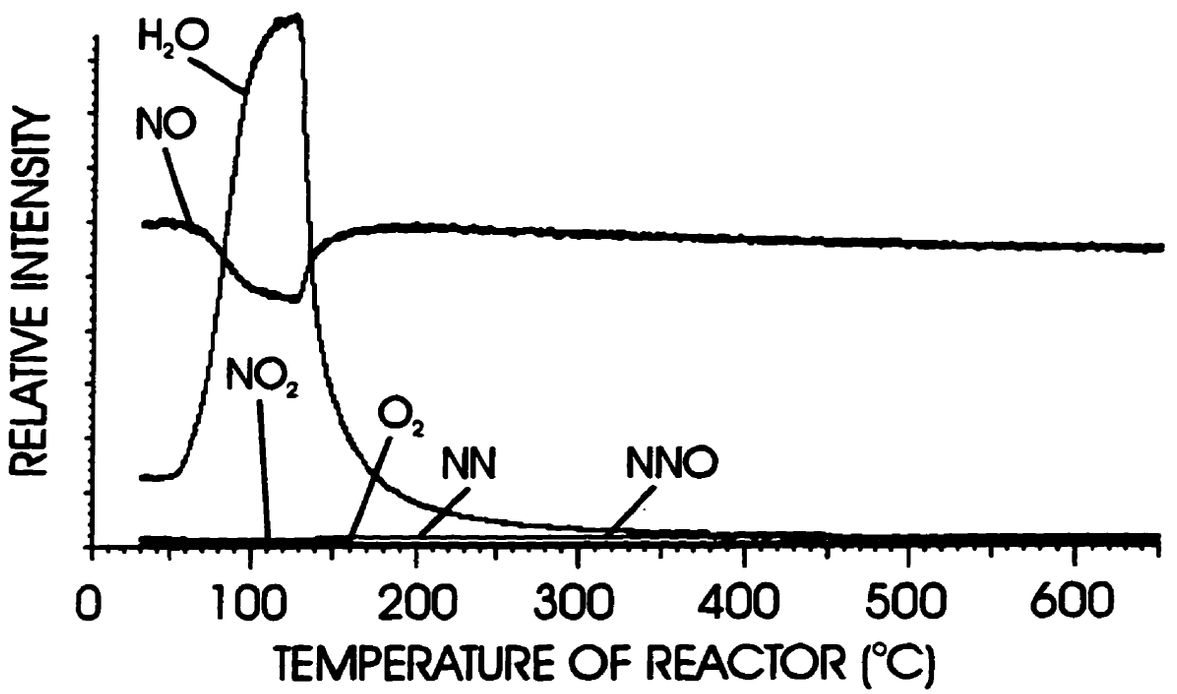

Fig.6.11 Temperature-programmed reaction of 0.075g (25.0μmoles) of KPW exposed to a continuous flow of 4950 ppm of NO. Heating rate=10°C/min and Flow rate=20 mL/min.

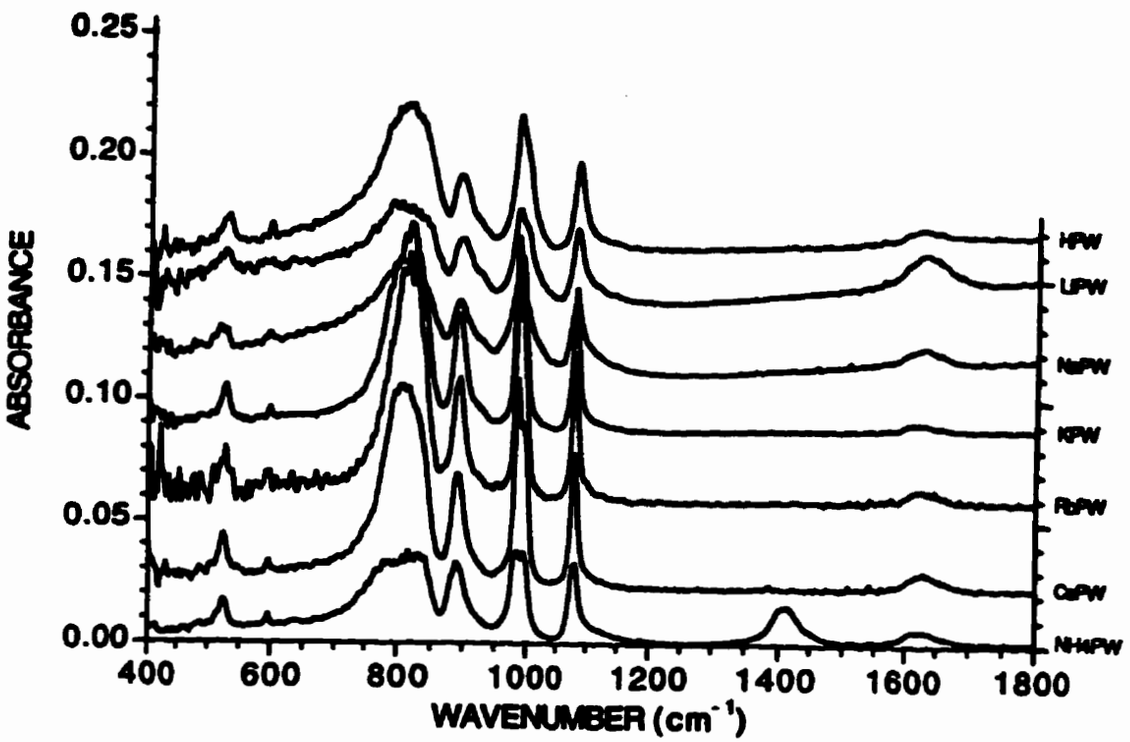

Fig.6.12 Normalized infrared spectra of HPW and derivatives after pretreatment in helium flow (20mL/min) at 300°C.
400-1800 cm^{-1} spectral region.

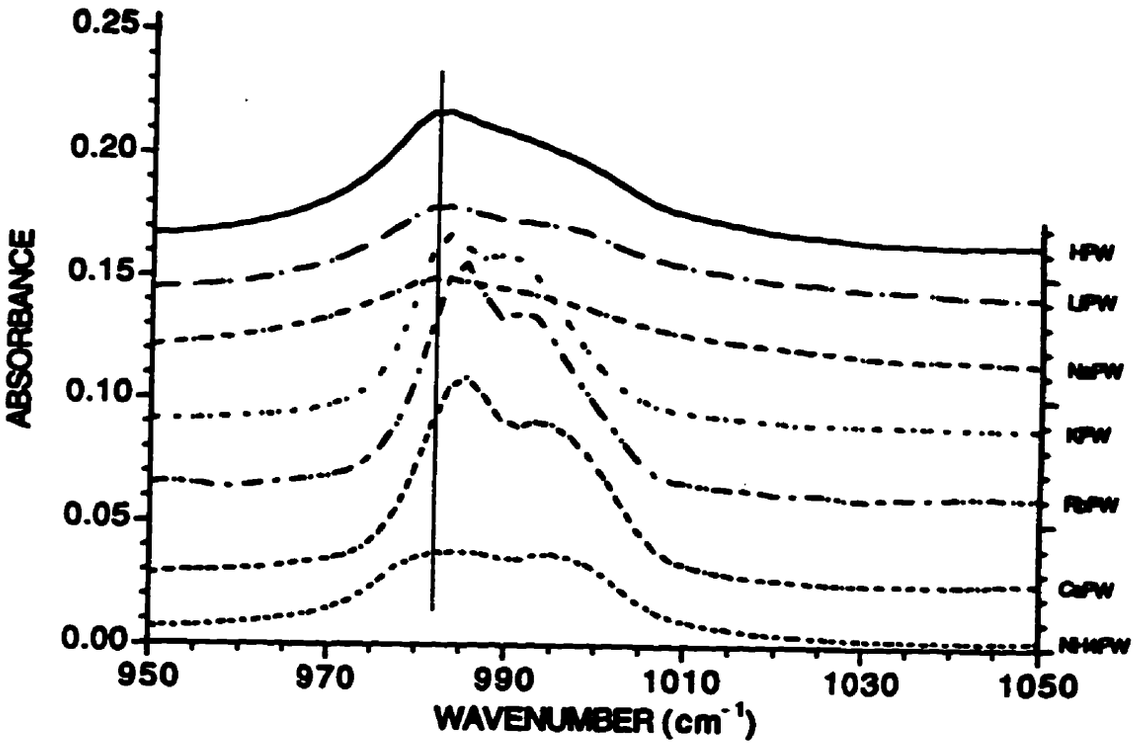

Fig.6.13 Normalized infrared spectra of HPW and derivatives after pretreatment in helium flow (20mL/min) at 300°C.
950-1050 cm^{-1} spectral region.

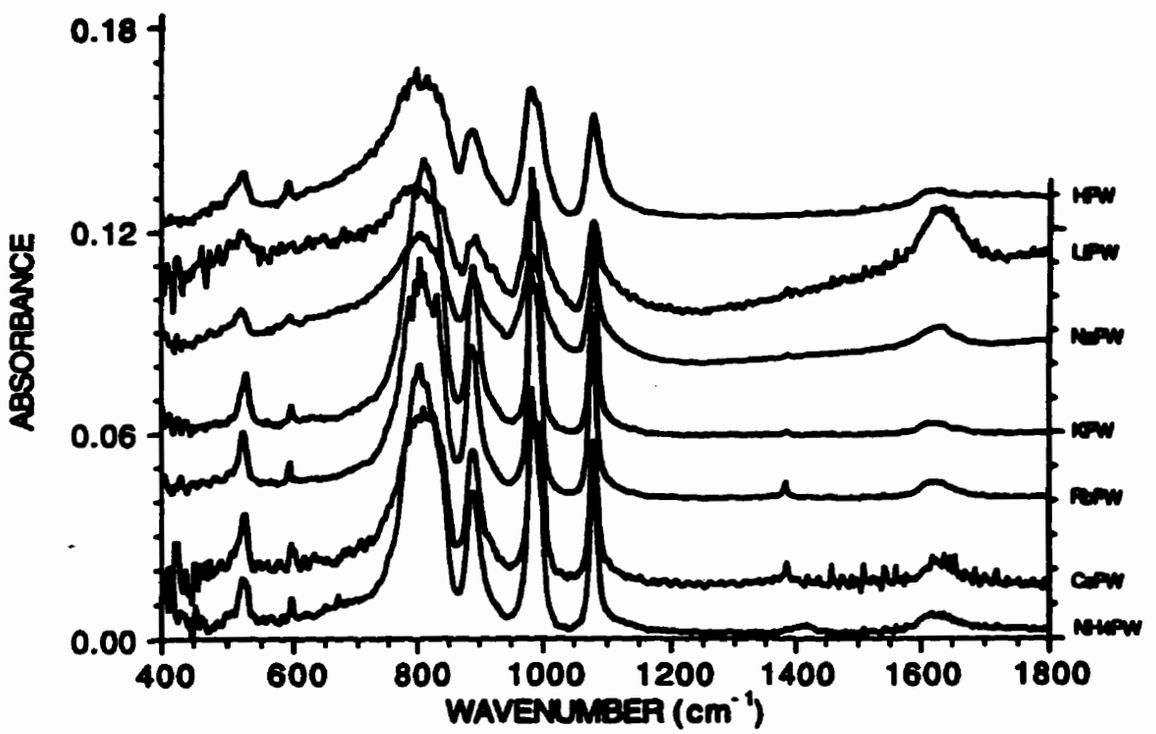

Fig.6.14 Normalized infrared spectra of HPW and derivatives after pretreatment in helium flow (20mL/min) and exposure to 85 μmoles NO_2 at 300°C.
400-1800 cm^{-1} spectral region.

An examination of the W-O_t bands, obtained with the salts between 950 and 1050 cm^{-1} (Fig.6.15), shows that the band observed at 981 cm^{-1}, with HPW, shifted to a lower wavenumber than observed in the absence of NO_2, and the relative intensity of the bands appears to have increased particularly for KPW, RbPW, CsPW, and NH_4PW.

B. Discussion

As seen in Chapter III, HPW exposed to NO_2 produces only vanishingly small quantities of N_2 and relatively large quantities of nitric acid through the reaction of NO_2 and the water molecules contained inside the bulk of the acid. After depletion of the water, NO_2 is irreversibly sorbed into the structure, apparently associated with the protons.

The results obtained on the salts of HPW provide supporting evidence for the role of the protons in the sorption of NO_2. Further, it was observed from the TPR results that HNO_3, apparently produced from the reaction of NO_2 and water, desorbs at approximately 100°C from KPW, RbPW, CsPW, and TlPW. Apparently, NO_2 did not diffuse into LiPW and NaPW. Further, no strongly held NO_2 molecules were seen desorbing at high temperature for any of these salts.

Relatively small losses of NO from the gas phase and vanishingly small evolutions of N_2 and NO_2 were found on exposure of HPW, LiPW, NaPW, and KPW to NO.

The absence of bands in the infrared spectrum which can be attributed to $[HNO_2]^+$ provide further support for the contention that protons are required for the irreversible sorption and protonation of NO_2.

The disparate behavior of LiPW and NaPW in comparison with that of KPW, RbPW, CsPW, and TlPW is tentatively attributed to the differences in microporosity and surface area, with the lithium and sodium salts having no microporous structure and low surface areas, while the remaining salts have both microporous structures and significantly high surface areas (see Refs.6.1 to 6.4 for micropore and surface area measurments).

The presence of the micropores may also facilitate entry of the water molecules into the bulk structure of the solid. Although NO is capable of entering the pore structure of the salts, there is little or no evidence of its reaction with water. The present observations suggest, however, that NO may either extract oxygen atoms from the anion or be oxidized by its decomposition product, although the formation of NO_2 and O_2 is insignificant.

The relative intensity of the infrared bands, particularly that from W-O_t at 982 cm^{-1}, seems, tentatively, to be related to the microporosity of the salts. For HPW, LiPW and NaPW, which are non-porous materials, the relative intensities of the W-O_t stretch are smaller than the intensities observed for KPW, RbPW, CsPW, and NH_4PW, which are porous materials. Moreover, for the porous catalysts, the position of the band has shifted to higher wavenumbers,

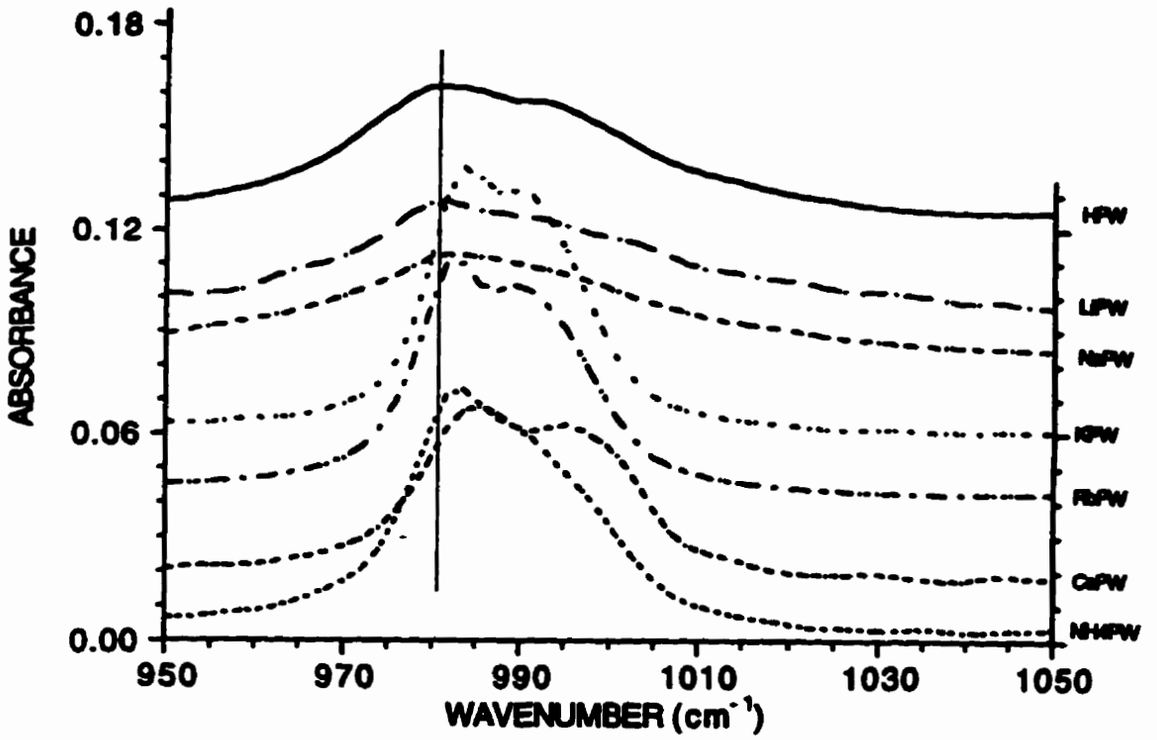

Fig.6.15 Normalized infrared spectra of HPW and derivatives after pretreatment in helium flow (20mL/min)and exposure to 85 μmoles NO_2 at 300°C.
950-1050 cm^{-1} spectral region.

and since the lattice distance between the Keggin units is larger in the porous than in the non-porous salts, vibration of the terminal oxygen atoms may be facilitated.

The formation of oxygen at high temperature (> 500°C), as observed from the TPR of NO_2 on the salts, could result from the reductive decomposition of NO_2 as in Equation 6.1.

$$2NO_2 \rightarrow O_2 + 2NO \qquad \text{(Eq.6.1)}$$

Although the participation of the catalyst in this process cannot be unambiguously established, it should be noted that, at the aforementioned temperature, little or no evidence for the formation of O_2 from NO_2 was found in the absence of the catalysts.

C. Conclusions

NO_2 interacts with the water on and in the microporous salts of HPW to produce HNO_3 which desorbs into the effluent stream at temperatures of approximately 100°C.

Little or no evidence was found for the irreversible sorption of NO_2 subsequent to the elimination of water from the salts. This suggests, as expected from the studies of the parent acid, HPW, that protons are required for the sorption of NO_2. Further, the NO_2^+ infrared band, observed with HPW after exposure to NO_2, was not seen with the salts which had previously been exposed to NO_2.

Although no formation of N_2 or N_2O was observed with the salts, at temperatures higher than 550°C, oxygen was observed, suggesting that partial reduction of NO_2 occurs.

REFERENCES

6.1 Highfield, J.G., and Moffat, J.B. *J.Catal.*, **88**, 177 (1984).

6.2 Moffat, J.B. *J.Molec.Catal.*, **52**, 169 (1989).

6.3 McGarvey, G.B., and Moffat, J.B. *J.Catal.*, **130**, 483 (1991).

6.4 Akimoto, M., Shima, K., Ikeda, H., and Echigoya, E. *J.Catal.*, **86**, 173 (1984).

CHAPTER VII

SORPTION AND REACTION OF NO AND NO_2 ON SUPPORTED HPW/SiO_2, BEFORE AND AFTER EXPOSURE TO GASEOUS AMMONIA

A. Results

HPW/SiO_2

On exposure of HPW supported on silica to pulses of NO_2, at 150 and 300°C, the predominant products are N_2 and NO with small quantities of O_2 and N_2O also evident in the reactor effluent (Figs.7.1A, 7.1B, and Table 7.1). As expected from the results found with pure HPW, a portion of the NO_2 lost from the gas phase is sorbed on the solid (Table 7.2), while the remainder is converted to the aforementioned products (Figs.7.1A and 7.1B). It is to be noted that no HNO_3 is detected.

Not surprisingly, the results are dependent on the loading of HPW on the support. At either temperature, the quantity of N_2 produced is highest at the lowest loading and decreases as the loading increases (Figs.7.1A and 7.1B). However, the production of nitric oxide is strongly dependent on the temperature of the reactor. At 150°C, NO reaches a maximum at 23.1% loading, while at 300°C the quantity produced is highest at a loading of 16.7% and decreases with further increases in the loading. NO_2 is removed from the gas phase through sorption on HPW, as well as conversion to N_2 and NO, with traces of O_2 and N_2O. At 150°C, the consumption of NO_2 increases to a maximum at 23.1% loading, while that at 300°C, although lower, is essentially independent of loading.

As noted, a portion of the NO_2 removed from the gas phase is sorbed by the solid. Since the sorbed NO_2 may not exist as such, the quantity held on the catalyst is expressed as the amount of nitrogen (N) (in whatever form) contained therein (Table 7.2). For the pure acid and each of the loadings, the quantity of nitrogen (N) retained on the solid is higher at 150°C than at 300°C. At 150°C, the retained amount increases with loading, reaching a value of approximately 2.5 moles of nitrogen (N) per mole of the anion for a loading of 75%, while at 300°C, the maximum is 0.5 mole of nitrogen (N) per mole of the anion at a loading of 16.7%.

The results of temperature-programmed desorption experiments on the supported catalysts (Fig.7.2), as prepared, show a low temperature peak at 200°C which increases in intensity and shifts to a higher temperature as the loading increases, as well as a smaller peak at 550°C. After exposure to NO_2 at 150°C (Fig.7.3), a peak is evident at 150°C, whose intensity

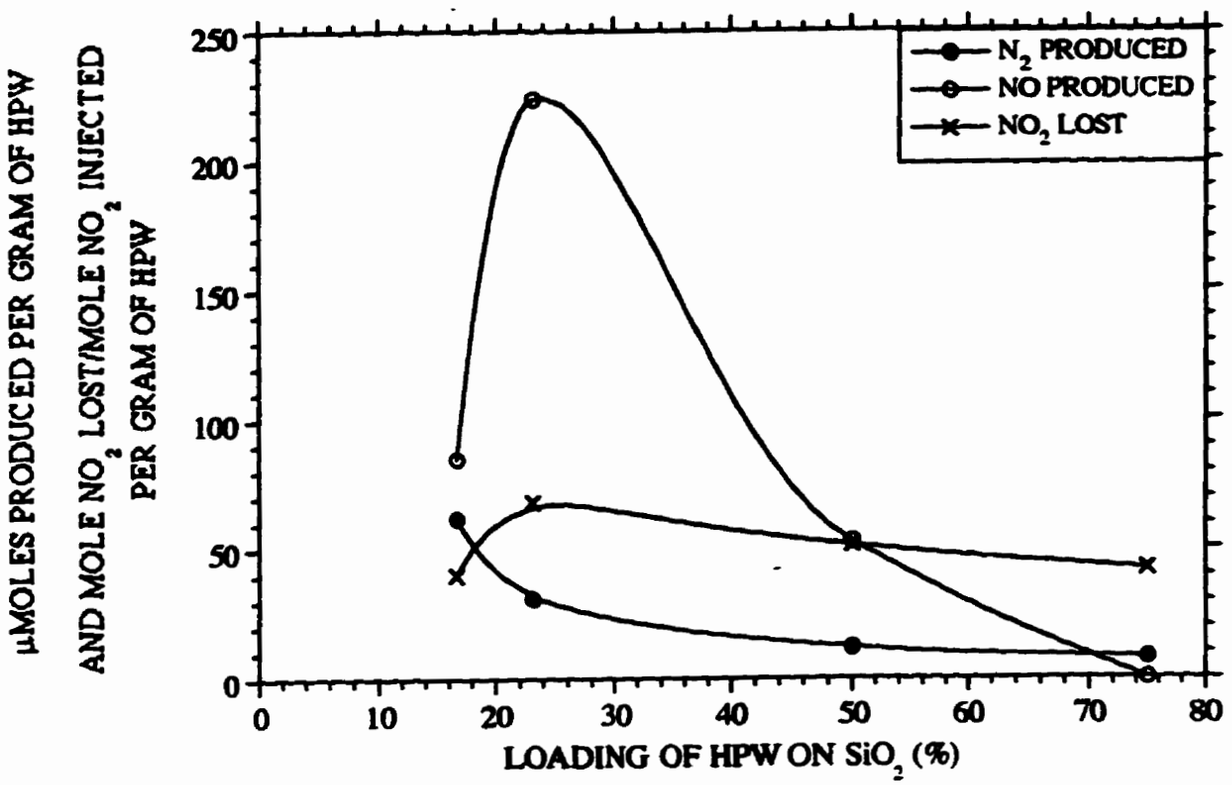

Fig. 7.1A Loading of HPW on SiO_2 on the production of N_2, NO and the NO_2 loss at 150°C. Single pulse experiments (17 µmoles NO_2) on 30 mg of supported catalyst for each loading. Each catalyst was pretreated in helium at the respective reaction temperature prior to the injection of NO_2.

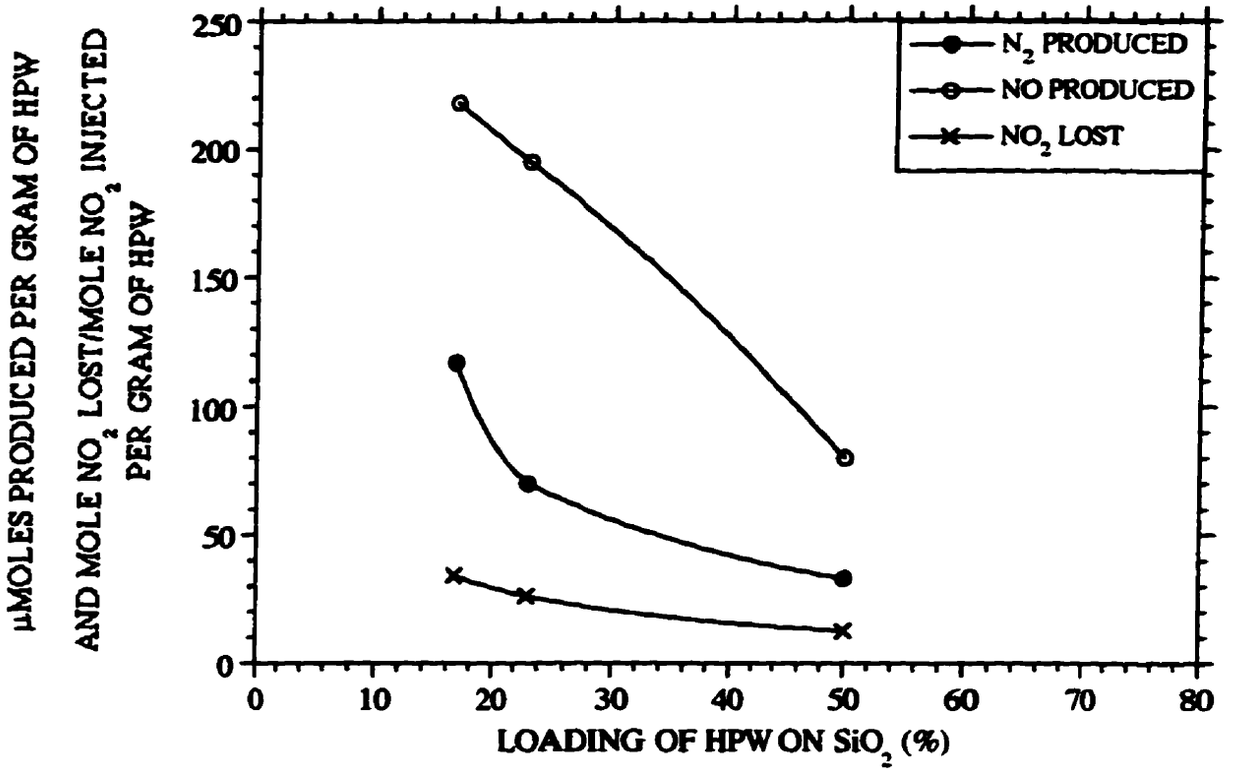

Fig. 7.1B Loading of HPW on SiO_2 on the production of N_2, NO and the NO_2 loss at 300°C. Single pulse experiments (17 µmoles NO_2) on 30 mg of supported catalyst for each loading. Each catalyst was pretreated in helium at the respective reaction temperature prior to the injection of NO_2.

TABLE 7.1

INJECTION OF NO_2 ON SiO_2

Temperature (°C)[a]	N_2[b]	NO[b]	N_2O[b]
150	1.1	20.7	0
300	3.1	26.2	0

a Pretreatment and reactor temperature for a reactor loaded with 30 mg of SiO_2.

b Results for the injection of 1 pulse of NO_2 (17μmoles). The results are presented in %mole per mole NO_2 injected.

TABLE 7.2

TOTAL NITROGEN SORBED ON HPW/SiO_2[a]

Loading[b] (weight %)	Temperature[c] (°C)	Quantity of Nitrogen-containing Species Sorbed[d] (μmole)	N/KU[e]
0.0	150	0.37	
	300	0.24	
16.7	150	1.8	1.1
(0.00500g)	300	0.79	0.5
23.1	150	2.8	1.1
(0.00692g)	300	0.18	0.1
50.0	150	10	2.0
(0.0150g)	300	0.70	0.1
75.0	150	20	2.5
(0.0225g)			

a Total nitrogen species sorbed on catalyst after exposure to 4 pulses of NO_2 (17 μmoles/pulse).

b %(w/w) loading of HPW over SiO_2. Reactor was packed with 30 mg of supported catalyst. () = mass of HPW in reactor (1mole HPW=2880.77g).

c Pretreatment and reaction temperature.

d Expressed as nitrogen atoms.

e Expressed as nitrogen atoms per Keggin Unit.

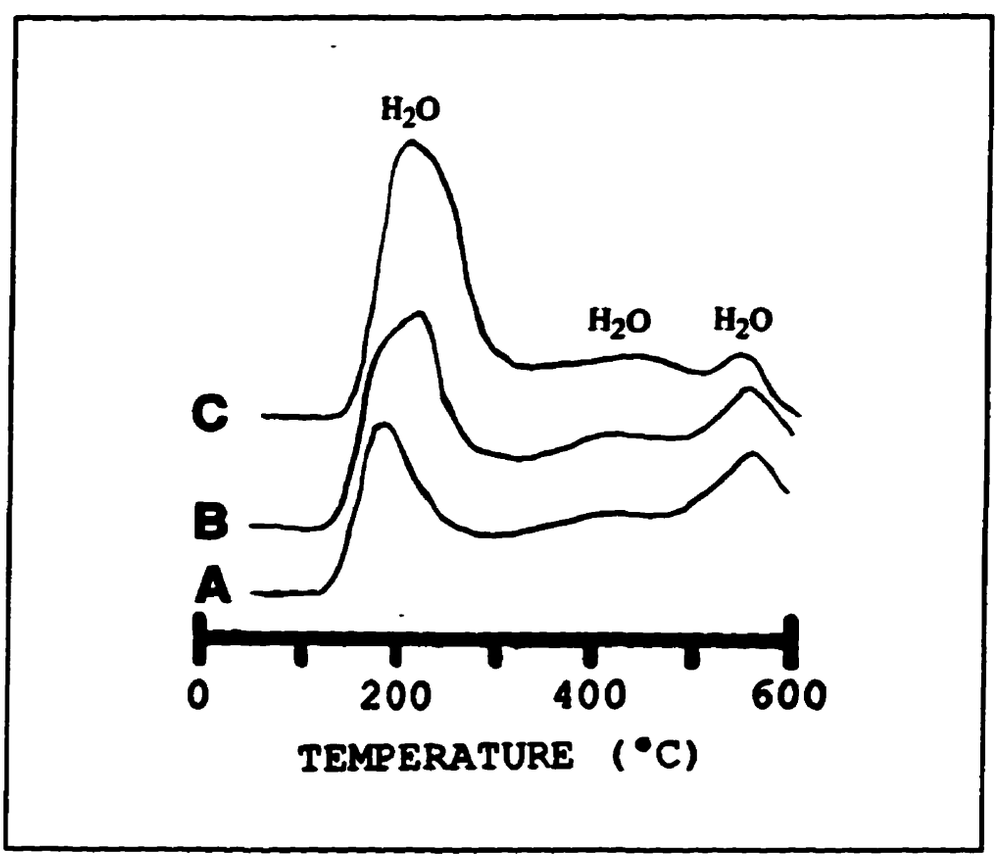

Fig. 7.2 Temperature-programmed desorption of A) 9.1%HPW/SiO_2, B) 16.7%HPW/SiO_2 and C) 23.1%HPW/SiO_2 as prepared. Helium flow rate, 45.0 mL/min; temperature rate, 60°C/min; mass of solid in reactor, 0.030 g.

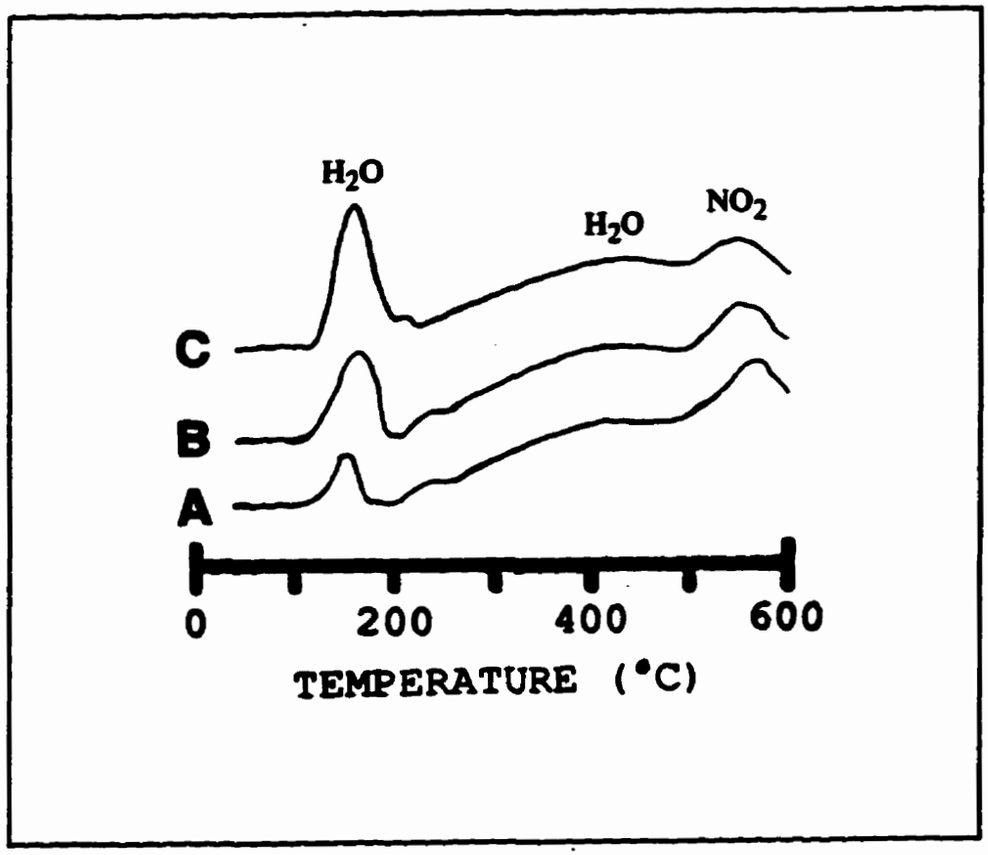

Fig. 7.3 Temperature-programmed desorption of A) 9.1%HPW/SiO_2, B) 16.7%HPW/SiO_2 and C) 23.1%HPW/SiO_2 pretreated in helium and saturated with NO_2 at 150°C. Helium flow rate, 45.0 mL/min; temperature rate, 60°C/min; mass of solid in reactor, 0.030 g.

again increases with increments in the loading. Vestiges of the aforementioned peak at 200°C are also evident, along with that at 550°C.

HPW/SiO_2 PRE-EXPOSED TO NH_3

On exposure of HPW/SiO_2, pretreated in helium and held at the desired temperature, to gaseous NH_3 followed by evacuation with helium and finally exposure to a pulse of NO_2, the principal products at 150°C are now N_2 and NO (Fig.7.4), with both experiencing decreases as the loading increases. A maximum in the ratio N_2/NO is observed at 23.1% loading. At 300°C, the quantities of these products are significantly lower, and N_2O is observed with decreases with the loading, again evident for all products (Fig.7.5). Although the effluent does not contain any NO at loadings higher than 75%, a maximum can be seen between 35 and 40% loading.

Aliquots of NH_3 were injected on a 23.1% loading to verify the saturation level (Table 7.3). The quantity of N_2 produced after the injection of NO_2 did not show any trend. However, the selectivity to NO increased with the NH_3 saturation level.

Introduction of consecutive pulses of NO_2 over a 23.1%HPW/SiO_2, previously exposed to NH_3, produced the expected decreases in the selectivity to N_2, at both 150 and 300°C (Figs.7.6 and 7.7, respectively). Unexpectedly, at both temperatures, the selectivity to NO increases after the first pulse, passes through a maximum at the second pulse, and then decreases. The selectivity to N_2O is vanishingly small at 150°C, but significant for the first pulse at 300°C.

The cumulative quantities of N_2, measured after 5 pulses of NO_2 for several loadings of catalyst pre-exposed to NH_3 followed by NO_2 at 150°C, correspond to approximately 10 moles/anion (Fig.7.8). With increasing loading, this decreases to approximately 1 mole/anion for a loading of 75%. In contrast, at 300°C, the aforementioned quantity varies relatively little with loading, ranging from 3, at the lowest loading, to 2, for the highest loading.

The results from temperature-programmed desorption on the solids, formed after injection of ammonia (6 mL at NTP) on the silica-supported HPW (Fig.7.9), show that, as the loading increases from 9.1 to 23.1%, the peak at 175°C decreases in intensity and shifts to higher temperatures (i.e. 210°C), while the peak at 550°C, attributed to the desorption of NH_3, increases. However, after exposure of the 23.1% catalyst, previously exposed to NH_3, to NO_2, the TPD obtained (Fig.7.9D) is similar to that shown in Figure 7.3.

As noted, when the catalyst is first pre-exposed to ammonia and then saturated with NO_2, the ammonia contained in the catalyst, as NH_4^+, reacts with NO_2 to produce, mainly, N_2. A portion of the NO_2 injected is sorbed by the catalyst. These sorbed NO_2 can in turn be reduced by the injection of ammonia. Figure 7.10 shows the quantities of N_2 and NO in the effluent of the reactor, for the different loadings at 300°C, after 1 cycle of regeneration (injection first of 6.0 mL NH_3, then saturation with NO_2, and again injection of 6.0 mL NH_3 and

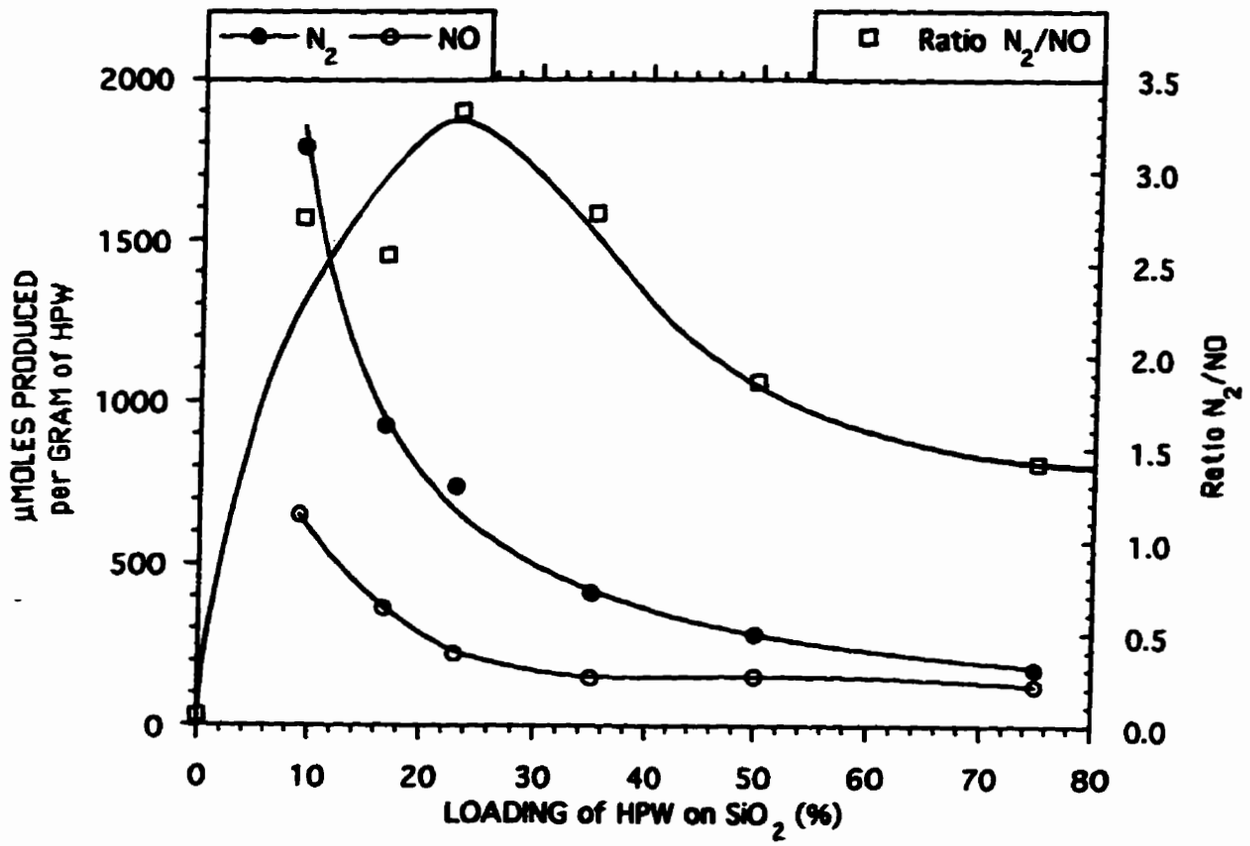

Fig. 7.4 Production of N_2 and NO as a function of the loading of HPW/SiO_2 at 150°C. Single pulse experiments (17 µmoles NO_2) on 30 mg of supported catalyst for each loading. Each catalyst sample was pre-exposed to 6.0 mL(25°C, 1 atm) of NH_3 at 150°C prior to the injection of NO_2.

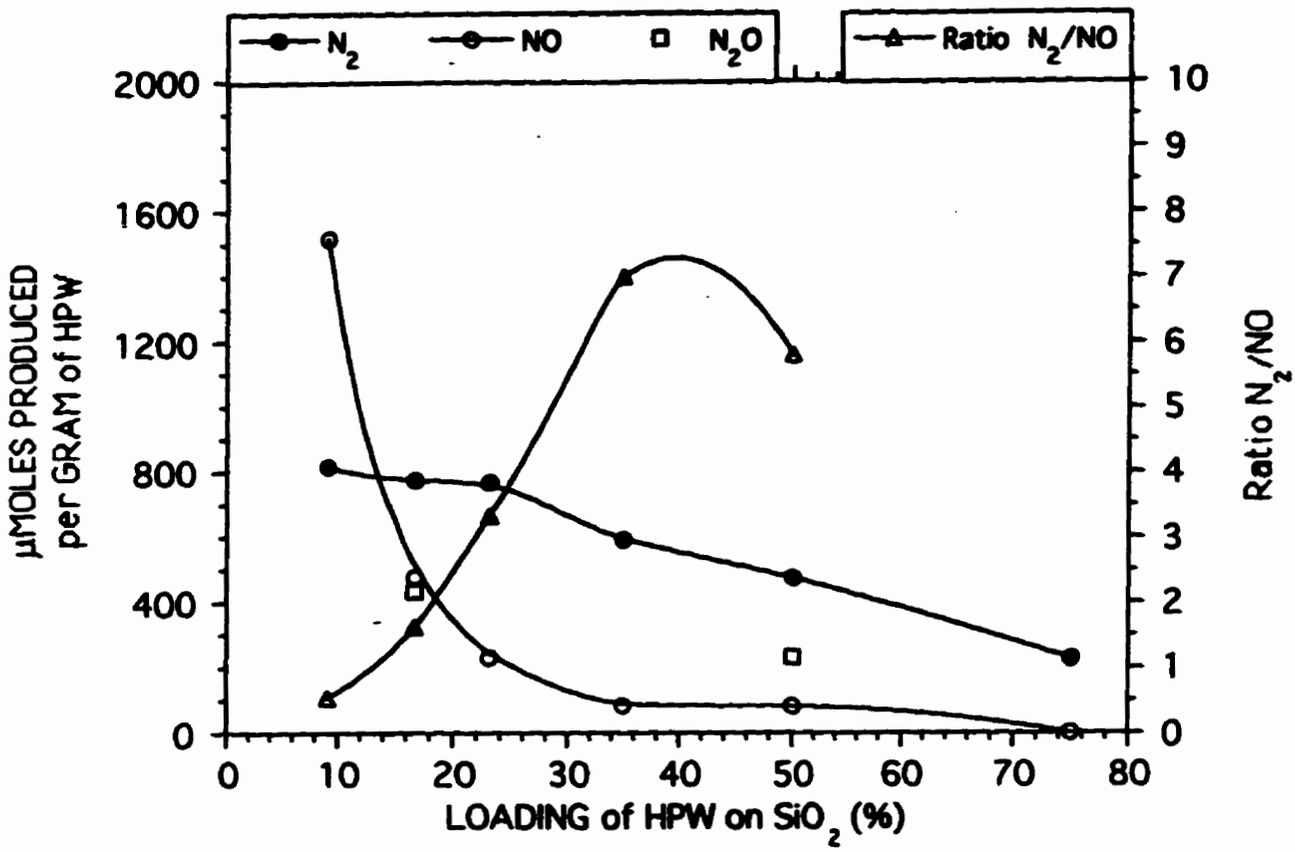

Fig. 7.5 Loading of HPW on SiO_2 effect on the production of N_2, NO and N_2O at 300°C. Single pulse experiments (17 µmoles NO_2) on 30 mg of supported catalyst for each loading. Each catalyst sample was pre-exposed to 6.0 mL (25°C, 1 atm) of NH_3 at 300°C prior to the injection of NO_2.

TABLE 7.3

EFFECT OF THE INJECTION OF NH_3 ON HPW/SiO_2 AND ON THE REDUCTION OF NO_2

Size of NH_3 Pulse (mL)[a]	N_2[b]	NO[b]	N_2O[b]
3.0	731	222	0
6.0	646	285	0
9.0	716	302	0

a Ammonia was injected in the reactor containing 30 mg of 23.1%HPW/SiO_2 kept at 150°C.

b Results for the injection of 1 pulse of NO_2 (17μmoles). The results are expressed in μmole per gram HPW (1mole=2880.77g).

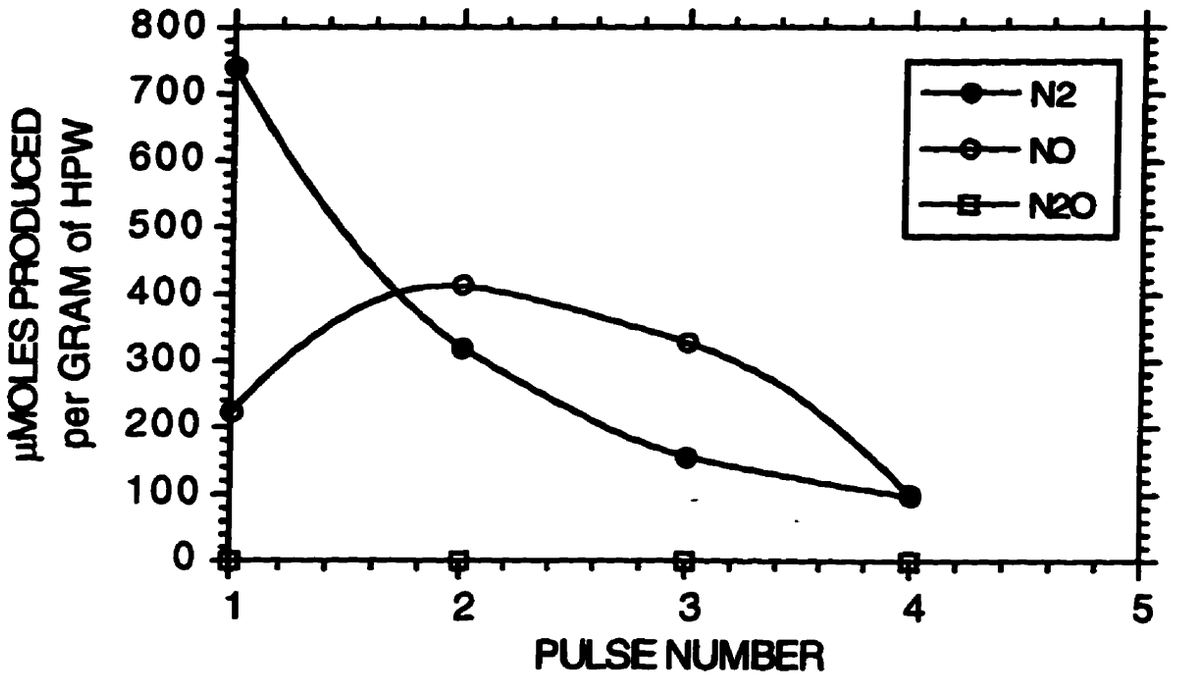

Fig. 7.6 N_2, NO and N_2O found in the effluent of the reactor for the injection of pulses of NO_2 (17 µmoles/pulse) on 30 mg of 23.1%HPW/SiO_2 sample kept at 150°C and pre-exposed to 6.0mL of NH_3.

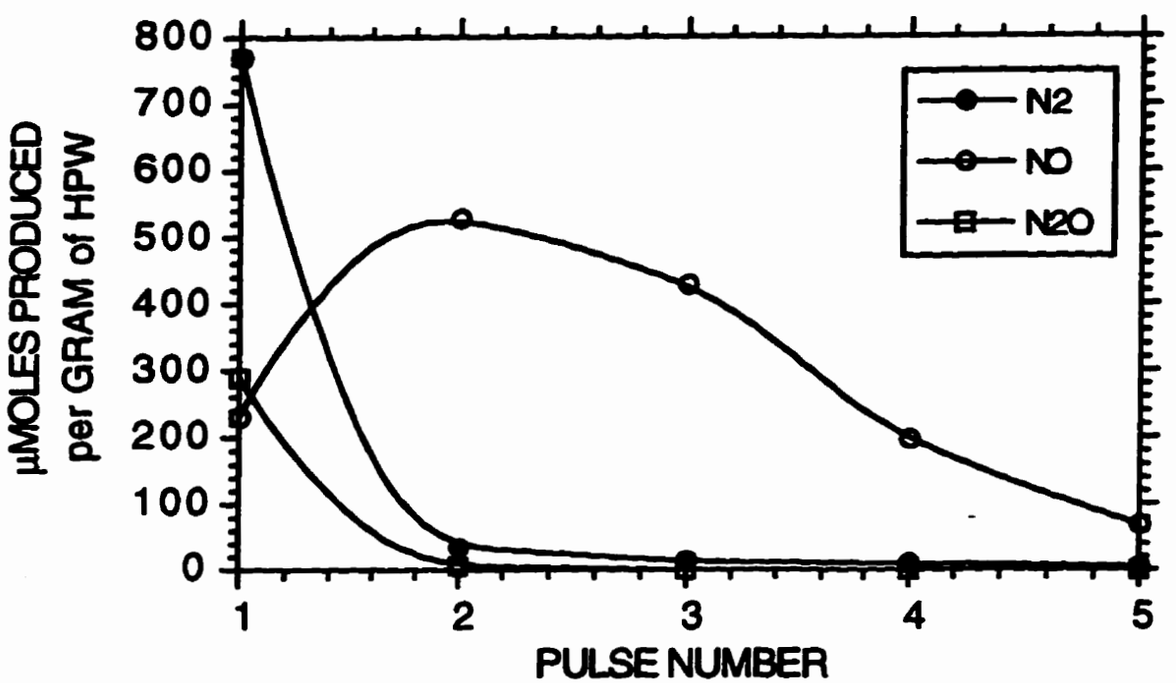

Fig. 7.7 N_2, NO and N_2O found in the effluent of the reactor for the injection of pulses of NO_2 (17 µmoles/pulse) on 30 mg of 23.1%HPW/SiO_2 sample kept at 300°C and pre-exposed to 6.0 mL of NH_3.

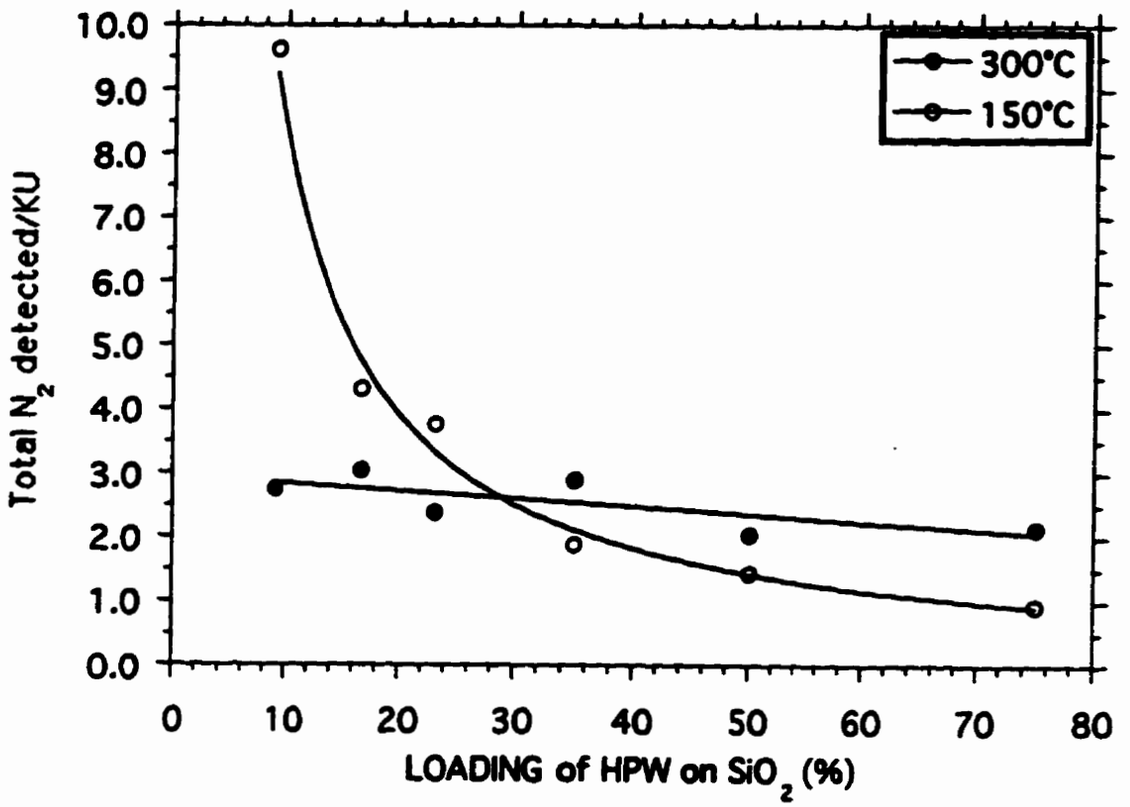

Fig. 7.8 Cumulative quantity of N_2 produced at 150 and 300°C from the injection of NO_2 (5 pulses of 17 μmoles each) on 30 mg of different loaded HPW/SiO_2 samples pre-exposed to 6.0 mL NH_3 at 150 and 300°C, respectively.

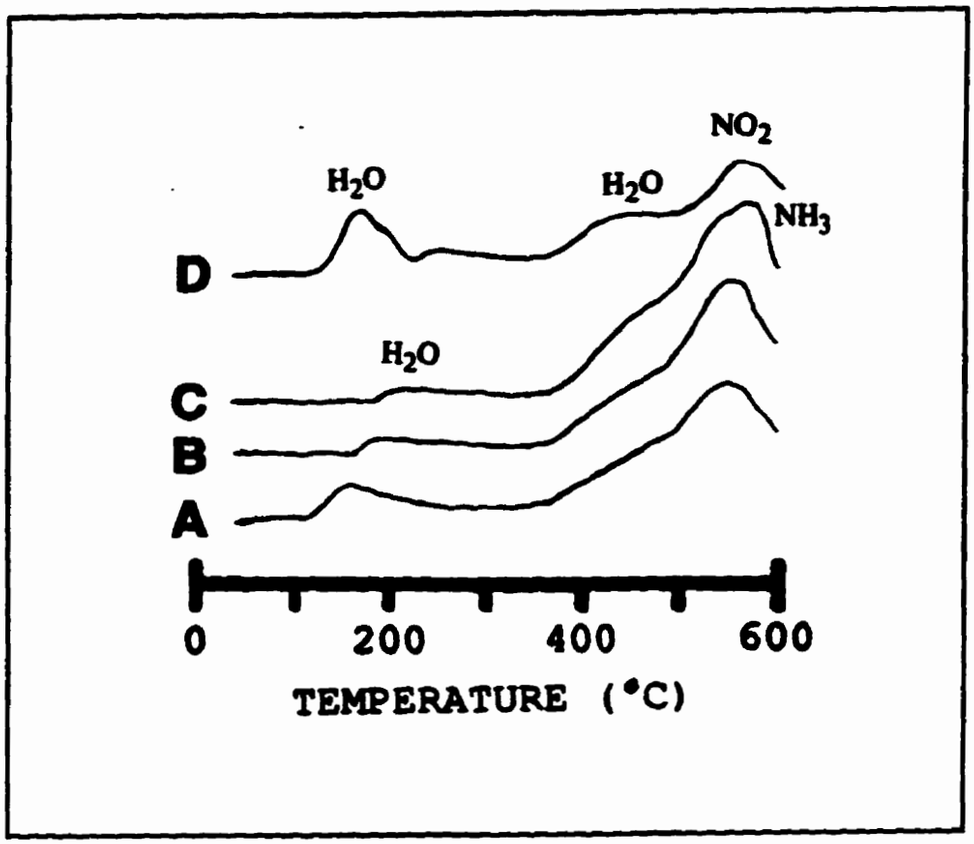

Fig. 7.9 Temperature-programmed desorption of A) 9.1%HPW/SiO_2, B) 16.7%HPW/SiO_2 and C) 23.1%HPW/SiO_2 pretreated in helium and saturated with ammonia at 300°C. TPD D) is as (C) for the exception of saturation with NO_2 at 300°C after the ammonia injection. Helium flow rate, 45.0 mL/min; temperature rate, 60°C/min; mass of solid in reactor, 0.030 g.

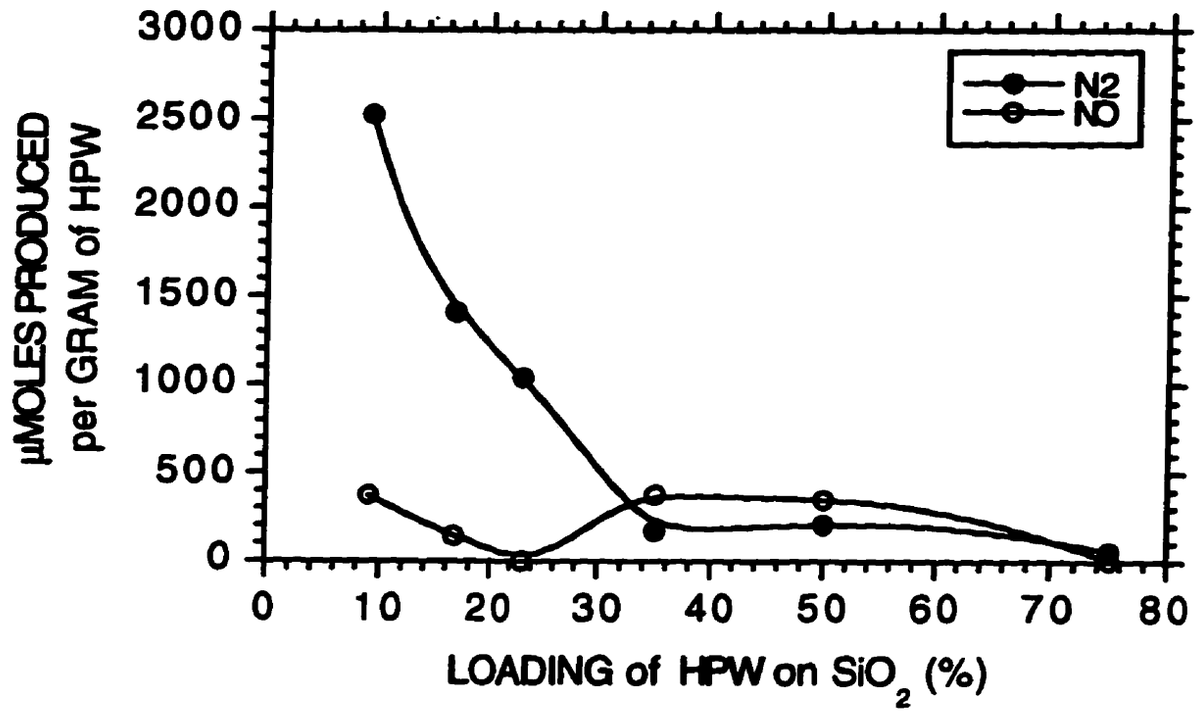

Fig. 7.10 Effect of ammonia injection (6.0 mL) on the production of N_2 when NH_3 is injected on samples of HPW/SiO_2 which were pre-exposed to ammonia first and then saturated with NO_2 in a first cycle. The reactor was kept at 300°C.

measurement of N_2 from the reaction). The relatively high value of N_2 detected for the smallest loading studied decreases rapidly with increasing loading. The selectivity to NO passes through two minima: one at 23.1%, and another at 75.0% loading. The second injection cycle of ammonia at 300°C produced little or no N_2O.

Repetitive regeneration cycles (Table 7.4) show that after three cycles, although the reduction of NO_2 to N_2 has decreased and that to NO has increased, the changes are relatively small.

The surface areas, after various pretreatments, are summarized in Table 7.5. The SiO_2 support suffers a significant reduction in surface area after loading, but exposure of the loaded catalyst to either NO_2 or NH_3, at 150°C, has little or no effect on the surface area. In contrast, exposure of the 23.1%HPW/SiO_2 catalyst to NH_3 at 300°C results in an increase in surface area, while the 50.0% loaded silica, after the same treatment, has a reduced surface area.

B. Discussion

HPW/SiO_2

The interaction between NO_2 and SiO_2-supported HPW results in the reduction of NO_2 to N_2 and NO, and in the sorption of NO_2 on the solid acid.

The reduction process is dependent upon the loading of HPW on silica with the selectivity to N_2 decreasing as the loading increases while the conversion of NO_2 increases, at least at 150°C (Fig.7.1A). It is to be noted that conversion here refers to loss of NO_2 from the gas phase, regardless of the means by which this occurs.

As noted in Chapter III, little or no NO_2 is reduced on pure HPW, at 150°C. Although the introduction of the support evidently encourages the reduction process (to N_2), it is clear that the support itself contributes relatively little to the reaction (Table 7.1). In view of the large differences in surface area between SiO_2 and the pure acid, the loading process obviously exposes a larger fraction of the acid to NO_2. However, as has been reported earlier (Ref.7.1), there is substantial evidence to support the contention that the interaction between the SiO_2 support and the acid is relatively strong, leading to an enhancement of the stability of the supported acid.

It is known (from Chapter III) that bulk HPW will sorb 3 NO_2/KU at 150°C and 0.8 NO_2/KU at 300°C. Based on the amount of HPW deposited on the silica, results from Table 7.2 show that, at saturation, for both 16.7 and 23.1% loadings, the total amount of NO_2 sorbed corresponds to 1.1 NO_2/KU. For the 50.0 and 75.0% loading, 2.0 and 2.5 NO_2/KU, respectively, were sorbed. However, at 300°C, with the 16.7, 23.1, and 50.0% catalysts relatively low sorption values are found.

TABLE 7.4

THE INJECTION OF NH_3 ON NO_2-EXPOSED HPW/SiO_2 FOR THE REGENERATION OF THE CATALYST[a]

Cycles[b]	N_2[c]	NO[c]	N_2O[c]
1	890	144	0
2	810	150	0
3	786	172	0

a Ammonia was injected in the reactor containing 30 mg of 23.1%HPW/SiO_2 kept at 300°C prior to the injection of NO_2.

b A cycle starts with the injection of 6.0 mL of NH_3 on the catalyst kept at 300°C and then NO_2.

c Results for the injection of 1 pulse of NO_2 (17μmoles). The results are expressed in μmole per gram HPW.

TABLE 7.5

SURFACE AREAS

Samples	Treatment[a]	Surface Area (m^2/g)
SiO_2	110°C-air	216.2
23.1%HPW/SiO_2	150°C-He	176.1
23.1%HPW/SiO_2	150°C-NO_2	169.5
23.1%HPW/SiO_2	150°C-NH_3	176.0
23.1%HPW.SiO_2	150°C-NH_3-NO_2	178.2
23.1%HPW/SiO_2	150°C-NH_3-NO_2-NH_3	158.0
23.1%HPW/SiO_2	300°C-NH_3	202.3
50.0%HPW/SiO_2	300°C-NH_3	149.5
HPW	150°C-He	9.3

a Pretreatment and treatment temperature-added gas(es) in order of injection at saturation conditions.

As noted earlier (Chapter III), NO_2 molecules are evidently capable of penetrating into the bulk structure of the solid acids, and the protons are apparently required for the sorption process (see Chapter VI). Since NO_2 molecules should be capable of entering the bulk of SiO_2-supported HPW, the relatively low values obtained for the number of sorbed molecules of NO_2 on HPW/SiO_2 must be attributed to a reduced ability of the protons to interact with NO_2, which may result from the binding of protons to the support itself. Alternatively, the existence of a small number of molecular layers on the support may not be sufficient to facilitate the sorption of NO_2.

Although the unexpected differences in the NO_2 reduction process on HPW and HPW/SiO_2 cannot be fully explained at this time, the observation that the reduction of NO_2 and the selectivity to N_2 are highest for low loadings suggests that the interactions between HPW and the silica support may play a role. The influence of the support on the anion may encourage the formation of oxygen vacancies, evidence for which has been reported earlier (Ref.7.2). Moreover, earlier work showed that N_2O was capable of providing oxygen for the vacancies (Ref.7.3), it is conceivable that NO_2 could function in a similar manner.

HPW/SiO_2 + NH_3

Exposure of HPW/SiO_2 to NH_3 results in the formation of a catalyst with strongly bound NH_3, the latter presumably in the form of NH_4^+. It is interesting to note, however, that at least, at 150°C, this process does not alter the surface area.

On exposure of the NH_3/HPW/SiO_2 catalyst to NO_2, reduction to N_2 and NO occurs with the selectivity to N_2 being approximately three times that to NO at 150°C. At both 150 and 300°C, the selectivities to N_2 and NO decrease with increase of the loading, when expressed per unit mass of HPW.

If it is assumed that sufficient NH_3 has been taken up by the catalyst to convert all protons, both those on the surface and those in the bulk, to ammonium ions, then the aforementioned dependence of selectivities on loading can be interpreted as indicative of an inability of NO_2 to penetrate into the bulk of the NH_3-saturated catalyst. However, the observation of the values for the total N_2 measured per anion, not too different from 3 (similar to the number of protons per anion), appears to contradict this, particularly at a reaction temperature of 300°C. Thus the increase of the surface area with decreasing loading would be a more important factor in the reduction of NO_2.

Interestingly, the reaction temperature appears to have relatively little effect on the selectivities to N_2 and NO with the NH_3/HPW/SiO_2 catalyst, although, at higher temperature (300°C), a significant selectivity to N_2O is noted.

Since NH_3 is strongly bound to HPW/SiO_2 (as evidenced from TPD), the NO_2 reduction process appears to be one in which NO_2, rather than reacting with gaseous NH_3, interacts with the NH_3 (as NH_4^+) on the catalyst. In view of the aforementioned values obtained for the nitrogen produced per anion, a probable stoichiometry for the NO_2 to N_2 reduction may be represented by

$$3NO_2 + 4NH_3 \rightarrow 3.5N_2 + 6H_2O \qquad \text{(Eq.7.1)}$$

and for the reduction of NO_2 to NO or N_2O

$$5NO_2 + 2NH_3 \rightarrow 7NO + 3H_2O. \qquad \text{(Eq.7.2)}$$
$$4NO_2 + 3NH_3 \rightarrow 3.5N_2O + 4.5H_2O. \qquad \text{(Eq.7.3)}$$

Nitrous oxide may also be generated from the decomposition of ammonium nitrate, which can form from nitric acid and ammonia.

It should be noted, however, that NO can be formed from the oxidation of NH_3 as

$$4NH_3 + 5O_2 \rightarrow 4NO + 6H_2O \qquad \text{(Eq.7.4)}$$

and NO can be oxidized to NO_2 as

$$2NO + O_2 \rightarrow 2NO_2. \qquad \text{(Eq.7.5)}$$

Exposure of the spent catalysts to gaseous NH_3 largely regenerates the catalyst, although the selectivities to N_2 and NO somewhat decrease and increase, respectively, after this process.

C. Conclusion

The reduction of NO_2 to N_2 is catalyzed by HPW/SiO_2 pretreated with gaseous ammonia. In the absence of the latter treatment, the reduction process is relatively less effective. Although the increased available surface resulting from the use of a support is evidently advantageous in enhancing the availability of the reductant, nevertheless, NO_2 is capable, as with pure HPW, of penetrating into the bulk of the supported material. The production of N_2 comes from a dual effect of the surface area and the quantity of NH_4^+ available for the reduction reaction, thus the reduction reaction is guided in part by the availability of the ammonium cations. At higher temperature, this dual role becomes almost insignificant since the penetration of NH_3 is the same regardless of the loading. The small difference only comes from the difference in surface area.

The formation of NO can be, most likely, explained by the decomposition of NO_2 on silica. But, at higher loading, the production of nitric oxide may also result from the reaction of Equation 7.4.

Regeneration of the supported catalyst can be achieved by injection of gaseous ammonia.

REFERENCES

7.1 Kasztelan, S., Payen, E., and Moffat, J.B., *J.Catal.*, **125**, 45 (1990).

7.2 Kasztelan, S., and Moffat, J.B., *J.Catal.*, **116**, 82 (1989).

7.3 Kasztelan, S., and Moffat, J.B., *J.Catal.*, **106**, 512 (1987).

CHAPTER VIII

SORPTION AND REACTION OF NO, NO_2, and N_2O ON SUPPORTED $HPMo/SiO_2$, BEFORE AND AFTER EXPOSURE TO GASEOUS AMMONIA

A. Results

$HPMo/SiO_2$

Single-pulse experiments at a variety of temperatures (SPE-VT), using the same catalytic aliquot, were carried out for NO_2 on 20.0% 12-molybdophosphoric acid supported on silica (20.0%$HPMo/SiO_2$) pretreated in helium. The quantity of N_2 produced remained at levels comparable to those obtained with silica itself (Fig.8.1). Although, the selectivity to N_2 with the supported HPMo is somewhat higher than that found with pure silica for a limited temperature range, between 400 and 550°C.

Both silica and $HPMo/SiO_2$ samples show similar selectivities to nitric oxide (Fig.8.2). The selectivity to nitric oxide shows a minimum (<2%) at 400°C, and at temperatures higher than 400°C the selectivity to NO is also similar for both SiO_2 and $HPMo/SiO_2$. However, below 400°C, the supported acid shows a higher selectivity than that observed for the silica alone.

The selectivity to oxygen, however small, is virtually the same for both silica and the supported acid (Fig.8.3). These samples show vanishingly small selectivities to O_2 from 150 to 300°C. The selectivity to O_2 increases for temperatures higher than 350°C and reaches a maximum of approximately 10% at 550-600°C. No nitrous oxide was detected in the gas phase during these experiments.

$HPMo/SiO_2$ PRE-EXPOSED TO NH_3

Single-pulse experiments of NO_2 on samples of $HPMo/SiO_2$ show that pre-saturation with gaseous ammonia (10 mL) considerably increases the selectivity to N_2 (Fig.8.4). For the 20.0%$HPMo/SiO_2$ sample saturated with NH_3 at 150°C, the selectivity to N_2 (17 μmoles of NO_2 is injected at each temperature) decreases rapidly with stepwise increase of the temperature. However, if the catalyst is saturated with NH_3 at each temperature (prior to the injection of NO_2) the selectivity to N_2 reaches a maximum of 70% at 500°C.

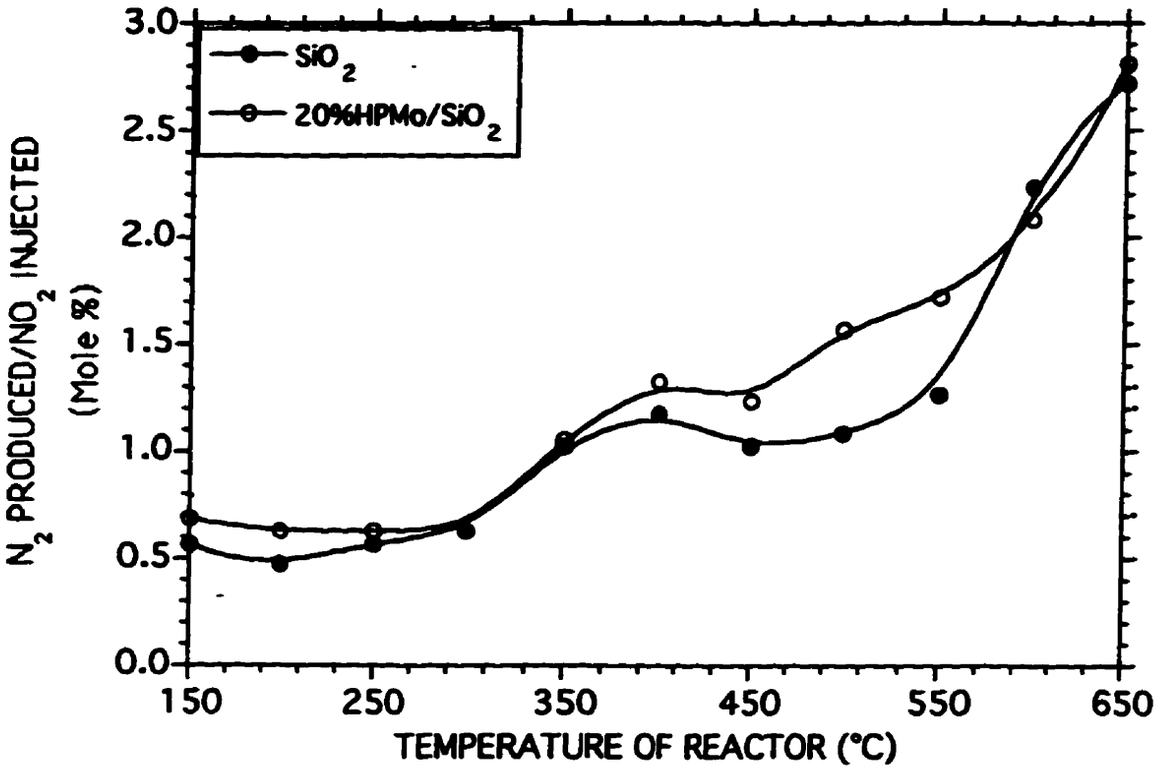

Fig. 8.1 Amount of N_2 found in the effluent from single-pulse experiments at a variety of temperatures (SPE-VT), from NO_2 on SiO_2; and NO_2 on 20.0%HPMo/SiO_2. The same catalytic aliquot was kept in the reactor for the series of temperatures. Mass in reactor = 50 mg; Pulse size = 17 μmoles NO_2; Helium flow = 20 mL/min.

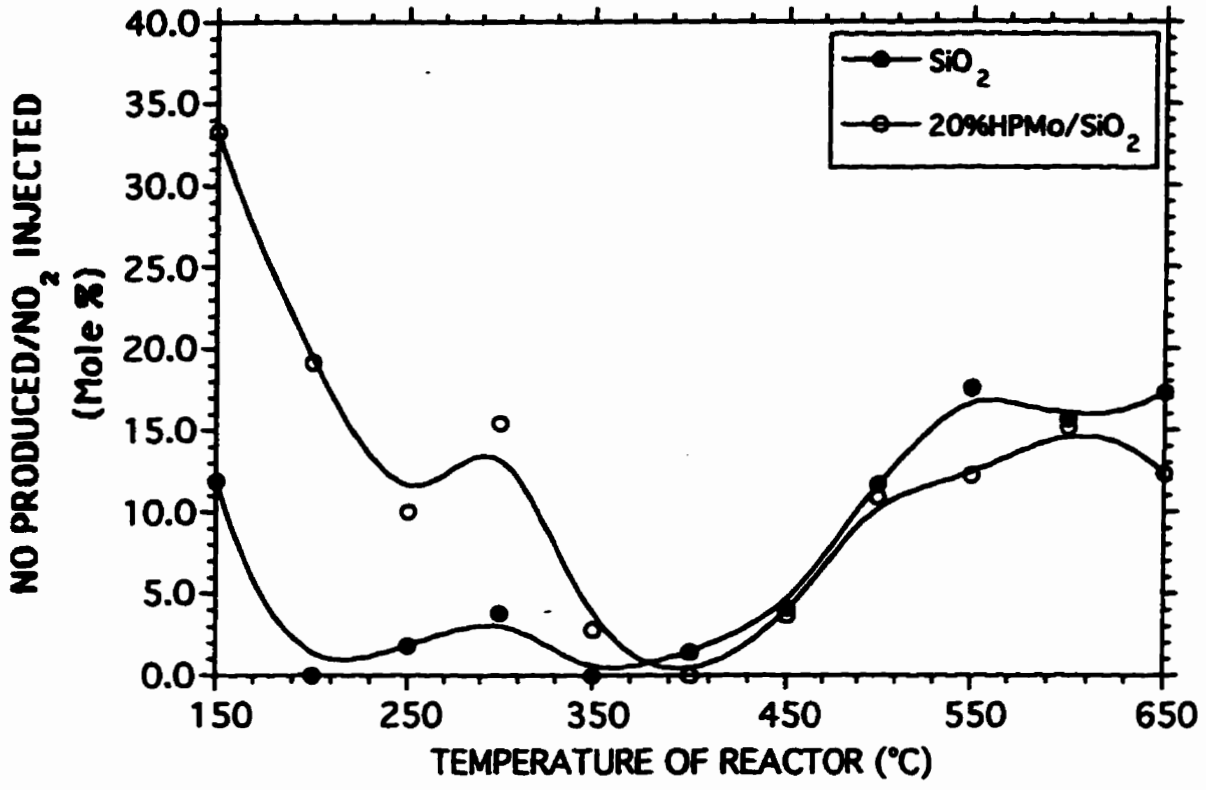

Fig. 8.2 Amount of NO found in the effluent from single-pulse experiments at a variety of temperatures (SPE-VT), from NO_2 on SiO_2; and NO_2 on 20.0%HPMo/SiO_2. The same catalytic aliquot was kept in the reactor for the series of temperatures. Mass in reactor = 50 mg; Pulse size = 17 μmoles NO_2; Helium flow = 20 mL/min.

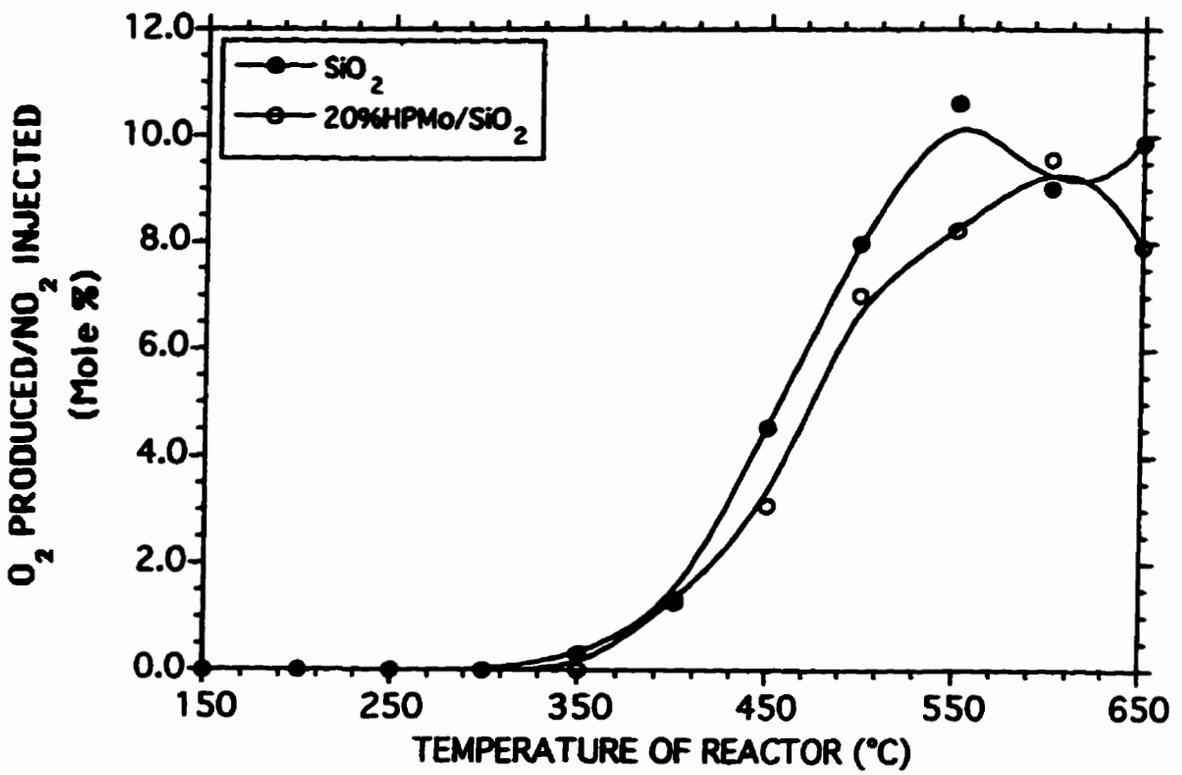

Fig. 8.3 Amount of O_2 found in the effluent from single-pulse experiments at a variety of temperatures (SPE-VT), from NO_2 on SiO_2; and NO_2 on 20.0%HPMo/SiO_2. The same catalytic aliquot was kept in the reactor for the series of temperatures. Mass in reactor = 50 mg; Pulse size = 17 μmoles NO_2; Helium flow = 20 mL/min.

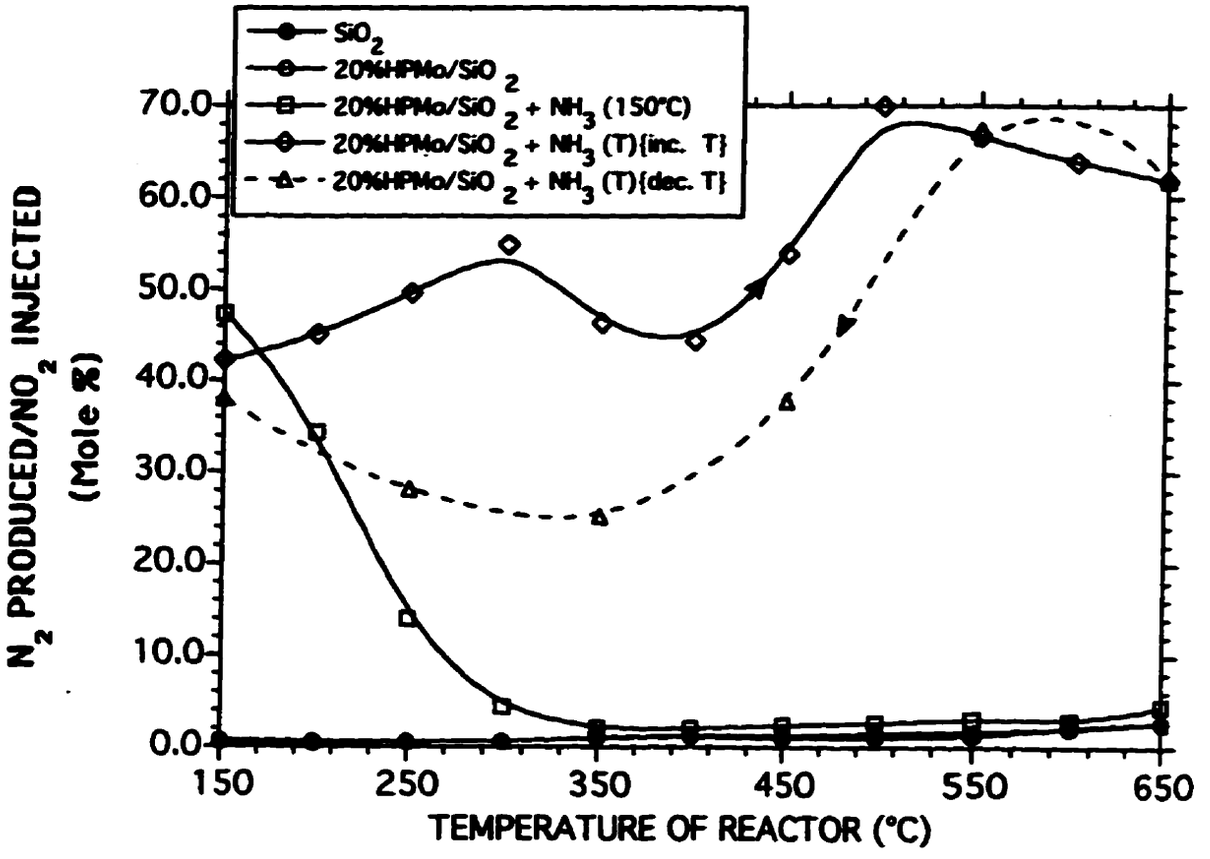

Fig. 8.4 Amount of N_2 found in the effluent from single-pulse experiments at a variety of temperatures (SPE-VT), from NO_2 on SiO_2; and NO_2 on 20.0%HPMo/SiO_2 pre-exposed to ammonia at 150°C only, or at each selected temperature (T). The same catalytic aliquot was kept in the reactor for the series of temperatures. Mass in reactor = 50 mg; Ammonia injected before pulse = 10 mL; Pulse size = 17 μmoles NO_2; Helium flow = 20 mL/min.

The results from the successive injection of ammonia and nitrogen dioxide, with stepwise decrease of the temperature of the reactor, are similar at 550°C to those found in the heating cycle but the selectivity to N_2 passes through a minimum at 350°C. The selectivity at 150°C in the cooling cycle is similar to that measured at the beginning of the heating cycle.

The presence of ammonia, as NH_4^+, on the catalyst decreases the selectivity to NO (Fig.8.5). Silica and the supported catalyst show decreasing selectivity to NO from 34% and 12%, respectively, at 150°C, to a minimum of 2-3% at 375°C, increasing to approximately 15% NO at 550-650°C.

The selectivity to NO is vanishingly small at 150°C when NO_2 is injected on the 20.0%HPMo/SiO_2 sample pre-exposed to ammonia at 150°C. The selectivity increases to a maximum of 12% at 300°C and decreases to 2-3% at 400°C. With further increases in temperature the selectivity to NO increases to reach a plateau of 10% at 550-650°C.

Exposure of the catalyst to NO_2 after saturation with NH_3 at the same temperature yields little or no NO between 150 and 250°C, but the selectivity to NO increases to a maximum of 38% at 350°C, followed by a decrease to a vanishingly small value between 450 and 650°C. In the cooling cycle, a maximum in the selectivity to NO is reached at approximately 300°C.

Surprisingly, the selectivity to O_2 is negligible for all samples up to 300°C but increases markedly for further increases in temperature with SiO_2, HPMo/SiO_2 and the latter samples saturated with NH_3 at 150°C (Fig.8.6). However, with the sample exposed to NH_3 and NO_2 at the same temperature, no evidence of O_2 is seen at any temperature.

Nitrous oxide was also found in the effluent of the reactor when NO_2 was injected on the 20.0%HPMo/SiO_2 samples saturated with ammonia (Fig.8.7). When the supported catalyst was pre-exposed to ammonia at 150°C only, the selectivity to N_2O at 150°C corresponds to approximately 0.5%. The selectivity rises slowly to a maximum of approximately 3% at 250°C to decrease to vanishingly small quantities at temperatures above 450°C. However, when ammonia is injected at each temperature prior to the injection of NO_2, the selectivity to N_2O rises from 0.5% at 150°C to a maximum of approximately 23% at 450°C to decrease to negligible values at temperatures above 550°C.

On exposure of 20.0%HPMo/SiO_2, pre-saturated with ammonia, to NO, the products in the effluent are N_2 and N_2O. The low conversion of NO can be seen from the high concentration of nitric oxide found in the effluent of the reactor (Fig.8.8). The concentration of NO in the gas phase remains high with the supported catalyst which was pretreated with NH_3 at 150°C only, but reaches a minimum of approximately 80% at 500°C. However when a 20.0%HPMo/SiO_2 sample is pretreated with ammonia before each injection of NO at each temperature, the conversion of NO remains low from 150°C to 300°C but increases to approximately 100% at 400°C.

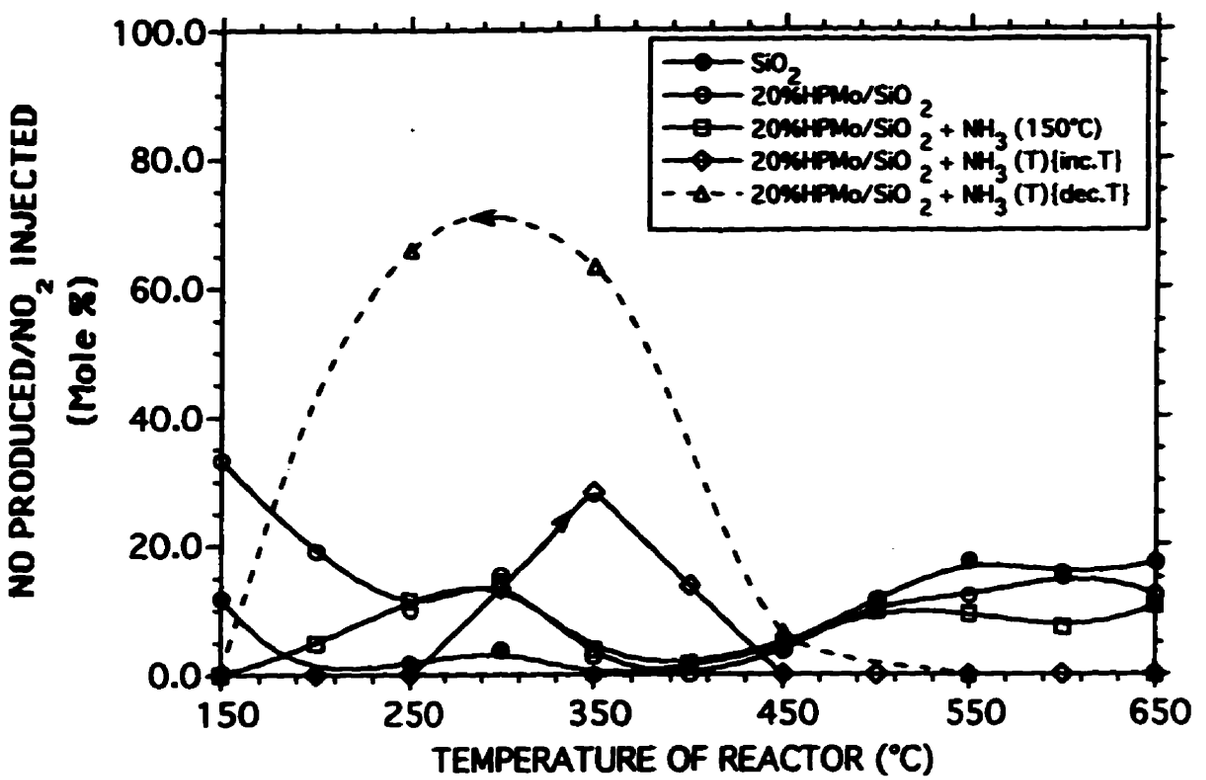

Fig. 8.5 Amount of NO found in the effluent from single-pulse experiments at a variety of temperatures (SPE-VT), from NO_2 on SiO_2; and NO_2 on 20.0%HPMo/SiO_2 pre-exposed to ammonia at 150°C only, or at each selected temperature (T). The same catalytic aliquot was kept in the reactor for the series of temperatures. Mass in reactor = 50 mg; Ammonia injected before pulse = 10 mL; Pulse size = 17 μmoles NO_2; Helium flow = 20 mL/min.

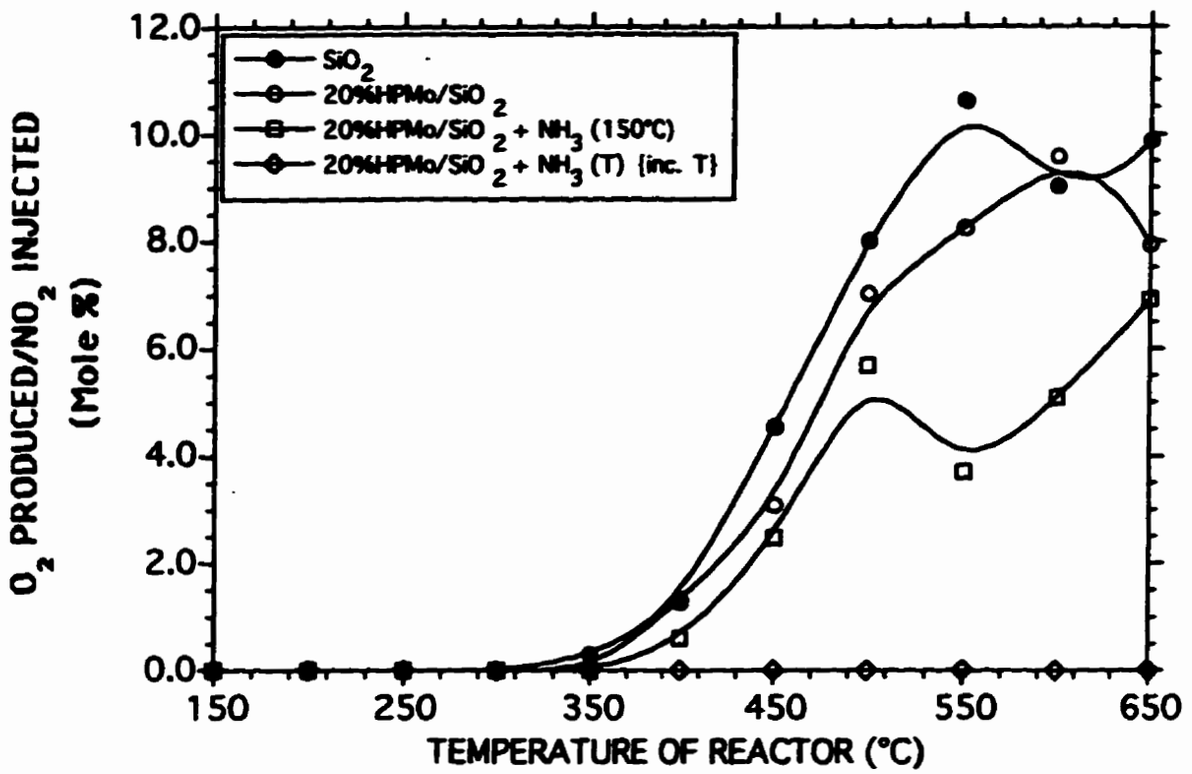

Fig. 8.6 Amount of O_2 found in the effluent from single-pulse experiments at a variety of temperatures (SPE-VT), from NO_2 on SiO_2; and NO_2 on 20.0%HPMo/SiO_2 pre-exposed to ammonia at 150°C only, or at each selected temperature (T). The same catalytic aliquot was kept in the reactor for the series of temperatures. Mass in reactor = 50 mg; Ammonia injected before pulse = 10 mL; Pulse size = 17 μmoles NO_2; Helium flow = 20 mL/min.

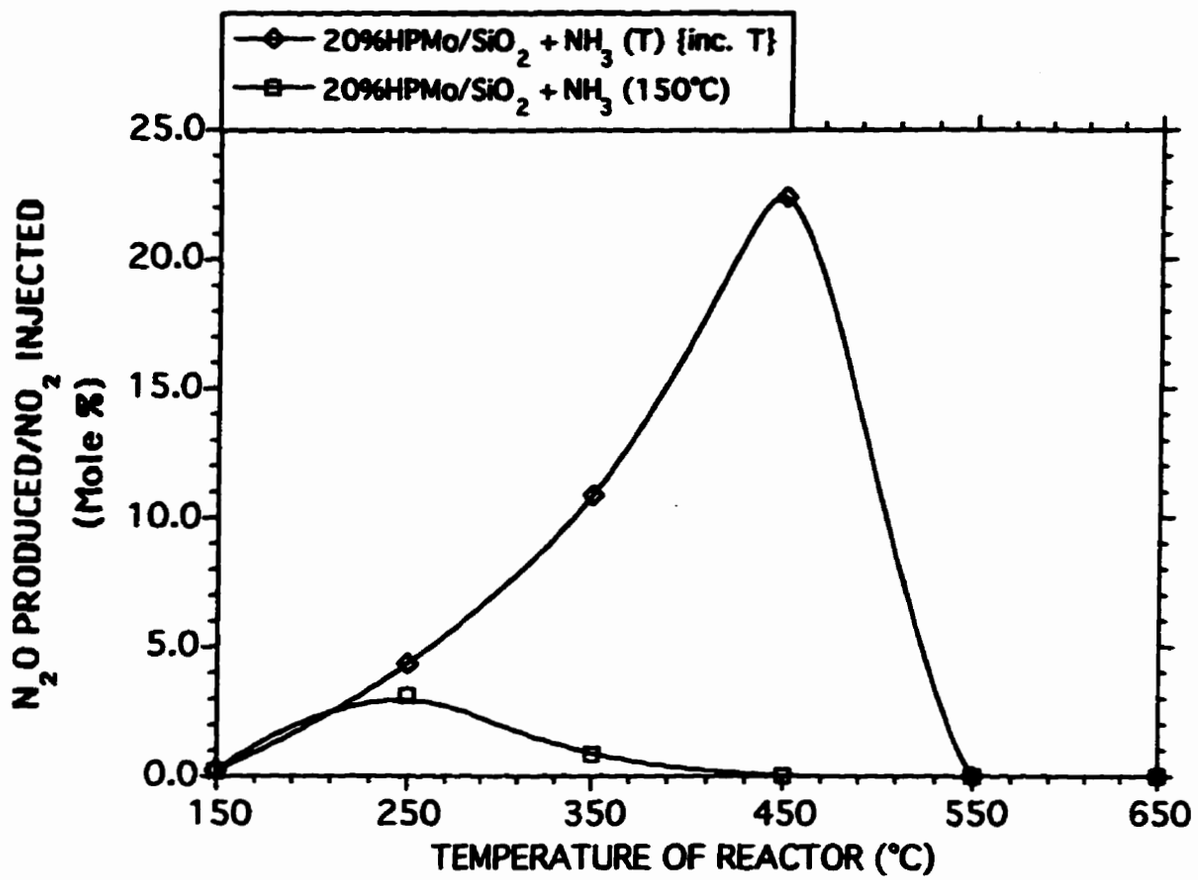

Fig. 8.7 Amount of N_2O found in the effluent from single-pulse experiments at a variety of temperatures (SPE-VT), from NO_2 on SiO_2; and NO_2 on 20.0%HPMo/SiO_2 pre-exposed to ammonia at 150°C only, or at each selected temperature (T). The same catalytic aliquot was kept in the reactor for the series of temperatures. Mass in reactor = 50 mg; Ammonia injected before pulse = 10 mL; Pulse size = 17 μmoles NO_2; Helium flow = 20 mL/min.

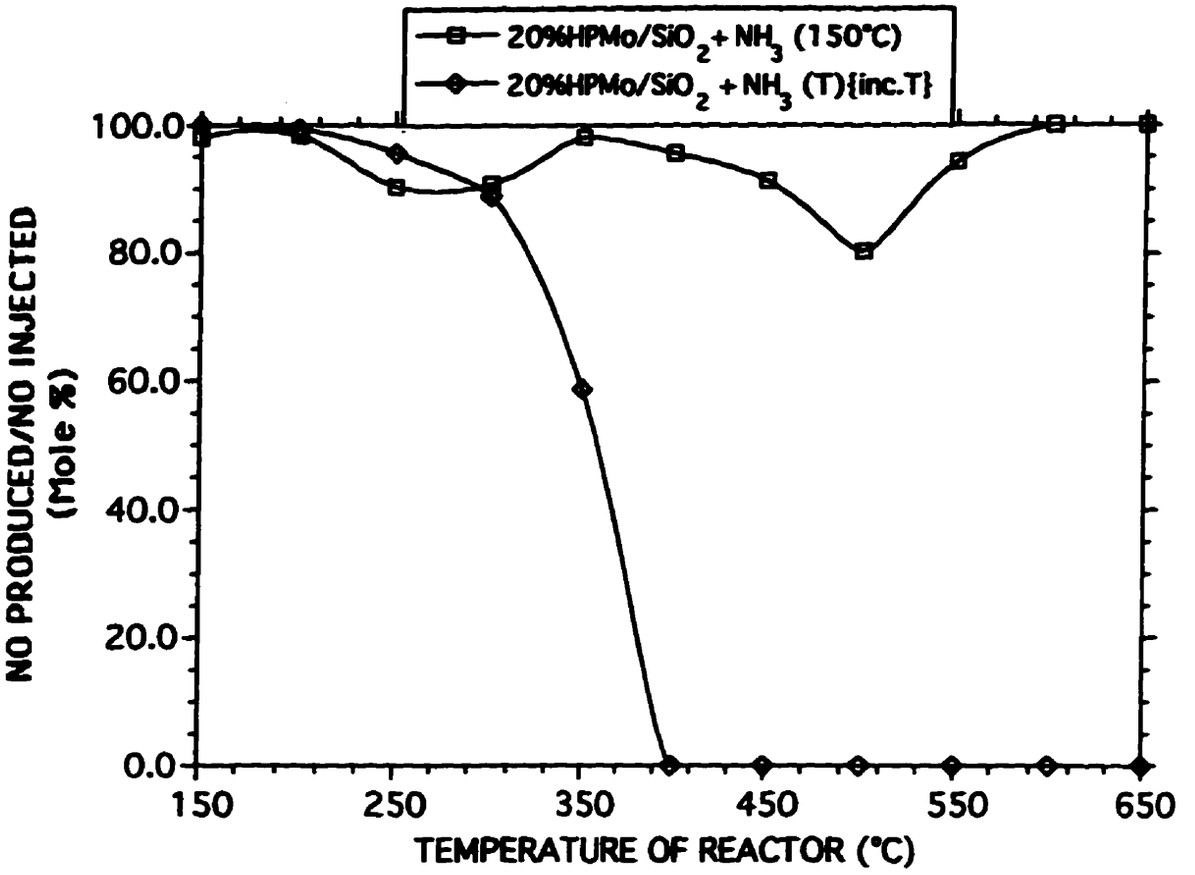

Fig. 8.8 Amount of NO in the effluent from single-pulse experiments at a variety of temperatures (SPE-VT), from NO on 20.0%HPMo/SiO_2 samples pre-exposed to ammonia at 150°C only, or at each selected temperature (T). The same catalytic aliquot was kept in the reactor for the series of temperatures. Mass in reactor = 50 mg; Ammonia injected before pulse = 10 mL; Pulse size = 10 μmoles NO; Helium flow = 20 mL/min.

Exposure of 20.0%HPMo/SiO_2 to NO after saturation with NH_3 at 150°C generally leads to smaller selectivities to N_2 than observed with NO_2 (Fig.8.9). However, with the samples saturated with NH_3 and exposed to NO at the same temperatures, the selectivities to N_2 increase to a maximum of approximately 60% at 450°C followed by a small decrease with further increase in temperature in a manner reminiscent of the behaviour with NO_2 (Fig.8.4). The selectivity to N_2O obtained with the catalyst saturated with NH_3 at 150°C also passes through a maximum at 400°C, however less nitrous oxide is produced than when NO_2 is injected on the catalyst (Fig.8.10).

In view of the absence of N_2O in the effluent at temperatures of 550°C and higher, a separate experiment in which N_2O was passed over the catalyst was carried out at 650°C (Table 8.1).

Selectivities to N_2 of approximately 56% were obtained for the first pulse, but these values diminished significantly for subsequent pulses. No other products were found in the effluent.

The TPD pattern for pure HPMo (Fig.8.11A) consists only in the desorption of water molecules. A relatively large peak desorbs at 50-300°C and the smaller peak desorbs at 440°C.

The TPD pattern for silica (SiO_2) (Fig.8.11B) also consists only in the desorption of small quantities of water molecules. The TPD displays two peaks at 90-250°C and 250-650°C, respectively.

The TPD pattern of 20.0%HPMo/SiO_2 (Fig.8.12A) displays two peaks resulting from sorbed water desorbing at 175°C and 250-500°C, respectively. A third peak at 525°C is due to the desorption of CO_2 (see Chapter IX). After exposure to ammonia (Fig.8.12B) the peaks attributed to water desorption are no longer evident. Small peaks due to the desorption of water and ammonia are seen from 525 to 650°C. The peak due to CO_2 appears at a slightly higher temperature. The TPD pattern of a sample of supported acid exposed first to ammonia and then to NO_2 at 150°C (Fig.8.12C) shows interesting features. Small quantities of NO_2 were sorbed on the supported catalyst but completely desorbed at 100°C. Vanishingly small quantities of water desorbed from 400 to 650°C. The peak due to CO_2 desorption has almost vanished as well as the peak for ammonia. However, a separate aliquot of the same sample exposed to NO at 150 and 450°C, Fig.8.12D and 8.12E, respectively, does not affect the CO_2 peak.

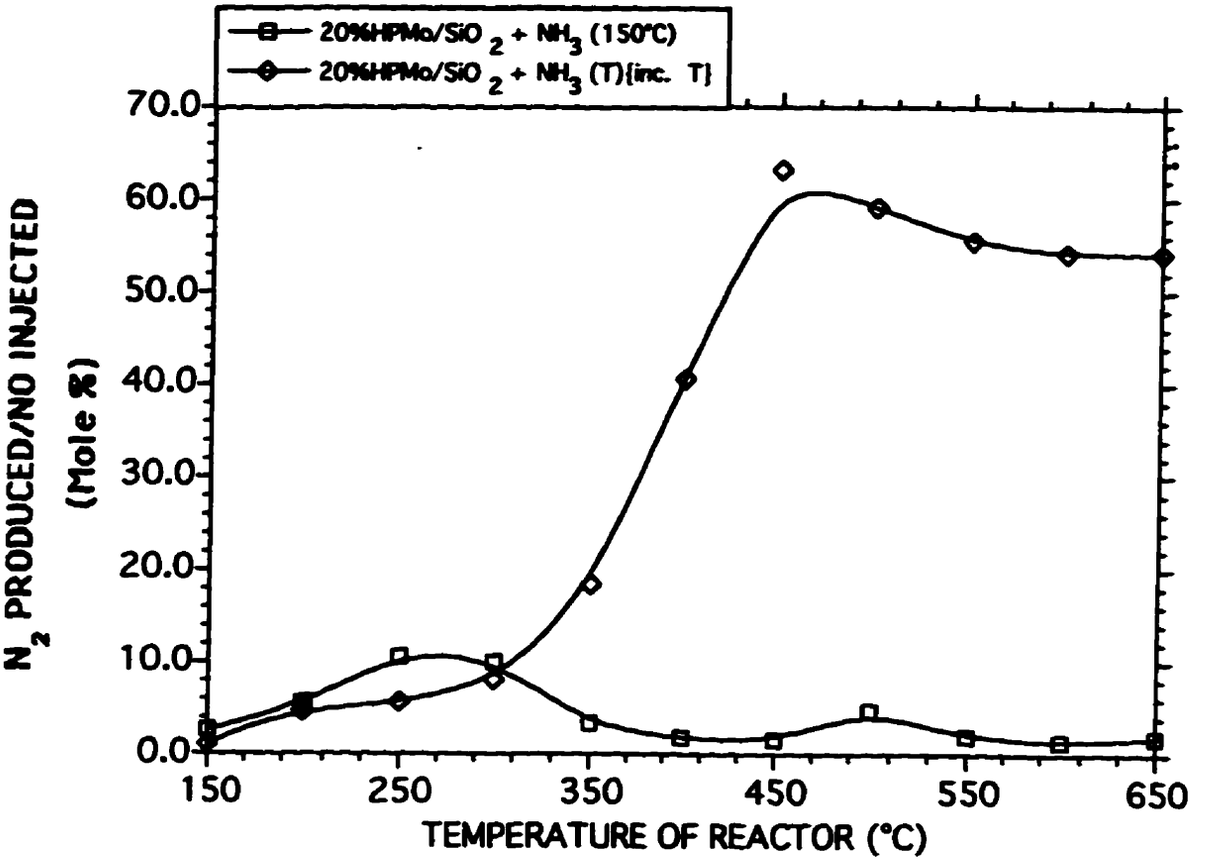

Fig. 8.9 Amount of N_2 in the effluent from single-pulse experiments at a variety of temperatures (SPE-VT), from NO on 20.0%HPMo/SiO_2 samples pre-exposed to ammonia at 150°C only, or at each selected temperature (T). The same catalytic aliquot was kept in the reactor for the series of temperatures. Mass in reactor = 50 mg; Ammonia injected before pulse = 10 mL; Pulse size = 10 μmoles NO; Helium flow = 20 mL/min.

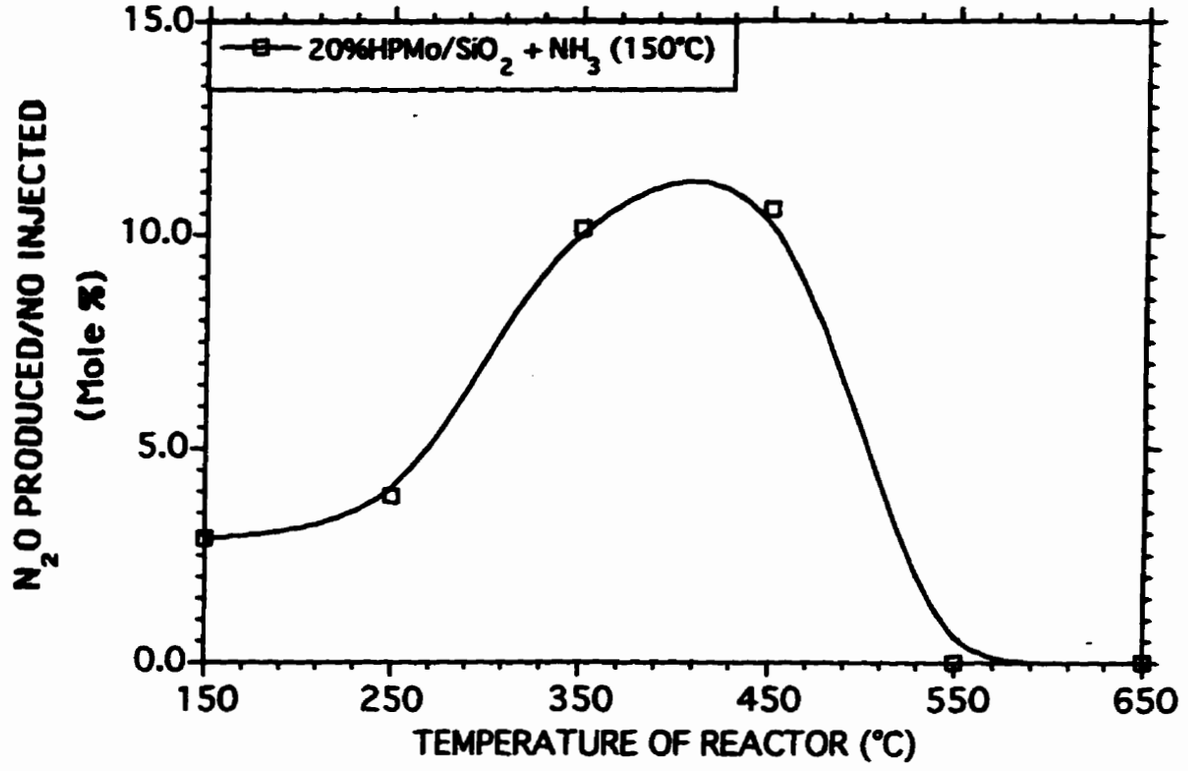

Fig. 8.10 Amount of N_2O in the effluent from single-pulse experiments at a variety of temperatures (SPE-VT), from NO on 20.0%HPMo/SiO_2 samples pre-exposed to ammonia at 150°C only, or at each selected temperature (T). The same catalytic aliquot was kept in the reactor for the series of temperatures. Mass in reactor = 50 mg; Ammonia injected before pulse = 10 mL; Pulse size = 10 μmoles NO; Helium flow = 20 mL/min.

TABLE 8.1

REDUCTION OF N_2O ON 20%HPMo/SiO_2 PRE-EXPOSED TO AMMONIA[a]

Pulse Number[b]	N_2 Selectivity (%)[c]
1	56.1
2	40.1
3	33.5

a 50 mg 20.0%HPMo/SiO_2 loaded into reactor and exposed to 10 mL (NTP) NH_3 at 150°C, then heated and held at 650°C.
b One pulse=4.1 μmoles N_2O.
c percent N_2 per N_2O injected.

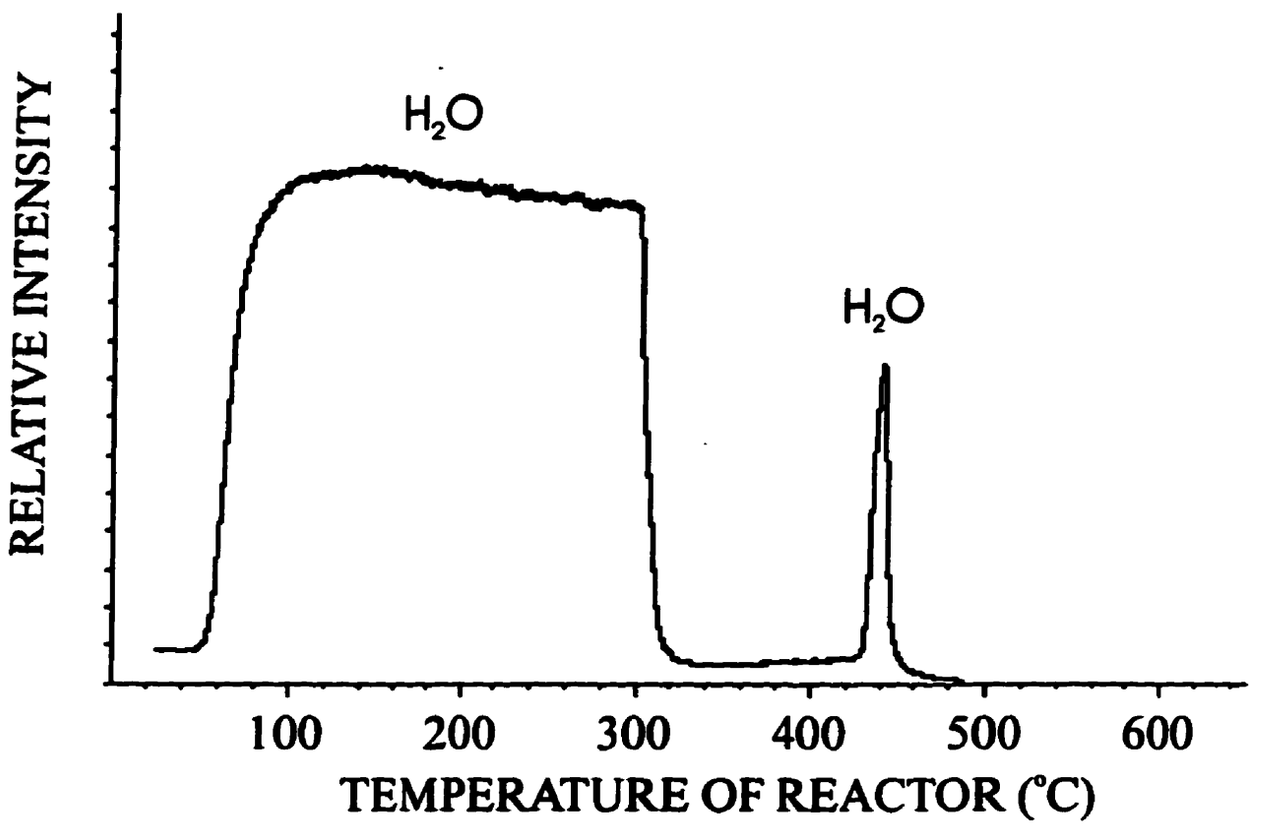

Fig. 8.11A Temperature programmed desorption of pure HPMo. Mass in reactor = 50 mg; Helium flow = 20 mL/min.

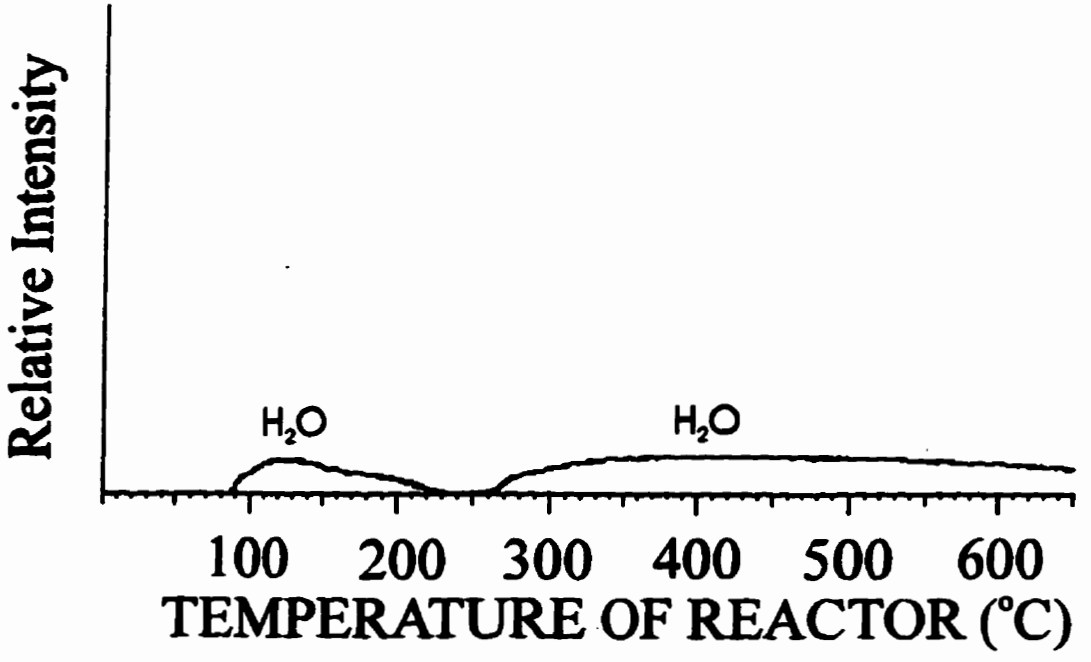

Fig. 8.11B Temperature programmed desorption of pure SiO_2. Mass in reactor = 50 mg; Helium flow = 20 mL/min.

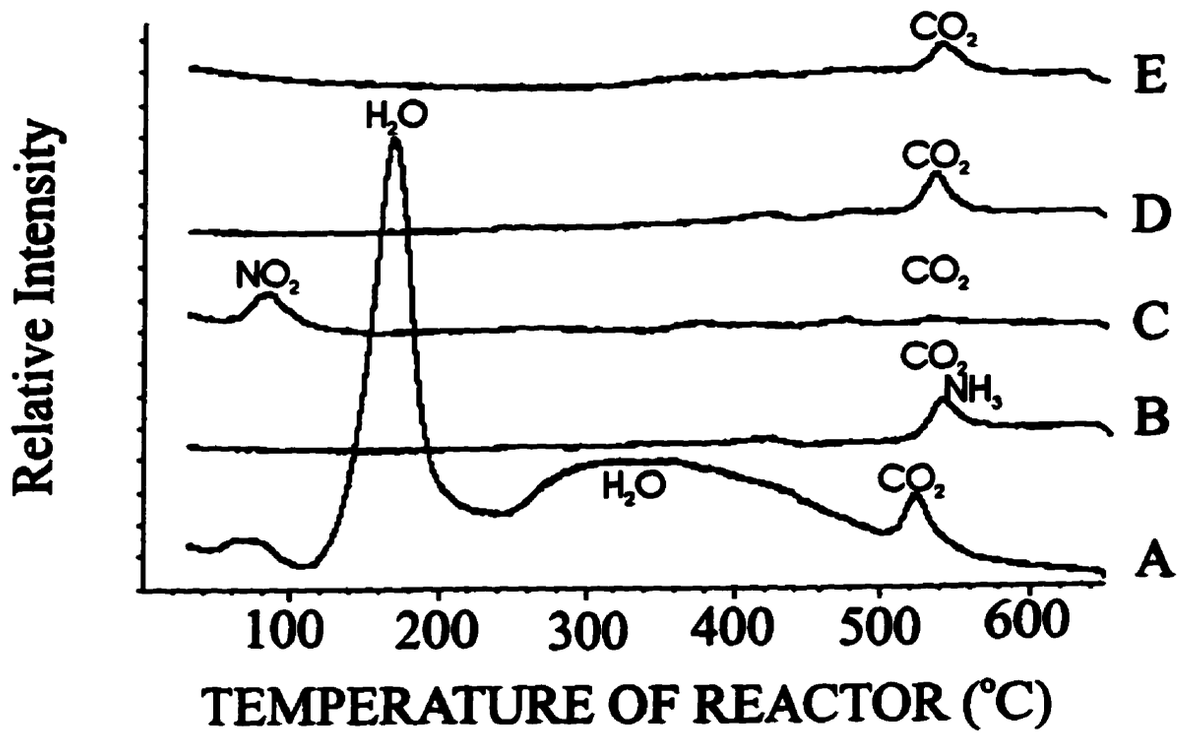

Fig. 8.12 Temperature programmed desorption of A) 20.0%HPMo/SiO_2 as prepared, B) 20.0%HPMo/SiO_2 pre-exposed to ammonia at 150°C, C) 20.0%HPMo/SiO_2 as B then exposed to pure NO_2 at 150°C, D) 20.0%HPMo/SiO_2 as B then exposed to pure NO at 150°C, E) 20.0%HPMo/SiO_2 as B then exposed to pure NO at 450°C. Mass in reactor = 50 mg; Ammonia injected = 10 mL; Helium flow = 20 mL/min.

B. Discussion

HPMo/SiO_2

From the single-pulse experiments at a variety of temperatures, it is clear that NO_2 is predominantly reduced to NO when passed over HPMo/SiO_2. The selectivity to N_2 for this catalyst is low. However, the N_2, NO, and O_2 selectivities are within the same range as with those found for HPW/SiO_2 (see Chapter VII). Moreover, the selectivities to N_2 and NO are larger for the 20.0%HPMo/SiO_2 catalyst than with the support alone, while that to O_2 with the former is lower than with the latter.

The SiO_2-supported HPMo has a somewhat higher activity than that of the bulk acid (Chapter III). No nitrogen was detected when the bulk acids were exposed to pulses of NO_2 at 150°C and 300°C.

HPMo/SiO_2 PRE-EXPOSED TO NH_3

Exposure of the supported HPMo to ammonia prior to the introduction of NO or NO_2 increases the selectivity to N_2 while decreasing that to NO. The higher surface area of the supported catalyst would be expected to facilitate the conversion of NOx but may also play a role in altering the selectivities. The results found for HPMo/SiO_2 are similar to those found with HPW/SiO_2 pre-exposed to ammonia (Chapter VII). Furthermore, the results on the reduction of NO on the silica-supported HPMo, with and without the presence of ammonia, also compare to those found by Mochida *et al.* (Ref.8.1).

Exposure of the catalyst to pulses of ammonia (at each temperature) restores the activity for the reduction of NOx. However, up to 550°C, significant quantities of N_2O are produced from both NO and NO_2. At temperatures above 550°C, little or no NO or N_2O are found in the gas phase. The results show the total reduction to N_2 (approximately 100% selectivity to N_2).

Since decomposition of the Keggin units in bulk HPMo is initiated at these high temperatures (see TPD results), at least a portion of the species existing at these temperatures will be decomposition products. However previously published data suggests that the introduction of a silica support enhances the thermal stability of HPMo (Ref.8.2).

Since MoO_3 is expected to be one of the decomposition products from HPMo, it is relevant to note that Mo atoms supported on alumina have been shown to promote the sorption of NO molecules (Ref.8.3).

HPMo (Chapter III) and HPMo/SiO_2 sorb vanishingly small quantities of NO or NO_2. Since semiempirical quantum mechanical (EXH) calculations have predicted that solid heteropoly acids containing tungsten as their peripheral metal atom should have a higher acidity than those with molybdenum as their peripheral metal atom (Ref.8.4), it is believed that the

acidic strength of HPMo is not sufficiently high enough for the sorption of NOx (see Chapter III).

C. Conclusion

The selectivity to N_2 and the conversion of NO_2 are slightly increased on introduction of a SiO_2 support with HPMo, compaired to the bulk HPMo. However, after saturation with gaseous NH_3, both the conversion of NOx and its reduction to N_2 are considerably increased. Furthermore, at high temperatures (>550°C), NO, NO_2, and N_2O are essentially completely reduced to N_2. At this time, the extent of the participation of the anion decomposition products, at these high temperatures, is not known.

REFERENCES

8.1 Mochida, I., Nakashima, T., and Fujitsu, H. *Bull.Chem.Soc.Jpn.*, **57**, 1449 (1984).

8.2 Kasztelan, S., Payen, E., and Moffat., J.B. *J.Catal.*, **112**, 320 (1988).

8.3 Valyon, J., and Hall, W.K. *J.Catal.*, **84**, 216 (1983).

8.4 Moffat, J.B., *J.Mol.Catal.*, **26**, 385 (1984).

CHAPTER IX

SORPTION OF CARBON DIOXIDE AND CONVERSION OF CARBON MONOXIDE TO CARBON DIOXIDE ON SUPPORTED AND UNSUPPORTED 12-TUNGSTOPHOSPHORIC AND 12-MOLYBDOPHOSPHORIC ACIDS

A. Results

SORPTION OF CARBON DIOXIDE

Temperature-programmed desorption of a sample of HPW, not previously intentionally exposed to CO_2 (Fig.9.1.1A), shows the characteristic water peaks at 100-300 and 400-500°C. In addition, a peak of desorbed CO_2 emerges at 580°C suggesting that strongly held CO_2 exists on the solid at lower temperatures. After saturation of HPW with CO_2, at 30°C, the water peak again appears but the CO_2 peak, at 580°C, has now intensified showing that CO_2 is readily sorbed (Fig.9.1.1B). After heating of HPW at 350°C, followed by exposure to CO_2, the lower temperature water peak has disappeared, while the higher temperature water peak and the CO_2 peak remain, but the intensity of the latter appears to have diminished somewhat (Fig.9.1.1C). However, after heating of HPW to 500°C followed by exposure to CO_2 only the peak due to CO_2 remains on the TPD (Fig.9.1.1D). After saturation of HPW with CO_2 at 30°C, followed by heating to 650°C, the sample was cooled to room temperature in a flow of dry helium and re-exposed to CO_2 at 30°C, and a TPD measurement was again carried out (Fig.9.1.1E). No water nor CO_2 peaks can be seen after the second TPD.

In contrast, HPMo, not previously intentionally exposed to CO_2 (Fig.9.1.2A), does not show any desorption of CO_2. Exposure of HPMo to a continuous flow of pure CO_2 (Fig.9.1.2B), at 30°C, shows the desorption of CO_2 with a maximum at 360°C. However, the TPD of 20.0%HPMo/SiO_2 (evacuated) (Fig.9.1.2C) shows that small quantities of CO_2 desorb between 200 and 650°C. After exposure to CO_2 at 30°C, the TPD of 20%HPMo/SiO_2 (Fig.9.1.2D) shows quantities of CO_2 desorbing between 200 and 650°C, with a maximum at 520°C.

To provide information on the role, if any, of the protons, the sodium salt of HPW (NaPW) was exposed to CO_2 (Fig.9.2). The lower temperature water peak is evident on the TPD scan, but the higher temperature water peak due to the associative desorption of water is absent, as would be expected for stoichiometric salts (Fig.9.2A). A small peak due to CO_2 emerges at 580°C. After exposure to CO_2 at 30°C, the TPD is virtually identical to that obtained prior to the exposure to CO_2 (Fig.9.2B).

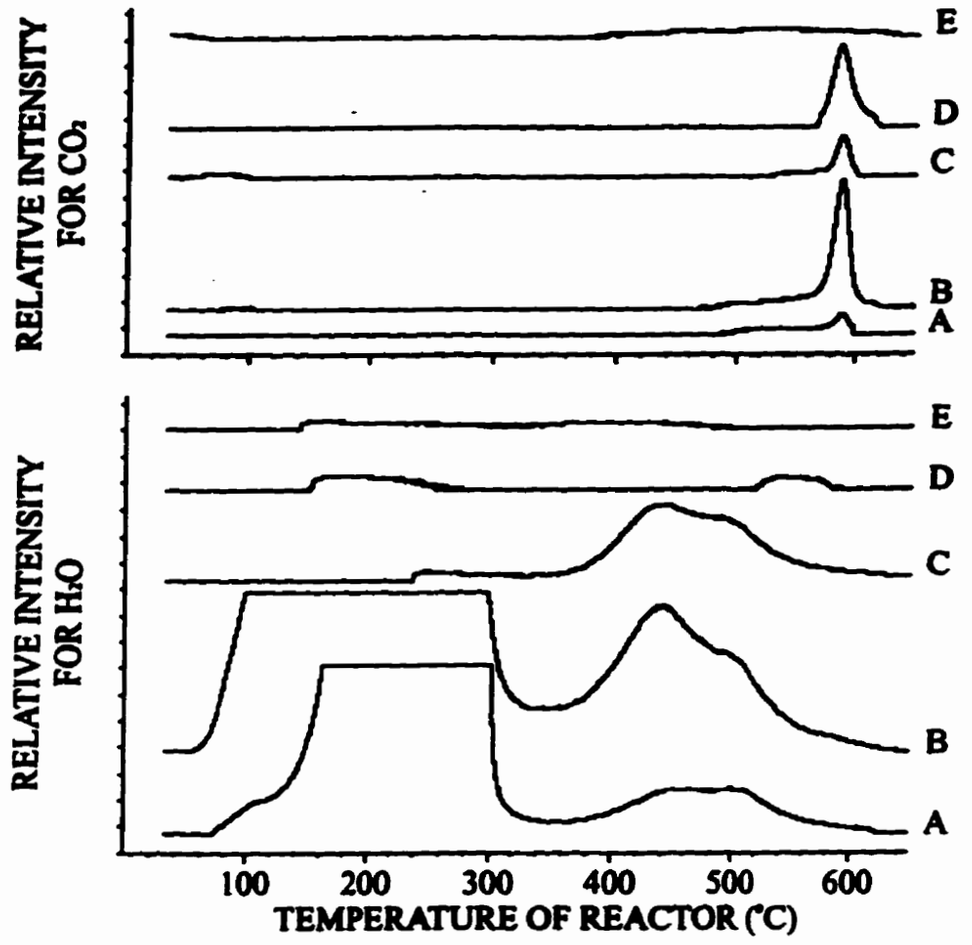

Fig.9.1.1 Water and CO_2 TPD of A) HPW evacuated at 25°C; B) of (A) exposed to pure CO_2 at 30°C; C) of (A) pretreated at 350°C and exposed to pure CO_2 at 30°C; D) of (A) pretreated at 500°C and exposed to pure CO_2 at 30°C; E) of (A) pretreated at 650°C and exposed to pure CO_2 at 30°C. All samples were exposed to pure CO_2 for 30 min before purging with helium at 30°C.

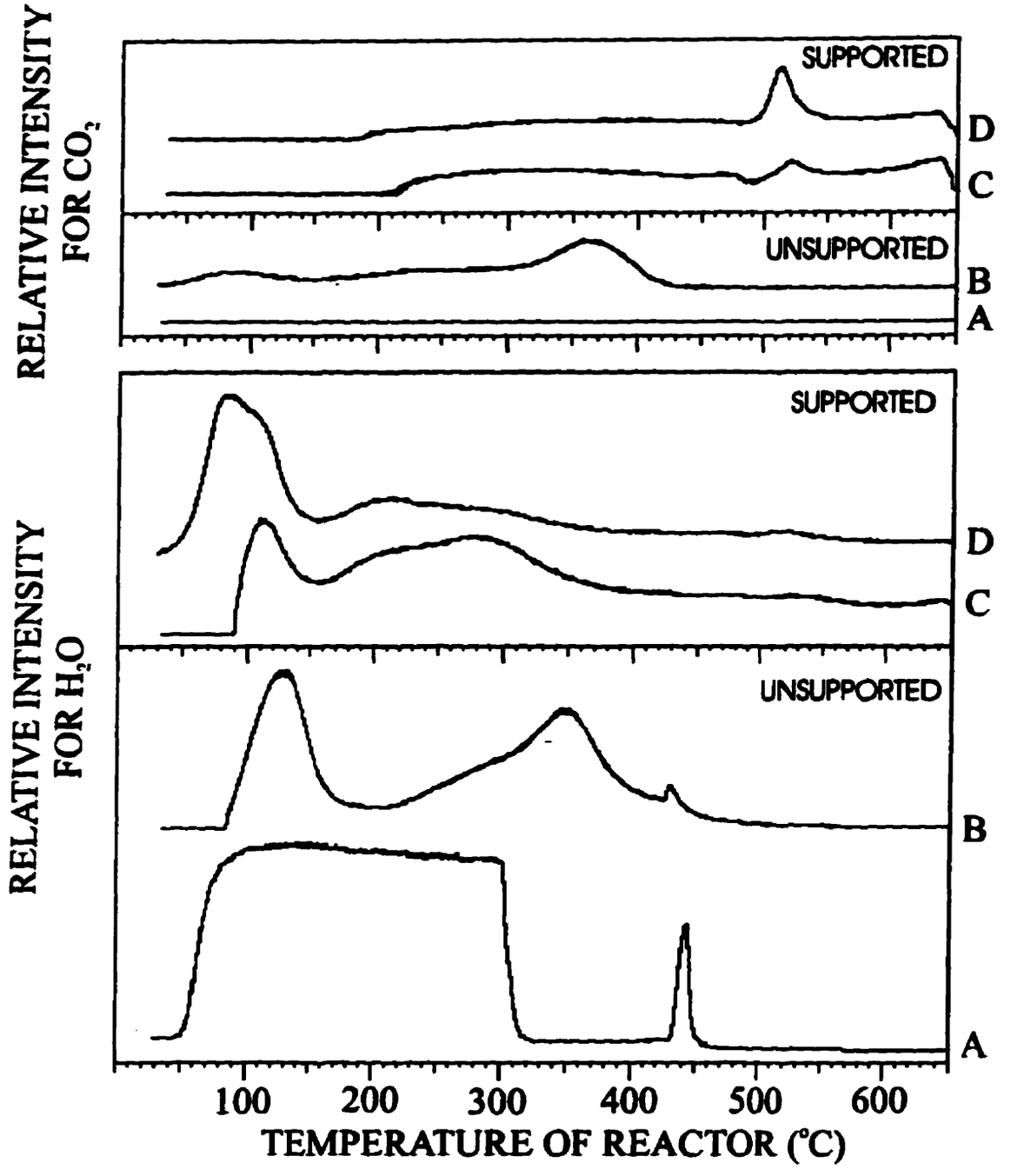

Fig.9.1.2 Water and CO_2 TPD of A) HPMo; B) of (A) exposed to pure CO_2 at 30°C; C) 20.0%HPMo/SiO_2 evacuated at 30°C; D) of (C) exposed to pure CO_2 at 30°C. All samples were exposed to pure CO_2 for 15 hours before purging with helium at 30°C.

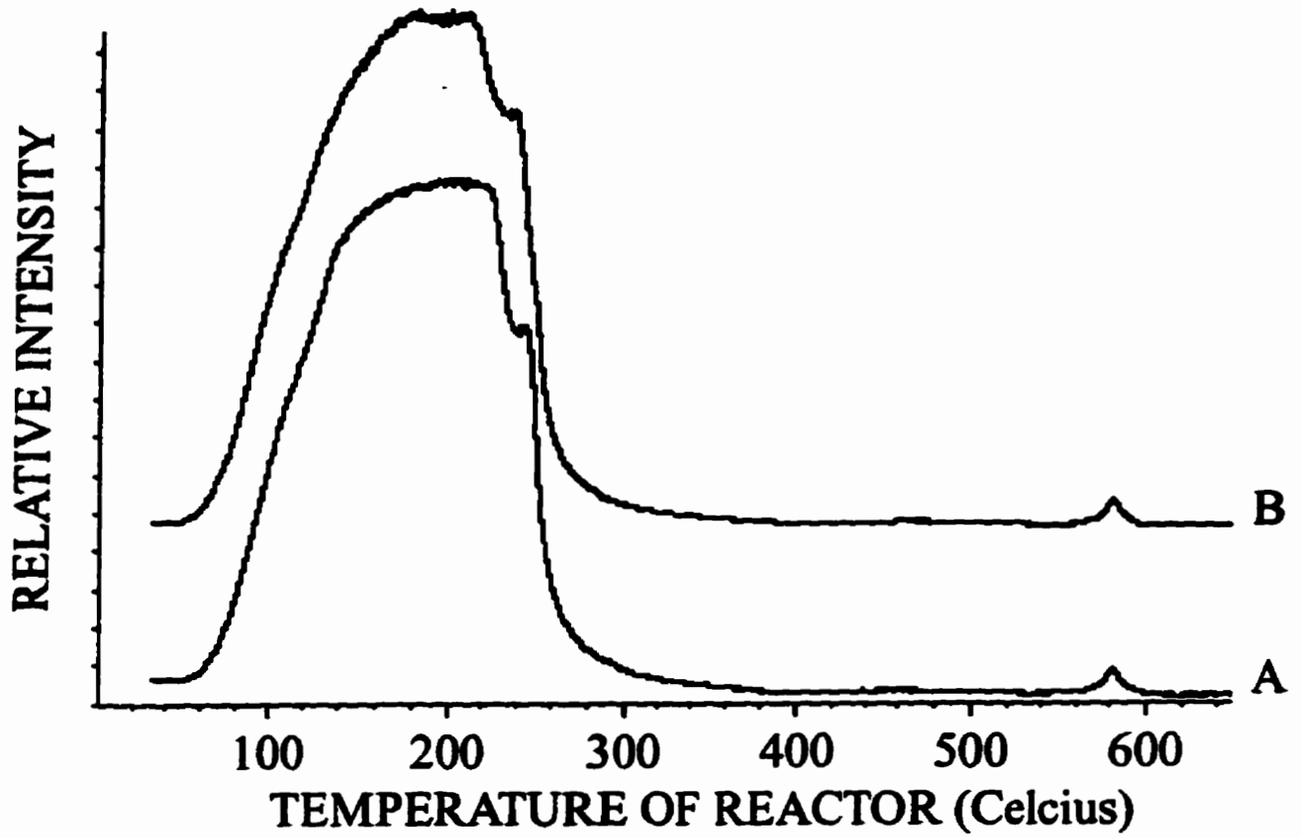

Fig.9.2 Total Ion-TPD of A) NaPW evacuated at 25°C; B) of (A) after exposure to pure CO_2 at 30°C for 22 hours.

To investigate the effect of loading of HPW on a high area support, temperature-programmed desorption experiments were performed on HPW loaded on SiO_2, as well as on the pure support after saturation with CO_2 at 300°C (Fig.9.3A). Regardless of the loading of HPW/SiO_2, approximately 0.3 CO_2/KU were desorbed from the samples. The amount of CO_2 detected increased slightly to 0.5 CO_2/KU with the bulk HPW.

In contrast, the results for the sorption of CO_2 on HPMo, at 30°C, and supported HPMo/SiO_2 (Fig.9.3B), show marked differences from those obtained with HPW and HPW/SiO_2. Generally, samples of HPMo/SiO_2 were found to sorb more CO_2 at room temperature. A maximum of 1.4 CO_2/KU was sorbed by the 9.0%HPMo/SiO_2 sample under the present conditions.

The temperature at which the catalysts are held has, in general, little effect on the amount of CO_2 sorbed, for a given acid catalyst (Table 9.1). No temperature effect can be seen from the sorption of CO_2 on 23.1%HPW/SiO_2 sample. Approximately 0.35 CO_2/KU were sorbed on the 23.1%HPW/SiO_2. Measurements for the 9.0%HPMo/SiO_2 sample showed that up to 450°C, the sample sorbed approximately 1.3 CO_2/KU. However, at temperatures above 450°C, the quantity of CO_2 sorbed decreased to approximately 0.15 CO_2/KU.

The sorption of CO_2 by the supported or unsupported acids is influenced by the pretreatment temperature (Table 9.1). However, the temperature has a greater effect on HPW than on HPMo samples. With the 23.1%HPW/SiO_2 catalyst, held at room temperature, more CO_2 is sorbed with increasing of the pretreatment temperature, but with the 9.0%HPMo/SiO_2 sample, the quantity of CO_2 sorbed remains almost the same from 30 to 450°C.

For samples of unloaded HPW, pretreated in helium and held at 300°C, the quantity of CO_2 sorbed decreases with the mass of catalyst contained in the reactor (Fig.9.4). This effect is small for the 9.0%HPMo/SiO_2 sample held at 30°C.

The quantity of CO_2 taken up by HPW at 450°C, as measured from the desorption at 580°C, increases linearly with the concentration of CO_2 in the gas phase, suggesting a Henry's law behaviour (Fig.9.5).

The time required to achieve apparent equilibrium in the CO_2 sorption process is, as expected, dependent on the nature of the adsorbent. With pure HPW, the quantity of CO_2 sorbed increases by a factor of approximately four for exposure times from 10 to 60 minutes (0.02 to 0.11 CO_2/KU, respectively), and by a factor of 10 (0.23 CO_2/KU) after 20 hours. In contrast, the quantity of CO_2 taken up by supported HPMo changes relatively little as the exposure time increases from 10 min to 20 hours (approximately 1.4 CO_2/KU for all exposure times).

In view of the discoloration of the samples on exposure to CO_2, Raman spectroscopic investigations appeared to be appropriate. The Raman spectrum of HPW shows a series of

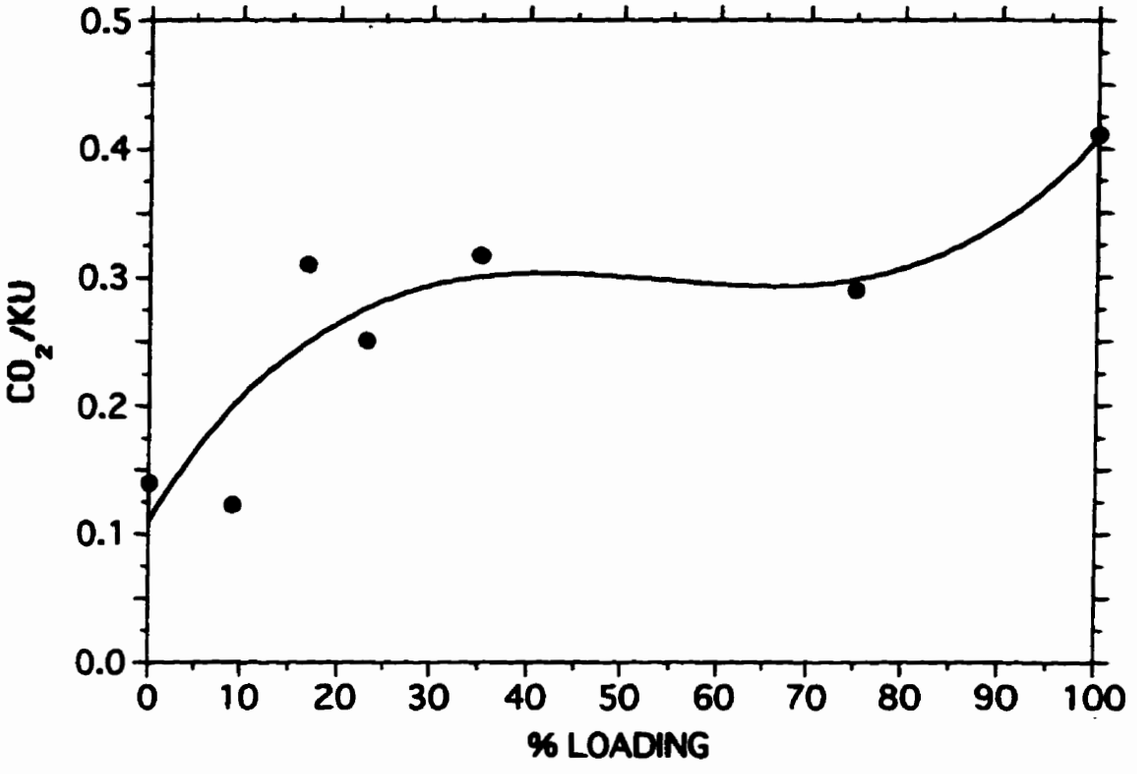

Fig.9.3A Loading effect on CO_2 sorbed (as measured by TPD) on samples of HPW loaded on SiO_2 (50 mg) pretreated in helium flow (40mL/min) and then exposed to pure CO_2 at 300°C for 22 hours. The aliquots were pretreated at the same CO_2 exposure temperature.

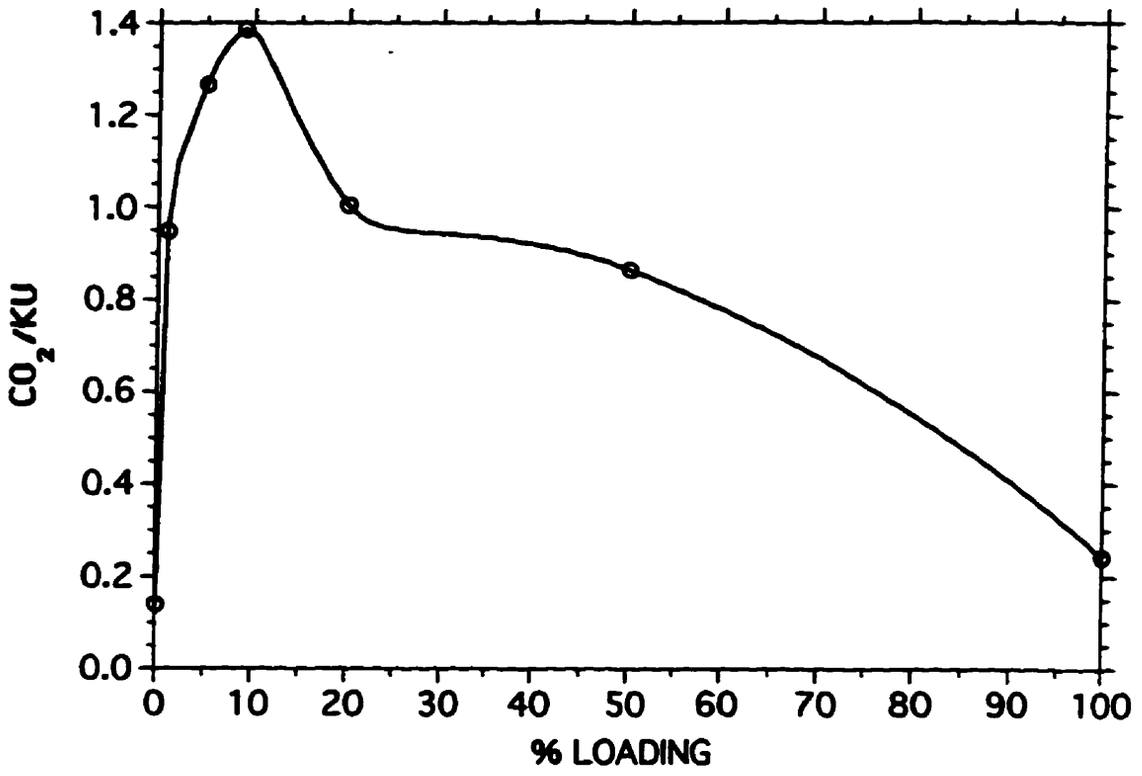

Fig.9.3B Loading effect on CO_2 sorbed (as measured by TPD) on samples of HPMo loaded on SiO_2 (50 mg) pretreated in helium flow (40 mL/min) and then exposed to pure CO_2 at 30°C for 22 hours. The aliquots were pretreated at the same CO_2 exposure temperature.

TABLE 9.1

EFFECT OF THE PRETREATMENT TEMPERATURE AND TEMPERATURE OF THE REACTOR ON THE SORPTION OF CO_2 ON HPW/SiO_2 AND HPMo/SiO_2

Temperature of Reactor (°C)	23.1%HPW/SiO_2[a] (CO_2/KU)	9.0%HPMo/SiO_2[a] (CO_2/KU)
30	-	1.39
150	0.22	-
250	0.21	-
300	0.25	1.30
450	0.34	0.17

Pretreatment Temperature (°C)	23.1%HPW/SiO_2[b] (CO_2/KU)	9.0%HPMo/SiO_2[b] (CO_2/KU)
30	-	1.39
300	0.11	-
450	0.54	1.37

a Same experimental conditions as in [b], but the samples were pretreated at the same temperature as the exposure to CO_2.

b Exposure of 50mg to CO_2 at 30°C for 22 hours after pretreatment in helium flow (40 mL/min).

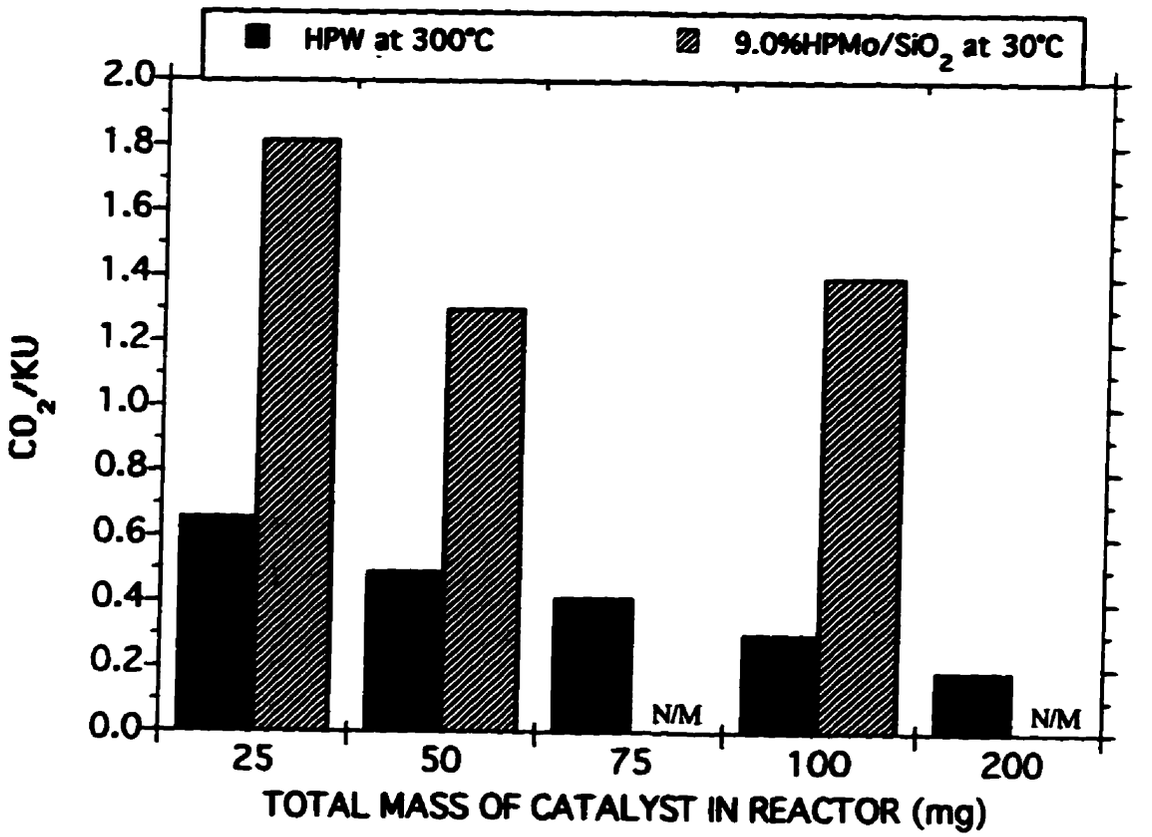

Fig.9.4 Effect of mass of catalyst inside the reactor on CO_2 sorbed (as measured by TPD) on samples of 9.0%HPMo/SiO_2 and HPW (50 mg) pretreated in helium flow (40 mL/min)and then exposed to pure CO_2 at 30°C and 300°C for 9.0%HPMo/SiO_2 and HPW samples, respectively, for 22 hours.

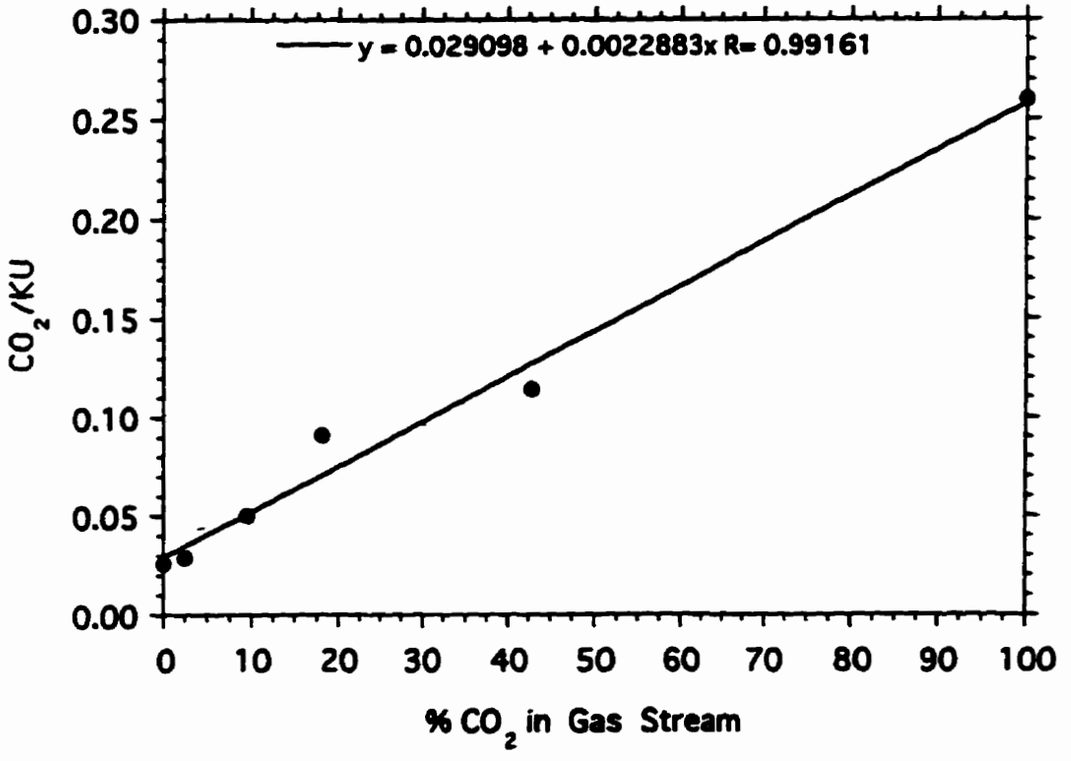

Fig.9.5 Effect of initial concentration of CO_2 in the gas stream on the sorption of CO_2 (as measured by TPD) on samples of HPW (50 mg) pretreated in helium flow (40 mL/min) and then exposed to pure CO_2 at 450°C for 30 min.

bands characteristic of the Keggin structure between 500 and 1200 cm^{-1} (Fig.9.6). The Raman spectra of the black particles, found after exposure to CO_2 at 450°C, show three new bands observed at 784, 1350, and 1590 cm^{-1}, respectively. The Raman line at 1590 cm^{-1} is characteristic of the degenerate E_{2g} mode of graphite, whereas the band at 1350 cm^{-1} is attributed to the A_{1g} mode of small crystallites in graphite (Refs.9.2a and 9.2b). After exposure to CO_2, the bands associated with the Keggin Units were less intense and slightly shifted to higher wavenumbers by about 10-20 cm^{-1}. With the particles which have not suffered discoloration, only that at 784 cm^{-1} was observed with additional shoulder bands.

For comparison, the Raman spectra of graphite and carbon black were measured (Fig.9.7).

CONVERSION OF CARBON MONOXIDE TO CARBON DIOXIDE

Temperature-programmed reaction (TPR) experiments, from 30 to 650°C, in which samples of HPW and HPW/SiO_2 are exposed to a flow of CO (8% in helium), without the addition of O_2, produce a CO_2 peak at 580°C.

The CO_2 produced from CO (without added O_2) at 600°C, on HPW/SiO_2, increased to a maximum at a loading of approximately 23% and decreases to a plateau for loadings from 35.0 to 100% (Fig.9.8). In contrast, that for HPMo/SiO_2 increases to a maximum at approximately 20% and then decreases continuously for further increase in the loading.

Exposure of NaPW to a flow of CO (without added O_2), while increasing the temperature, shows that no CO is sorbed and no CO_2 is produced.

The conversion of CO to CO_2 (without added O_2), on 50mg 23.1%HPW/SiO_2 and 20.0%HPMo/SiO_2, is relatively independent of the temperature of the reactor for 500°C and lower (Fig.9.9). At temperatures less than 300°C, no CO_2 is produced. Above 500°C, the selectivity to CO_2 increases sharply to 3.2% at 650°C with the HPMo/SiO_2 catalyst.

The conversion of CO to CO_2 (without added O_2) shows a disparate dependence on the mass of the catalyst contained in the reactor (Table 9.2). With 23.1%HPW/SiO_2 at 600°C, the dependence of the conversion on the mass is small and apparently nonsystematic, while with 20.0%HPMo/SiO_2, the conversion increases monotonously with the mass. It is of interest to note that the conversion per unit mass of catalyst, obtained with the latter catalyst, is virtually constant.

The conversion shows a trend with the initial concentration of CO in the reactant stream, which is similar to the effect of catalyst mass. With HPW/SiO_2 (Fig.9.10), the conversion passes through a maximum, while with HPMo/SiO_2 (Fig.9.11), a steady decrease is observed.

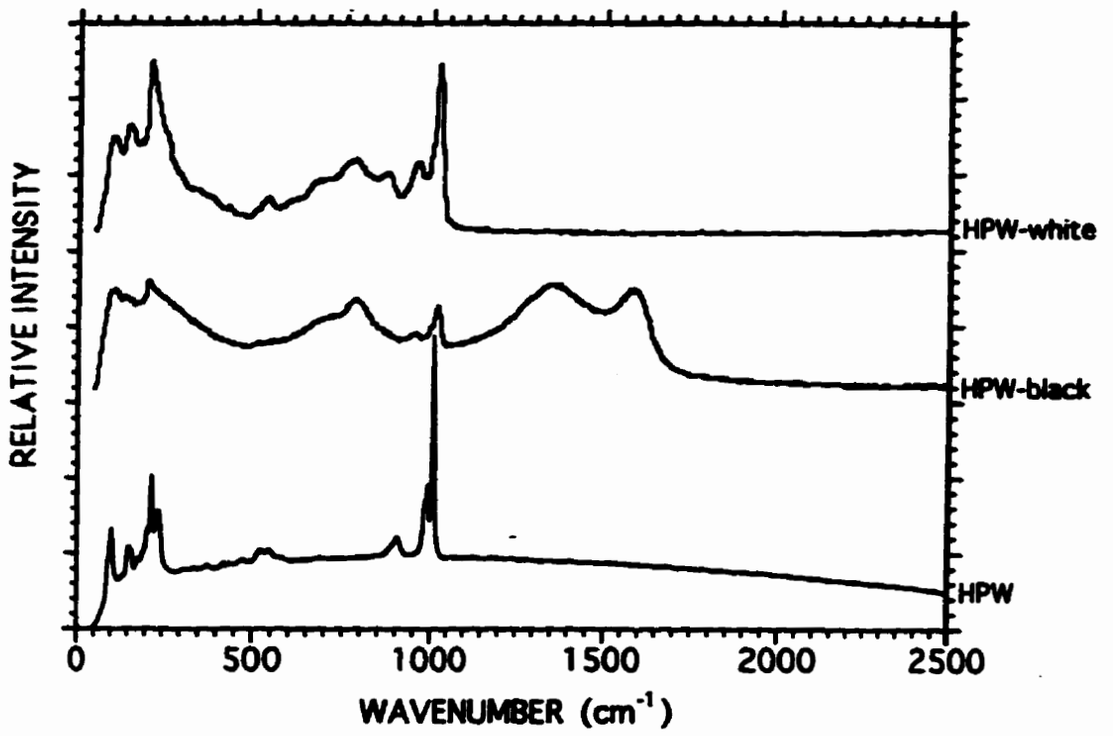

Fig.9.6 Raman spectra of HPW at 25°C; and of black and white particles from HPW exposed to pure CO_2 at 450°C for 22 hours.

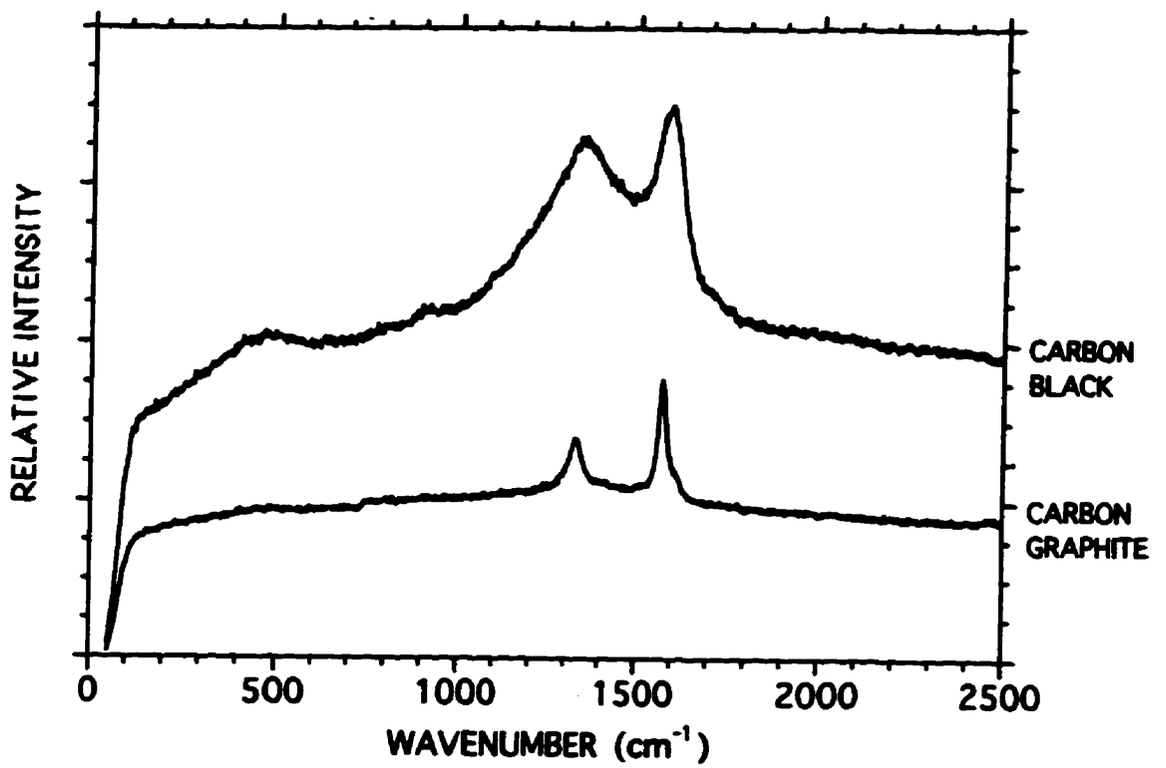

Fig.9.7 Raman spectra of carbon graphite and carbon black.

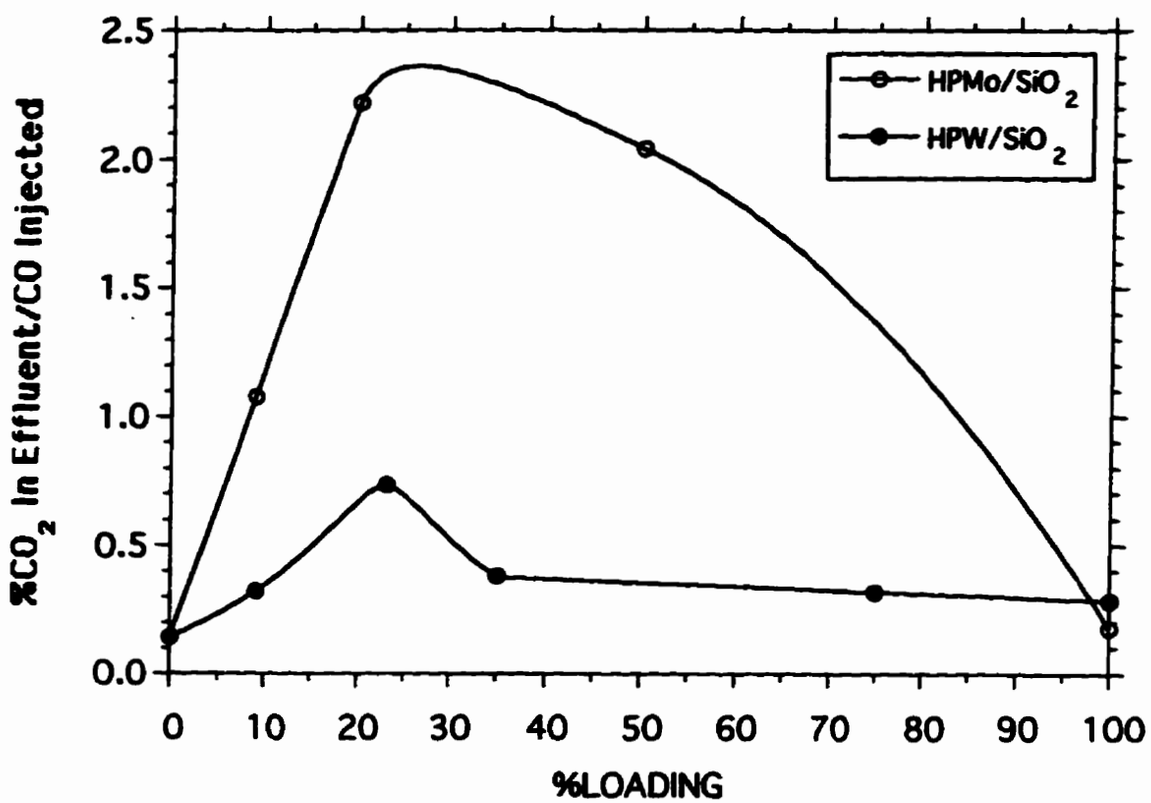

Fig.9.8 Loading effect on the oxidation of CO (8% CO/He at 40 mL/min) to CO_2 (as measured by ICR) on HPW and HPMo on SiO_2 samples (50 mg) pretreated and exposed to CO at 600°C. Integration time = 30 min.

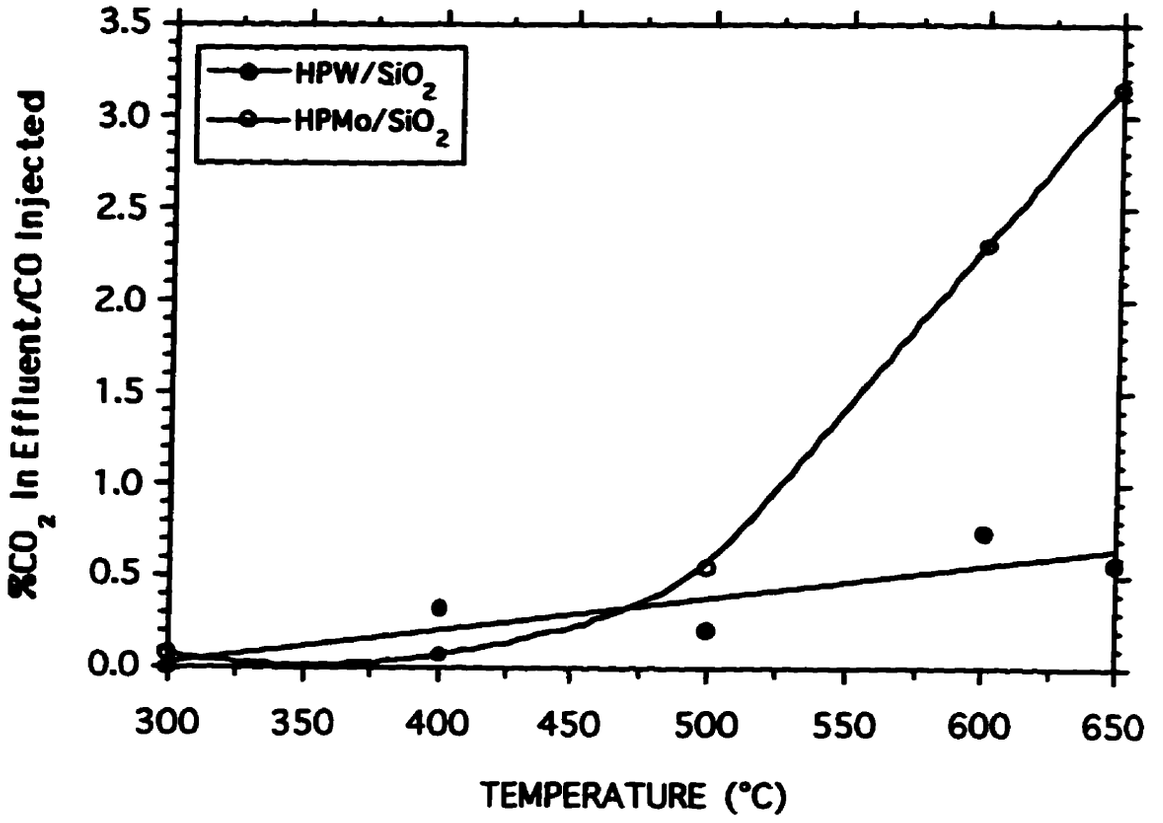

Fig.9.9 Reaction temperature effect on the oxidation of CO (8% CO/He at 40 mL/min)to CO_2 (as measured by ICR) on 23.1% HPW and 20.0% HPMo on SiO_2 samples (50 mg) pretreated and exposed to CO at the respective temperatures. Integration time = 30 min.

TABLE 9.2

EFFECT OF THE MASS OF CATALYST IN THE REACTOR ON THE CONVERSION[a] OF CO TO CO_2 AT 600°C

Mass of Catalyst (mg)	23.1%HPW/SiO_2 (%Conv.)	20.0%HPMo/SiO_2 (%Conv.)
25	0.31	1.23
50	0.75	2.30
100	0.44	3.39

a Conversion = %CO_2 produced/CO injected; Integration time = 30 min.

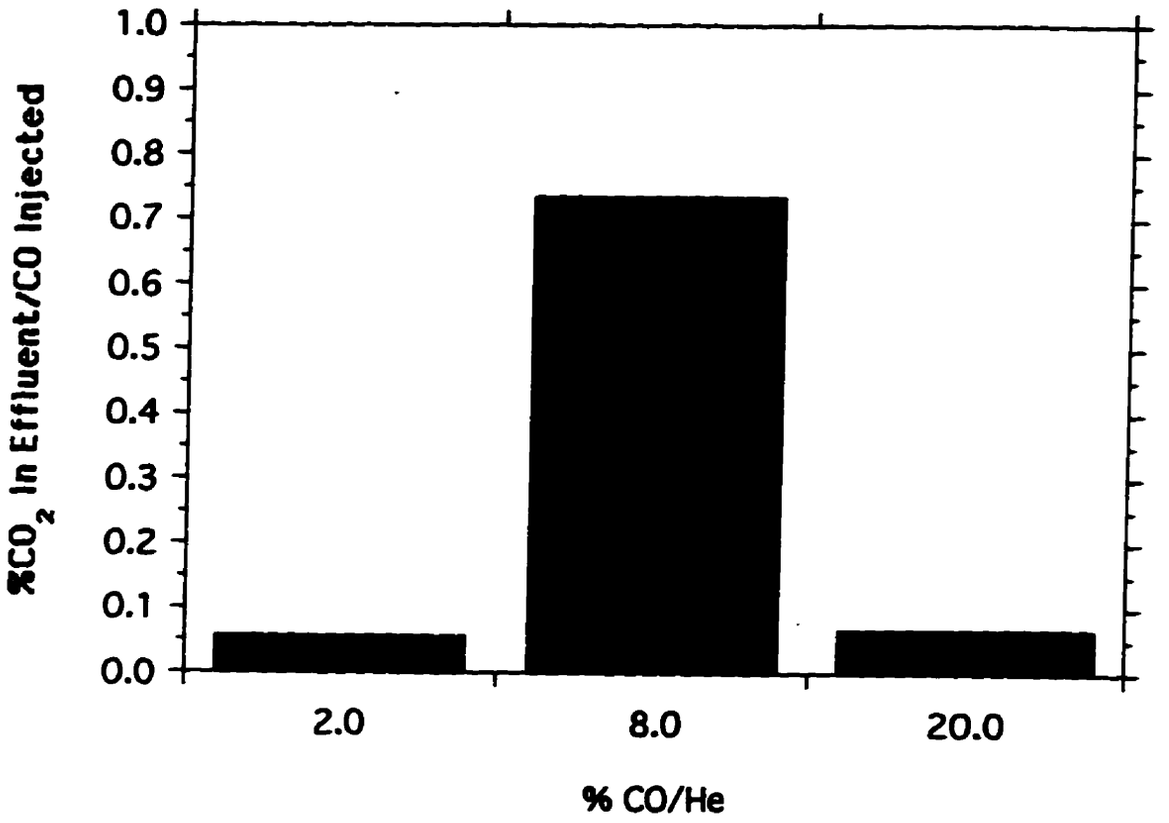

Fig.9.10 Effect of initial concentration of CO in stream on the oxidation of CO (40 mL/min) to CO_2 (as measured by ICR) on 23.1% HPW/SiO_2 (50 mg) pretreated and exposed to CO at 600°C. Integration time = 30 min.

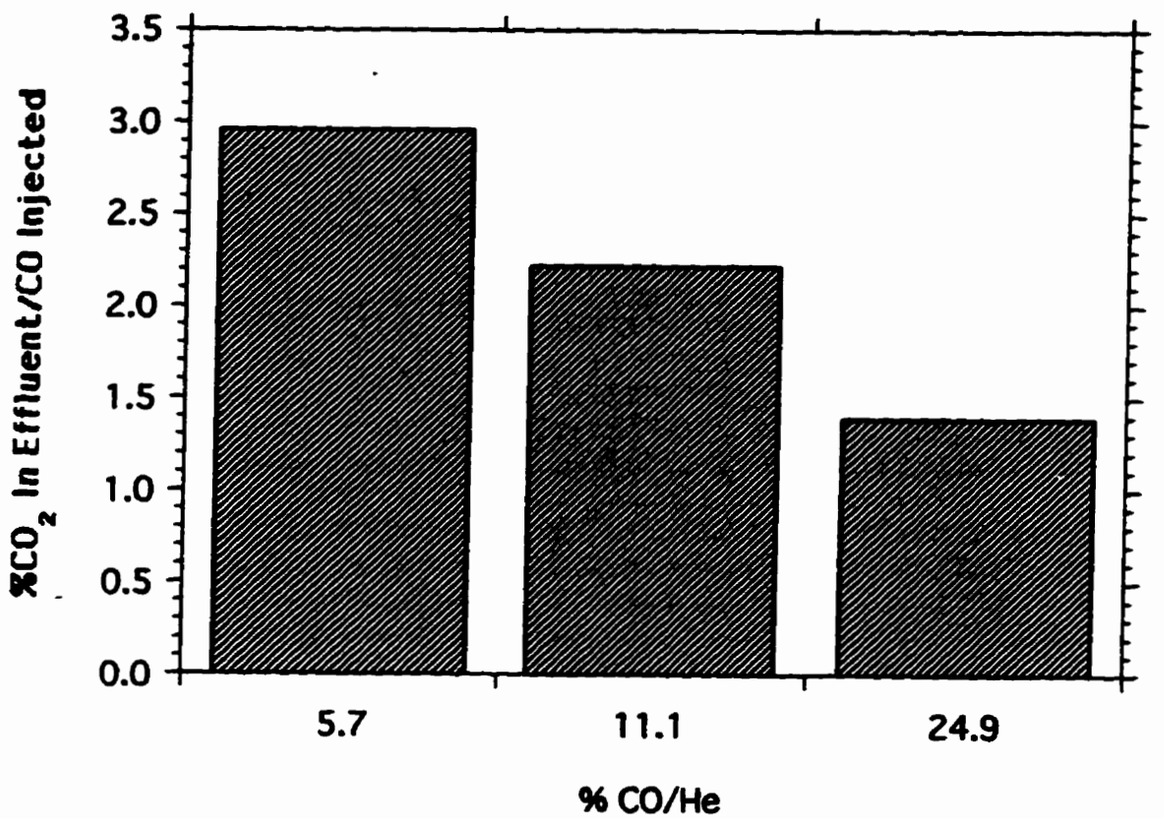

Fig.9.11 **Effect of initial concentration of CO in stream on the oxidation of CO (40 mL/min) to CO_2 (as measured by ICR) on 20.0% $HPMo/SiO_2$ samples (50 mg) pretreated and exposed to CO at 600°C. Integration time = 30 min.**

During the conversion of CO, a black deposit formed on the catalysts. The addition of relatively small quantities of O_2 to the gas stream alleviated the discoloration and improved the conversion by a factor of three (Fig.9.12).

To investigate the mechanism of the oxidation of CO to CO_2, in the absence of O_2, experiments were performed with $C^{18}O$. Table 9.3 shows the product compositions obtained with HPW/SiO_2 and $HPMo/SiO_2$ samples. At both 500 and 600°C, $HPMo/SiO_2$ shows a higher activity than HPW/SiO_2. However, the selectivity to unlabelled carbon dioxide (OCO), at 600°C, is larger with the latter catalyst.

Temperature-programmed reaction of $C^{18}O$ on HPW/SiO_2 (Fig.9.13A) reveals that significant amounts of $C^{18}O$ are transformed to CO. Further, the oxygen exchange is concurrent with the desorption of H_2O from the catalyst. As the temperature increases above 350°C, the oxidation of $C^{18}O$ to OCO increases steadily, while the oxidation of $C^{18}O$ to $^{18}OC^{18}O$ becomes negligible at temperatures higher than 550°C. In contrast, with $HPMo/SiO_2$ (Fig.9.13B), CO is only observed to form from about 500°C, with a sharp increase from 550°C and a maximum at 580°C.

The maximum in selectivity to CO occurs at a temperature similar to that for ^{18}OCO. However, the selectivity to OCO passes through a maximum at 570°C. $^{18}OC^{18}O$ begins to emerge at 550°C, and its selectivity reaches a plateau at 610°C.

As shown earlier, the carbon deposits on the catalysts can be alleviated by injection of oxygen on the catalyst bed (see Fig.9.12). Injection of pulses of oxygen on the catalyst previously saturated with $C^{18}O$, led to product compositions somewhat dissimilar from those summarized in Table 9.3 (Table 9.4 and Table 9.5).

Two distinctions between the results obtained with the two catalysts are evident. Water ($H_2{}^{16}O$) is obtained in the product only with $HPMo/SiO_2$ and, unlike HPW/SiO_2, all of the added oxygen is consumed in the first pulse by the former catalyst, resulting in a higher conversion of the labelled CO held on the catalyst.

B. Discussion

ADSORPTION OF CARBON DIOXIDE

Although CO_2 is evidently present on the untreated tungsten-containing catalyst, after exposure to CO_2, the CO_2 desorption peak increased in intensity providing further evidence for the chemisorption of CO_2. After exposure of the acid to CO_2, the continued presence of the high temperature water desorption peak demonstrates that the protons largely remain in the structure.

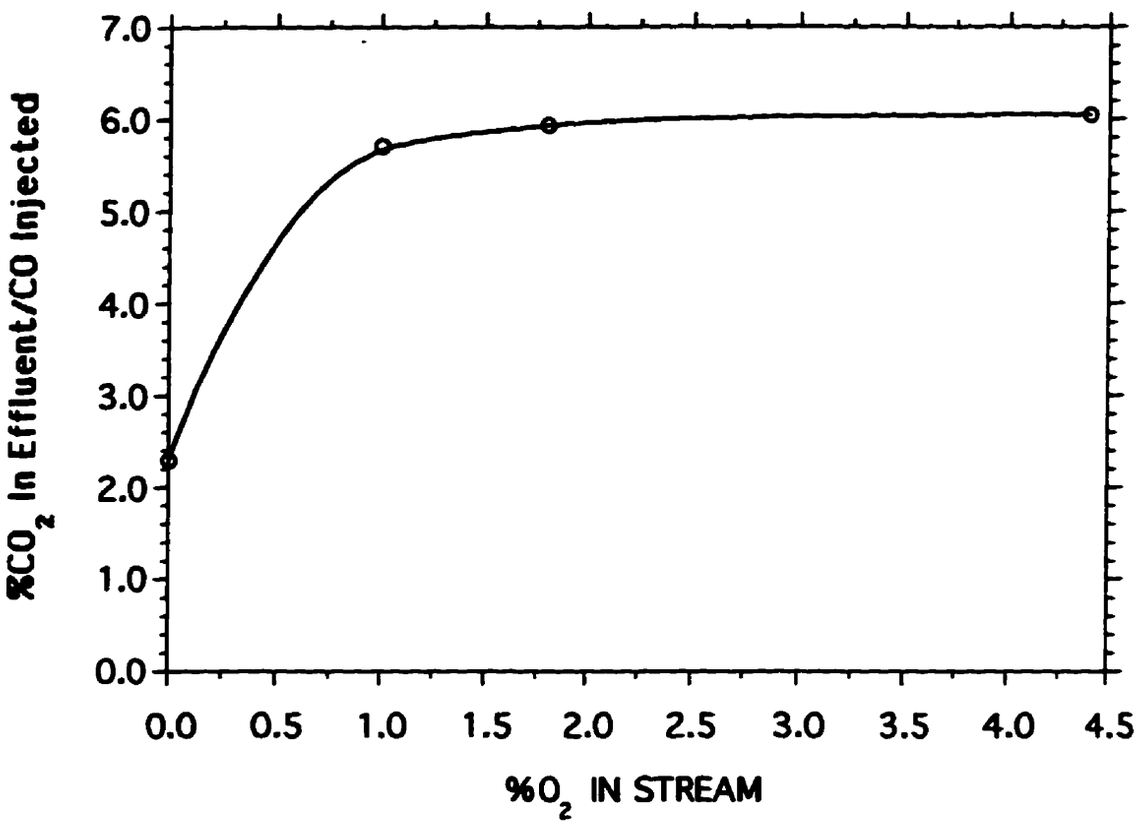

Fig.9.12 Effect of adding oxygen in the gas stream on the oxidation of CO (8% CO/He at 40 mL/min) to CO_2 (as measured by ICR) on 20.0% HPMo/SiO_2 samples (50 mg) pretreated and exposed to CO at 600°C. Integration time = 30 min.

TABLE 9.3

%CO, CO_2, AND OXIDATION PRODUCT RATIO (HPW/HPMo)

23.1%HPW/SiO_2 + 8%C*O at 500°C

Mass	Molecules	%(Product/CO* injected)
28.0	CO	4.3
44.0	OCO	1.3
46.0	^{18}OCO	1.1
48.0	^{18}OC^{18}O	0.3
		7.0

20.0%HPMo/SiO_2 + 8%C*O at 500°C

Mass	Molecules	%(Product/C*O injected)	Product Ratio (HPW/HPMo)
28.0	CO	18.8	0.2
44.0	OCO	2.0	0.7
46.0	^{18}OCO	4.4	0.3
48.0	^{18}OC^{18}O	6.1	0.05
		31.3	

Integration time=60 min, Mass in reactor=50 mg

23.1%HPW/SiO_2 + 8%C*O at 600°C

Mass	Molecules	%(Product/C*O injected)
28.0	CO	2.8
44.0	OCO	1.2
46.0	^{18}OCO	1.7
48.0	^{18}OC^{18}O	0.6
		6.3

20.0%HPMo/SiO_2 + 8%C*O at 600°C

Mass	Molecules	%(Product/C*O injected)	Product Ratio (HPW/HPMo)
28.0	CO	8.7	0.3
44.0	OCO	0.2	6.0
46.0	^{18}OCO	1.5	1.1
48.0	^{18}OC^{18}O	5.9	0.1
		16.3	

Integration time=30 min, Mass in reactor=50 mg.

* = isotope 18.

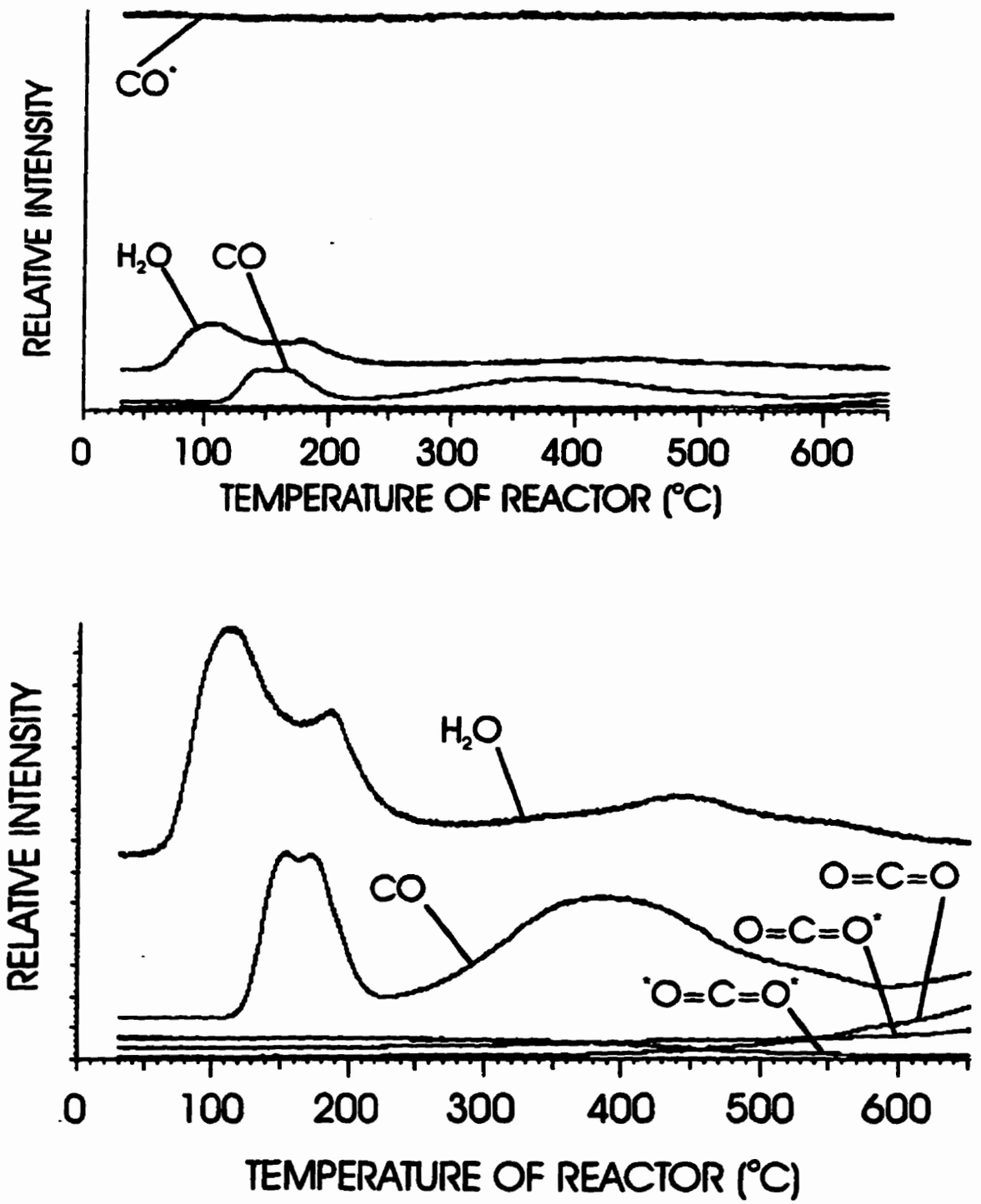

Fig.9.13A TPR of $C^{18}O$ (8% $C^{18}O$/He and 15 mL/min) on 50 mg of 23.1%HPW/SiO_2. * = isotope 18.

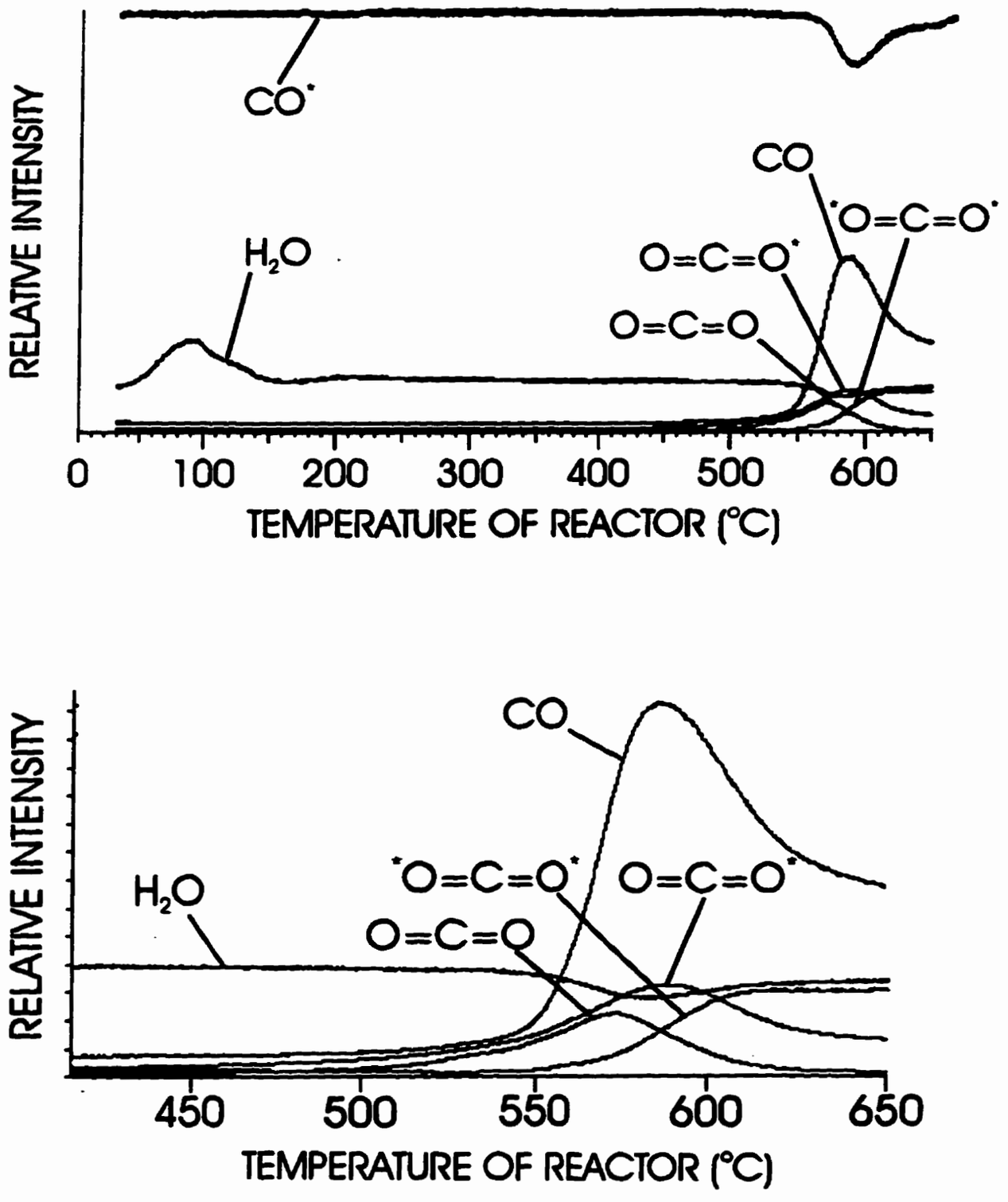

Fig.9.13B TPR of $C^{18}O$ (8% $C^{18}O$/He and 15 mL/min) on 50 mg of 20.0%HPMo/SiO_2. * = isotope 18.

TABLE 9.4

PRODUCT COMPOSITION FROM INJECTION OF OXYGEN ON CATALYSTS SATURATED WITH $C^{18}O$ (FIRST PULSE)

Injection of 50 µl O_2 after exposure of 23.1%HPW/SiO_2 to 8%C*O at 600°C for 1 hour (First Pulse)

Mass	Molecules	%(Product/O_2 injected)
30.0	$C^{18}O$	0.2
32.0	OO	97.4
34.0	^{18}OO	0.9
44.0	OCO	0.2
46.0	^{18}OCO	0.02
48.0	$^{18}OC^{18}O$	1.3
50.0	MF	0.1
64.0	MF	1.5
66.0	MF	0.2
76.0	MF	0.01

Injection of 50 µl O_2 after exposure of 20.0%HPMo/SiO_2 to 8%C*O at 600°C for 1 hour (First Pulse)

Mass	Molecules	%(Product/O_2 injected))
18.0	HOH	4.6
22.0	MF	0.07
23.0	MF	0.1
24.0	MF	0.08
28.0	CO	66.5
29.0	MF	1.0
30.0	$C^{18}O$	29.6
32.0	OO	0.0
34.0	^{18}OO	0.0
40.0	MF	1.0
44.0	OCO	11.1
46.0	^{18}OCO	19.5
48.0	$^{18}OC^{18}O$	11.0
60.0	MF	0.0
62.0	MF	0.0
76.0	MF	0.0

Mass in reactor=50 mg, MF=Molecular Fragment.
* = isotope 18.

TABLE 9.5

PRODUCT COMPOSITION FROM INJECTION OF OXYGEN ON CATALYSTS SATURATED WITH $C^{18}O$ (SECOND PULSE)

Injection of 50 µl O_2 after exposure of 23.1%HPW/SiO_2 to 8%C*O at 600°C for 1 hour (Second Pulse)

Mass	Molecules	%(Product/O_2 injected)
30.0	$C^{18}O$	0.1
32.0	OO	100
34.0	^{18}OO	0.9
44.0	OCO	0.2
46.0	^{18}OCO	0.0
48.0	$^{18}OC^{18}O$	0.02
50.0	MF	0.0
64.0	MF	0.0
66.0	MF	0.0
76.0	MF	0.0

Injection of 50 µl O_2 after exposure of 20.0%HPMo/SiO_2 to 8%C*O at 600°C for 1 hour (Second Pulse)

Mass	Molecules	%(Product/O_2 injected)
18.0	HOH	3.3
22.0	MF	0.04
23.0	MF	0.04
24.0	MF	0.0
28.0	CO	28.9
29.0	MF	0.3
30.0	$C^{18}O$	2.8
32.0	OO	80.1
34.0	^{18}OO	0.7
40.0	MF	0.4
44.0	OCO	6.3
46.0	^{18}OCO	5.4
48.0	$^{18}OC^{18}O$	1.8
60.0	MF	0.05
62.0	MF	0.03
76.0	MF	0.02

Mass in reactor=50 mg, MF=Molecular Fragment.
* = isotope 18.

The results with HPMo are significantly different from those found with HPW. While only small quantities of CO_2 are sorbed on the bulk HPMo, substantial amounts are sorbed on the HPMo/SiO_2. Temperatures of 520 and 580°C were required for CO_2 to desorb from HPMo and HPW containing samples, respectively. However, the high temperature water peak was not observed after sorption of CO_2, suggesting that the CO_2 may be hindering the extraction of anionic oxygen atoms by the protons.

NaPW, HPW and silica pretreated at 650°C, sorb vanishingly small quantities of CO_2. Since under these conditions, relatively few protons are present within these materials, their presence is apparently a necessary condition for the chemisorption of CO_2.

Remarkable differences are observed in the sorption of CO_2 by the two supported and unsupported solid acids. While pure HPW sorbs twice as much CO_2 as pure HPMo, the supported HPMo sorbs substantially more CO_2 than supported HPW. Although such differences for the pure acids may be attributed to differences in acidic strengths, as suggested in the comparative studies of the sorption of NO_2 (Chapter III), such a rationalization appears to be inappropriate for the supported acids.

The number of water molecules or protons present in the catalysts is dependent upon the temperature to which the catalyst has been heated. The effect of the pretreatment temperature on the sorption of CO_2 suggests that the accessibility of the protons as well as the environment surrounding the protons is important for the sorption of CO_2. This effect is more evident with HPW than with HPMo, which may be attributed to the higher acidic strength and consequent higher binding energy of the water molecules in the former solid. Further, from the results of NaPW exposed to carbon dioxide, it is evident that the protons play an important role for the sorption of CO_2.

The Raman results demonstrate clearly that carbon deposits exist at the surface of the samples. As estimated from the I_{1350}/I_{1590} ratio of 1.5 for HPW, the carbon particle size of 30-35 Å corresponds to that expected for disordered graphite (Ref.9.3). Thus, heating the catalysts to 520 and 580°C, for HPMo/SiO_2 and HPW (orHPW/SiO_2), respectively, will result in the carbon atoms extracting the anionic oxygen to produce CO_2.

$$Mo{=}O + C \rightarrow Mo\square + CO \qquad \text{(Eq.9.1)}$$

$$Mo{=}O + CO \rightarrow Mo\square + CO_2 \qquad \text{(Eq.9.2)}$$

or

$$W{=}O + C \rightarrow W\square + CO \qquad \text{(Eq.9.3)}$$

$$W{=}O + CO \rightarrow W\square + CO_2 \qquad \text{(Eq.9.4)}$$

The disappearance of the high temperature water peak (in the TPD results) with HPMo can be rationalized by the consumption of the protruding oxygen atoms (of the anions) during the desorption of CO_2. Also, it is possible that the protons are oxidized to water as the reduction of CO_2 proceeds. However, the disappearance of the associative water peak with HPW is difficult to observe since little CO_2 is being reduced to carbon. Further, the depletion of carbon and the formation of CO_2 (during the TPDs) apparently occurs after the extraction of the protons because no water can be detected during the former process. Alternatively, the extraction of anionic oxygen atoms (those normally available to the protons) would also hinder the formation of the associative waters.

The attribution of the 784 cm^{-1} Raman band is unclear. Observations from measurements of the sorption of CO on nickel suggest that the band could be due to bridge sites W-C or Mo-C (Ref.9.3). These sites would then offer a nuclei for the growth of carbon particles of approximately 30Å in dimension. Alternatively, the 784 cm^{-1} Raman band may be attributed to the bending mode for sorbed CO_2 which has been observed at 650-820 cm^{-1} on a variety of metals (Ref.9.4a).

Tentatively, the mechanism for the reduction of CO_2 to carbon graphite could be similar to that of Ayers (Ref.9.4b), where a 4 electrons (from the oxygen atoms) mechanism is involved. In a first step CO_2 (in the presence of two protons) would be reduced to CO, which would be reduced (also with two protons) to C. The protons and the oxygen atoms (from CO_2 and CO) would form water.

$$CO_2 + 2H^+ + 2e \text{ (from } O^{2-}) \rightarrow CO + H_2O \qquad \text{(Eq.9.5)}$$

$$CO + 2H^+ + 2e \text{ (from } O^{2-}) \rightarrow C + H_2O \qquad \text{(Eq.9.6)}$$

Alternatively, the disproportionation of CO_2 is also a possibility which cannot be rejected.

$$2CO_2 \rightarrow 2CO + O_2 \qquad \text{(Eq.9.7)}$$

$$2CO \rightarrow CO_2 + C \qquad \text{(Eq.9.8)}$$

Although no oxygen was observed in the gas phase, it is conceivable that O_2 is used for the regeneration of oxygen vacancies.

Another important factor is the diffusion of the molecules into the samples. Both type of catalysts are affected by the diffusion of CO_2 (seen from the mass of catalyst used inside the reactor, the initial concentration of CO_2 in the gas stream, and the time of contact), HPW being more affected than HPMo. Since CO_2 is a non-polar molecule, it is not expected to interact or

diffuse easily into the heteropoly acids. Further, the role of the protons is important in the reduction of CO_2, and the number of CO_2 (from the oxidation of the carbon deposits) per KU was found to be smaller than the stoichiometry of three protons per Keggin Unit. The formation and accumulation of carbon atoms at the surface of the catalysts would hinder the diffusion and subsequent reduction of CO_2 by the protons (Refs.9.5 to 9.9).

The present results give some insights pertaining to the mechanisms governing the interaction of molecules with the heteropoly oxometalates.

CONVERSION OF CARBON MONOXIDE TO CARBON DIOXIDE

A flow of CO (8% in helium) passed over HPW or HPMo samples heated from 30 to 650°C, produced a CO_2 peak at 580°C demonstrating that CO was oxidized to CO_2 on the catalysts in the absence of added O_2. Carbon monoxide was not sorbed as such since no peak of CO could be observed. Portion of the CO_2 produced was, again, strongly bound to the solid (in whatever form). Further, the oxidation of CO on loaded samples showed a maximum conversion at approximately 20% of loading. This result is similar to results reported earlier in which maxima in conversion (for a given reaction) were observed at loadings in the vicinity of 20% (Ref.9.10). It is of interest to note that earlier XPS, Raman, and NMR studies have shown that at loadings greater that 20-25% crystallites of HPW begin to form on SiO_2 (Ref.9.11).

The selectivity to CO_2, from the oxidation of CO, was greater with HPMo/SiO_2 than for HPW/SiO_2 samples. The results for the conversion of CO to CO_2 are reminiscent of those for the sorption of CO_2. As for the sorption of CO_2, the oxidation of CO also depends on the anion composition and surface of the catalysts exposed.

Exposure of NaPW to a flow of CO, while increasing the temperature, showed that no CO is sorbed and no CO_2 is produced. This suggests that protons are required for the oxidation of CO. The small quantities of CO_2 produced from CO over SiO_2 may, tentatively, be attributed to the protons from the silica, or the disproportionation of CO (Eq.9.8). However, CO_2 may also result from the oxidation of CO by oxygen atoms from the decomposition of CO.

The results show that the oxygen atoms in HPMo are more labile than those in HPW, since the yield is greater with the former than the latter. It is worth noting that the rapid rise in the production of CO_2, for HPMo at 500°C, corresponds approximately to the temperature at which HPMo/SiO_2 would thermally decompose to release CO_2 when previously exposed to CO_2. For HPW/SiO_2 this decomposition temperature was found to be higher (>580°C) than those employed in the present work. However an increase in the production of CO_2 occurs at temperatures above 600°C. Nevertheless, as previously explained, heteropoly compounds and their decomposition products exist at the surface of the silica at temperatures greater than 600°C.

Experiments with $C^{18}O$ were performed to provide further information on the oxidation of CO. Since the $C^{18}O$ used contained only traces of CO (<2%), the formation of CO, ^{18}OCO and OCO results primarily from the extraction of oxygen atoms from the cluster compounds (Eqs.9.2 and 9.4). The formation of $^{18}OC^{18}O$ may be attributed to isotopic exchange between sorbed species and gas phase $C^{18}O$, or the oxidation of $C^{18}O$ by ^{18}O from dissociated $C^{18}O$.

CO may form from the sorption of $C^{18}O$, its dissociation to C and ^{18}O, and reoxidation of C with oxygen atoms from the clusters or water molecules. With HPW/SiO_2, the maximum for the formation of CO was found at much lower temperatures than that at which the anions decomposed but, with $HPMo/SiO_2$ the formation of CO was observed at temperatures greater than 550°C. More surprising is the fact that HPW samples formed relatively more CO at temperatures as low as 150°C. No evidence for the sorption of CO (or $C^{18}O$) was found.

As mentioned earlier, the disproportionation of $C^{18}O$ (Eq.9.8) is also possible. Using Tables 9.3 to 9.5 (at 600°C), the quantities found in Table 9.6 were calculated. The results indicate that little disproportionation is occurring on the catalysts, but mainly isotopic exchange and anionic extraction.

Only small quantities of water desorb from $HPMo/SiO_2$ samples above 550°C, while substantial quantities of CO were detected, the oxygen of which evidently has been extracted from the anions. Cho and Stock showed that at high temperature the rate of CO dissociation was approximately half that of direct oxidation with Rh/Al_2O_3 catalysts (Ref.9.12). However, at low temperature the rate of CO dissociation was of the same order of magnitude as the rate of CO oxidation to CO_2. They also observed the formation of carbon at the surface, which could also reduce the rate of dissociation of CO at the surface. Nevertheless, the mechanism for the oxidation of CO to CO_2 was ultimately controlled by the dissociation rate. It is also conceivable that, in the present study, the rate of dissociation also controls the mechanism for the oxidation of CO to CO_2. However, the rate of oxidation of CO (or $C^{18}O$) to (total) CO_2 increases with the isotopic exchange (see Table 9.3 and 9.4). The rate of the reaction is expected to decrease if controlled by the dissociation of $C^{18}O$ (Ref.9.13). Thus, the rate of CO oxidation to CO_2 is slower than the rate of CO (or $C^{18}O$) dissociation.

The two types of catalysts have similarities and subtle differences. Both can oxidize carbon monoxide to carbon dioxide. The molybdenum catalyst produces CO by isotopic exchange between the $C^{18}O$ molecule in the gas phase and the anionic oxygen atoms. However, with the tungsten catalyst, the $C^{18}O$ combines with the anionic oxygen to form carbon dioxide (^{18}OCO), since this is not concomitant with the formation of CO. However, regardless of the oxygen exchange mechanism, $HPMo/SiO_2$ is more effective than HPW/SiO_2 for the oxidation of carbon monoxide, as expected from the lability of the oxygen atoms (Ref.9.14).

TABLE 9.6

TOTAL SORBED CARBON AND CARBON DIOXIDE DURING THE OXIDATION OF CO ON HPW/SiO_2 AND HPMo/SiO_2[a]

Catalysts	Carbon Sorbed[b] (C sorbed per KU)	Total CO_2 in gas phase[c] (CO_2 produced per KU)
23.1%HPW/SiO_2	0.021	19
20.0%HPMo/SiO_2	1.4	30

a Calculated from results of Tables 9.3 to 9.5, at 600°C.
b From Tables 9.4 and 9.5, calculated from the total carbon found in the gas phase.
c From Table 9.3, calculated from total CO_2 found at 600°C.

Under continuous reaction conditions, H_2O was only observed with $HPMo/SiO_2$, which would indicate that some oxygen atoms from the Keggin Units are being extracted, as well as protons, possibly due to the temperature at which the reaction proceeded.

The contact of CO with the heteropoly acids, as with the sorption of CO_2, produces an accumulation of carbon over the catalysts. The presence of the labelled molecules, including ^{18}OO, after reaction of the catalysts with $C^{18}O$ followed by injection of O_2, indicates that a portion of the ^{16}O in the anions has been replaced by ^{18}O. Alternatively, the existence of perhaps strongly held $C^{18}O$ could also be responsible for the formation of the labelled oxygen molecules, however, evidence of which was not observed by TPR or Raman spectroscopy.

The observed decrease in the conversion of CO, may tentatively be attributed to the inhibition of the process by carbon deposits, which seems to eventually stop the oxidation reaction of CO to CO_2. The carbon deposits block the active sites, but it is possible to remove these carbon deposits by the addition in the feedstream of oxidants (like O_2, or NO_2) to oxidise the sorbed carbonaceous species (Ref.9.15).

C. Conclusion

The heteropoly acids reduce CO_2 to carbon. The loading of these acids on silica promotes the reduction of CO_2. The presence of the protons are required for the reduction of CO_2. Raman spectroscopy shows that carbon deposition occurs on exposure of the catalysts to CO_2. The sorbing capacity for CO_2 (in whatever form) depends on the acidic strength, thus on the composition of the anions.

The oxidation of CO to CO_2 occurs on HPW/SiO_2 and $HPMo/SiO_2$ in the absence of added oxygen, with the latter catalyst being more effective for this purpose.

REFERENCES

9.1a Hodnett, B.K., and Moffat, J.B. *J.Catal.*, **88**, 253 (1984).

9.1b Moffat, J.B. Heteropoly Compounds: Solid Acids With Guarded Protons, in *Catalysis by Acids and Bases*, Elsevier Science Publishers B.V., Amsterdam, Netherlands, 1985.

9.2a Tuinstra, F., and Koenig, J.L. *J.Chem.Phys.*, **53**, 1126 (1970).

9.2b Wang, Y., Alsmeyer, D.C., and McCreery, R.L. *Chem. of Materials*, **2**, 557 (1990).

9.3 Stencel, J.M. Raman Spectroscopy for Catalysis, Van Nostrand Reinhold, New York, NY, 1990.

9.4a Wambach, J., Freund, H.-J. CO_2 Activation on Transition Metal Surfaces, in *Carbon Dioxide Chemistry: Environmental Issues*, The Royal Society of Chemistry, Cambridge, UK, 1994.

9.4b Ayers, W.M., An Overview of Electrochemical Carbon Dioxide Reduction, in *Carbon Dioxide Chemistry: Environmental Issues*, The Royal Society of Chemistry, Cambridge, UK, 1994.

9.5 Dadyburjor, D.B., and Zhenyu, L. *Chem.Eng.Sci.*, **47**, 645 (1992).

9.6 Bonardet, J.L., Barrage, M.C., and Fraissard, J. *J.Molec.Catal. A:Chemical*, **96**, 123 (1995).

9.7 Lee, H.H *A.I.Ch.E. J.*, **40**, 2022 (1994).

9.8 Baptist-Nguyen, S., and Subramaniam, B. *A.I.Ch.E. J.*, **38**, 1027 (1992).

9.9 Muhammad, O.H.J., and Kam, E.K.T. *Chem.Eng.Sci.*, **51**, 2939 (1996).

9.10 See for example: Kasztelan, S., and Moffat, J.B. *J.Catal.*, **109**, 206 (1988).

9.11 Kasztelan, S., Payen, E., and Moffat, J.B. *J.Catal*, **125**, 45 (1990).

9.12 Cho, B.K., and Stock, C.J. *J.Catal.*, **117**, 202 (1989).

9.13 Atkins, P.W., Physical Chemistry, Fourth Edition, W.H. Freeman and Company, New York, 1990.

9.14 Moffat, J.B., *J.Mol.Catal.*, **26**, 385 (1984).

9.15 Puri, B.R., Surface Complexes on Carbons, in *Chemistry and Physics of Carbon*, Volume 6, Marcel Dekker Inc., New York, NY, 1970.

CONCLUSIONS

The work reported here serves two purposes: (1) to provide further information on the surface, bulk and catalytic properties of the heteropoly oxometalates, in particular by use of nitrogen and carbon oxides as probe molecules and (2) to investigate the potential of these solids as catalysts for the removal and conversion of the aforementioned environmentally disadvantageous gases. In regard to the coming regulations, where catalysts will have to operate under fuel-lean conditions (net oxidizing), it is believed that the present heteropoly compounds could represent a breakthrough in oxides of nitrogen catalytic control.

The first section deals the reactions and interactions of nitrogen oxides on the parent acids (Chapter III). The composition of the anion may be altered by changes in the central atom or the peripheral metal element, while the Keggin structure is retained. By studying 12-tungstophosphoric and 12-tungstosilicic acids the effect of the central atom can be evaluated and comparison of the results from the former with those of 12-molybdophosphoric acid allow the effect of changes in the peripheral metal elements to be determined.

While the central atom has little effect on the properties of the heteropoly acids for the sorption of NO_2, the solid acids containing tungsten show superior sorption properties to those containing molybdenum. Earlier work has shown that the former acids are stronger acids than the latter. Nitrogen dioxide molecules are shown to be capable of penetrating into the bulk structures of the solid acids, in particular HPW and HSiW, and interacting with both the surface and the interior water molecules to produce HNO_3 which is released from the solid. After consumption of the water NO_2 associates with the protons to form $[HNO_2]^+$ and up to 3 molecules of NO_2 per anion are retained on the solid.

Although relatively insignificant quantities of NO were found to sorb on the acids, after sorption of NO_2 nitric oxide sorbed up to equimolar amounts of NO_2, with the resulting formation of N_2O_3. No evidence was found for the reduction of either NO_2 or NO to form N_2.

The absence of sorption of NOx on the alkali metal salts of HPW (Chapter VI) provides evidence for the participation of the proton in the sorption process.

Liquid and solid sorbents have been used in the past to control the NOx emissions (Ref.1.6). Solutions of ferrous sulfate, potassium hydroxide, or potassium permanganate were used and offered between 15-50% NOx removal. Silica gel, zeolites, and carbon were also used as solid sorbents. At best, silica gel and zeolites offered 89% NOx removal, while 55% for

carbon. The sorbents were later regenerated but only 80-90% recovery could be attained. The use of liquid and solid sorbents generates considerable amounts of waste if the sorption is irreversible.

The direct sorption of NO_2 by the heteropoly acids offers interesting prospects. As it was seen in Chapter III, NO_2 sorbs on the solid heteropoly acids (those containing tungsten). Over 90-95% removal can be attained under the present conditions. Further, increasing the mass of the catalyst inside the reactor will increase this figure. The chemisorbed NO_2 can react with water vapour to produce nitric acid (and vice versa) without damaging the Keggin structure. In this reaction, the heteropoly acids are true catalysts. Further, it is our belief that the NO_2-saturated heteropoly acids could also be used in many other catalytic reactions which would need a pool of nitrogen dioxide or $[HNO_2]^+$.

Because the heteropoly acids are unable to reduce NO_2 to N_2 under net reducing conditions, a direct comparison with the TWC is not possible here. However, the heteropoly acids could be compared to the ZSM-5 (Ref.1.13) or VPO (Ref.1.17) catalysts since they are to be operated under fuel-lean conditions. Even though this is highly speculative, it is possible that the reduction of NO_2 might be possible under real or simulated (net oxidizing) conditions.

In the standard SCR process (also net oxidizing), gaseous ammonia is directly injected in the gas stream before the catalyst bed. Great quantities of ammonia escape to the atmosphere (5-10 ppm). This problem results in higher costs, as well as release of NH_3 into the atmosphere. Another concern for the industries is the temperature at which the catalyst bed must be heated for the efficient reduction of NOx. Low temperatures (100-200°C) are preferred in order to diminish the cost of operation. Presently, the maxima in NOx conversion with V_2O_5 and TiO_2 are approximately 55% (at 300°C) and 40% (at 400°C), respectively (Ref.1.18a).

In view of the use of ammonia for the selective catalytic reduction of NO_X in the industries, as well as the ammonia slip problem, NO and NO_2 were injected on ammonium salts of heteropoly acids (Chapters IV and V). In the present work, the heteropoly ammonium salts were prepared from their respective parent acid by precipitation with any ammonia source (i.e. ammonium carbonate, ammonium nitrate, etc.). They do not require calcination at high temperatures, but they only need to be heated at the reaction temperature. The surface structure of the ammonium salts is well known and unlike the heteropoly acids, they possess a high surface area. The direct advantage is that no gaseous ammonia needs to be injected while the reduction process takes place.

Nitrogen dioxide is directly reduced to N_2 and is the principal product found in the effluent at temperatures of 100-200°C. However, at temperatures higher than 200°C, nitrous oxide is released to the gas stream in great quantities from the thermal decomposition of ammonium nitrate and the direct reaction of nitric acid (formed from the reaction of NO_2 and

catalytic H_2O) with the ammonium cations. In the reduction process the ammonium are thus consumed by both NO_2 and nitric acid.

Although little nitric oxide can be reduced directly by the ammonium heteropoly salts, the reduction of NO to N_2 at low temperature can be promoted by pre-exposing the ammonium salts to NO_2 or HNO_3. Further, during the reduction of NO_2 or NO, no ammonia was released to the gas phase.

Table C.1 presents the observed capacities for both sorption and reaction on the present heteropoly compounds. Only the values found for the injection of NO_2 are presented in the table since most of the work related to nitrogen dioxide and, under fuel-lean conditions, NO_2 is the main oxide of nitrogen found in the gas stream. Further, the $N_2/(N_2O+NO)$ ratio is presented in the last column as an efficiency indicator (in regards to N_2). It is to be noted, however, that the values presented in this table are those for the total capacity (or saturation), and this would not be the case if operated under practical conditions.

From the total capacities found in Table C.1, both ammonium 12-tungstophosphate and ammonium 12-molybdophosphate can reduce NO_2 to N_2. Generally the capacity to N_2 increases with the temperature of the reactor, but the production of N_2O starts at $T > 200°C$. The efficiency indicator (last column) shows that NH_4PW-150°C and NH_4PMo-400°C are those which give the cleanest gas stream. Moreover, increasing the mass of catalysts in the reactor bed (Table 4.3) will results in a higher conversion and a cleaner exhaust. However, the ammonium 12-molybdophosphate irreversibly losses its structural integrity when exposed to NO_2 at temperatures greater than 400°C. Ammonium 12-tungstophosphate sorbs quantities of NO_2 (by protonation) after consumption of the NH_3 (as NH_4^+) in the reaction. In addition, at 150°C, the surface of the salt becomes saturated with ammonium nitrate, which reduces the selectivity to N_2, from NO_2, but increases that from NO. NH_4PW can also be regenerated by injection of ammonia, which in turn reduces the chemisorbed NO_2 to N_2. However, in the process, the heteropoly ammonium salt losses its original surface area, thus its efficiency.

Since the selectivity to N_2 is inferior in the gas phase reaction of NO_2 and NH_3, NH_4PW (as well as NH_4PMo) is considered to be a catalyst, in which it promotes the formation of N_2. More precisely, since the ammonium cations are consumed during the course of the reaction, the heteropoly ammonium salts are known to be catalo-reactants.

Once again, a direct comparison between the heteropoly ammonium salts and the catalysts used commercially in the NOx SCR process is impossible. A cost-effective analysis including the price of the catalyst bed, the heating costs, the amount of ammonia used, and the cost for regeneration (if possible) would be needed to show which catalyst is better. In view of the figures presented above (from Ref.1.18a) and the ammonia slip problem, NH_4PW offers an interesting alternative.

TABLE C.1

OBSERVED CAPACITIES OF HETEROPOLY OXOMETALATES TO NO_2

Catalysts	Temperature (°C)	NO_2 sorbed (NO_2/KU)	N_2 produced (N_2/KU)	N_2O produced (N_2O/KU)	NO produced (NO/KU)	Efficiency indicator ($N_2/(N_2O+NO)$)
HPW[a]	150	2.9	-	-	-	-
HPW	300	0.8	-	-	-	-
HPMo	150	0.1	-	-	-	-
HPMo	300	0.0	-	-	-	-
NH_4PW[b,c]	150	?	0.62	trace	0.09	6.9
NH_4PW[b,d]	300	3.0	1.0	1.8	trace	0.56
NH_4PMo-A[e]	150	?	0.58	trace	0.31	1.9
NH_4PMo-A[e]	300	0.0	1.6	0.91	0.0	1.9
NH_4PMo-A[e]	400	0.0	1.4	0.15	0.76	1.5
NH_4PMo-B[f]	150	?	0.19	0.0	0.37	0.51
NH_4PMo-B[f]	300	0.0	1.7	0.74	0.0	2.3
NH_4PMo-B[f]	400	0.0	2.0	0.03	0.28	6.5
23.1%HPW/SiO_2[g]	150	1.1	4.0	0.0	2.9	1.4
23.1%HPW/SiO_2[g]	300	0.1	2.5	0.90	4.0	0.51

a 1.6 HNO_3/KU produced at 150°C during saturation with NO_2 (0.45 HNO_3/KU produced during regeneration).

b Prepared from stoichiometric amounts of ammonium carbonate and HPW (washed).

c Originally contained 2.3 NH_4^+/KU.

d Originally contained 2.1 NH_4^+/KU.

e Prepared from stoichiometric amounts of ammonium nitrate and HPMo (unwashed).

f Prepared from stoichiometric amounts of ammonium carbonate and HPMo (unwashed).

g Pre-exposed to NH_3 prior to saturation with NO_2.

NOTE: TO CONVERT VALUES TO MOLE OF PRODUCT PER GRAM OF CATALYST:

1 mole KU= 2877.77g (PW) or 1822.25g (PMo).

Because of their poor mechanical properties, and in some case their water solubility, the heteropoly acids and salts are not well suited to be used in an industrial reactor system. However, it was clearly shown in the past that these problems can be avoided by the use of a proper support. Further, supporting the heteropoly acids improves not only the mechanical properties but also the surface and catalytic characteristics (i.e. greater surface area, higher thermal stability, and different pore structure).

The silica-supported ammonium 12-tungstophosphate shows a greater capacity to N_2 from the reduction of NO_2 (Chapter VII). However, because of the nature of the support and the reactivity of NO_2, the capacity to NO is also high. From the previous results, it is clear that the support contributes to the formation of NO. Under reducing conditions, nitrogen dioxide on V_2O_5, TiO_2, and Al_2O_3 shows a high selectivity to NO (11.9%, 29.8%, and 36.1%, respectively) and no capacity to N_2 (Ref.1.31). In this fashion, NH_4PW/SiO_2 is a superior catalyst for the reduction of NO_2. V_2O_5/SiO_2 (at 180°C) was found to be also efficient (96% total conversion) for the decomposition of NOx (Ref.1.21).

Although the formation of N_2 is enhanced with the supported heteropoly salt, the overall process is less efficient (see the efficiency indicator on Table C.1) than the bulk materials. The surface integrity, however, is kept intact. Finding a NO_2-inert support is imperative to improve the catalyst. A possible support could be one of the high surface area IA-heteropoly salts (or thallium salt). It was found in Chapter VI that these salts were inert to NO_2. Supporting the heteropoly acid (HPW) on CsPW (then exposed to gaseous ammonia), for example, might give an improved, low temperature, mechanically stable catalyst for the decomposition of NO_2 under fuel-lean conditions.

The last Chapter of the present work presents the sorption and reaction of oxides of carbon (COx) by the heteropoly oxometalates (Chapter IX). The characterization and quantification of the sorption of CO_2 and oxidation of CO was initiated because of the results observed with the silica-supported HPMo. A CO_2 desorption peak was observed in the TPD of the supported acid. This was never mentioned in the literature even though the peak at 580°C was seen on the published TPDs. The present results show that both bulk and supported acids can sorb quantities of CO_2. Moreover, the heteropoly acids (supported or not) are capable of oxidizing CO to CO_2 under net reducing conditions. The sorption and conversion values measured are small and more research needs to be done to improve these values. However, the present results teach us about the surface and catalytic properties of the heteropoly oxometalates having the Keggin structure.